CRANFIELD UNIVERSITY

Alireza Alghassi

Prognostics and Health Management of Power Electronics

School of Aerospace, Transport and Manufacturing
IVHM Centre

PhD Thesis
Academic Year: 2015 - 2016

Supervisor: Dr Suresh Perinpanayagam

September 2016

CRANFIELD UNIVERSITY

School of Aerospace, Transport and Manufacturing
IVHM Centre

PhD Thesis

Academic Year 2015 - 2016

Alireza Alghassi

Prognostics and Health Management of Power Electronics

Supervisor: Dr Suresh Perinpanayagam

September 2016

Abstract

Prognostics and health management (PHM) is a major tool enabling systems to evaluate their reliability in real-time operation. Despite ground-breaking advances in most engineering and scientific disciplines during the past decades, reliability engineering has not seen significant breakthroughs or noticeable advances. Therefore, self-awareness of the embedded system is also often required in the sense that the system should be able to assess its own health state and failure records, and those of its main components, and take action appropriately. This thesis presents a radically new prognostics approach to reliable system design that will revolutionise complex power electronic systems with robust prognostics capability enhanced Insulated Gate Bipolar Transistors (IGBT) in applications where reliability is significantly challenging and critical. The IGBT is considered as one of the components that is mainly damaged in converters and experiences a number of failure mechanisms, such as bond wire lift off, die attached solder crack, loose gate control voltage, etc. The resulting effects mentioned are complex. For instance, solder crack growth results in increasing the IGBT's thermal junction which becomes a source of heat turns to wire bond lift off. As a result, the indication of this failure can be seen often in increasing on-state resistance relating to the voltage drop between on-state collector-emitter. On the other hand, hot carrier injection is increased due to electrical stress. Additionally, IGBTs are components that mainly work under high stress, temperature and power consumptions due to the higher range of load that these devices need to switch. This accelerates the degradation mechanism in the power switches in discrete fashion till reaches failure state which fail after several hundred cycles. To this end, exploiting failure mechanism knowledge of IGBTs and identifying failure parameter indication are background information of developing failure model and prognostics algorithm to calculate remaining useful life (RUL) along with ±10% confidence bounds. A number of various prognostics models have been developed for forecasting time to failure of IGBTs and the performance of the presented estimation models has been evaluated based on two different evaluation metrics. The results show significant improvement in health monitoring capability for power switches.

Furthermore, the reliability of the power switch was calculated and conducted to fully describe health state of the converter and reconfigure the control parameter using adaptive algorithm under degradation and load mission limitation. As a result, the life expectancy of devices has been increased. These all allow condition-monitoring facilities to minimise stress levels and predict future failure which greatly reduces the likelihood of power switch failures in the first place.

Keywords:

Prognostics and Health Management, Power Electronics, Insulated Gate Bipolar Transistor, Integrated System Health Management, Remaining Useful Life, Condition-Based Monitoring, Coffin-Manson Rule, Failure Mechanisms.

Acknowledgements

I would like to express my sincere thanks to my supervisor, Dr Suresh Perinpanayagam, for all his support and encouragement. I would like also to thank Dr Mohammad Samie and Dr Tarapong Sreenuch for technical discussions, valuable comments and constructive suggestions which helped me to have a better understanding of the research problem.

I take this opportunity to thank the head of the IVHM Centre, Professor Ian K. Jennions, for helpful discussions on my presentations at technical reviews. I am thankful to my colleague, Dr Omer Faruk Eker, for helpful discussions about prognostics during the initial stages of the PhD. I would also thank my colleague, Payam Soulatiantork, from University of Politecnico di Milano for his collaboration in advance stress control studies. I express my thanks to Rajkumar Choudhary, Dr Faisal Khan and Barry James Nel for reviewing my papers. I also express my thanks to all colleagues at the IVHM Centre for all their support and joyful company.

Very special thanks to my parents and my brother and sisters for always supporting and encouraging me at every stage.

Table of Contents

List of Figures

List of Tables

List of Abbreviations

AI	Artificial Intelligence
AIN	Aluminium Nitride Substrate
ANFIS	Adaptive Neuro-Fuzzy Inference System
ANN	Artificial Neural Networks
ARMA	Auto-Regressive Moving Average
NAR	Nonlinear Autoregressive
CBM	Condition-Based Modelling
CM	Condition Monitoring
CMOS	Complementary Metal Oxide Semiconductor
CTE	Coefficient of Thermal Expansion
DBC	Direct Bonded Copper
DBN	Dynamic Bayesian Network
DDM	Data-Driven Modelling
DP	Damage Prognosis
DWNN	Dynamic Wavelet Neural Network
EHM	Engine Health Management
EKF	Extended Kalman Filter
EoL	End-of-Life
FEA	Finite Element Analysis
FET	Field Effect Transistor
FFNN	Feed Forward Neural Network
FMECA	Failure Mode, Effects, and Criticality Analysis
FMMEA	Failure Modes, Mechanisms, and Effect Analysis
FSM	Fuzzy Sugeno Model
GA	Genetic Algorithm
GPR	Gaussian Process Regression
HCI	Hot Carrier Injection
HHMM	Hierarchical Hidden Markov Model
HMM	Hidden Markov Model
HPC	High-Pressure Compressor
HS	Health State
HSMM	Hidden Semi Markov Model
HUMS	Health and Usage Monitoring System
IEEE	Institute of Electrical and Electronics Engineers
IGBT	Insulated Gate Bipolar Transistor
iR	Infra-Red
ISHM	Integrated System Health Management
IVHM	Integrated Vehicle Health Management

KF	Kalman Filter
MA	Moving Average
MAD	Mean Absolute Deviation
MCS	Monte Carlo Simulation
MD	Mahalanobis Distance
MLE	Maximum Likelihood Estimation
MSE	Mean Squared Error
MTBF	Mean Time between Failures
MTTR	Mean Time to Restore
NASA	National Aeronautics and Space Administration
NBTI	Negative Bias Temperature Instability
NF	Neural Fuzzy
NN	Neural Network
OBD	On-Board Diagnostic
OC	Operating Condition
PbM	Physics-Based Modelling
PCBs	Printed Circuit Boards
PDF	Probability Distribution Function
PF	Particle Filter
PHM	Prognostics and Health Management
PoF	Physics of Failure
POF	Potential of Failure
RA	Relative Accuracy
RCM	Reliability Centred Maintenance
RMSE	Root Mean Squared Error
RNN	Recurrent Neural Network
RUL	Remaining Useful Life
SEE	Single Event Effect
SHM	Structural Health Monitoring
SSBP	Simple State-Based Prognostics
TDDB	Time-Dependent Dielectric Breakdown
TDNN	Time Delay Neural Network
SEPIC	Single-Ended Primary Inductance Converter
SHM	System Health Management
VHM	Vehicle Health Management
VQ	Vector Quantisation
IR	Ideal RUL

1 Introduction

1.1 Scope of Research

Power electronics is becoming significant at all levels of energy conversion. Power switching modules, such as Insulated Gate Bipolar Transistors (IGBTs), are one of the main components in power conversion systems. Generally, all power switches, power electronic devices and modules have a non-zero probability of failure and the overall system using them will also demonstrate this degree of unreliability. Generally, power switches suffer from wide-ranging failure that could be classified as packaging problems (e.g. wire bond lift off, substrate solder joint crack and die-attached failure), dynamic latch up, and loose gate control voltage thermal runway, during exposure to thermal variation and high electrical stresses. Within this classification, faults introduced by irreversible physical changes in the packaging, known as extrinsic failures, are dominant failures, whilst other physical changes, known as intrinsic failures, are mostly triggered by dominant failures. These faults have a great impact on reducing the reliability of the power system in highly-reliable applications, such as chemical/nuclear and space/aeronautic/medical industries. In cases of extreme dependence on the severity of the environmental conditions and the load operating conditions, replacement of malfunctioning devices may be difficult, and thus, earlier failure prediction and on-line repair are the only options. With regard to failure prediction, industry fabrication is still in its infancy and no datasheets with typical characteristics are available to build prognostics models. Power electric and electronic systems of industrial applications, such as space and aerospace applications, are comprised of electronic boards integrating various complicated electronic power switches and converters. To facilitate integrated system health management prognostics, it is necessary that the

system is monitored properly and the degradation profiles of these power electronic components are obtained. Monitoring and collection of vital signals from active components for extracting appropriate features, with a standard level of reliability, suitable for prognostics and estimating RUL, are a prerequisite for monitoring the state of the system's health.

1.2 Research Background

In the long-term vision, the ambition of health monitoring and prediction of future behaviour of power electronics become a great interest of an underlying research for an innovative new generation of the powertrain system. "Prognostics" also becomes an interesting part of an advanced health management tool to handle prediction and forecasting anomalies and failure regions which reduce system downtime. Furthermore, within the field of PHM, creating prognostics models for estimating the RUL of a system continues to consume time and require expensive resources and historical data. PHM, which is considered to be one of the most challenging disciplines in condition-based maintenance (CBM), had rarely been applied to power electronic modules and therefore is relatively immature in this field. This may be due to the fact that the development of wear and damage models that enhance more interactive reliable power electronics switches are comparatively complex to indicate the end of life. In addition, scattered intermittent faults populated in power electronic devices may not necessarily lead to failure. This becomes really difficult for developing prognostics algorithms to distinguish switch degradation from incipient faults and threats that may arise from early impending failure [1].

Current prognostics approaches for power electronics can be classified into three different methods: (1) Data-driven approach, (2) Physics of failure (PoF), (3) Fusion method or hybrid model which consists of a combination of the data-driven and PoF approaches.

The data-driven approach to prognostics is highly dependent on a sufficient amount of online measurement data which is not easy to obtain for

model training in real time in order to predict future status and remaining useful life estimation. However, the data can be obtained from experiment data to train the model [2]. PoF is an analytical model of the degradation process based on the knowledge of failure mechanisms which uses damage parameters in calculation of the RUL. Although developing physics-based models for such complex systems may not be feasible because mapping the physical structure's model parameters with prognostics features is still an ongoing challenge for designers. The hybrid model aims to fuse both the data-driven and PoF methods to compensate for the imperfections of both models [3].

1.3 Hypothesis

Enhancing power modules with system health management provides a substrate upon which power electronics designers can implement their architectures with the security of knowing that, if degradation occurs, the remaining useful life of the component/system is estimated. Additional care through self-awareness features is taken automatically to avoid the power converter from being faced with actual faults while the healthy passive devices (e.g. capacitors, inductors and resistors) keep functioning properly. Having power switches with embedded estimated degradation models allows significant health monitoring locally in each component. This will allow the industry to benefit in terms of significant maintenance cost reduction and low-carbon electricity generation.

The main novelty and aim of this project are to develop versatile prognostics for IGBTs' packaging and to investigate how signals from electrical parameters that monitor thermo-mechanical stress, can be used for failure prediction and protection as well as to modify the control strategy and reliability assessment. Feature extraction provides facilities in which just one parameter of an IGBT as a precursor provides relevant signals that can be used for detection if degradation or failure is from the die or packaging of the IGBT. The goal of this would be to exploit real-time health monitoring technology to overcome the above limits by adopting the game-changing concept of real-time prognostics for power

electronics, allowing industry to benefit in terms of significant maintenance cost reduction and low-carbon electricity generation.

Within this context, this three-year EPSRC funded PhD project on embeddable and efficient prognostics and health management of power electronics which can be derived from ageing test data and conditions. The model can be adapted to the available data set and the results help in decision-making. The dynamic of the model can be integrated into RUL calculation method which results in enhancement of the potential of failure for power electronics components "IGBTs". This, in turn, improves the prognostics capability for IGBTs module. This will contribute to the following research objectives via the methodologies described in sections 1-5:

- Light real-time prognostics development for IGBT conditional health monitoring
- Compare and contrast various prognostics health assessment
- Improve IGBT reliability
- Implementation, assessment and justification.

1.4 Research Methodology

The research methodology outlines the research goals and objectives in a structured approach as shown in Figure 1-1 through a number of scientific and technical steps. The ultimate goal in employing precursor parameters of prognostics for life extension of power modules requires us to look for parameters that can be used for prognostics of IGBTs. This has been widely addressed in much research conducted by other researchers. However, prognostics capability concepts have been rarely applied to power electronic modules because failure in power electronic modules is difficult to identify in real time. Hence, this thesis contributes a number of prognostics techniques utilising parameters that have been investigated by other researchers. This avoids repetition of previous research in the field and develops real-time condition monitoring. In this regard,

the research method presented in this thesis contributes to the evaluation of RUL using:

- Statistical techniques (e.g. Poisson distribution and Gamma distribution models),
- Artificial intelligence techniques (e.g. Time Delay Neural Network, Fuzzy Logic)
- Hybrid data-driven method
- Analytical method.

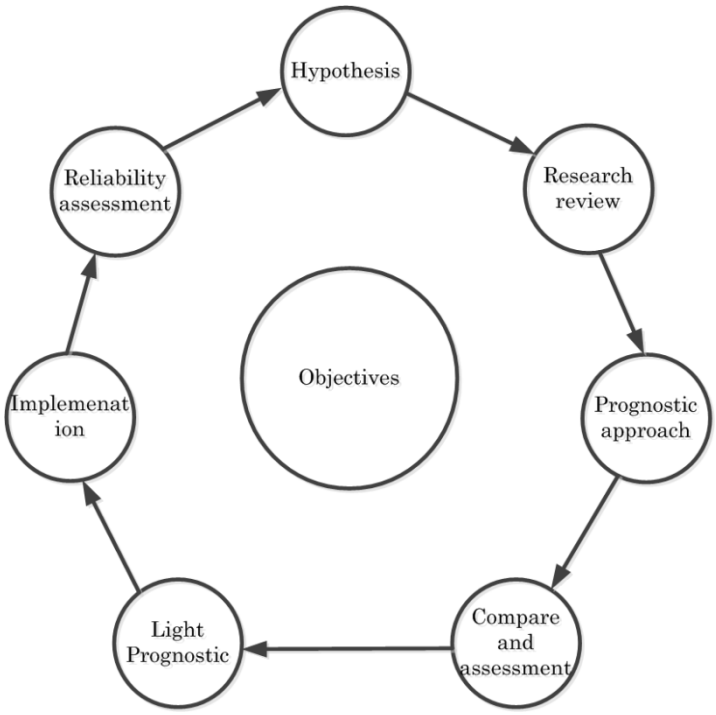

Figure 1-1 Flowchart of the research methodology

This research methodology then evaluates and assesses RUL estimation derived from each technique leading us to critique design policies/rules for formulating a light prognostics and real-time processing approach that addresses which techniques under which conditions are more suitable for a particular application. Finally, the research is followed by assessment and justification of the hypothesis. The research outcome through various comparisons highlights the benefit of using these techniques which are the improvement of the

paradigms of future power electronic reliability. The research methodology fulfils the project's contributions to the objectives through the following tasks:

- **Research review:** The current state-of-the-art of power electronics prognostics has been properly addressed in the literature. This leads us toward existing knowledge in regard to figuring out the gap of knowledge in developing robust prognostics techniques. We, however, justify if the selected precursor parameters addressed by other researchers is really right failure indication parameter within power electronics fault indicator parameters. This is conducted through a pre-processing step that involves identifying precursor parameters amongst several different parameters data set, noise filtering and classification.

- **Research collaboration** to collect reliability data from other research centres that have been active in the field, including NASA, the Power Electronics Group Centre at the University of Nottingham.

- **Prognostics modelling:** Classification of failure data use for early anomaly detection, and robust statistical failure modelling using the light embeddable Monte Carlo propagation technique to simulate remaining useful life. A hybrid model time delay neural network (TDNN) and analytical integration have been implemented to eliminate the uncertainty of failure modelling and a statistical model approach is studied. Expert knowledge incorporates with unified model-based prognostics has been developed in order to be scalable with IGBT operating condition factors.

- **RUL estimation and prognostics evaluation:** Prognostics results have been simulated and RUL estimation performance of models was evaluated using a well-known common evaluation metric method to quantify the accuracy of the prognostics results and to obtain light prognostics performance.

- **Hypothesis evaluation:** Implementing a case study of DC-DC Single-Ended Primary Inductance Converter (SEPIC) in real time that has a precursor parameter of light prognostics employed for modifying the

control strategy of a power module to extend the lifetime of the module while the lifetime itself is assessed by light prognostics.

- **Publication:** Research contribution in well-known high-impact international publications to distribute its findings to other research centres.

1.5 Research Assumptions

Although research has been already conducted to develop prognostics for IGBTs, there is still a lack of knowledge about whether precursor parameters and results derived from prognostics can be employed for modifying the control strategy of power modules. For the purpose of this radically novel research, it is impossible to find results from published research that test a similar hypothesis. Hence, we have conducted the validation steps considering the following assumption:

It is assumed that the physics-based prognostics of IGBTs can be used as a reference for prognostics evaluation. We accept this assumption because physics-based models are mainly based on the well-known Coffin-Manson law and a creep model of the material properties of IGBTs' packaging structure and junction temperature. On the other hand, other prognostics techniques are mainly based on collected data and training iterations that either needs data to be collected from a huge number of IGBT prototypes or proper training algorithms. Both the IGBT prototypes and the training algorithms are random. Physics-based models can be a precise prognostics reference as the uncertainty has less impact on the results.

1.6 Research Outcomes

The research conducted by this thesis delivers as follows:

1. Steps to approach failure model learning and a light prognostics algorithm specific to power switches.

2. Prognostics policies and rules leading us to guidelines for a suitable prognostics approach for particular power converter applications. The results have prioritised and categorised maintenance policies in different prognostics implementations, such as less computational power consumption and less complexity of implementation, improvement of the confidence boundary for decision-making, and elimination of model uncertainties.
3. Stress minimisation and improvement of power converter reliability by fusing health management parameters with the control strategy.

The scientific contributions of IGBT health management are outlined as follows:

1. Investigating dominant failure in IGBT module using an empirical failure model.
2. Develop a novel real-time data-driven prognostics model based on a statistical approach.
3. The development a robust fusion prognostics approach involves building neural network models of failure with the intuition of uncertainty and a probabilistic approach to estimate the end of life of an IGBT.
4. The development of an electro-thermal model for an IGBT module and estimating the junction temperature and feature extraction of the obtained thermal stress.
5. Introducing control stress minimisation in order to improve the lifetime of the IGBT as it is imposed to thermal stress due to the variation of the load conditions.

1.7 List of Publications

A list of publications that contributed to the IGBT prognostics literature during this research listed below:

Journal papers:

1. ***A. Alghassi***, S. Perinpanayagam, M.Samie, T. Sreenuch; "*Computationally Efficient, Real-Time, and Embeddable Prognostic Techniques for Power Electronics*", IEEE Transactions on Power Electronics 2014.

2. M. Samie, ***A. Alghassi***, S. Perinpanayagam, and et. al.; "*Developing Prognostic Models Using Duality Principles for DC-to-DC Converters*", IEEE Transactions on Power Electronics, 2014.

3. T. Sreenuch, ***A. Alghassi***, S. Perinpanayagam, and Y. Xie; "*Probabilistic Monte-Carlo Method for Modelling and Prediction of Electronics Component Life*", (IJACSA) International Journal of Advanced Computer Science and Applications, Vol. 5, No. 1, 2014, pp. 96-104.

4. M. Samie, M. S. Motlagh, ***A. Alghassi***, S. Perinpanayagam, and et. al.; "*Principle of Duality in Prognostics*", International Journal of Advanced Computer Science and Applications 01/2014.

5. ***A. Alghassi***, M. Samie, and S. Perinpanayagam, "Stochastic RUL Calculation Enhanced With TDNN-Based IGBT Failure Modeling," *Reliability, IEEE Transactions on*, vol. PP, no. 99. pp. 1–16, 2015.

6. M. Samie, M. S. Motlagh, ***A. Alghassi***, S. Perinpanayagam; " *Feasibility of Generalized Hybrid Prognostic for Impedance Source DC-DC Converter using Vector Quantization-Based Pattern Search* ", Special Issue of the IEEE Transactions on Power Electronics on Impedance Source Converter Topologies and Applications, accepted, January. 2016.

Conference Proceedings:

1. ***A. Alghassi***, S. Perinpanayagam and I. K. Jennions., "*Prognostic capability evaluation of power electronic modules in transportation electrification and*

vehicle systems", in Power Electronics and Applications (EPE), 2013 15th European Conference on, 2013, pp. 1-9.

2. ***A. Alghassi***, S. Perinpanayagam and I. K. Jennions., "*A simple state-based prognostic model for predicting remaining useful life of IGBT power module*", in Power Electronics and Applications (EPE), 2013 15th European Conference on, 2013, pp. 1-7.

3. ***A. Alghassi***, P. Soulatiantork, M. Samie, S. Perinpanayagam, M. Faifer., "*Reliability Enhanced Powertrain Using ANFIS Base Prognostics Model*", in PHM, IEEE International Conference on, 2015.

4. ***A. Alghassi***, P. Soulatiantork, M. Samie, S. Perinpanayagam, M. Faifer., "*Reliability Enhanced Powertrain Using Fuzzy Base Prognostics Model*", in Power Electronics and Applications (EPE), 2015 17th European Conference on, 2015.

5. M. Samie, ***A. Alghassi***, S. Perinpanayagam, and et. al.; "*Reliability Enhanced EV Using Pattern Recognition Techniques*", IEEE International Electric Vehicle Conference, Florence, Italy; 2014.

6. M. Samie, M. S. Motlagh, ***A. Alghassi***, S. Perinpanayagam, and et. al.; "*Realising Duality Principle for Prognostic Models*", The Ninth International Multi-Conference on Computing in the Global Information Technology, Spain; 2014. (Best Award Paper)

7. M. Samie, ***A. Alghassi***, S. Perinpanayagam., "*Unified IGBT Prognostic Using Natural Computation*", 2015 IEEE International Conference on Digital Signal Processing (DSP), Singapore; 2015.

8. ***A. Alghassi,*** P. Soulatiantork, M. Samie, S. Perinpanayagam, M. Faifer., " Fault Tolerance Enhance DC-DC Converter Lifetime Extension", Procedia CIRP Proceeding of the 5th International Conference in Through-life Engineering Services, 2016, pp, accepted, November 1-2. 2016.

9. P. Soulatiantork, ***A. Alghassi,*** M. Faifer, S. Perinpanayagam., “IGBT Thermal Stress Reduction Using Advance Control Strategy", Procedia CIRP Proceeding of the 5th International Conference in Through-life Engineering Services, 2016, pp, accepted November 1-2. 2016.

10. M. Samie, ***A. Alghassi***, I. K. Jennions., “Experiment Results of Failure Progression from Low Power Wires", Procedia CIRP Proceeding of the 5th International Conference in Through-life Engineering Services, 2016, pp, accepted November 1-2. 2016.

11. Robin. K. Sebastian, S. Perinpanayagam, ***A. Alghassi***., " Prognostic Reasoner based Adaptive Power Management System for a More Electric Aircraft", 8th Annual Conference of the Prognostics and Health Management Society 2016 (PHME 16), Denver, Colorado, USA; 2016, accepted, October 1-6. 2016.

2 Literature Review

The purpose of this chapter is to provide a literature review of the logistic capabilities of CBM includes prognostics and diagnostics. The several conventional hierarchical prognostics methods are discussed for power electronic switches (i.e. IGBT). Next, a description of various IGBT structures and IGBTs' failure mechanisms are presented. In the conclusion of this chapter, the more challenging parts of the prognostics models that cause complexity in the area of intelligent maintenance are discussed.

2.1 Prognostics and Health Management

Reliability is the definition of a product capability that can rely on its normal performance. This is initially in the design stage and is intended to perform without failure within a specific life cycle frame. Prognosis is the process of predicting the future health state of a product by realising the current degradation and expected nominal operational condition. Furthermore, calculation of a number of lifetimes left is conducted by extrapolating the performance of the product degradation process up until to the expert defined failure threshold using light versatile failure models and algorithms [4], [5]. These models and algorithms may need to integrate the sensing and interpretation of relevant recorded data for assessing and predicting the reliability of a product in its actual application environment. It is necessary to identify the failure modes and mechanisms that can take place in electrical components in the first step for employing a PHM system [6], [7]. To identify the main failure mechanisms, the precursor parameters, such as voltage, current, temperature, amongst others, have to be identified and monitored. The recorded data and interpretation of the working environment and loading conditions are then used in a PHM system to help predict the remaining lifetime. The condition

monitoring can be developed for the product using various techniques to indicate and interpret the health condition through the sensory parameters [5]:

i) Degradation parameters, such as an operating parameter, have deviated from their nominal values.
ii) Electrical degradation, such as material cracking (e. g. solder crack), and interfacial delamination cause an increase in electrical voltage and resistance.
iii) Environment life cycle variations, such as temperature, vibration, and humidity variation in ambient.

The maintenance procedure can be planned according to the information of the product's health and life cycle conditions. The new product has the advantage of health monitoring information being concurrently designed according to the appropriate life cycle environment [5]. Most of the safety critical mechanical systems and structures, such as aircraft engines and structures, propulsion systems and rotary gears and equipment, have benefited from the advanced sensory measurement platform which has contributed to online diagnostics and prognostics tools. Thus, mechanical systems are relatively known for online health monitoring with considerable useful knowledge of conditional health monitoring [8], [9].

Today, improving the reliability of power electronics devices is a key requirement for future technologies as it protects systems from various reliability issues [10], [11]. A revolutionary step is to equip power electronics with an Integrated System Health Management (ISHM) unit, which offers solutions to enhance the reliability of power conversion devices via failure prediction, detection, and mitigation techniques [12]. Prognostics and diagnostics are the key players for power electronic systems in service planning, predictability maintenance which minimise unscheduled maintenance through effective timely repair actions and result in maintenance cost reduction, minimising the down state of the equipment. Diagnostics focuses on the detection, isolation and identification of failure when they occur whilst prognosis

focuses on predicting failure before it occurs. This means that technical prognostics could be understood as an extending/complementary element of technical diagnosis. Prognosis can be referred to as the ability to predict how much time is left or RUL before a failure occurs given an observed machine condition variable and a past operational profile. The observed condition can be attributed from the physical characteristics or process performance of its failure. For instance, some condition parameters that can be used in prognostics are acoustic data, temperature, moisture, humidity, weather, voltage and current [13].

Technical prognosis, which is considered a part of PHM, is a relatively new field of research and it is still considered as the weakest point in the condition-based maintenance processing chain. There are several applications of prognostics methods but the results and accuracy vary and are not always sufficient even if researchers so claim. Although several patents have been registered and many journals and conference papers have been published, the field of technical prognosis is still quite new and not well researched. In particular, robust real system applications are still missing [14].

2.2 CBM in Power Electronics

The desire and need for efficient maintenance in advance and complex machinery become progressively vital over the last few decades. The goal for the industry is to reduce unscheduled maintenance and maximise system/component availability and functionality. Predictive maintenance has become more ambitious recently for power electronics systems and the associated challenges have been addressed. The paradigm shift of the early fault detection and protection in revolutionary electronic systems enables prognosis and health management for power electronic switches. CBM is a predictive and preventive maintenance strategy with real-time monitoring which indicates signs of upcoming failure, helps to optimise and adapt the functionality and the reliability of power conversion applications with integrated trending possibility of single or of several condition parameters. The aim of CBM is to reduce

maintenance costs by reducing unscheduled downtimes and furthermore to minimise spare part costs [15]. Having in situ intelligent condition monitoring improves efficiency and reliability and increases operating time significantly. The characterisation of the system behaviour is part of the CBM in order to be able to develop the model to indicate the current health state and predict failure. Therefore, CBM implies to be backed up by the relevant disciplines of PHM and Integrated Vehicle Health Management (IVHM).

The preliminary concept of the reliability for the power generation (e.g. wind turbines) and power conversion (e.g. AC-DC converters) are an imperative role for the IVHM maintenance framework. As a potential maintenance application, fault detection capability improves real-time condition monitoring to detect an abnormality. This also prevents catastrophic failure which is a requirement of pre-emptive maintenance and prognosis model prerequisites for planning predictive maintenance.

2.2.1 Diagnostics and Prognostics in CBM

Diagnostics and prognostics approaches are the main two aspects of the CBM [16].

- Predictive Maintenance (RCM, CBM)

Designing a prognostics capability for power electronics requires understanding the physical or electrical degradation, such as solder cracking, wire bond corrosion, packaging structure's layer delamination, and increase in electrical resistance, threshold voltage or thermal resistance, changes in a lifecycle environment, such as ambient temperature and humidity, vibration, and shock. Such information results in better model development for predictive maintenance which will be an intuitive adaptive model to determine the schedule of maintenance actions. Predictive maintenance is classified into two categories: CBM (condition-based maintenance) and RCM (reliability-centred maintenance). RCM emphasises much broader and deeper failure mechanisms (e.g. FMECA) and analysis to perform two tasks: first, to analyse and categorise

failure modes and second, to assess the degree of risk and system functionality and maintainability of the asset [17].

Diagnostics is a complementary tool for CBM which deals with fault detection and the location of the faults. This information can be helpful for providing maintenance decision-making and informative feedback for improving model-based monitoring for prognostics. It aims to detect the incipient failure and failure progression to prevent catastrophic failure. This will help to increase the time between failures for upcoming component failure which improves system availability and safety.

A prognostic gives a probabilistic forecast of the system's or component's future health based on the current health and historic condition failures before they happen [4]. It would be necessary to provide data that can be used for modelling the future health level by trending the current health level up to failure status and predicting RUL [16]. It is considered to be one of the most challenging keys and potential payoffs of CBM for enabling power electronics with advance warning, extending maintenance cycles and residual life computation. Figure 2-1 depicts the platforms of diagnostics and prognostics in CBM.

In power electronics applications, the term "Prognostics and Health Management", as shown in Figure 2-2, is manifesting current health state of the system through both conditional monitoring and data processing. Health assessment function provides feature extraction, state detection using pattern recognition and clustering which are supporting steps for the fault detection and diagnostics. Furthermore, failure model effectively to be developed for forecasting future health state and prognostics algorithm computes RUL. Finally, the decision-making unit provides scheduled maintenance actions related to the current health of the asset. All this informative health information is used in satisfactory operating conditions before the incipient failure happens in downtime which can be controlled in a fault avoidance unit.

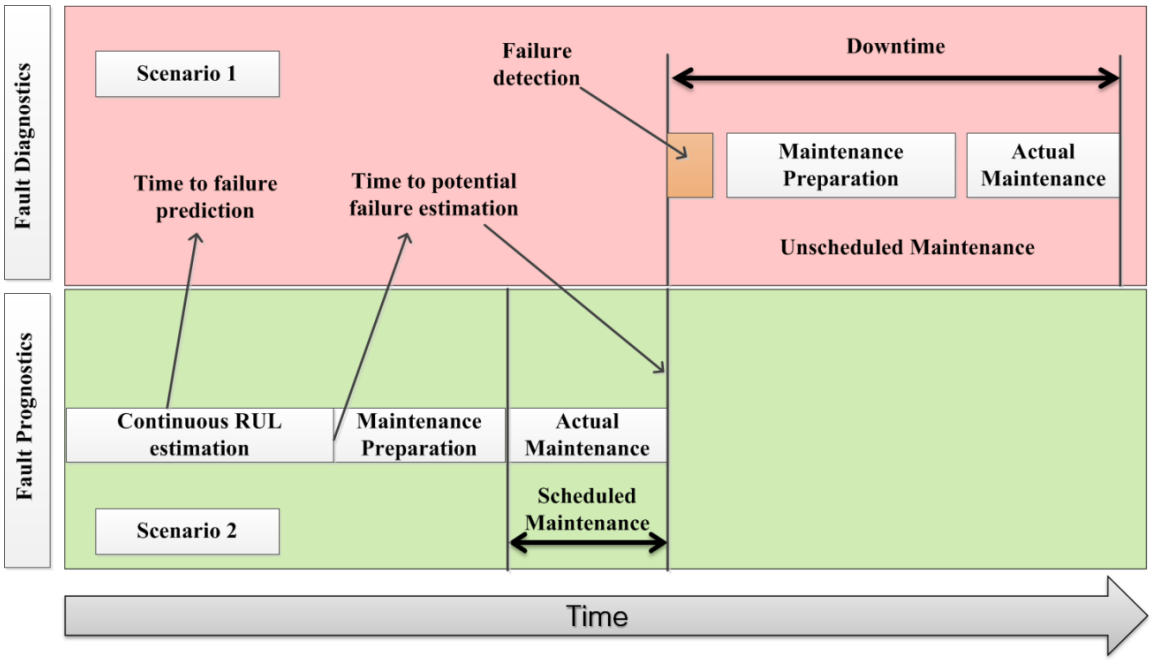

Figure 2-1 Diagnosis and prognosis in CBM

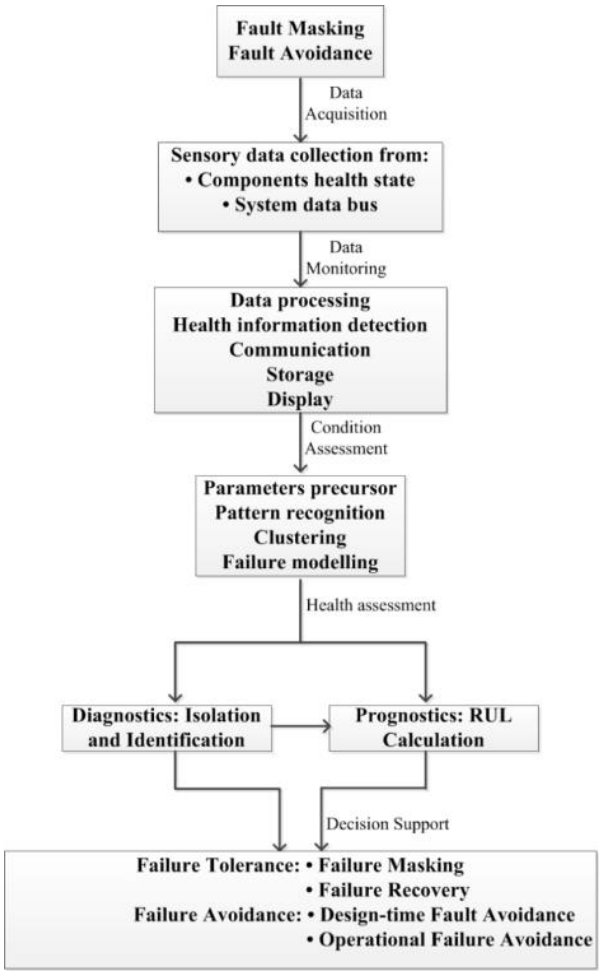

Figure 2-2 Power electronics PHM overview

2.2.2 CBM Challenges

It is noted that the prediction can basically be done based on failure rates and the operation of components under operating conditions, whereas it is generally impossible to develop the prediction model based on a single data source or one set of environmental factors. Thus, a wide variety of failure data sources from different operating conditions needs to be pre-processed in terms of populated noise and uncertainty information in order to be able to design accurate failure rate modelling. With real-time measurement for monitoring, the old components in place can be difficult to retrofit with sensors. The lack of factual data can be the main reason to competence CBM for quantifying lifecycle prediction of products. Lifecycle prediction is needed in real services to monitor MTBF and MTTF of complex systems through reliability programmes. However, there are practical evaluations of system reliability that enable customers to access the products lifetime with a tangible value. MTBF (Mean Time between Failures) is for providing time to repair in the interval where during useful life typically displays the number of hours to failure. The desired MTBF can be used as quantifiable objectives in order to avoid maintenance cost exceed replacement cost. Furthermore, MTTF (Mean Time to Failure) is the numeric value requires an intrusive programme that could introduce the indication of the product's end of life.

Essentially, there is an increasing need for failure detection technologies to provide state-of-health or early warning information which can detect abnormality at an earlier stage. It is possible to increase the time to failure or the duration of the potential of failure (POF) (see Figure 2-3). On the other hand, prognostics results can be used for optimisation of system controls to extend the overall RUL. In order to justify the usefulness of prognostics, the duration of POF must be quite long. Therefore, it is important to know which feature must be monitored to detect malfunction at an early stage. For example, if the monitored parameters persistently deviate by more than 3δ (Std) as a detection error over the flat region, this implies that there is an abnormality at this time [17].

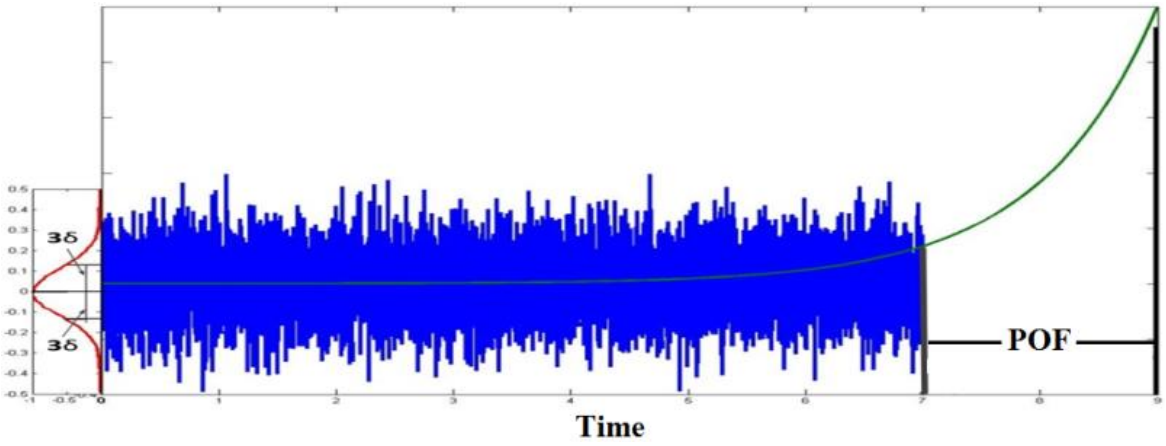

Figure 2-3 Potential of failure interval

2.3 Benefit of CBM in Power Electronics

Recent surveys of maintenance strategies in US industry indicate one-third of every dollar spent on maintenance is wasted due to inappropriate maintenance plans. The premise of diagnostics and prognostics in CBM has a significant effect on reducing unnecessary and improperly carried out maintenance and results in reducing scheduled maintenance costs and mission failure. The capabilities of the systems to prevent upcoming component failure will be included using real-time detection and estimating the health state. In addition, prognostics piece becomes the function of using in the monitoring to make predictions. Fault detection and prognostics become significantly effective parts for decision making where the safety and reliability are the paramount concern in power electronics. This will save greatly 50% maintenance cost and enable power electronics with 80% end-of-life prediction capability. CBM in power electronics strives to maximise the availability at the optimal time and MTBF of the component by identifying incipient failures before they become catastrophic failures [18]. The overall benefits of CBM have been evaluated to significantly improve the overall performance and operation of systems in highly-integrated power conversion systems.

2.4 Review of Prognostics Approaches

In condition-based maintenance, prognostics can be defined as a controlled engineering discipline that focuses on the prediction and estimation of the future course of a system or component that tries to establish when the system/component starts to slowly develop irregularities and faults to the point where it eventually malfunctions. A system or component has malfunctions mean that it can no longer operate accordingly. The predicted lifecycle of a system or component is referred to RUL. This is used in decision-making for contingency mitigation and maintenance. There are various scientific techniques used that help constructs the prognostics of a system or component, including failure mode analyses, early detection of ageing signs, and damage propagation models. Failure mechanisms are often used in conjunction with system lifecycle management to create PHM disciplines. PHM is also sometimes known as system health management (SHM). Within the field of transportation applications, it is either known as vehicle health management (VHM) or engine health management (EHM).

Four main technical approaches related to building prognostics models can be categorised into data-driven approaches, PoF approaches, knowledge-based models, and hybrid approaches.

Data-driven models (DDMs) employ and develop models based on routinely collected sensory data from operating conditions and/or past historical reliable data instead of formulating an analytical model based on the physics of failure of the system or expert knowledge of the failure propagation. DDMs strive to track the degradation of power electronics and significant failure can be predicted for the components using projection techniques (e.g. regression, machine learning, Hidden Markov Models (HMMs), and neural networks). They basically depend on the past run-to-failure data to forecast future degradation [19].

Data-driven prognostics [20] are mainly based on statistical and learning techniques from the theory of pattern recognition and machine learning

approaches that help identify and detect trends and changes in the individual phases of a system's state. A way to predict trends in nonlinear systems is by using classical data-driven methods, such as stochastic models, an autoregressive model, the bilinear model, the projection pursuit, etc. Soft computing techniques that involve using various types of neural networks (NNs) and neural fuzzy (NF) systems have also been commonly adopted to deal with data-driven forecasting of a system state [21], [22]. This prognostics approach applies to applications that have complicated system architecture, i.e. systems that incur high costs when developing an accurate prognostics model. Thus, adopting this approach to deal with complex systems will lead the prognostics of a system to be much faster and cheaper to set up as compared to other approaches. In contrast, data-driven approaches may have wider confidence intervals than other approaches which mean they will require a substantial amount of data for training purposes [23].

There are various strategies used to develop data-driven prognostics which involve the analysis of either (1) modelling cumulative damage and then extrapolating out to a damage threshold, or (2) directly learning from the data based on the remaining useful life.

As it is lengthy and rather a costly process to fail each and every system one by one, we thus seek to obtain the run-to-failure data which refers to the main fundamental setbacks, especially for new systems. In order to retrieve adequate data-driven prognostics, the accelerated ageing data should be extracted cautiously from a number of similar/related products by using appropriate measuring tools. This means that both the quality and quantity aspects of the data-driven prognostics will add to the cost, especially since the data sources may have been derived from a wide range of factors, including temperature, pressure, oil debris, currents, voltages, power, vibration and acoustic signal, spectrometric data, as well as calibration and calorimetric data. As a result, it is important to fully understand what parameters and signals will be necessary to measure, and which features will need to be extracted from the noisy and high-dimensional data [20], [21], [23].

2.4.1 Statistical Models

The degradation model structures are based on probabilistic distributions and tuned using the run-to-failure data obtained from the accelerated ageing experiments. Again, the ageing data sets are used to train the statistical model depending on what probability distributions are employed. The distribution of the statistical approach is defined by two parameters: scale, which is comparatively dependent on the proportion of time to failure and shape which is an indication of the distribution of data alongside with scale parameters [24]. The Weibull distribution, the most suitable probability function, can be used for lifetime estimation of the data analysis. The trained statistical model and testing data set are used to support the calculation of the RUL. Data-driven methods based on the statistical approach are subjected to two different approaches. The first approach is known as a direct estimation of RUL in which the direct condition monitoring (CM) preserves the damage propagation to manifest the underlying health state, and the RUL prediction is evaluated up until a predefined threshold value (e. g. solder crack, thermal resistance). In contrast, the second indirect approach initially needs to estimate a damage progression model using indirect condition-monitoring data from the system's health state (e.g. sensory information, temperature, voltage, current) and then, propagates the expected data through the model until a predefined threshold for the RUL calculation is reached. The difficulty with the second method is that obtaining a reliable failure data set is often challenging due to non-identical devices and complete knowledge of the component is often unavailable [2]. Several models covering almost all statistical approaches are categorised as direct and indirect CM for RUL estimations. The model based on direct CM data is regression-based, Wiener processes, Gamma processes and Markovian-based models. For statistical models based on indirect CM data, some of the approaches which have been included are stochastic filtering-based, covariate-based hazard and HMM and semi-Markov models (SMM).

Overall, RUL calculation is one the most challenging tasks of PHM for high, medium and low-density power electronic modules, such as IGBTs,

MOSFETS and BJTS, etc. We attempt to present a comprehensive review through a statistic-based model in RUL prediction of power electronic modules.

Sreenuch et al proposed a probabilistic Monte-Carlo framework to predict the RUL of an IGBT with TO-220 packaging. The probability distribution functions (PDF) are used to model the degradation process occuring during accelerated ageing tests. The parameter of the model is defined using Maximum Likelihood Estimation (MLE). The RUL and confidence bounds are calculated by estimating the mean, median and ±10% statistics values of the simulated degradation path, respectively [22].

Alghassi et al implemented the simple state-based prognostics (SSBP) method to estimate the RUL of the IRG4BC30K IGBT. The SSBP model is a statistical model for modelling the failure mode that evolves through a finite number of discrete states. The model implementation process involves three steps: clustering, cluster evaluation and RUL calculation [25].

Saha et al [18] implemented a particle filter algorithm for the prediction of the RUL of a punch through (PT) IGBT. The algorithm was implemented on data obtained by performing high-temperature power cycling ageing tests on a planar PT IGBT IRG4BC30KD manufactured by International Rectifier. The trend of the IGBT collector-emitter current (I_{CE}) at turn-off was fit with an exponential degradation model. A third-degree polynomial was used for the regression fit as given by the equation below.

$$I_{CE} = e^{(P_1 t^3 + P_2 t^2 + P_3 t + P_4)}$$

As the coefficients of the polynomial fit were highly correlated, only the trend of the first coefficient P_1 with time was analysed over the ageing lifespan and used for tracking among the correlation coefficient matrix. This trend was then used in the particle filter (PF) framework for remaining useful life prediction. The framework consists of extracting features from sensor data and using these features to estimate and track the system behaviour. During the state estimation and tracking step, model parameters can also be learned from

the feature data. The state estimation and tracking continue until a diagnostic trigger enable the state prediction and RUL estimation steps.

This thesis proposes a new data-driven approach for power electronics components (e.g. IGBTs) which addresses issues in previous IGBT prognostics.

In [14], Celaya et al proposed an empirical degradation model based on the increase in the observed drain to source on-state resistance ΔRDS(ON) as the degradation process for six aged devices for a power MOSFET IRF520Npbf in a TO-220 package. This condition-monitoring parameter represents the failure process due to die-attached failure mechanisms as the only active degradation during the ageing process. The exponential model is formed as a first-order linear discrete model for using Bayesian tracking algorithms like an extended Kalman filter (eKF) for on-line RUL estimation calculation at time tp.

In [26], Patil et al introduced a prognostics framework for non-punch through and field stop IGBTs (NPT IGBTs) which includes the Mahalanobis distance (MD) as the diagnostic parameter. The MD was evaluated using healthy baseline data and transformed into a normal distribution for anomaly detection. The PF is performed for future health prediction of the component using the $V_{CE\,(ON)}$ as a precursor parameter. This parameter indicates the health state of the die attached and wire bonds through changes in thermal resistance which effectively causes to increase in the $V_{CE\,(ON)}$. The first step in this approach is to propagate a number of particles through the probabilistic laws to estimate the initial state. In this approach, a multi-model distribution can be presented for the evolution of the system health state. The second step is to estimate the next state based on the previously updated system state as the posterior pdf. The system state is presented by the set of associated particles which characterise the prior and posterior distribution, and also set of associated weight denoting Markov probability of the discrete state.

Azarian et al proposed a PF approach predicting RUL of IGBTs in wind turbine applications. In this approach, the second-order least squares regression has been driven based on $V_{CE\,(ON)}$ measurement from power cycling ageing

experiments to present the behaviour of the component failure. The RUL calculation is triggered when failure threshold value reaches 20% rise in the $V_{CE(ON)}$. In this research, they claim the ageing process for run-to-failure data collection lasts for 21.4 minutes and the result of RUL estimation at the measurement time detection of 11.8 minutes shows 20.8 minutes with an accuracy of 2.6% prediction error. The mean time RUL prediction was simulated with boundary levels and was presented with the Gaussian probability distribution of the particles at the end of life estimation [27].

Celaya in [28] has used the Gaussian Process Regression (GPR) technique for lifetime prediction of power MOSFETs based on on-state resistance degradation due to thermal and power cycling accelerated ageing tests. The monitoring parameter was computed as the ratio voltage and current across the drain and source of the device. The raw data was filtered by taking the mean of the data reading over one minute's duration window length. The RUL prediction is described by a mean function and used as an output parameter and the dynamic behaviour of the system incorporates with uncertainty. The covariance function is designated to compute the response of uncertainty.

Alghassi et al presented a light-weight statistical prognostics approach as an alternative to the EKF and PF. In this approach, the model is constructed based on the probability of failure for 9 different discrete phases from the decomposed historical run-to-failure data of $V_{CE(ON)}$. The probability model is formed utilising the duration of the failure phase as a versatile feature in order to aid the model propagation, with lifetime estimation effectively requiring only 0.3ms computing time for each measurement [17].

2.4.1.1 Artificial Neural Network (ANN)-Based Model

ANN is a data-processing has been acquired in black box tool which is attracted to prognostics field. This can be used in a modelling system which conventional models including complex nonlinear physical model are not either analytically exist or practically difficult for modelling. This model consists of

three layers: input layer, hidden layer and output layer. All layers are in interaction with different neurones, inspired by the human brain neurone structure, the so-called synapses, and connected with associated numerical weights. ANN is formed in mapping inputs to outputs through training a network of between set of n-dimensional real input and output. ANN is usually used in pattern recognition due to the ability of a having synthesised process via numeric information from multiple channels. In prognostics, ANN is well-known machine learning used to model a trend of non-linear failure objects by classifying the training data. However, the number of hidden layers and the number of participated nodes become a complicated issue in the training process as the feedback connection requires for learning the dynamic of the model. Also, two types of training methodologies are mainly defined thus far in the ANN machine-learning technique, namely supervised and unsupervised training. In supervised training, the network is trained from the input/output data set from direct health indicators or indirect sensory data to adapt to the changes of data and this requires a large set of training data. In contrast, unsupervised learning is widely used in clustering analysis and pattern mining for finding hidden clusters in unlabelled data by using primary functions of networks. The self-organising map is one the most widely-used architectures for unsupervised learning algorithms. Zhang and Ganesan have used the technique for developing multivariable fault indices for monitoring rotating machinery [29]. Eker et al used an unsupervised learning algorithm (e.g. k-means clustering) for evaluating the health state indices of railway turnout [30]. Several types of neural networks are considered in supervised model prediction, such as a feed-forward neural network (FFNN), recurrent neural network (RNN), time-delay neural network (TDNN) and dynamic wavelet neural network (DWNN). FFNN is constructed from multiple series of layers where the first layer is connected to the input and each subsequent layer consists of a number of neurones which perform the summation of the weights from the previous layer. The network output is formed by the summation of the output of the hidden layer's weight which can be called the output layer [31]. Byington et al used FFNN to obtain model prediction of the control valve position in the electro-hydraulic servo valve from the F/A-18

stabiliser actuator which has used the principle of electric current signature analysis in tracking the degradation of the actuator, and a KF was taken apart to calculate the RUL of the actuator [32]. RNN was proposed in the 1980s for modelling time series and is formed of multi-layer perception with distinction allowing a hidden unit to retain information from previous calculations as it has a "memory" which is a model capable of complex sequence prediction [33]. Yam et al successfully applied the RNN approach for prediction of nonlinear time-based trends for critical equipment of power plants in order to avoid loss of parts before reaching major maintenance [34]. Yu et al presented a type of RNN, known as the Elman recurrent neural network (ERNN), which has shown the potential of promising the prediction of feature signature reading from a boring process sensor with 95% confidence levels [35]. TDNN is proposed and developed by Waibel in the 1980s and is inspired from neurobiology where the time delay occurs in axons due to different conduction times and the length of the axon fibres [36]. TDNN is typically similar to FFNN; however, the input signals are augmented by introducing time delay varying activation on the inputs and propagates through in a similar way to feed-forward fashion connection. This network architecture is used to model the dynamic of the set of input properties, and also identifies the behaviour of the series inputs [37].

Alghassi et al used TDNN for the development of failure modes for IGBTs, and a statistical approach was fused to model for RUL estimation.

DWNN can act as a real-time prognostics tool which can be trained in a time-dependent way by either using the gradient descent technique or the generic algorithm for prediction and classification issues. The sensory data is recorded with time information for training the DWNN in a dynamic fashion, also enabling the model to update the component's remaining life distribution [38]. Gebraeel et al used a feed-forward and back-propagation neural network to model bearing degradation signals and update the failure time with sensory information to compute the RUL for the components based on the DWNN approach [39].

Oukaour et al [40] developed an approach to distinguish defective IGBTs from healthy IGBTs. In this study, power cycling tests were performed on IGBT modules by subjecting them to a cyclic DC collector-emitter current ICE of 20A with 30 seconds power on and 20 seconds power off. Four parameters, namely the collector-to-emitter on-state voltage VCE, the case temperature Tc, the junction temperature Tj and the junction-to-case thermal resistance $R_{th\text{-}jc}$, were monitored during the tests. The healthy IGBT state was established by applying small DC currents to the IGBT from 200mA to 16A by steps of 200 mA with 30 seconds power on and 1-second power off. The $V_{CE\ (sat)}$ and Tj measurements were performed during this test. After determining the healthy IGBT state, the device was power cycled to failure. The $V_{CE\ (sat)}$ and Tj were monitored during the ageing tests. A neural network based classifier scheme was implemented to determine a boundary that could be used to identify defective IGBTs, as shown in Figure 2-4 [40].

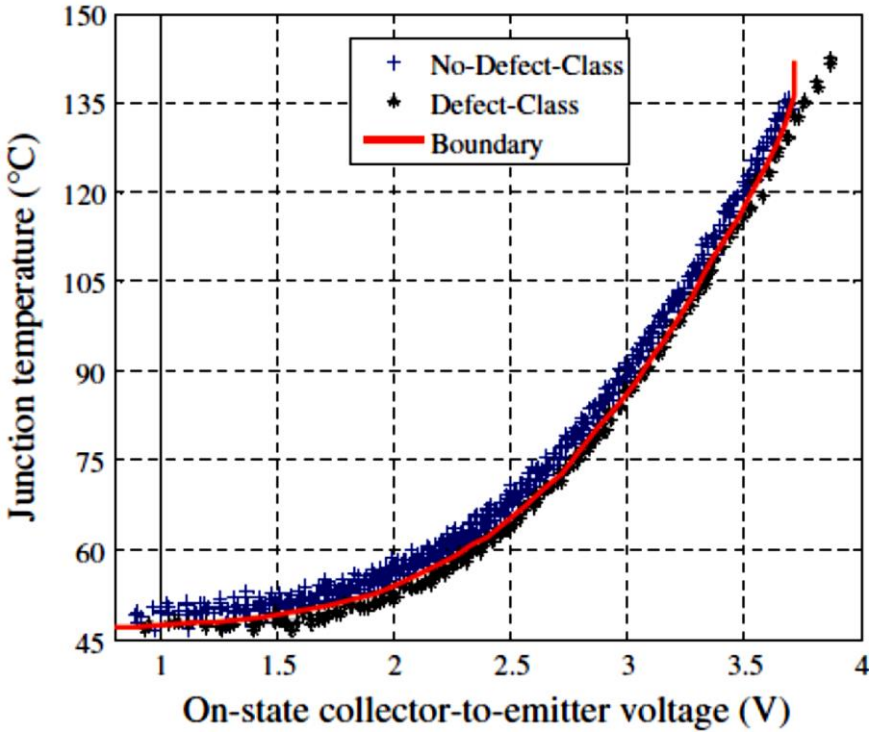

Figure 2-4 Boundary to distinguish defective IGBTs from healthy IGBTs

2.4.2 Knowledge-Based Models

In contrast to the data-driven and physics-of-failure approaches which require large samples of real reliable run-to-failure data of systems and accurate mathematical models for physical systems, respectively, knowledge-based models (KBA) utilise graphical models, such as Bayesian networks and rule-based reasoning, and this requires an implicit reasoning technique, such as ANN, to observe previous failure history from the data repository assess the health state of the system. This model becomes more promising as there is no need for a complex model, an expert system and fuzzy logic that are typically employed in this application [41]. Expert systems have long been used in diagnostics tools, and are currently becoming a more interesting subject for implementation in the prognostics field. Expert systems integrate human knowledge from previous experience with explicit reasoning techniques, such as rule-based techniques (e.g. IF-THEN), to allow system software language to realise the lifetime of the system [42]. This can be more problematic when an increase in the number of inputs requires a consistent combination rule to address the desired output [43]. As the system condition is upgraded or reconfigured, the knowledge base also needs to be updated during the process. A rule-based technique also needs to be prepared to address the domain knowledge of the failure phenomena in different conditions. Fuzzy logic can provide a robust rule to examine the sequence of failure mechanisms by configuring the membership function to map numerical values of the degradation feature. In expert systems, the logic covers the true and false statement, and this can be considered to be a major defect of the approach in that some important data will be effectively excluded, making it difficult to define a precise membership function [44]. A fuzzy system is an effective way of overcoming the above deficiencies by applying the algorithm to both the knowledge base and the fuzzy rule base. The data received from sources will be pre-processed and converted to a fuzzy form to be compared with a set of fuzzy rules. A few rules are selected and manually developed which represent the number of possible input and output combinations. This process, known as fuzzification, is about to define the membership function which finds the mapping between input data and particular fuzzy variables. The next step is

about defuzzify the resulting data into numeric output values. The extensive use of fuzzy systems has contributed significantly to control systems with the physical device's current state, and output of the controller to control the system behaviour. Thus, this process also can be used in prognostics models [45].

Feng et al proposed a new fuzzy expert system in real-time condition monitoring of a chemical pulp mill. In this expert system approach, the reasoning inference engine of the fuzzy system is driven by the dynamic fuzzy rules. Thus, the rule is time-dependent and detects the change in the dynamic membership function of input/output and is fired due to changes in working conditions [42].

Chinnam et al presented a neuro-fuzzy approach for performing online RUL estimation of a physical system under degradation conditions. The method was implemented for measuring online data from thrust force and torque acting on the drill bit for a drilling operation. A Sugeno fuzzy inference model (FIM) is used to address the potential of failure by extracting strong experiential knowledge of the degradation signal. The model considers predominately the torque degradation profile in reliability assessment. The model was trained by 8 samples from drill bits and 2 samples from network testing for estimating online reliability [45].

Alghassi et al proposed a prognostics capability algorithm for active power electronics devices (IGBTs) based on an adaptive neuro-fuzzy inference system (ANFIS) failure model. In this approach, 4 samples of the run to the failure of two parameters, namely measurement junction temperature (T_j) and $V_{CE\,(ON),}$ and the dynamic of inputs variable are used to train fuzzy Sugeno model (FSM) reasoning to map the dynamic membership function of the output to input. The failure data was collected from emulated failure mechanisms of solder fatigue degradation in IGBT simulation modelling. The prognostics results were evaluated with the root mean squared error (RMSE) against the probabilistic model, and results have shown significant improvement compared to the ANFIS model approach [46].

2.4.3 Model-Based Approach

Model definition, as the first step for model-based prognostics, requires understanding the failure mechanisms of the system enhanced with PoF models and this is often a difficult task because establishing an accurate physical model is difficult to achieve. The aim is to integrate a physical model of the system to estimate the RUL which can be achieved using either through micro or macro levels. The model is driven as such is known for model-based prognostics [47], [48], [49].

In contrast to physical expressions used in micro-levels (also recognised as a material level) which is the integration of the damage propagation with relevant series of model dynamic equations, macro-level models use mathematical frameworks at a system level to make sense of relations among system input, system state, and system variables. The mathematical model often builds in simplified converged form but this may decrease the accuracy of the failure model. This model also suffers from a lack of expert knowledge in developing robust mathematical models which may add uncertainties and accordingly increase inaccuracy in the developed model [12], [50], [23].

In power electronics, PoF is an approach that employs knowledge of power electronic modules' life-cycle loading and failure mechanisms to perform reliability modelling, design, and assessment. The approach is based on the identification of potential failure modes, failure mechanisms, and failure sites for the power electronic module at a particular life cycle loading condition. The stress at each failure site is obtained as a function of both the loading conditions and the geometry and material properties of the power electronic module [51]. The second method is the PoF for lifetime prediction based on Coffin-Manson models, Norris-Landzberg models, or Bayerer's models [52]. The lifetime expectancy (in numbers of cycles) of an IGBT is experimentally obtained from the given environmental and load condition [53]. The cumulative fatigue (or damage) of an IGBT is calculated based on stress amplitude at each individual stress level and also from various actual operational conditions. Furthermore, RUL can be then expressed when incremented damage reaches a critical

threshold. Thereafter, the number of cycles to failure is used to estimate the life usage of the device [54].

The PoF method has been employed for estimating life usage of the wear out mechanisms of the materials in power electronics packaging modules. It can be noticed that the early fault detection and estimation of the current degradation level are often difficult [55].

Gu et al developed a PoF model for the RUL estimation of the printed circuit boards (PCBs) under vibration load for electronics application. The finite element analysis is developed to calibrate the analytical model to calculate the strain stress at the solder interconnection using sensory data indicating solder joint vibration fatigue of critical components under certain vibration loading. The time to failure obtained using a cumulative damage model incorporates the extracted cycle-counting algorithm for the solder strain and validated based on the resistance in-situ measurement [56].

Musallam et al [13], [57], [58] have developed an integrated real-time electro-thermal model to estimate the junction temperature of an IGBT module. The estimation has been carried out for different layers of the structure of the active device package which is difficult to access for real-time measurement. A rain-flow algorithm was employed to extract features from the temperature profile vs. time data, such as the number of cycles for different ranges of thermal cycling. The obtained knowledge enhances the Coffin-Manson model to estimate the end-of-life of the IGBT bond wire interconnects and the substrate solder joints under nominal operating conditions using the Palmgren-Miner accumulated damage rule.

Kovacevic et al developed a comprehensive the energy-based lifetime model for a power electronic module based on the physical behaviour phenomena of the solder interconnections. The proposed model is based on Clech's algorithm, which unlike the Coffin-Manson model, explains the properties of the junction temperature, i.e. frequency, dwell-ramp time, minimum/maximum temperature [52].

Yin et al proposed a PoF-based prognostics approach for power electronic modules. The reliability assessment was carried out in real time under thermal cycles with different temperature swings. A linear thermo-mechanical model of the solder interconnect was formulated using the information of plastic strains under different load conditions to estimate the lifetime of the module [59].

Huang and Mawby developed a prognosis method for an inverter based on the physical IGBT and freewheeling diode. The Coffin-Manson equation is constructed based on the modified accumulated creep strain based model for only one failure mode, die-attached solder fatigue. The rain-flow counting method incorporating the damaged accumulated after one temperature profile was conducted to calculate the estimated lifetime using Miner's rule [60].

Ji et al presented a precursor parameter in-situ monitoring methodology to diagnose the health of wire bond interconnection degradation in IGBTs and estimation lifetime of the device. Furthermore, the forward voltage bias V_{CE} and V_F are selected and indicated wire lift-off and integrated into the power drive for the IGBT and diode, respectively, with both parameters dependent on the high current and die junction temperature [61].

Xiong et al [7] proposed a real-time diagnosis and prognosis tool to forecast the critical failure region of an IGBT power module applicable in the automotive industry. In this study, power cycling tests were performed on Toshiba 600V/800A IGBT modules for approximately 10,000 hours. The stressing was performed by the application of repeated cycles of a 400A current pulse (1 second), followed by a 20A current pulse (0.5 seconds) and a dwell period (8.5 seconds). During the test, the collector-emitter voltage at saturation $V_{CE\,(sat)}$ was monitored continuously. A sudden drop of the $V_{CE\,(sat)}$ followed by a rise was observed. The authors suspected an initial solder joint degradation before wire-bond failure eventually caused the failure of the power module.

Based on the test results, the authors proposed a quasi-real-time IGBT failure model prognosis. The prognostics approach of the authors consisted of a prognostics check-up routine that would be implemented at a pre-set frequency

and current during vehicle turn-on and turn-off. During the check-up, the $V_{CE\ (sat)}$ of the IGBT module would be compared with a look-up table of healthy data. Any variation of the $V_{CE\ (sat)}$ over 15% would signal an alarm. Although the authors reported this approach as a prognostics approach, the remaining useful life of IGBTs was not reported [62].

Ginart et al [63] performed a study of IGBTs to develop an online ringing characterization method to detect early IGBT faults in power drives. The authors proposed the analysis of ringing characteristics of current and voltage transitions during switching as a feature for the evaluation of IGBT ageing. In this study, IGBTs were aged by exposing the active device to more heat generated from the junction temperature and switching it on and off until device latch-up occurred. A few times after latching occurred, the transistors were turned off. After the transistors recovered, they have aged again in a similar manner. The transistors latched after recovery but at a lower temperature and for a shorter ageing duration in comparison to the previous ageing. The transistors were evaluated using a custom ringing platform. It was observed that transistors that had latched multiple times had more damped voltage responses to an input gate pulse. The damped responses observed are shown in Figure 2-5.

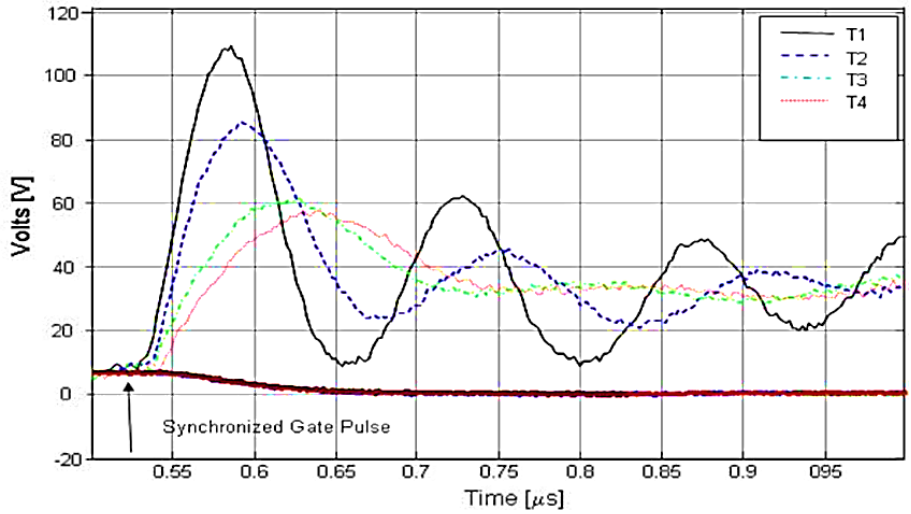

Figure 2-5 Changes in the ringing characteristic of the new (i.e. T1) and aged (T2, T3, and T4) IGBTs [63]

The authors speculated that the damped response was due to defects in the gate oxide which increased the channel resistance and hence, the damping in the power drive system. Hot-carrier injection and time-dependent dielectric breakdown were suggested as possible failure mechanisms in operation that could have resulted in the observed damped response [63].

Lu et al [64] analysed an IGBT power electronic module for railway applications. Based on a reliability analysis, the lifetime of the module was determined to be limited to the lifetime of the wire bond, bus bar, chip and substrate solder interconnects. The authors estimated the lifetime of the power module based on a strain-based model for each of the solder interconnects. In this study, no comparison of the predicted lifetime was made with experimental results.

Patil et al [14], [65], [66] developed a fusion prognostics framework for an IGBT module. The approach has used a failure mode, mechanism, and effect analysis (FMMEA) to identify failure mechanisms in order to enable parameters to monitor degradation and fault isolation and trending, furthermore, prognostics is developed to be capable of addressing critical failure mechanisms and relevant physics-of-failure models for RUL calculation.

2.4.4 Prognostics Cells

Prognostics cells are devices which have the same failure modes and mechanisms as the real power electronics devices but their failure modes occur much sooner. They are embedded in the actual product and are monitored. With regard to the failure time of the real power semiconductor module, the lifetime of prognostics cells is pre-calibrated [67]. Therefore, prognostics cells will produce an early warning of failure and their failure time can be employed to predict the remaining life of the power electronic modules. In the power semiconductor, where the common failure modes, such as the hot carrier damage, metal migration, are far worse at geometries below 0.25 μm, prognostics cells have been employed for prediction of semiconductor reliability. Prognostics cells are a

suitable way of providing an early warning of a system failure when it is impossible to embed sensors in the failure site in power electronic modules. Prognostics cells are used for wear out failure prediction in power semiconductors [13].

Goodman et al [68] described the benefit of the canary method to fail before catastrophic failure for the benefit of integrated circuit protection. The method also calls prognostics cells mounted down on the chip or circuit calibrated with respect to the time of circuit's actual failure. The failure mode is expected to be the same for both prognostic cells and main circuit, and meant to provide early warning of failure in all service operating conditions prior to the circuit board meets failure. The canary prognostics design has the capability of foreseeing failure in the same environment as the actual chip but at the relatively accelerated rate. These cells were developed for example (i.e. 0.35, 0.25, and 0.18 micron) in complementary metal oxide semiconductors (CMOS) to predict failure as a result of time-dependent dielectric breakdown (TDDB), hot carrier injection (HCI), and negative bias temperature instability (NBTI).

2.4.5 Hybrid Prognostics Model

Initially, hybrid approaches intended to bring together the strengths of the data-driven and model-based approaches integrates them in one prognostics algorithm. This can be done in 1) pre-processing data-mining and 2) post-processing for prognostics model learning. The first approach is about feature extraction and classification techniques for run-to-failure data sets. The second technique is applied for eliminating uncertainties which occur during model learning. In general, this will narrow down the ambiguities of the prognostics model as a result of the uncertainty interval of each individual prognostics model [69], [70].

A hybrid model involves with failure mode analysis, component failure parameters, pattern recognition of the parameters of the components, and data driven for machine learning. This is a versatile technique in prognostics and

provides more accurate diagnostics (e.g. anomaly detection and parameter isolation) and overcomes the drawbacks of data-driven and physics of failure models but it is a relatively new area in prognostics and considered to be promising and cost-effective. Liao and Kotting [71] reviewed the development of the hybrid prognostics method that has employed the advantages of various types of prognostics capability. They categorised the hybrid approach with the combination of three main types of prognostics: data-driven models, knowledge-based models and physics-of-failure based models as follows:

The H1 type approach leverages the underlining expert knowledge domain of the system health state and converts them in appropriate membership functions which then integrates with data-driven models for the system's RUL estimation.

In the H2 category, knowledge-based models can be used for diagnostic tools which are enhanced with physics-of-failure models to estimate future failure propagation.

Samie et al developed a novel prognostics model using mathematical modelling of physical systems, and also graph and duality theories of the subsystem's topology for a single phase DC-to-DC Cuk converter and its dual version (D-Cuk). The degradation profile has induced to both Cuk and its dual circuit as a time series data, signals such as input/output voltage and current are measured accordingly. The input/output impedances and admittances are calculated to implicate system transfer function with a number of time-dependent Tee and Pi models. The damage model fuses with energy relaxation (tr) from the Cuk converter, Δtr, attenuation, and the current of load (from D-Cuk) are used by a fuzzy RUL estimator to estimate the remaining useful life of the Cuk's dual circuit [72].

The H3 type hybrid model includes two different types of data-driven approaches, wherein in the absence of direct measurement of the failure growth, one can be used as an estimation of the internal system's health to extrapolate

the future health state. The results are enhanced with another data-driven approach to generate RUL predictions.

Alghassi et al developed a novel prognostics model for a power electronics active device (IGBT). The power cycling ageing dataset has been used for the development of failure modelling based on the TDNN approach. In addition, health state classification incorporates with probabilistic Monte Caro RUL calculation to significantly reduce the uncertainty occurring from an incomplete failure model. Thus, the technique enables effective health state indication plus improves the accuracy of the RUL calculation [73].

Hybrid prognostics under the category H4 is intuitive to leverage the advantage of both data-driven and physics-of-failure models to strengthen RUL prediction.

Pecht et al [4] developed A fusion prognostics method for estimating the RUL of electronics systems. The fusion method is a combination of data-driven and physics-of-failure methods. It benefits from the merits of both methods while eliminating some of their drawbacks. In this method, the anomalies exhibited in the monitored data are detected by data-driven methods and the remaining useful life prediction can be conducted by a combination of data-driven and physics-of-failure methods when the anomalies are detected or at any time when remaining useful life prediction is needed by users [65].The fusion prognostics method for remaining useful life prediction is shown in Figure 2-6. The fusion prognostics method can be implemented as the following steps [65].

As is obvious in Figure 2-6, the precursor parameters and the load of the power converter are measured. Then, the total power dissipation of the power electronic module is calculated and then based on this and a compact electro - thermal model of the power electronic module, the temperature of various parts of the power electronic module are estimated. At the same time, precursor parameters of the power electronic module are monitored and compared with a healthy behaviour baseline. If anomalies are detected, a counting algorithm is run and operates automatically on the temperature-time data and identifies the

full and half cycles of the temperature profile. Lifetime models for various failure mechanisms of the power electronic module are then integrated with the output of the counting algorithm to estimate the life consumption of the power electronic module [65].

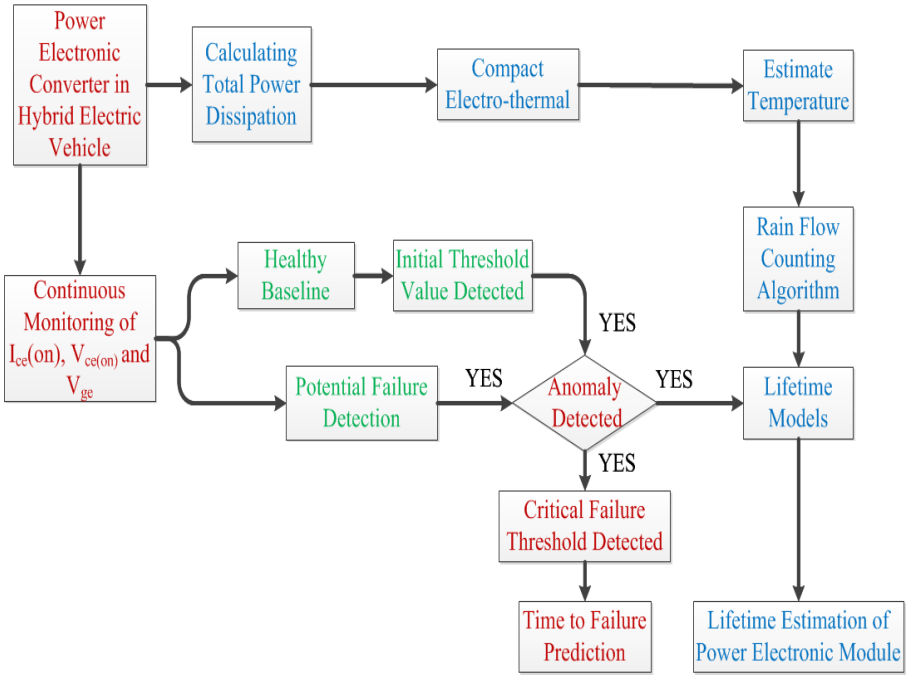

Figure 2-6 The hybrid method of category H4 proposed in prognostic lifetime of power module

The advantages and disadvantages of prognostics approaches are summarised in Table 2-1 [74].

Table 2-1 Benefits and Drawbacks of Prognostics Models

	Advantages	Disadvantages
Physics-Based Models	**-Prediction results depend on fidelity model.** **-Does not depend on historical data.** **-Just calibration may be needed to adjust the model for different conditions.** **-Provide a root cause analysis and maintenance decision.**	**-Difficult to obtain underlying physical failure processes.** **-Computationally expensive to run the high-fidelity model in the real-time process.** **-Difficult to determine intermittent faults.** **-If the component is redesigned, it would be necessary to repeat the extended process of evolving the model.**
Data-Driven Models	**-Can be applied to complex systems.**	**-Lack of identification of failure mechanisms.** **-Require large amounts of data (e.g. historical data**

	-Easy to be implemented. -The more data is available; the more physical behaviour can be gained. -Suitable for diagnostics. -More robust and adjustable in optimisation performance.	for training), increased complexity in computation. -Deal with sources of uncertainty (e.g. process noise, measurement noise) presents inefficiently uncertainty in long-term monitoring.
Prognostics Cells	-No need to sense data. -Possibly a low-cost option.	-Need to pre-calibrate with product lifetime. -Replacement cells need to be recalibrated with the aged condition of the product.
Precursor Monitoring	-Indicates relatively direct failure progression. -Easy to characterise changes with failure. -Easy to be implemented.	-Relatively time-consuming and costly. -Difficult to characterise for a large number of usage profiles.
Hybrid Prognostics Models	-Provide detailed knowledge of the failure mode and effect analysis. -Determine the failure mechanisms for root cause analysis. -Determine parameters for in-situ monitoring. -Detect intermittent failure. -Identifying all sources of uncertainties lie within the prediction results.	-Need both accurate and noiseless data. -An inaccurate model or noisy data may bias each other, and accordingly, alleviates disadvantages.

2.5 Insulated Gate Bipolar Transistor (IGBT)

IGBTs are well-known active power transistor devices which are widely used in highly-effective modern appliances, such as power conversion, in the renewable energy sector, electrified railway traction, more electric aircraft (e. g. Boeing 787) and electric cars. This device is the gate drive voltage control using the characteristics of a field effect transistor (FET) that insulates the gate from high power density capability which allows the device to have high current density with the low voltage saturation capability of the output performance of the conventional bipolar power transistor [75]. It has also the advantage not to latch during a short circuit.

The IGBT was first experimentally demonstrated by Baliga in 1979 [76]. Plummer and Scharf in 1980 also experimentally demonstrated the IGBT and provided a quantitative analysis and models for the device [77], [78]. Becke and Wheatley filed what is considered the seminal patent on IGBTs in 1980 which was subsequently awarded in 1982 [79]. The first IGBT devices were commercially available from General Electric in 1983. Currently, IGBTs are widely used in medium-frequency (20-200 KHz) and medium-power (10KW-1MW) applications, such as switch-mode power supplies (SMPS), AC motor drives, uninterrupted power supply (UPS) and inductive heating. High voltage and high current IGBTs (6500V, 200-400A) are used in electric traction applications for locomotives and streetcars [79]. Companies that manufacture IGBTs include Toshiba, Infineon, Microsemi, ON semiconductor, International Rectifier, IXYS, Hitachi, Fuji Electric, Fairchild Semiconductor, Dynex, Powerex and Siemens.

The vertical cross-section of an IGBT structure in Figure 2-7 illustrates the three terminal configurations of the device layout where the collector forms the bottom node of the device under the additional punch through a p+ layer which enables fast switching turn off by injecting holes into the drift region to neutralise the leftover electrons. This leads to lower on state resistance. The emitter region occupies a similar region of the source for a metal oxide semiconductor field effect transistor (MOSFET) at the vicinity of the gate region [79].

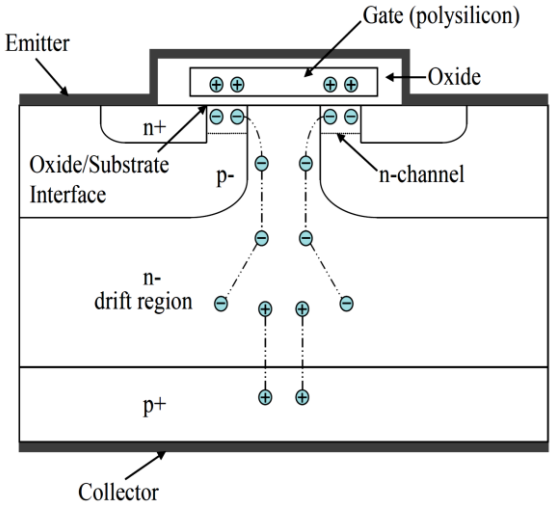

Figure2-7 Schematic of n-channel IGBT operation [79]

As mentioned above, an IGBT is a voltage control and by just applying small positive voltage on the gate to maintain the switch in conduction mode with a unidirectional current. Basically, the positive carries from the injected p+ layer into the drift region allows the current flow through the collector to the emitter. In addition, the switching speed of the device can be simply improved by adding an extra n+ layer as the buffer right above the p+ layer to evacuate the remaining charge in the drift region.

IGBTs are classified based on the orientation of the gate as planar or trench. In planar structures, the gate is parallel to the collector. In trench IGBTs, the gate is vertical to the collector terminal. In the planar IGBT, electrons flow through a horizontal channel and then downwards to the collector. This current path leads to higher losses during conduction. The trench IGBT, on the other hand, has a single direction of current flow, from the emitter, through the vertical channel down to the collector. This path lowers the conduction loss of the trench IGBT, and minimises the use of silicon, allowing for the reduced size of the trench IGBT for a given voltage rating in comparison to the planar IGBT [79].

IGBTs are further classified as punch-through (PT), non-punch-through (NPT) and field stop (FS), as shown in Figure 2-8. The punch-through IGBT is manufactured using an expensive epitaxial process. The electric field punches through and terminates in the p+ layer (buffer layer). The non-punch-through IGBT is manufactured using a less expensive float zone silicon process. In this device, the electric field terminates in the drift region. For a given voltage rating, the NPT IGBT is smaller than a PT IGBT. The field stops IGBT is manufactured using the inexpensive float zone process and has a buffer layer that is used to terminate the electric field. It is the smallest for a given voltage rating among the three technologies [79].

The conduction loss is a function of the on-state collector-emitter voltage $V_{CE\ (ON)}$. The $V_{CE\ (ON)}$ is a function of the n-drift region thickness. From Figure 2-8, it is obvious that the punch-through and field stop IGBTs have thinner drift

regions in comparison to the non-punch-though IGBT. Therefore, the punch-through and the field stop IGBTs have lower conduction loss in comparison to the NPT IGBT. However, the NPT IGBT can sustain large currents, such as in short circuit events, due to the thicker n-drift region [79].

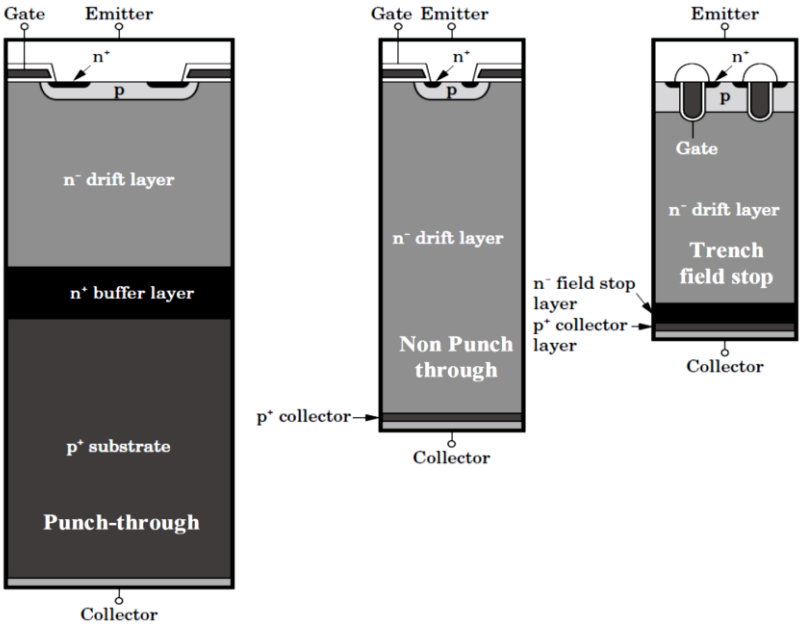

Figure 2-8 Overview of IGBT technologies

The switch-off losses in IGBTs are based on the time required for the holes in the drift region to recombine with electrons and be swept out of the device through the collector. The punch-through IGBT uses the heavy-hole injection to reduce conductivity losses. These excessive holes lead to high switching losses for punch-through IGBTs in comparison to the NPT IGBT and field stop transistors [79].

Trench IGBTs, due to their vertical gate structure, have lower $V_{CE\ (ON)}$. Hence, trench IGBTs have lower conduction losses in comparison to planar IGBTs. A modification of the trench IGBT to include a field stop buffer layer leads to a reduction in switching losses as well. The trench IGBT configuration in comparison with the planar structures is shown in Figure 2-8 [79].

Overall, an IGBT is a power electronic switching device gaining popularity because of:

- The high input impedance
- The high current carrying capacity
- High switching speed
- Low switching losses.

In power electronics converters, power semiconductor switches, such as IGBTs, MOSFETs, diodes, capacitors and inductors are mainly used to convert input quantity values of the electricity supply into load demand quantity values by using the switching configuration. All quantity values such as voltage and current amplitudes, voltage and current frequency generate a number of input and output phase and phase delays. Power electronics converters have implemented in different power conversion demands as shown in Figure 2-9.

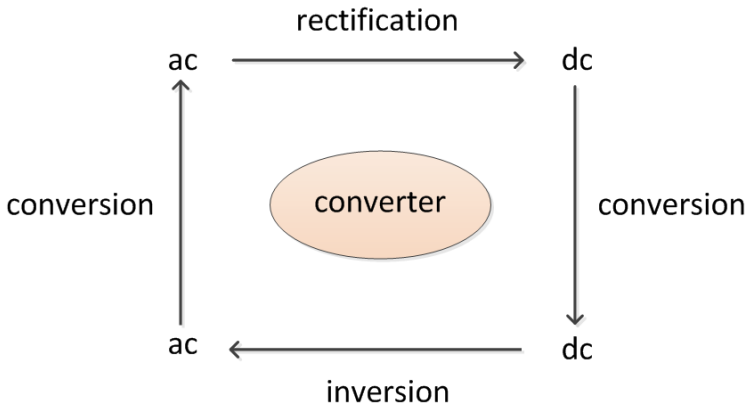

Figure 2-9 Overview of definition of power electronic converter

In order to model the reliability of power electronic components, it is necessary to understand the failure mechanisms and identify the precursors of failure as well as of ageing under various operating conditions and environmental stress to predict the malfunctioning of the component.

2.6 IGBT Failure Mechanisms

Most failures in power electronic modules are due to thermal effects, but other failures, such as mechanical vibration, may also be significant. The failure

mechanisms for thermally-induced failure are thermal cycling and power cycling. Thus, the thermal cycling capability has induced the substrate solder joint fatigue phenomena at between the substrate layers that have attached to the base plate via solder joint layer. Furthermore, thermal expansion during a converter load cycle drives stress–strain cycles within the device and packaging. solder cracking and bond wire lift-off on the die are the dominants failure in IGBT packaging which fairly happens due to power cycling capability. Moreover, the energy lost through hysteresis causes crack propagation in the solder or at the bond wire/device interface. Failure may be precipitated by thermal runaway due to the increased resistance caused by a reduction in the active device area as the solder area decreases or the bond wire lifts off.

The two major failure mechanisms of IGBTs are intrinsic and extrinsic faults that are related to IGBTs' physics and packaging, respectively. The phenomenon of intrinsic failure mechanisms in power electronics includes hot carrier injection, the latch-up mechanism (i.e. sudden collapse of the collector to emitter voltage), dielectric breakdown and electromigration, whereas extrinsic faults consist of wire lift off, die solder delamination and substrate solder degradation [80]. On the other hand, the ageing of power electronics systems resulting from harsh operating conditions and environmental stress are two potential failure modes of stress and causes of catastrophic failure in IGBTs.

One of the most important defects relevant to electric stress is related to dielectric breakdown [81], [82]. This defect mechanism occurs in between the channels of the gate oxide, the emitter and collector. It is noted that the gate oxide degrades when the dielectric layer wears out due to a strong electric field 10MV/Cm or above and electrostatic discharge [83]. The gate structure includes a thin oxide layer which is used to isolate the gate from the MOS transistor and due to a large voltage spike, punches through and causes an immediate breakdown [84]. HCI, an intrinsic failure mechanism, is considered as either being the primary cause of TDDB or wearing out of chips under harsh operating conditions [85]. Under the high electric field, the carriers (electron/hole) have sufficient energy to break through the Si/SiO2 barrier which causes leakage

current through the oxide, whereas high temperature causes gate oxide breakdown. As a result of hot electron injection which leads to excessive leakage current, the IGBT's turning off time is effectively increased and causes subsequently gate voltage losses to control collector current (i_C). Hence, HCI has a major effect on the long-term reliability of power electronic components [14]. Another intrinsic failure phenomenon is an electro-migration failure which might occur when the current is unevenly distributed among wire bonds. The reason is that the current density is much higher in the vicinity of around some bonding wires. With an increase in temperature will cause an adjustment in the interconnection of the wire bonding which eventually resulting in a break in the cross section of the wires. As a result, the conductor resistance and overall temperature of the devices are increased [86], [87].

Power electronic modules are always working in certain duty cycles from the requirement of an inductive load along with a defined switching frequency operating condition. This will result in instantaneous power dissipation during freewheeling diode recovery mode and IGBTs conduction mode plus turn on and turn off mode. Furthermore, the growth of the wear out mechanisms in power electronic modules adds more adverse operating conditions in the modules.

Furthermore, implementing a non-optimum thermal management design causes external electrical dysfunctions. Thus, inappropriate thermal management will accelerate the packaging degradation inside the module, which in turn triggers abnormal behaviour, such as short circuit, over-current, or over-voltage, and over time contributes more stress to the components. The harsh environment and load condition impact can also pose a severe stress issue for the power module. Overall, it is important to determine the failure signature in order to enable health management to derive precious information regarding the origin of the failure. Obviously, the operating conditions for active devices become more adverse during wear out mechanisms due to thermal fatigue mechanisms [88], [89].

2.6.1 Thermal Fatigue

In long-term reliability, packaging wears out is one of the important limiting factors that power electronics suffer from. The thermo-mechanical effects on power module wear-out depend on the package materials, geometries, usage conditions (external cooling system, air temperature, etc.). Usage conditions produce thermal cycles on the package assembly, which induce thermal stresses and strains that produce the so-called thermal fatigue. The term fatigue is driven by the exhausted material mechanics which is degraded due to a cyclic load on the component. The following are the failure mechanisms which are dominant for packaging technology [90], [91].

2.6.1.1 Reconstruction of Metallisation

Power cycles are capable of inducing cyclic expansion and contraction stresses on the upper metallization of the device due to large thermomechanical mismatch with the silicon die. Such stresses are not tolerated and with a certain degree of freedom can go beyond the elastic limit, and eventually they reach the relaxation region where the mechanical processes led through (e. g. diffusion creeps, grain boundary sliding or by plastic deformation through dislocation glide). This mechanical stress phenomenon leads to the extrusion of the aluminium grains which are dependent on the texture of the metallization. This finally can result in aluminium reconstruction which causes an increase in sheet resistance of the metal. This can be observed and monitored by changing in $V_{CE(ON)}$.

2.6.1.2 Wire-Bonding Fatigue

Wire-bonding occurs under varied working conditions from temperature swing stress which is predominately induced by power dissipation in the silicon die. This will result in fatigue due to shear stress which occurs in between the wire pad and the wire-bonding. This will continue till that they disconnect from dying itself. As a result, they will become sudden open circuit failure. Two

related phenomena can be observed: one can be initial crack propagation in the vicinity of the wire bonding heel, and the second is observed as wire-bonding lift-off. The problem is due to inappropriate wire bonding process which mechanically initiates a crack on the wire-bonding heel. Mechanical stress is inevitable and causes the wire-bonding to age which eventually becomes wire lift-off failure due to the high coefficient thermal expansion (CTE). The failure phenomenon can be seen in contact resistance which can be monitored externally by $V_{CE\,(ON)}$.

2.6.1.3 Solder Joint Fatigue

The thermo-mechanical fatigue is seen as the main failure mechanism for power electronic modules. The power module constructs of seven layers of the materials to which they are attached to each other in order to conduct heat transformation to ambient. The most susceptible part is the solder which is used to join the die attach ceramic substrate and the ceramic substrate base plate. The solder (i.e. the tin-silver, indium or tin-lead alloys) is critical material that is used frequently in multi-chip power electronic modules, and it has a good electrical characteristic. The more challenging part is when a material with copper metallization is going to be a solder with the property of a standard lead-tin alloy. At the central of the solder joint two materials tin and lead are formed together and during accelerating ageing the copper which is more brittle than the tin-lead starts often early to receive thermo-mechanical fatigue. The crack will appear often at the outside corners pointing and edges which are responsible for rising up stress at this location. The crack continues to propagate towards the centre of the solder joint in the source of high temperature where the module is located.

2.6.1.4 Summarised IGBT Failure Mechanisms

The intrinsic failure mechanisms in power electronics include hot carrier injection and dielectric breakdown and electro-migration, while extrinsic faults consist of latch up, wire lift off, die solder delamination and substrate solder

degradation [80]. These are summarised in [87]. Power electronic modules are subject to two potential failure mode stresses: the first is associated with high electric fields and the second is due to high temperatures. One of the most common defects which are relevant to electric fields is dielectric breakdown [81], [82].

Table 2-2 Identifying IGBT Failure Mechanisms

Failure Mechanisms	Failure Type	Failure Mode
Full-cycle temperature swings due to power dissipations and self-heating of wire bonds	Bond wire fatigue	Extrinsic
Coefficient of Thermal Expansion (CTE) mismatches between wires and silicon	Bond wire lifts off	Extrinsic
Thermo-mechanical stress due to temperature cycles	Bond wire heel cracking and fractures	Extrinsic
Large thermo-mechanical stress and mismatches due to stiffness of the silicon and materials that cause junction temperature at the centre of the die to rising	Aluminum reconstruction and metallurgic damage	Extrinsic
Thermal and thermo-mechanical stress during operation propagates micro-cracks and aluminium metallization	Current leakage	Intrinsic
Sharp stress level at the pre-existing damage points for brittle materials	Fatigue crack propagation	Extrinsic
Thermo-mechanical cycling and residual deformation in the bond wires	Corrosion of the wires	Extrinsic
High-temperature swings and mismatch in the various intermetallic layers with solder between them	Solder fatigue and voids	Extrinsic
During transients: High electrical energy produces excessive charging energy in IGBT which leads to excessive current flow through the gate oxide and high voltage drop across the IGBT. Results in loss of gate control.	Static and dynamic latch up	Intrinsic

Energetic particles in the form of heavy particles, such as electrons, interact with cosmic neutron rays and burst localised which leads to catastrophic failures. (Cosmic rays)	Single event effect	Intrinsic

2.7 Summary of Prognostics Challenges in IGBTs

The reliability of power electronics is a vital issue for the commercial success of industrial applications. Initially, in such applications, IGBT module life cycle expectancy is estimated at several thousand of hours. However, their lifetime under excessive temperatures or in other harsh environments will be much shorter, depending on the application, i.e. pulsed power. As a solution, diagnostic and prognostics approaches are the two principal aspects of CBM [92] that are developed to increase the useful lifetime of IGBTs by monitoring critical parameters such as V_{CE}, I_{CE}, etc. [15].

As systems mainly work in critical harsh and noisy environments, sensory data is highly polluted with noise. Hence, robust prognostics models that mitigate uncertainty are necessary. However, a wide range of numerical and statistical methods, as well as well-known machine learning approaches, have been employed for the development of prognostics models. Incomplete failure model becomes the imponderables of uncertainties involves with surrounding future health estimation which has not been taken into account.

Figure 2-10 summarises the basic knowledge needed to develop data-driven and model-based prognostics. As shown in this figure, the development of prognostics models is generally started with the definition of a model for model-based prognostics that requires understanding the physics-of-failure of the IGBT component. It is often a difficult task to establish an accurate physical model. On the other hand, data-driven approaches start with accelerated ageing tests followed with pre-processing (filtering) and classification for eliminating noise from collected data, and damage model formulation followed by RUL estimation. There is also an important initial step (known as the feature extraction step) to

investigate which signals should be monitored that would allow prognostics to be successfully developed based on features extracted from those signals [72].

The next chapter describes the accelerated ageing test in power electronics, and two different ageing processes and data manipulation of each experimental data collection.

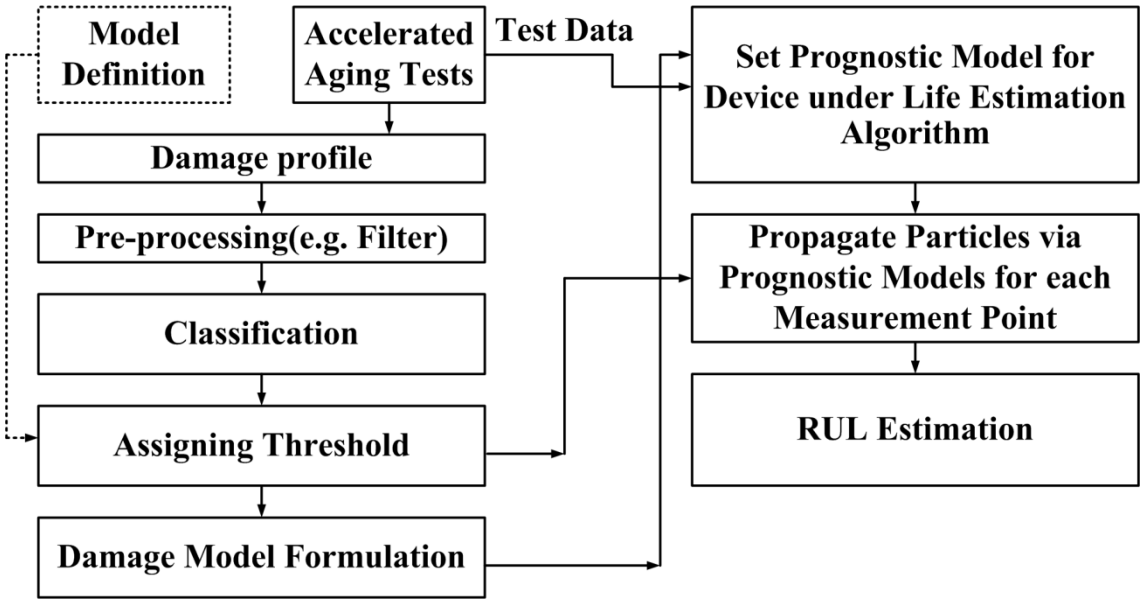

Figure 2-10 Algorithm to develop prognostics model

3 Accelerated Ageing Test

In order to create a prognostics model, it is important to collect reliability information in the form of a degradation profile that covers failure data under various types of operating conditions. It takes a long time for failures to progress in actual operating conditions. It is thus necessary to employ a number of different techniques to accelerate failure mechanisms. These techniques, known as accelerated ageing tests, are divided into three main categories: thermal cycling [53], [93], [94], [95], power cycling [96], [97], and electrical overstress [98]. It is noteworthy that due to the nature of failures, different failures are induced under different ageing experiments. Hence, it is necessary to collect degradation information which is accelerated by different types of accelerated ageing tests. For example, wire bond failure is the dominant failure for IGBTs in relatively highly-accelerated thermal and power cycling ageing tests [99]. However, other mechanical failures, such as solder joints and metallization, can dominate the failure mode in lower temperature condition stress testing. The accelerated ageing test is useful in identifying these dominant failures. Furthermore, it is worth mentioning that there is also an important initial step to investigate what signals should be monitored that could allow prognostics to could be successfully developed based on features extracted from those signals [100].

3.1 Thermal Cycling

Thermal cycling may be characterised as follows. In high-frequency cycling, with a time period of tens of milliseconds, the device temperature varies with the load current during an inverter modulation cycle. The modulation frequency is typically between one and a few hundred hertz, depending on the load characteristics. For most of the time, the relatively high frequency

compared with the heat sink time constants results in low amplitude cycling. In fact, it is assumed that the low amplitudes are sufficiently small to be ignored.

However, at low modulation frequencies, the amplitude may approach tens of degrees. Therefore, these cannot be ignored. Low-frequency cycling, with a time period of many seconds, is due to the variation in the average (RMS) load current throughout the load cycle because the inverter loads change. This may significantly vary over several seconds or minutes and may result in a change in the junction temperature of more than 50°C.

Deep thermal cycling, with a time period of many minutes or hours, is caused by operational changes, i.e. a rise and fall in the device temperature as the inverter comes in or out of use. For example, if the electric vehicle is used twice a day, two peak-to-peak thermal cycles of 100°C may result from this pattern of use. Despite the low frequency of this cycling, the high amplitude has a severe effect on device reliability. This is particularly the case from a cold start (down to −40°C).

Traditionally, device and packaging reliability have been tested by using accelerated thermal cycling, which may be active, using the device to heat itself, or passive, where the heat is applied externally. The number of cycles to failure is given for the mean temperature Tm and temperature range ΔT during the test. This is often used by device manufacturers as a means to evaluate packaging performance.

Several studies have explored power device reliability in relation to device temperature. The stress–strain locus is calculated directly from the transient device temperature profile, which is followed by a fatigue model applied to the stress and strain variations to predict the number of cycles to failure. The energy absorbed by the packaging materials in each cycle is calculated from the material temperature rise in order to predict the crack growth and the number of cycles to failure. A large sample of IGBT modules was tested across a wide range of cycle conditions, giving the only known comprehensive data set for the thermal reliability of IGBT power modules.

All these methods share the difficulty that the interaction between failure mechanisms for different temperature cycling conditions is not known with certainty. It is suggested that above a range ΔT of 130 K, the dominant mechanism is solder cracking, whereas, below 130 K, it is bond wire lift off. Also, different mechanisms gave rise to nonlinear damage accumulation that was observed with temperature ranges of 80 K–110 K interleaved during a thermal cycling test [101], [95].

3.1.1 IGBT Thermal Cycling Data Repository

NASA Ames conducted thermal cycling accelerated ageing tests to determine the associated failures mechanisms on the International Rectifier IRG4BC30KDPBF IGBT. Initially, the temperature was set within the maximum operating junction temperature 150°C. Then, it was increased beyond the safe operation in order to induce thermo-mechanical. And, due to the difference in a thermal coefficient mismatch between different IGBT's structure layers several failures such as latch-up, thermal runaway and loss gate control have been considered. Several parameters, such as transient and steady state collector-emitter ON voltage $V_{CE\ (ON)}$, the collector-emitter current, device case temperature, and transient and steady state gate voltages have been monitored in order to be able to identify the precursor parameters that indicate the degradation on the die. The $V_{CE\ (ON)}$ was measured across the collector-emitter terminals of the transistor where the emitter is directly connected to the ground of the power supply and the collector with a resistor is in series with the positive lead of the power supply. And also configuration consists of gate voltage 15 V which the gate was driven by an independent power supply. Initially, by looking at the parameter data sets, it can be noticed the $V_{CE\ (ON)}$ increases monotonically in a discrete manner while the phenomena die to attach voids migrated and degraded over the ageing cycles. Due to very harsh operating conditions, the eligibility of the data sets for assessing IGBT reliability is the major challenge.

The IGBT accelerated ageing experiments are designed to study the ageing characters of the IGBT and develop the algorithm of prognostics for

prediction of the remaining useful life. The IGBT degradation data set is acquired from the ageing process system, which is provided by the AMES laboratory of the National Aeronautics and Space Administration (NASA) [22]. The data set can be used to design and develop prognostics algorithms for semiconductor components, such as IGBTs, which have been increasingly used in modern multiple vehicle systems. IGBT accelerated ageing experiments belong to the project in NASA to investigate the degradation characterisations of electronic components [102]. As electronic components have an increasing consumption in new generation aircraft and vehicles, and the amount of electronic failure will also become significant. Fault diagnostics and prognostics, estimation of remaining useful life and health management play a vital role in avoiding catastrophic failure, improving aircraft reliability, reducing maintenance cost and increasing performance.

IGBT accelerated ageing experiments are based on the ageing platform which induces the degradation and electronic faults into the test system. Prevalently, four kinds of accelerated ageing methods are widely used in accelerated ageing experiments, namely thermal cycling, hot carrier injection, electrical overstress and time-dependent dielectric breakdown stimulus. The IGBT functional failure, such as die solder degradation and wire lift, were brought by the thermal cycling accelerated ageing approach. Hot carrier injection could accelerate electrons and holes pass into the gate oxide, which could result in the increase of the IGBT threshold voltage. IGBT condition mutation and lighting could be caused by the electrical overstress due to the excessive voltage, current or power. The breakdown of the IGBT gate oxide will occur when the charge injection exceeds the threshold which is caused by the increase of the temperature in the gate oxide when it is being operated. Accelerated ageing approaches, such as thermal cycling and electrical overstress, are used in IGBT accelerated ageing experiments to speed up the degradation and failure of the IGBT in experimental environments which simulate scenarios of industrial practical applications. Precursor parameters, such as collector voltages, collector currents, gate voltages and currents, and environmental parameters, such as

temperature, are monitored and recorded to be utilised for IGBT diagnosis and prognosis research [103].

The experiment data and measurements are shared on the website of NASA as an open database which can be used to develop prognostics algorithms available to academic and industrial researchers. The IGBT accelerated ageing measurements and sensory data collection from the IGBT accelerated ageing experiment platform is shown in Figure 3-1.

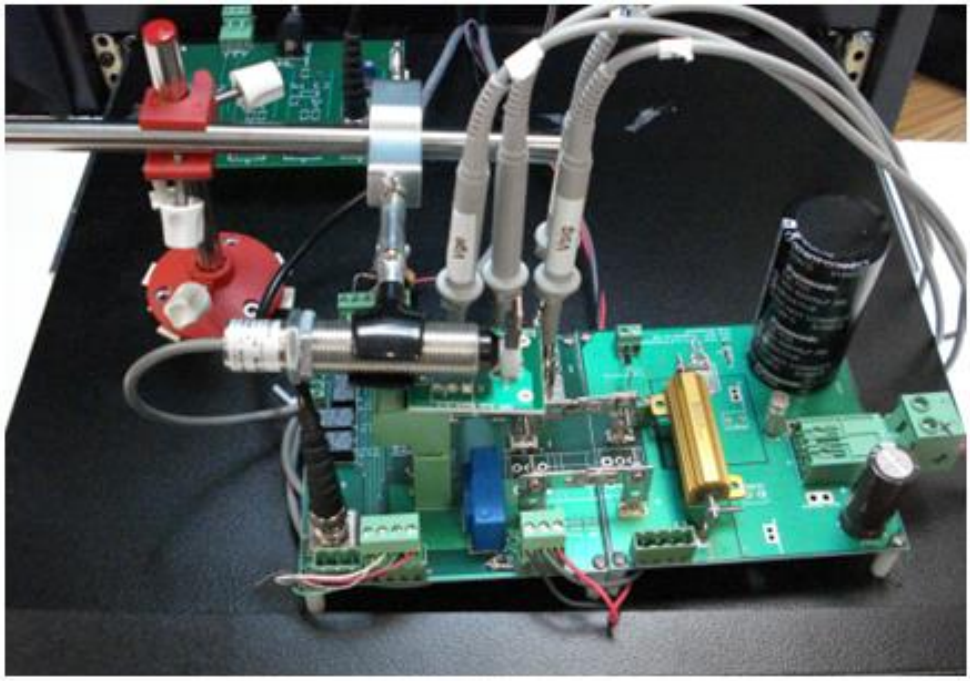

Figure 3-1 IGBT accelerated thermal cycling ageing experiments hardware [104]

The data set includes the measurements recorded from IGBT experiments (or operating) environment, and survey data is representing the deterioration of IGBT in the experiments. This data set contains mass data from thermal overstress ageing experiments, including several parameters being recorded continuously, such as collector current, collector voltage, gate voltage, package temperature, etc. [104]. These data and parameters were monitored and recorded constantly until IGBT failure in accelerated ageing experiments. The data set was formatted in a data array which could be read by MATLAB to facilitate analysis and processing of the data in subsequent research and investigation [22].

The aim of data processing is to gain useful information from the data with the approach of analysis and sorting. Collector-emitter voltage is selected as a precursor parameter for the IGBT ageing prognostics [25]. The profile of the V_{CE} collected from the ageing experiment is presented in Figure 3-2. The collector-emitter voltage of the IGBT presents a monotone increasing in the whole ageing process and the V_{CE} also presents a fluctuation and oscillation during this process, but the V_{CE} falls quickly at the end of the ageing process when the IGBT begins to fail. The whole ageing process is more than 10,000-time units [22].

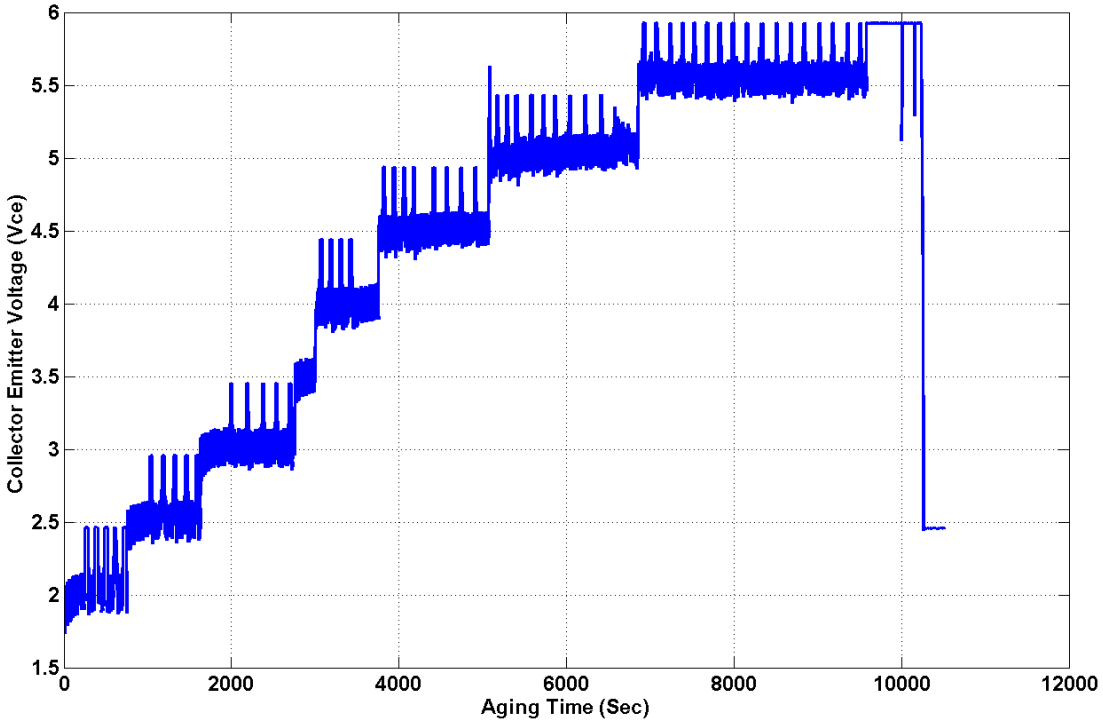

Figure 3-2 IGBT collector-emitter voltage profile

The ageing data of raw V_{CE} as a precursor parameter are processed by low-pass filtering, and its filtered profile is shown in Figure 3-3. It can be seen that V_{CE} presents an increase step by step during the whole IGBT ageing process. The data is now clean and more suitable for analysis. The variation of V_{CE} in the whole ageing process could be separated into 8 stages, and the values of V_{CE} for each phase are discretely different. Seven IGBTs were used in the accelerated ageing experiment. It can be seen that the degradation stages are

clearly separated from one another. The V_{CE} voltage value is approximately 2.45V at the start of the ageing process. The degradation states can be determined by the level of V_{CE}. In this particular IGBT, V_{CE} increases about 0.5V discrete step at each degradation phase [22].

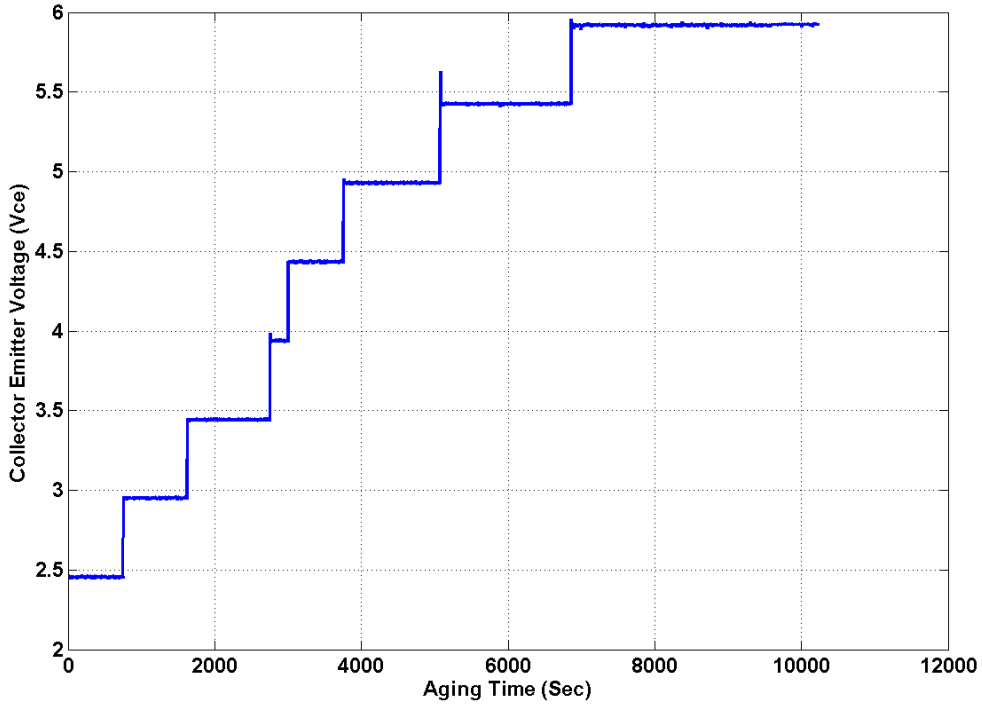

Figure 3-3 IGBT collector-emitter voltage after filtering and K-Mean clustering

3.2 Power Cycling

IGBTs are designed to work below the nominal characteristic temperature (i.e. 150°C). However, in railway traction and automotive applications, they could experience increased thermal cycling (rise and fall of temperature) which leads to thermo-mechanical stress on the weakened part of the IGBTs' packaging interconnections [105]. To simulate this environment in a laboratory set-up, accelerated ageing techniques, such as power cycling, are used. This type of reliability testing can be used to characterise failure mechanisms more accurately than traditional thermal cycling inside an environmental chamber due to the flow of current through the IGBT, and heat dissipation which is similar to what is experienced in the application. The induced failure

mechanisms depend on the testing conditions and have various levels of degradation similar to real industry applications. Power cycling tests are used to define failure modes and estimate the reliability of standard power electronic module IGBTs [101].

In power cycling tests, the IGBT actively heats up due to the amount of power dissipated at the junction during a constant load cycle. The load cycle also depends on the pull time and change in junction temperature. These results in strain and stress between the aluminium wire and silicon die, as well as between the die and insulation substrate, where differences in CTE initiate cracks at the bonding surface and creep in the solder joint and substrate layer. Finally, peel progression of the copper metallization and crack propagation in the solder joint lead to the aluminium nitride substrate (AlN) failure mode and wire bond liftoff, respectively [17].

The Power Electronics Group at Nottingham University has carried out a power cycling ageing test for IGBT power electronic devices under high thermal stress values up to 60°C for the baseplate temperature and 120°C for the die. The failure mode involves wire bond lifting off and progressively ending before reaching the open circuit. The device is assembled using Dynex technology of the alumina-copper using Direct Bonded Copper (DBC) for heat conduction and relatively low conductivity of alumina, and aluminium wire bonds (see Figure 3-4) [17]. The test bench is equipped with a switched current supply and a constant current power supply to heat and cool a die sample. Each IGBT die is soldered and wire bonded onto a substrate tile. A coupon is used to hold the die and to constantly dissipate heat through the heatsink and water coolant loop. This also allows the temperature to be measured using an infra-red (iR) sensor.

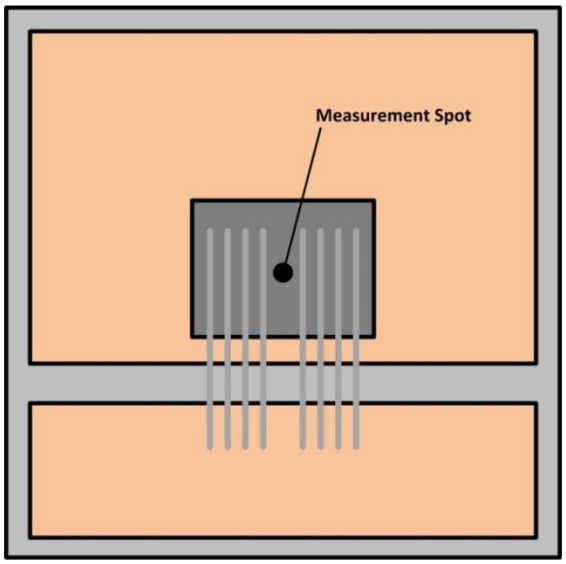

Figure 3-4 Proposed sample [17]

The custom test bed provides a coolant at a constant 20°C using a chiller unit (Thermo Fisher-Scientific A200-A25) and the coolant flows in a U-shape circuit through the heat-sink. The four coupons sit in recessed areas on the upper surface of the heat-sink. The supported infra-red sensors above the coupons used are Micro-Epsilon CS-SF15-C1 miniature pyrometers. These can be configured to output an analogue voltage, proportional to temperature, in the 0-5V range using a USB programming kit (TM-USBK-CS USB Kit) (see Figure 3-5) [17].

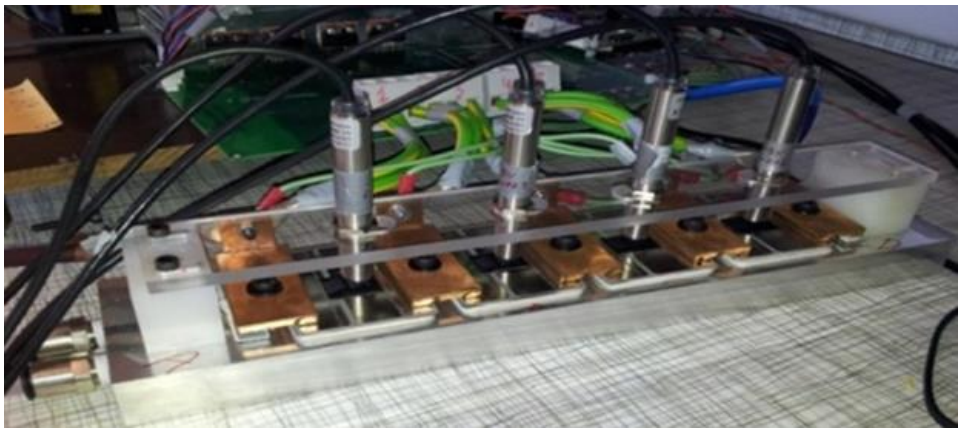

Figure 3-5 Actual heat sink assembly, iR sensor support and iR sensor [17]

The voltage signal from the iR sensor can also be used to visualise the temperature cycling in real time using Labview or similar software. Each coupon is allowed to heat up within the range of operating junction temperature (60°C to 120°C). Once the reading from the iR sensor indicates the temperature has reached the upper bound, then the bypass switch (designed to keep the temperature within a hysteresis bound) diverts heat away until the temperature drops to the lower limit. On the other hand, if the iR sensor indicates the temperature has fallen to the lower temperature bound, the bypass switch will be disabled and the cycle repeats until the safety temperature-bound which is set to prevent the device to from open-circuit failure. Such a test bench is needed to age the component under various operating conditions subjected to various mission profiles, which characterise the operational environment. It is expected to work under ambient, high-temperature cyclic and intermittent loading conditions (i.e. power cycling) which ultimately induces more stress on the weak parts of the device [106].

An iR sensor is used to monitor the temperature of each die, and when the temperature reaches below or above some specified threshold, the heating current will be automatically removed. The temperature is constantly recorded and the collector-emitter voltage is measured as a precursor and recorded during each heating cycle. Each of the test beds is controlled independently and they are allowed to heat up until the iR sensor indicates the temperature has reached the upper limit of 120°C. The bypass switch diverts the heating current away from the test bed so it starts to cool until the iR sensor indicates that the temperature has fallen to the lower limit of 60°C and the bypass switch stops and this power cycling is repeated. The typical temperature waveform during cycling is shown in Figure 3-6 [100].

Power cycling ageing tests enable monitoring and measurement of temperature and electrical parameters. The junction temperature and the collector-emitter are measured and recorded constantly until the IGBT fails in accelerated ageing experiments. The data set is formatted in a data array fashion which can be read by MATLAB to employ reliability analysis on the raw

data for conducting data pre-processing. It was noticed during tests that wire lift off occurred because of thermal expansion mismatches between the wire bond and solder contact points after short-circuit failure [17], [100].

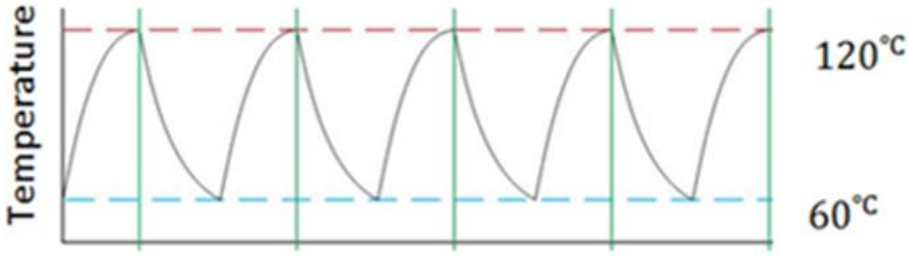

Figure 3-6 Temperature cyclic [100]

3.3 Data Pre-processing

Following the transfer of data to MATLAB, it is necessary to conduct pre-processing which makes the reliability information suitable for developing a prognostics model (i.e. data-mining). Data-mining comprises pre-processing (filtering), classification (discretising), formulating a degradation model, and propagation (RUL simulation) [107], [108]. The $V_{CE\ (ON)}$ parameter indicates increases in non-monotone discrete steps including noise until the IGBT fails and before an open circuit occurs for 4 IGBT samples (see Figure 3-7).

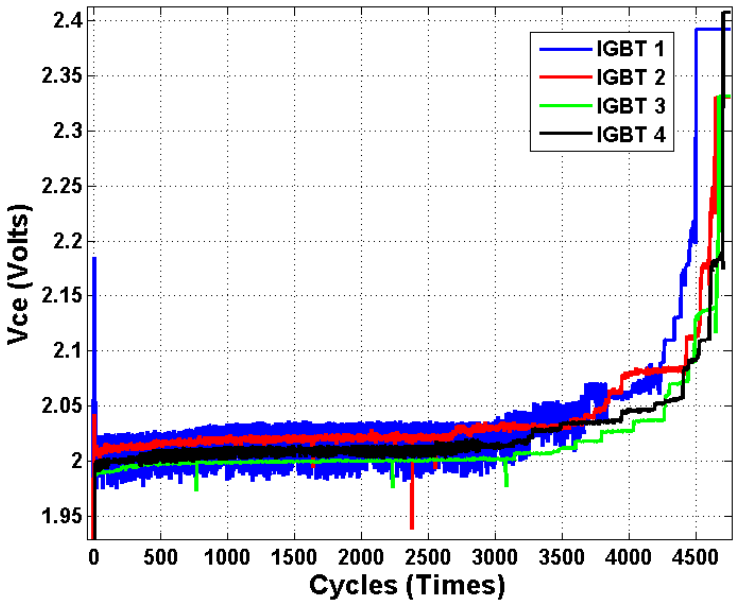

Figure 3-7 Four IGBT run-to-failure data set samples [110]

The V_{CE} measurement enables the detection of wire bond lift off or emitter metallization damage [109], [61], [26]. The V_{CE} variation due to the degradation process is very small and requires a very high degree of accuracy for this measurement. As shown in Figure 3-7, the V_{CE} voltage precursor indicates a sudden fall at the end of the ageing process when the IGBT fails after more than 4,500-time units [17].

IGBT raw data sets have inherent noises which obscure the trend underlying the samples. The first IGBT sample has shown an obvious peak. This is due to the initial value setting of the PID controller which is the input value of the PWM generator. This spike is eliminated after the first control loop iteration where the PID sets its output according to the reference input. The $V_{CE\ (ON)}$ is obtained from a standard power cycling experiment to failure and this will be formatted into a dimension to be used in the data-mining analysis. Initially, the raw data set is processed using a 1-pole low-pass filter in MATLAB with initial correspond setup according to the data set properties where the time between samples (T=1sec). And, the filter time constant (τ=200 sec) attempts to reduce internal noise as a dispersion sensitivity to reveal the true value of the ageing data of raw V_{CE}. The drawback of this filter is that it imposes delays on the data set. In Figure 3-8, the green plot represents a low-pass filter with RC delay of 1,000-time units, the magenta plot depicts a symmetrical low-pass filter with RC delay of 1,000-time units and the blue plot represents the raw data.

As a solution, asymmetrical low-pass filter (i.e. moving averages filter) is proposed to overcome the lagging. The advantages of the moving average filter, as in Equation (1), is that it results in more weighting of the population of data and less delay in filtering, and while minimising noise, it effectively smoothes the data set and can be a better use for data pattern recognition or classification as an essential step for developing stringent prognostics modelling [17].

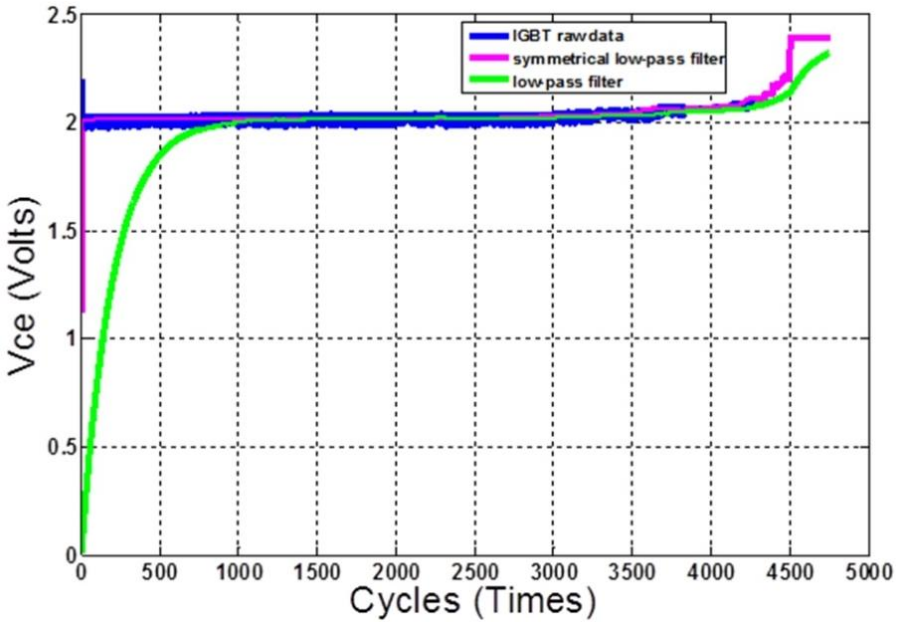

Figure 3-8 First VCE sample after filtering [110]

The parameter j denotes the reading points of both filtered and non-filtered test data. Xi is non-filtered test data at reading point i. n shows the length of the first relaxing points which are varied from test data to test data. n is set to 1,000 for the data test shown in Figure 3-8.

$$MA_j = \sum_{i=j}^{n} \frac{x_i}{n-j} \quad (1)$$

$$n = 1000$$

$$j = 1,2,2,\ldots,n-1$$

The rate of filtering windows increases when it reaches close to the relaxing point, whereas the length of the defined window becomes increasingly smaller. After noise elimination, the data set is clean enough and suitable to be separated into different health states (see Figure 3-9). Therefore, classification, an important part of the data-mining approach, is performed for accurate and efficient RUL computation.

It is noted in Figure 3-9 that the ageing process started at almost 2V and degradation is progressed for more than 4,500 cycles, whereas the failure has occurred at about 2.4V.

The monitoring data and experiment's parameters are recorded and collected to transport into the software platform which is used as data formation and data storage. IGBT diagnostic and prognostics investigation will be based on this data set. Prognostics algorithm for RUL prediction will be developed, and Monte-Carlo simulation (MCS) is used in the prognostics algorithm which will be described in more detail in the subsequent sections.

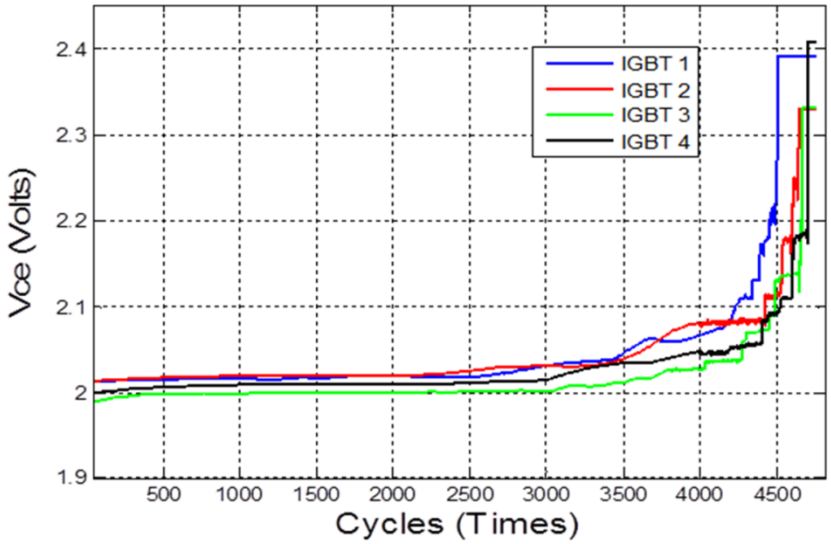

Figure 3-9 Four IGBT run-to-failure data sets after filtering [110]

4 IGBT Probabilistic Data-Driven Prognostics Modelling

In this chapter, it is considered to contribute the novel prognostics technology development in the PHM for the power electronics active devices. Undoubtedly, the detection of an IGBT fault prior to prognosis or even after diagnosis is of critical importance for a healthy converter operation system. Conventional vehicles are equipped with on-board diagnostic (OBD) systems which are capable of detecting a "happened" fault and flag it up to the driver of the vehicle [17], [109]. In the event of an IGBT failure, the detection must be quick enough (ideally, less than 10μs) to prevent a fault from propagating, which places a limitation on the hardware setup [17].

Hence, a comprehensive approach to the development of a prognostics framework for IGBTs is required. There is a need to develop methods to predict the RUL of IGBTs to prevent system stoppage and costly failures. Prognostics technology is aimed at high-technology sectors, for example, the automotive or aerospace industries, for ensuring safety and customer satisfaction. Most modern vehicles monitor their systems to ensure correct operation. If a fault is detected or predicted, the user of the vehicle is usually notified before the fault has had a detrimental effect on the vehicle. Modern vehicles also monitor their usage and change their service intervals accordingly. The reliability of IGBTs directly affects the reliability and performance of these vehicle systems. In recent years, a series of research work about IGBT reliability, failure mode and ageing analysis has been carried out, and a suitable prognostics method for IGBTs and an efficient algorithm for predicting IGBTs' RUL have become increasingly important.

This chapter proposes a new data-driven approach for power electronics components which addresses issues in previous IGBT prognostics. The defect in [1], [26] are dependent on the propagation by time steps. However, it is not computationally feasible to perform several Monte-Carlo simulations. In the proposed novel prognostics algorithm, the dependency of RUL efficiency on the time step is eliminated and an MCS is carried out at different degradation phase durations.

As a result, the RUL time consumption is significantly reduced and a considerably improved prognostics feasibility model is embeddable. The aim of this chapter is to develop a computationally efficient and embedded real-time prognostics approach. In this regard, we propose a novel probabilistic prognostics model for each degradation phase of the system for estimation of the health state of the IGBT component. RUL simulation is performed using the Monte-Carlo technique (multiple runs) of the degradation model up to the predefined end-of-life threshold. In this approach, the RUL calculation is carried out using the probabilistic model as a function of the component's life duration. This modelling technique uses the historical degradation data to construct the probability of failure during operating conditions. The data set is discretised in different states which have different durations. Therefore, the probabilistic model is formed utilising the duration of the failure phase in order to aid the model propagation, which effectively reduces the total computing processing [17].

4.1 Classification

Classification is an important part of the data-mining prognostics approach which is mostly used in supervised learning. In classification, the important part is to group similarities. In the field of data mining, vector quantization (VQ) is known as a classical quantization technique that models the probability of density functions using the distribution of prototype vectors. VQ clustering is proposed to divide a large set of vectors into groups so that members of the group share similarities in their properties with a group representative. For instance, the different regions of the feature (e.g. V_{CE}) divide into vectors

with similar and minimum centroid distance within the vectors and K-mean as a clustering technique is used for grouping vectors and identifying the best set of clusters such that data within a cluster are more similar to each other.

A VQ technique is one of the most powerful techniques in data compression and information retrieval to manage size and meaning of metadata while maintaining an acceptable level of quality and fidelity within the core of ISHM systems. Using this technique, a codebook which consists of a bank of codewords of failure patterns is created by iterative clustering algorithms conducted on different parts of the systems (partitions). The codebook constitutes the core of the reference model with which prognostics models and features of partitions of the system are linked to representative patterns of the system from the reference engine. Then, the health state of any partition is estimated based on the similarities of query failures (failure pattern of that partition) with similar patterns (codewords) from the codebook. In other words, the prognostics of systems are created from using the similarities gathered from the failure patterns of partially-related systems within the different shared partitions. The accuracy of the prognostics model and the estimated lifetime is highly dependent on the accuracy of the codebook, selecting the right codewords from the codebook, and the mechanisms used to effectively reconstruct and track failure objects based on the specific failure feature queried. Applying such a technique to IVHM systems may open a new avenue in the design of reliable systems by the creation of a VQ-based reference engine that develops prognostics of a system based on the prognostics and failure patterns of its counterparts [17], [111].

This starts with given a data set X= {x1,…,xn} to create a k-dimensional space which is mapped from a vector space of R^k onto a finite set of vectors Y = $\{y_i: i = 1, 2, ..., N\}$ where y_i is center of i^{th} reign known as a Voronoi centre, or preferably known as codeword i. Hence, a set of all Voronoi centres (Y) generates a codebook. All locations within any region are closer to the centre (codeword) of that reign than to any other. Thus, determining K clusters $R1, \ldots, Rk$ (with $Ri \cap Rj = \emptyset$, for $i \neq j$, and Rj=X). Therefore, associated with each codeword, y_i, is a

nearest neighbour region called a Voronoi region or centroids of cluster Rj, and it is defined by [112]:

$$V_i = \{x \in R^k : \|x - y_i\| \leq \|x - y_i\|, for\ all\ i \neq j\} \quad (2)$$

The representative codeword is determined to be the closest in Euclidean distance from the input vector as defined by the following equation:

$$d(x, y_i) = \sqrt{\sum_{j=1}^{k} (x_j - y_{ij})^2} \quad (3)$$

where x_j is the j^{th} component of the input vector, and y_{ij} is the j^{th} component of the codeword y_i. Now it is worth to find a $(k.d)$-dimensional vector of centroids and corresponding clusters in order to develop typical loss function.

$$\sum_{j=1}^{K} \sum_{x \in Rj} \|x - yj\|^2 \quad (4)$$

A standard K-mean algorithm is useful to optimise the cluster vector. The algorithm (see Figure 4-1) starts with VQ processes which follow with clustering failure objects in the form of codewords. Each VQ is comprised from a) determining the centroid coordination of the degradation profile in a k-dimensional vector; b) determining the distance of each object to centroids and finally, d) codebook generation and codeword indexing. An index matching step then assigns the most appropriate group of objects based on minimum distance to the failure object codeword (find the closest centroid). The same process is continued up until the outcome leads to a number of codewords of failure objects

that will be correlated with the same duration codewords for a number of different samples that have similar properties and specifications [113].

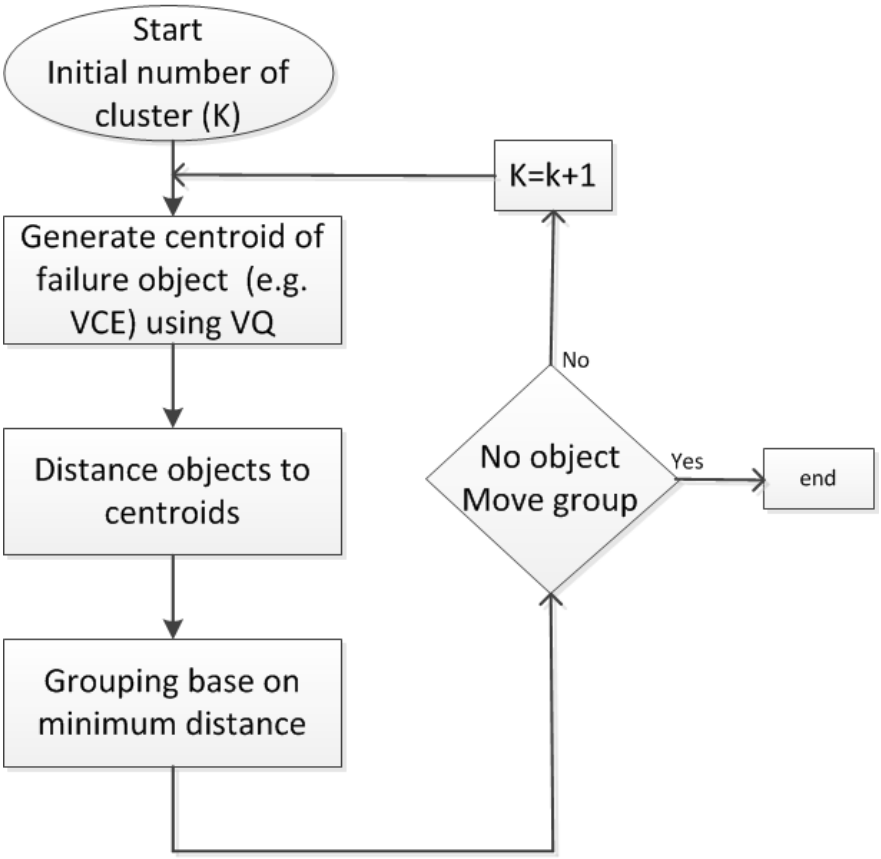

Figure 4-1 K-mean algorithm

The degradation process is now classified into different health state processes and each degradation state increases about 0.054V in a discrete manner which corresponds to one wire bond lift off. Figure 4-2 depicts 10 health states and each state lasts for a period of time before it reaches the subsequent state [17].

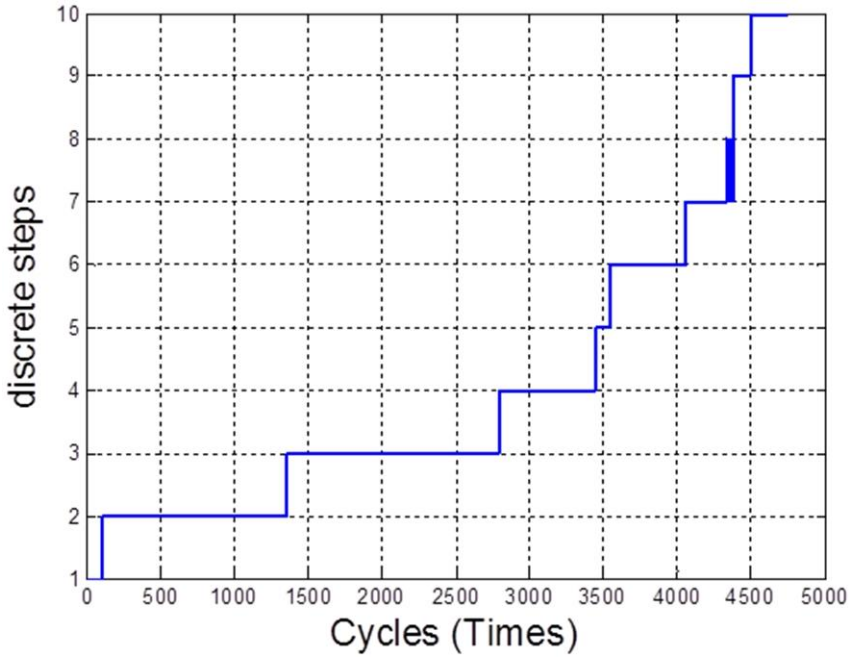

Figure 4-2 Classified ageing data

4.2 Developing the Failure Model

Figure 4-3 depicts the overall process of the data-mining algorithm development for the IGBT V_{CE} data set collected from power cycling experiments. Initially, the ageing data of raw V_{CE} as a precursor parameter is processed by low-pass filtering. Then, the state of degradation is discretised in the form of the hidden health condition. The estimation model as a failure model (degradation model) is then structured from the training data set using conventional statistical models (Gamma, Poisson, etc.). Subsequently, the trained model is used with the test data to estimate the current health of the component up until a predefined threshold state where it fails gradually in a discrete manner. This information is then used with an MCS to predict the remaining useful life of the IGBT. The outline of the algorithm is described in Figure 4-3 [17].

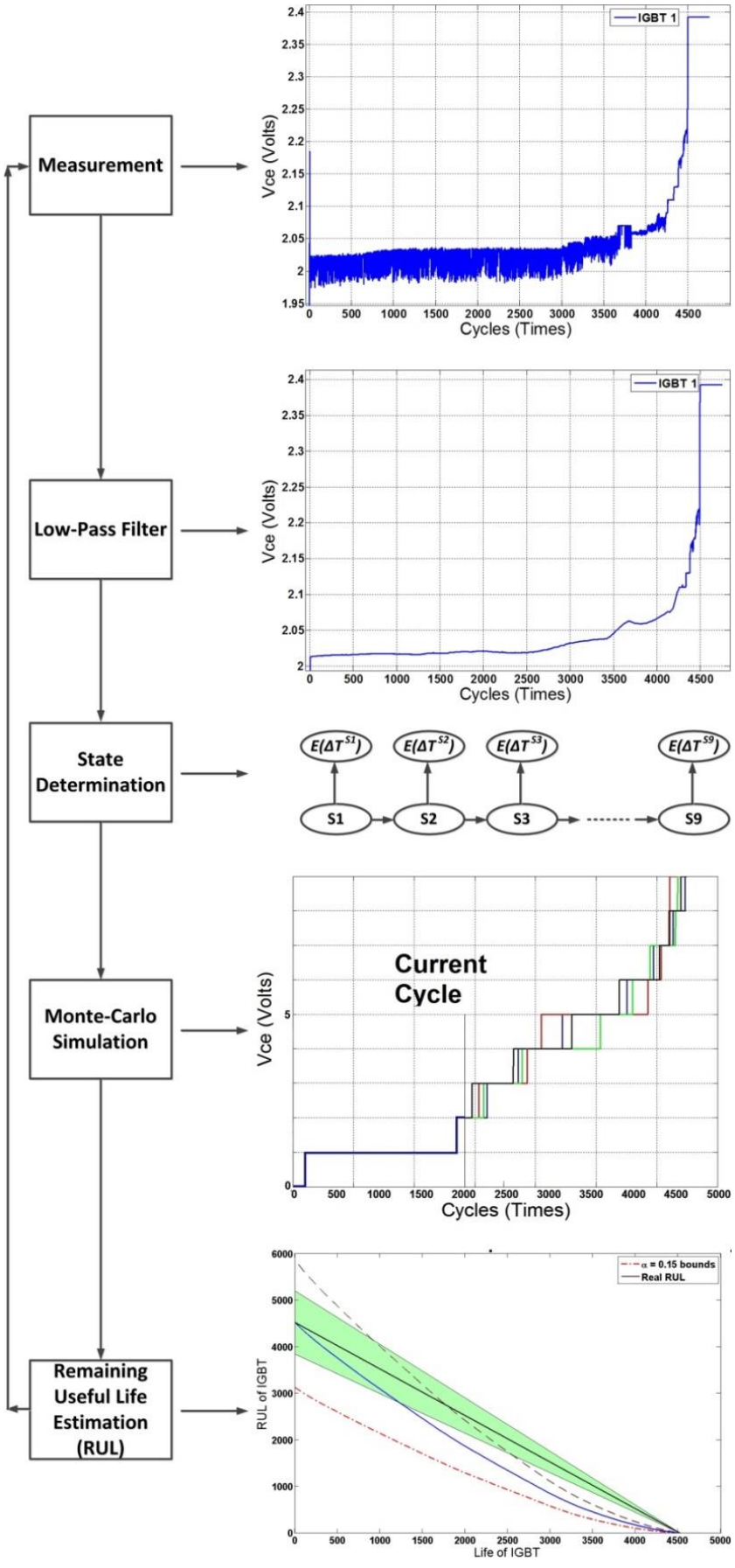

Figure 4-3 The proposed algorithm process [17]

4.2.1 **Problem Formulation**

As mentioned in the previous section, the noise-free ageing data was discretized into different steps (phases). The phase durations of the run-to-failure of four IGBT samples are recorded after using a quantized cluster validity index and are displayed in Table 4-1. The highest number of the failure progression occurs at the tenth health state [114].

Table 4-1 records the run-to-failure degradation process of 4 IGBT samples used in the accelerated ageing experiment. The columns are the time durations of each degradation phases. It can be seen that an IGBT will degrade and undergo 10 degradation phases before it eventually fails. Each phase will last for a period of time before the degradation progresses further to the next phase. Take the first IGBT for example. The operational use life of IGBT-No.1 is 4,498-time units, and the duration of the IGBT staying in its first degeneration phase is a one-time unit. Then, the IGBT degraded into the second degradation phase and stayed 109-time units before its further degradation to step into the third degradation phase, and so on, until the IGBT had stayed for 111-time units in the last phase wherein the IGBT continued to degrade and completely failed [17].

Table 4-1 IGBT Degradation Phase Duration [17]

Duration of Each Degradation Phase	IGBT No.	1	2	3	4
	1ST Phase	1	2	2	2
	2nd Phase	109	132	61	117
	3rd Phase	1,245	955	1,069	1,561
	4th Phase	1,440	1,429	1,940	1,296
	5th Phase	656	866	317	341
	6th Phase	88	164	645	480
	7th Phase	521	879	266	394
	8th Phase	282	94	145	331
	9th Phase	45	78	209	85
	10th Phase	111	6	17	91
	IGBT Life	4,498	4,605	4,671	4,698

A stochastic model is used in this section because the occurrence of the IGBT degradation is assumed to have followed a non-homogenous probability distribution process which renders the occurrence of a random event. As a result, the failure pattern follows the statistical approach in which the mean and standard deviation are the main parameters for tuning the probability functions (see Table 4-2). Hence, the prognostics model can be formulated with statistical distribution models [17].

Table 4-2 Probability Distribution Function [17]

Models	Density Functions	Parameters
Gamma	$f(T_i = x) = x^{k-1}\left(e^{\frac{-x}{\theta}} \Big/ \Gamma(k)\theta^k\right)$	κ, θ
Poisson	$f(T_i = x) = \frac{e^{-\lambda}\lambda^k}{k!}$	Λ

Both can be modelled into each individual degradation phase. The duration time (ΔT) of the degradation is considered to be a random variable which can be a random parameter for the PDF. The duration of each degradation process is used as a parameter λ for the Poisson PDF and K, θ for the Gamma PDF [114].

In this chapter, the histogram of the limited (four) run-to-failure samples will not provide the precise distribution. As such, two distributions have been selected: the Gamma and Poisson distributions. Two major types of distributions have been identified: 1) the distribution which has mean (λ) and standard deviation (δ), i.e. Gaussian, exponential, Weibull distributions, etc.; 2) the distribution with solely δ = λ, i.e. Poisson, binomial distributions, etc. All the listed distributions in Type 1 will work in a similar manner and vice versa for the Type 2 distribution. Therefore, each distribution has been peaked up from both types randomly. The Gamma distribution has been chosen as it is associated with mean and standard deviation parameters, whereas the Poisson distribution involves only a mean parameter [17].

Unlike the binomial probability distribution that observes the number of events occurring during a given number of repeated trials, there is a different probability distribution that observes the number of events that occur in a specific region or within a given time interval that is independent of any other events occurring in any set of the disjoint time interval. In this case, it is appropriate to use the Poisson distribution model which is developed by the French mathematician, Simeon Denis Poisson. Basically, both the binomial and Poisson distributions are discrete. Hence, this chapter aims to presents the feasibility of Gamma and Poisson models in the problem formulation of prognostics [17].

4.2.2 Degradation Model Optimisation

MLE is used as an objective function to maximize the density probability function (i.e. Poisson distribution function). The Poisson distribution ($P(x_i|\lambda) = \left[\frac{\lambda^{x_i}.e^{-\lambda}}{x_i!}\right], x_i \geq 0$) is the probability distribution of IGBT data (x_i) given Poisson parameter λ. The MLE method is used to estimate the underlying rate parameter (λ) for the Poisson process in order to generate the probability of occurrences for each λ. The first step is to write the joint probability mass function in this case because x_i is a discrete random variable of positive integers. Hence, each 'λ' is the times over a specific time interval or the mean number of occurrences in the given specified time interval. As all discrete random variables are independent, the probability distribution depends on λ which constructs the probability of exactly 'x' occurrences. The product of individual density functions can be obtained when the probability of measuring x number of events that occurs in one unit of measurement is followed using this formula:

$$P[x_1, x_2, \dots, x_n|\lambda] = \prod_{n=1}^{N} \frac{\lambda^{x_n} e^{-e\lambda}}{x_{n!}} = c.\, e^{-\lambda_N}.\lambda^{\sum_{n=1}^{N} x_n} \quad (5)$$

The next step would be to calculate the maximum of this probability mass function with respect to λ. This can be done by taking a logarithm which simplifies the product of exponents. This is equivalent to finding Max λ [115].

$$\log\left(\mathrm{c}.\,\mathrm{e}^{-\lambda_N}.\lambda^{\sum_{n=1}^{N} x_n}\right) = -N\lambda + \left(\sum_{n=1}^{N} x_n\right).\ln\lambda \qquad (6)$$

Then, taking the derivative from Equation (5) and setting it to zero ($\frac{\partial}{\partial_\lambda} = 0$) produces $\hat{\lambda}MLE$ [24]:

$$\hat{\lambda}MLE = \frac{1}{n}\sum_{n=1}^{N} x_n$$

For the Gamma distribution, there are two modelling parameters, κ and θ, to be estimated. MLE generically is formulated as:

$$\hat{\theta} = \frac{1}{\kappa N}\sum_{i=1}^{N} x_i \qquad (7)$$

The maximum likelihood criterion is a fairly general one, and also, fairly powerful to show the true value (the maxima) in close form algebraically. The true maximum likelihood estimator $\widehat{\theta}$ and $\hat{\lambda}$ MLE parameters converge to the true parameter value λ. Using the analytical MLE method, estimation of the best fit of the modeling parameter λ for tuning the Poisson distribution is performed [116] (see the estimated values in Table 4-3 and Table 4-4 which summarise the parameters for 10 uncorrelated degradation phases obtained from MLE of the Poisson and Gamma distributions, respectively).

Table 4-3 MLE for Poisson Probability Distribution [17]

MLE	**Model 1**	**Model 2**	**Model 3**	**Model 4**	**Model 5**	**Model 6**	**Model 7**	**Model 8**	**Model 9**	**Model 10**
λ	2	98	1210	1531	520	330	520	211	126	70

Table 4-4 MLE for Gamma Probability Distribution [17]

MLE	Model 1	Model 2	Model 3	Model 4	Model 5	Model 6	Model 7	Model 8	Model 9	Model 10
K	0.6646	0.6020	0.4284	0.3378	0.3086	0.2692	0.2389	0.2456	0.2578	0.2964
θ	694.9	766.9	1053.3	978.3	576.5	458.4	372.9	153.0	63.3	20.0

In Figure 4-4, the black discrete plot is the optimized parameters of all four IGBT samples, using the MLE function, which has shown the tracking of the trend of the first IGBT sample as an example.

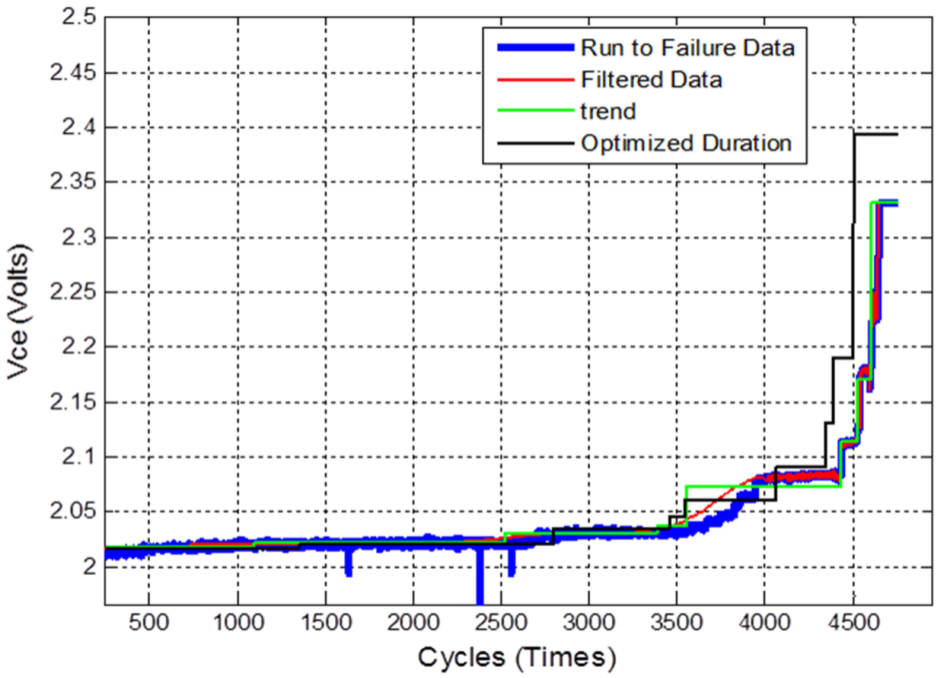

Figure 4-4 The estimated parameter tracks the trend of the IGBT data set [17]

4.2.3 Prognostics Approach

In the previous chapter, the IGBT degradation models have been developed based on probabilistic distributions and tuned using the data obtained from accelerated ageing experiments. Based on the degradation profiles shown in Figure 3-8 and Figure 4-2, the degradation process can be observed by tracking the V_{CE} measurement values. The profile indicates that V_{CE} monotonically

increases in discrete steps. In this chapter, MCS is utilised to generate the degradation paths to represent the duration the IGBT stays in different degradation phases [17].

In this chapter, the prognostics algorithm is described in detail and is shown in Figure 4-5. Feature extraction (i.e. duration), clustering, and duration optimisation using MLE functions are obtained before model estimation. The threshold value must, therefore, be defined for the propagation stage. In this regard, the ninth state is predefined as a threshold state which almost indicates the end of the component's life. This is an essential step for the data-mining process which the degradation model propagates up until the predefined threshold state.

A cross-validation technique is used to assess the accuracy of the predictive degradation model (Poisson model, Gamma model). Therefore, in this chapter, the first three IGBT samples are chosen as the training data set and the fourth as the test data. In the next iteration, the first training data set is shifted to the second training data set and the second training data set is shifted to the third and so on, until the first data set reaches the last one. The test data will then be rotated one by one for all four IGBT data sets. The PDF (e.g. Poisson function) is used to estimate the expected value using mean parameter λ value [17].

Next, nine stochastic models are built based on nine degradation phases which look similar to a Markov model structure as shown in Equation (8).

$$\frac{1}{N}\sum_{i=1}^{4}\sum_{j=1}^{9}\Delta T_{(S_j)}^{(j)} = E(\Delta T^{S_j}) \quad (8)$$

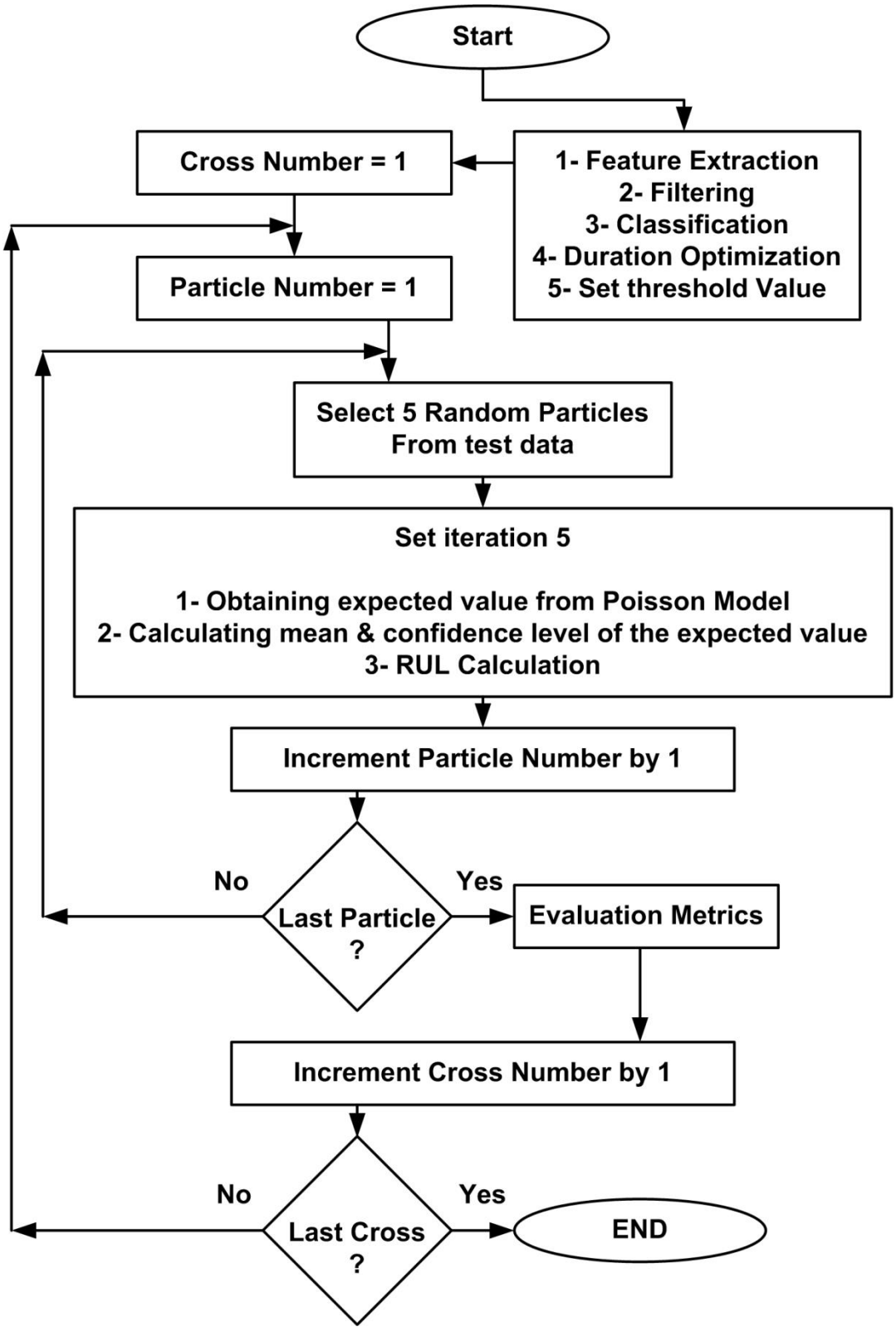

Figure 4-5 Prognostics approach algorithm [17]

After the states are parameterized by mean duration $E(\Delta T^{S_j})$ for all degradation phases (see Figure 4-6), the degradation model based on stochastic probability density functions (Poisson probability distribution) are constructed in the form of a Markov model structure, the next step is to calculate the end of life of the component [30].

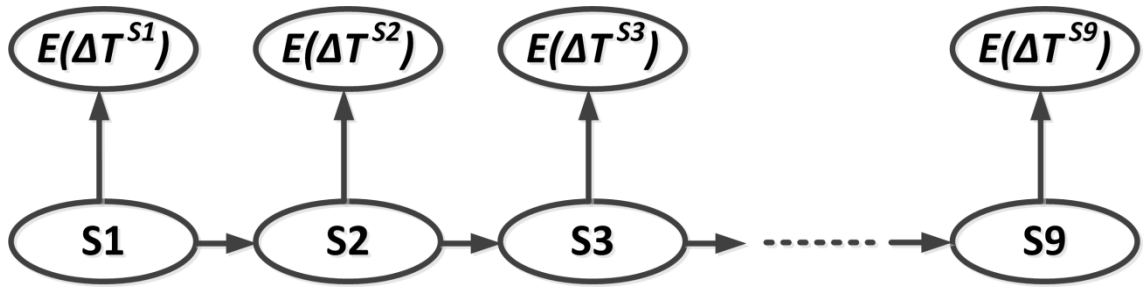

Figure 4-6 Degradation model's structure for prognostics [17]

4.2.4 **RUL Estimation**

The feasibility of RUL estimation presents as the useful life left on an IGBT component at a particular time of measurement. The approach depends on past observed IGBT degradation data which is processed to construct an estimated model based on the duration parameter of the failure data using the Poisson and Gamma distribution functions. Both Poisson and Gamma models are conducted with the same RUL estimation format. Due to this similarity, only the RUL estimation for the Poisson process is described. However, whilst both are conducted with the same process, the results for both emphasise differences in RUL calculations which will be explained in the next section. The degradation model is constructed using the Markov approach and MCS are used to estimate the value up to a predefined threshold state [117]. Then, the RUL (i.e. mean, median and confidence bounds) is calculated using the distribution of simulated RULs based on the duration of the degradation phase. Firstly, the particle is peaked up from the selected data set and propagated through the degradation

model up until the predefined threshold state 9. The propagation is iterated 5 times according to the algorithm (see Figure 4-5).

Before incrementing at a particle number, the mean of the expected value is calculated using MATLAB command Poisstat and subsequently, using Poissfit to return a 90 percentile confidence level of the optimised parameter. The 10 percentile bounds of the expected value are also calculated using Poissinv. To successfully estimate the RUL of the IGBT component, this process will continue up until the last particle of the selected test data set is greater than the length of the test data and if not, the particle is incremented by one. The same process is to be repeated for all data points. Subsequently, the process moves to calculate the prognostics evaluation metric using the RMSE method. Cross-validation is performed to evaluate the prognostics results by changing the test sample one by one after the RMSE value is calculated for each individual test sample. The RUL of the component is calculated using the operation time (opt) measured at t_0, using Equation (9), e.g. IGBT1 shown in Figure 4-7 [118].

$$\text{RUL } (IGBT_1) = \text{component life } (igbt_1) - \text{operation time } (t_0) \quad (9)$$

$$\text{C\_life } (igbt_1) = t_0 + \Delta t_{rem}^{s3} + \Delta t_4{}^{s4} + \Delta t_5{}^{s5} + \Delta t_6{}^{s6} + \Delta t_7{}^{s7} + \Delta t_8{}^{s8} + \Delta t_9{}^{s9} \quad (10)$$

where C_life is component life, and ΔT is generated by a MCS which presents the duration of the relevant degradation phase. It follows the model distribution based on the duration of the degradation phase, and it is optimised using the MLE function. As is noted from Figure 4-7, t_1 is the ending time of the last degeneration phase and is ready to jump into the next degradation. If the random value Δt_{rem}^{s3} is equal to $(E[\Delta t^{s3}] = \Delta T)$ for the duration of $\Delta T \leq t_1$, then the random value (Δt_{rem}^{s3}) would be equal to 0. In the case of $\Delta T \geq t_1$, Δt_{rem}^{s3} is equal to $\Delta T - t_1$, this means the component health state is still in this degradation phase, and it also continues in the same degradation phase [17].

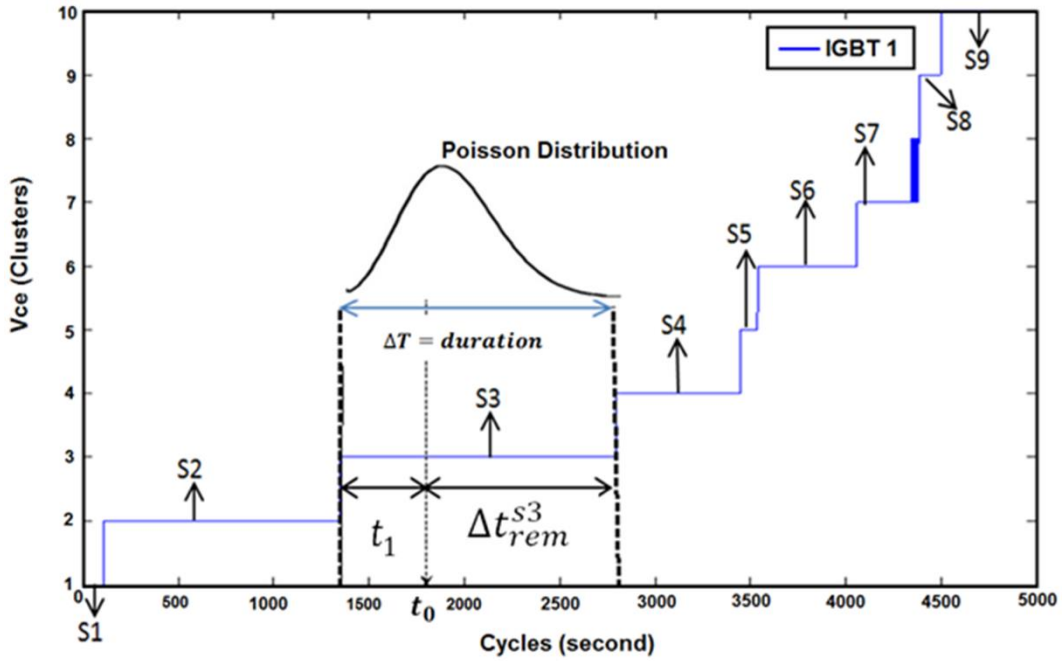

Figure 4-7 Constructed Markov model and MCS for RUL calculation [17]

4.2.5 Stochastic RUL Simulation Results

For both estimation models, the prognostics methods have tested all four IGBT data sets and the results are depicted by a series of polylines. In this process of calculation, at the beginning, the convergence of the RUL estimation is high and it will decrease towards the end of the real RUL. At each measurement point, the degradation phase of the IGBT is predicted and the end of the degradation process is forecasted.

Figure 4-8 shows the whole IGBT prediction life results, which are validated with test samples using the cross-validation technique for the prognostics results, computed using a Poisson distribution model depicted in Figure 4-8, in which the straight red line represents real RUL. The scattered red and green plots are used as ±10% confidences levels, respectively. The scattered blue line is the mean value of the RUL prediction. They are used as baselines to show the MCS results during the degradation process.

It can be noted that the 90 and 10 percentiles confidence width bonds are very narrow and unrealistically close to the mean during the whole prediction

and do not provide meaningful information for decision-makers due to the fact that the Poisson distribution does not have a standard deviation parameter. At the beginning of the execution, the mean is quite divergent and linear with sudden changes reflecting the number of discrete changes in the degradation phase but slowly becomes convergent with the real value once the V_{CE} measurement is updated and reaches the end of the component's life [17].

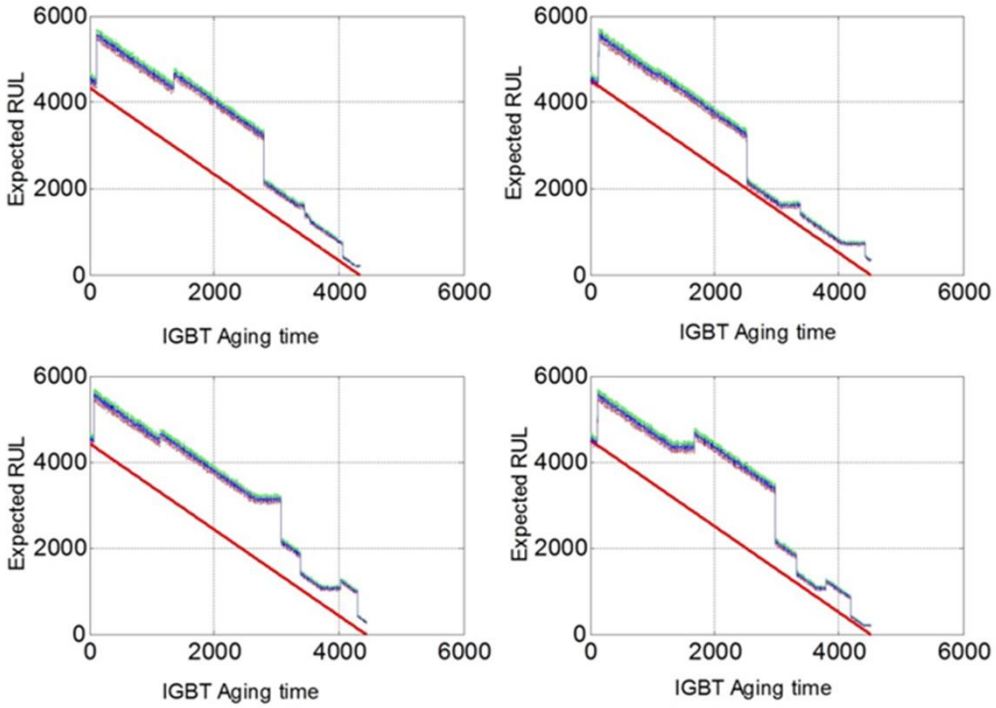

Figure 4-8 RUL prediction results using Poisson distribution [17]

In contrast to the Poisson process, initial results for the Gamma process were populated with uncertainty which provides meaningless information for the decision-maker. The reason for this controversy is the Poisson distribution's mean value (λ) is equal to the standard deviation (δ) which causes confidence intervals to overlap with the mean value. As a result, uncertainty is trapped in between the narrow confidence bounds and does not appear in simulation results. The advantage of the Gamma-based estimation model is to have such a large confidence bound which provides meaningful information for decision-makers in comparison with the Poisson process. To resolve the problem of

uncertainty, and to make the Gamma-based RUL estimation more appropriate for the decision-maker, we propose FIFO (i.e. First-In First-Out) buffering.

A FIFO buffer is a useful way to store and smooth the estimated values using averaging FIFO buffer sizes. This will conduct further care to reduce uncertainty for increasing accuracy of the RUL estimation and improve confidence bounds. Conventional estimation models are relatively inefficient in that they reserve a large amount of uncertain data and unwanted information and this will propagate for the whole RUL process calculation and become stale. This leads to ineffective pre-fetching when the Monte-Carlo method simulates the RUL estimation. We propose an alternative structure to store an estimation value in a predefined FIFO buffer size (e.g. 550 buffer sizes). All estimated data are placed at the bottom of the buffer and removed from the top. The mean buffer is maintained in direct correlation with the FIFO buffer. Thus, this method reduces stale uncertainty data and allows a more accurate reconstruction of the Monte-Carlo RUL simulation [17].

The MLE estimation value of the PDF (e.g. Gamma, Weibull distributions, etc.) is returned in a vector (i.e. phat) which contains elements $\{a_1, a_2, a_3, \dots, a_n\}$ and fetches into a FIFO buffer where the size of the buffer is optional. However, if the buffer size extends to the length of the component life, then the excess buffering of the estimated RUL causes high latency where the RUL estimation simulation is slightly off from the real RUL at the beginning (see Figure 4-10). It can be noted in Figure 4-9 that the first element fetches into the FIFO buffer frame and has shifted the next part when the second element arrives, and will continue until all buffer sizes (550) are occupied with estimation elements. Simultaneously, the mean buffer keeps recording the average of the FIFO buffer elements as it increases (see Equations (11) and (12)). Once it becomes bigger than the size of the buffer, the first element fetches out. Additionally, averaging of the FIFO buffer creates a single number at the end of the buffering that represents the typical distance where the buffer sample is from the average. This phenomenon is essentially equivalent to the DC offset (i.e. mean value). This will shift the estimated RUL , and needs to be eliminated because provides

significantly longer divergent of tracking real values. The elimination of the DC value is identical to the equation: μ−min (μ) where μ is mean value [17].

$$\text{If buffer size } = S \leq 550 \Rightarrow \{b_1, b_2, b_3, \dots, b_s\} = \frac{\sum_{n=1}^{n=s} a_n}{s} \quad (11)$$

$$\text{If buffer size } = S > 550 \Rightarrow \{b_1, b_2, b_3, \dots, b_s\} = \frac{\sum_{n=(s-550)}^{n=s} a_n}{s} \quad (12)$$

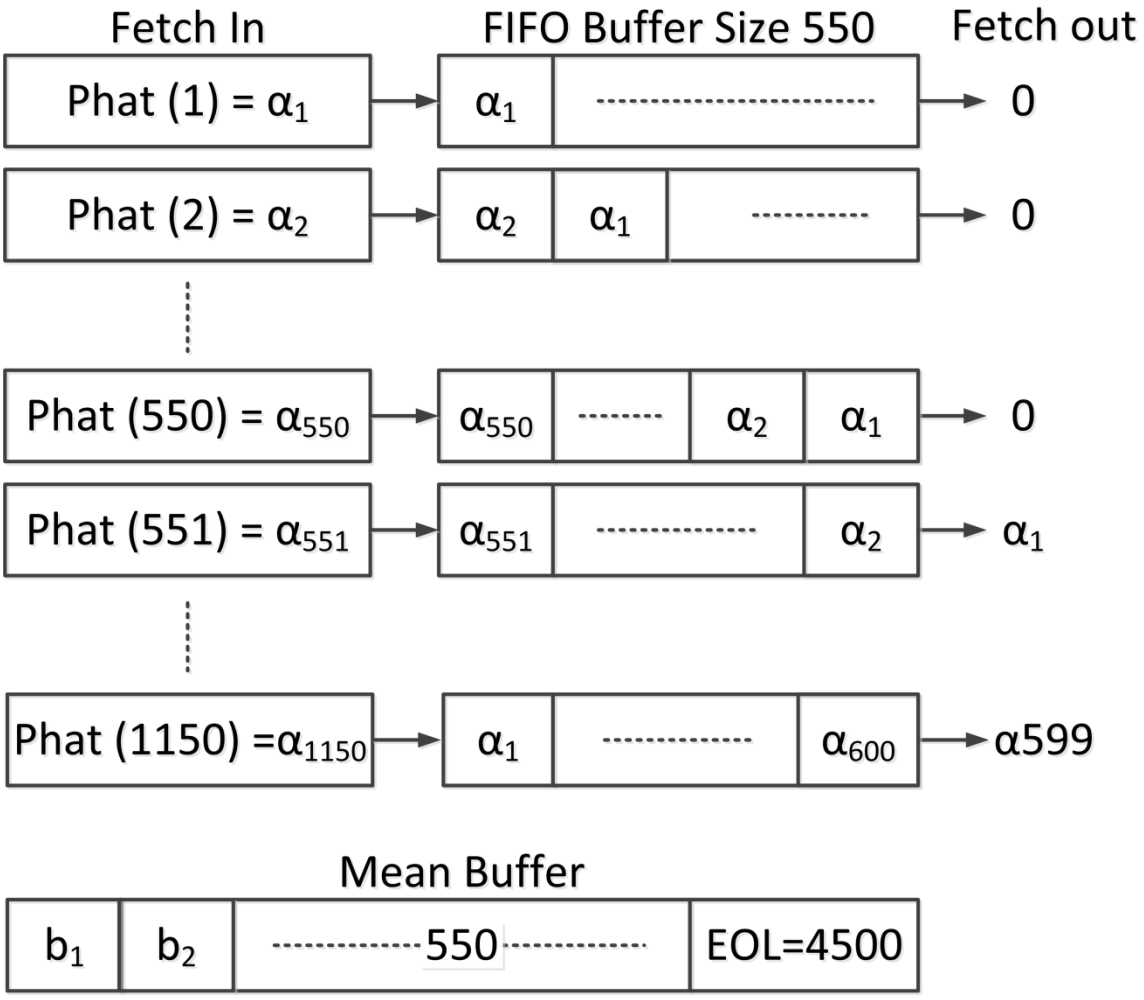

Figure 4-9 Implementing FIFO buffer for prognostics approach [17]

Figure 4-10 shows 4 IGBT samples of RUL prognostics results. The results are computed based on a Gamma distribution model with the implementation of the FIFO buffer. As can be seen in Figure 4-10, the results are promising for early failure findings and improve decision-making based on ±10% confidence

levels. The straight red dash lines are used as the real RUL values. This is used as the baseline to indicate how well the prognostics algorithm performs during the test. In Figure 4-10, the blue scatters plots are the mean value of the RUL prediction. The green and red plots are the 90 and 10 percentiles of the Monte Carlo simulated degradation paths. At the beginning of the rendering test, the RUL prediction is slightly higher than the real RUL value. However, the predicted RUL slowly converges to the real RUL values as the operating time reaches the end of the component life [17].

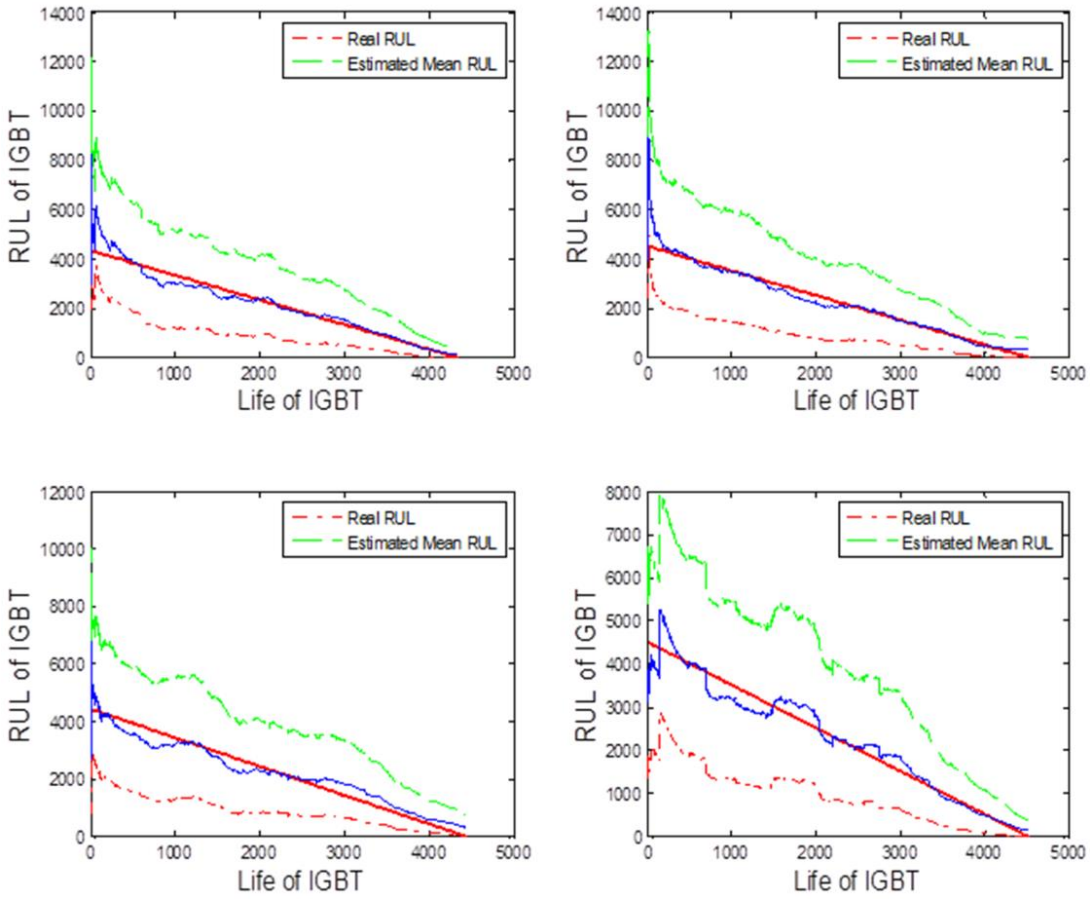

Figure 4-10 RUL prediction results using Gamma distribution [17]

4.2.6 Prognostics Evaluation Metric

The errors between the predicted and real RUL values reflect the performance of the IGBT prognostics approach. In this chapter, the prediction (or prognostics) error is defined by:

$$E_r = RUL_R - RUL_P \tag{13}$$

where E_r is the error value between the predicted and real values, RUL_R is the real RUL value of an IGBT and RUL_P is the predicted value obtained from the prognostics algorithm. Using Equation (13), the prognostics accuracy can be quantitatively calculated using:

$$P_{pr} = \frac{E_r}{RUL_R} = \frac{RUL_R - RUL_P}{RUL_R} \tag{14}$$

The difference between the estimated value and the real RUL is considered as an error and the standard deviation of the error is recognised as the RMSE value. This prediction metric renders the accuracy and precision for all prognostics methods. Therefore, in this research, RMSE is used to evaluate the prognostics results of the Poisson and Gamma distribution models [45]. A smaller value for RMSE means a more accurate result is produced by the prognostics model. If the $\hat{x_i}$ is the estimated and x_i is the real value, then the RMSE can be calculated using the following equation of mean squarer error (MSE).

$$\text{MSE} = \frac{1}{n}\sum_{i=1}^{n}(\hat{x_i} - x_i)^2 \tag{15}$$

$$\text{MSE} = \frac{1}{T_f}\sum_{i=1}^{T_f}\left(RUL_{P\,i} - RUL_{R\,i}\right)^2 = \frac{1}{T_f}\sum_{i=1}^{T_f}(Er_i)^2 \quad (16)$$

$$\text{RMS} = \sqrt{\frac{1}{n}\sum_{i=1}^{n}(\widehat{x_i} - x_i)^2} = \sqrt{\frac{1}{T_f}\sum_{i=1}^{T_f}(Er_i)^2} \quad (17)$$

Table 4-5 and Table 4-6 summarise the mean-based RMSEs of the Poisson and Gamma distribution models of the 4 IGBT samples, respectively. The Poisson model has lower RMSE values in comparison to the Gamma model. Comparing the RMSE of the predicted RULs, the IGBT test sample number 2 has the smallest RMSE value for the Poisson model, whereas the IGBT test sample number 1 has the smallest RMSE value for the Gamma model. The rest of the other IGBT test samples have similar prognostics results.

Table 4-5 Prognostics Performance Metric of Poisson Distribution [17]

RUL Estimation Metric	**IGBT 1**	**IGBT 2**	**IGBT 3**	**IGBT4**
RMSE %	0.286	0.200	0.258	0.272

Table 4-6 Prognostics Performance Metric of Gamma Distribution [17]

RUL Estimation Metric	**IGBT 1**	**IGBT 2**	**IGBT 3**	**IGBT4**
RMSE %	0.3317	0.3397	0.3485	0.3319

4.3 Summary

In this chapter, the prognostics algorithm represents a Monte Carlo RUL simulation and is based on a Markov stochastic duration model using Poisson and Gamma distribution functions. The $V_{CE\,(ON)}$ is chosen as the best degradation indicator and precursor parameter. A degradation profile is obtained using the duration of the degradation process and the degradation phase is parameterized for the PDF to be integrated into the prognostics algorithm for RUL estimation. It can be seen that the algorithm is capable of recalculating the RUL based on

the measurement updates and merging it with the real RUL profile. The RMSE result indicates a good prognostics performance using the cross-validation technique. In contrast to the Poisson process, the Gamma process needs FIFO buffering for the improvement of the prognostics results as uncertainty was an issue with the Gamma process. In contrast to current state-of-the-art prognostics, this thesis represents a light-weight simulation-based prognostics approach because the RUL calculation takes less time, about 0.3 ms for each measurement point. Therefore, it could be implemented efficiently in a real-time prognostics calculation and is capable of providing an advanced failure warning and preventing costly power electronic system downtimes and failures [17]. The next chapters will discuss hybrid prognostics approach to developing degradation models with the TDNN approach and fuse the MCS for calculating the area under the estimated IGBT's TDNN degradation model for RUL estimation and present the proposed RUL algorithm.

5 IGBT Hybrid Prognostics Model

This chapter bases its study on failure data sets derived from a power cycling test rig wherein IGBTs were exposed to cyclic temperatures similar to those encountered in railway traction applications. We introduce an approach for the development of a time delay neural network for failure modelling using health state classification fused with probabilistic Monte-Carlo RUL simulation, thus enabling a significant reduction of the uncertainty occurring from an incomplete failure model and enhancing the clear indication of the current health state as well as an improvement the RUL calculation. This has been successfully employed in the accurate and robust prediction of the current degradation of the device and allows better decisions to be made regarding scheduling of maintenance policies in IVHM.

5.1 The Motivation of the Hybrid Model for IGBT

The collection of data requires accelerated ageing tests which are used to fail device parts at high temperatures in a shorter time frame under various working conditions, such as high baseplate temperature (60°C to 100°C) and large temperature swings (60°C to 120°C), these values depending on system applications. In an accelerated ageing test, the particular wear-out mechanisms which are of interest accelerate to cause failure. The part/device is monitored throughout the test, noting the critical parameters for the particular device. Accelerated ageing tests which are used to obtain a detailed understanding of IGBT failure modes, and in turn, determine parameters are indicative of the various failure mechanisms. Employing these precursor parameters are prerequisite to develop a forecasting model for observing significant changes in the current health of the device and predicted failure [95]. However, precursor

parameter identification for power electronics prognostics is challenging due to the representation of the uncertainties in the degradation profile for the precursor parameter. The precursor is also used to monitor direct or indirect failure mechanisms trend in order to enable the prognostics model estimates the longest possible remaining useful life (RUL). This tool is applied to facilitate the power electronics with predictive maintenance. Hence, an advanced approach to the development of a prognostics tool for IGBTs is required. This could then be used to forecast failures, improve system life and reduce unnecessary maintenance [119].

Following the identification of parameters which are a precursor to failure, the feature extraction (i.e. mean, median) and clustering of the collected data (i.e. finding the number of states for the degradation profile) are carried out to provide information for training a prognostics model. The trained model is given a predefined threshold value which is used in the prognostics algorithm. Data-driven methods are subjected to two different approaches. The first approach is known as a direct estimation of RUL in which the model learns directly from the damage data set. In contrast, the second indirect approach initially needs to estimate a damage progression model and then propagates the expected data through the model until a predefined threshold for the RUL is reached. The difficulty with the second method is that obtaining a reliable data set is often challenging due to the diverse devices and incomplete knowledge of the component [2].

Following the classification/clustering step, a damage model is created using data-mining techniques that ultimately models the failure mechanisms of the IGBT. Although there are a number of popular conventional numerical methods (such as KF, PF, machine-learning approaches, support vector machines [120], etc.) used for developing degradation models in a wide range of different applications, only a few of them have been employed so far for the modelling of degradation of IGBTs. A Kalman Filter tunes and updates the parameters of the model on stream noisy input test data for linear systems. In contrast, a PF updates the parameters of the model with the most weighted

samples generated from a probability distribution of the system which mitigates the degeneracy of particles by a number of iterations.

In general, developing a versatile physical model for both the KF and PF is necessary to present a degradation model that avoids the main disadvantages of both techniques. The KF can be a good estimator if it is given a precise state-space model which constructs from all interpretable unobservable dynamic parameters of the component. Overall, imprecise knowledge of the model parameter and inaccurate initialization of the filter lead to inconsistency with the true component failure model [121]. Our proposed hybrid prognostics approach overcomes the complexity of developing the PoF, learns the degradation pattern online, and adapts itself with the dynamic of the parameter trend which will create a robust failure model.

In [26], Patil et al proposed early anomaly detection implementing MD using on-state collector-emitter voltage V_{CE} and collector-emitter current (Ice) as precursor parameters and a PF approach to calculating RUL before catastrophic failure occurs. Patil et al present an anomaly detection parameter which is used as a diagnostic parameter. However, the mean time of failure estimation has considerable divergent from failure parameter. The RUL accuracy evaluation metric involves on-going examining the estimation results. Evaluation is just conducted from anomaly detection till the predefined failure threshold thus, the efficiency of the results will be expected highly greater than 21% prediction error and less precision.

Celaya et al develop a prognostics algorithm technique using an extended KF for a MOSFET component [1]. The algorithm claims to be a versatile candidate for component-level RUL calculation. The on-state resistance of the device is chosen as a precursor parameter which has increased due to die-attached degradation process. The accuracy of the prognostics results has been challenged using evaluation metric relative Accuracy (RA).

In [18], Saha et al implement a PF to calculate RUL and use the Monte Carlo (MC) method for simulation results. The reliable run-to-failure data set

was obtained by conducting thermal overstress accelerated ageing tests on an IRG4BC30KD IGBT. A third-order polynomial fit of the tail of the Ice waveform was used to create a failure precursor model. In [18], data manipulation and model-based learning using regression analyses were performed while offline. Furthermore, the PF has implemented on a model-based approach for just the tail of the collector-emitter current parameter which has less duration of POF. This will not be appropriate estimation either for predictive or corrective maintenance Saha's model has not been developed for the entire degradation process and the strategy of failure model learning close to critical condition will not be applicable for maintenance decision-makers.

5.2 Testing Significance of IGBT Data Set

The Chi-squared goodness-of-fit is a robust statistical test used to examine the difference in relationships between nominal variables. In this case, it is used to validate the significance of the expected distribution for the given data set. The chi-square test is named after the British statistician Karl Pearson to analyse the probability of the bet on a roulette wheel in a Monte Carlo casino. This testing method is used in the s number of IGBT samples $B1, \ldots, Br$ have n data points $X1, \ldots, Xn$ into these samples independently of each other with probabilities:

$P(Xi \in B1) = p1, \ldots, P(Xi \in Br) = pr$, so that $p1 + \ldots + pr = 1$

Let v_j is the number of data points in the j^{th} sample:

$v_j = \#\{\text{data points } X1, \ldots, Xn \text{ in the sample } Bj\} = \sum_{i=1}^{n} (Xi \in Bj)$

Then, the expectation of the random data points in the j^{th} sample will be np_j since

$\mathrm{E}v_j = \sum_{i=1}^{n} EI(Xi \epsilon Bj) = \sum_{i=1}^{n} P(Xi \epsilon Bj) = np_j$

Convergence in distribution of the data set is close if the computed statistic test is not large and the null hypothesis H_0 is true. The distribution of the data fits with the expected distribution if the variables are independent. By the theory of the Pearson says that we know the random variable of the last sample if we have the number data points for s-1 sample.

$$\sum_{j=1}^{s} \frac{(v_j - np_j)^2}{np_j} = X^2{}_{r-1} \tag{18}$$

During the prevalent power, cycling accelerated the ageing process, emitter wire bonds were lifted off and damaged. The collector-emitter voltage on state tracks the degradation and is presented as the precursor parameter for developing IGBT prognostics in this thesis. During the duration of the degradation process, the $V_{CE\ (ON)}$ measurement shows an increase in non-monotone fashion in discrete steps with noise until the failure of the IGBT. The V_{CE} indicates failure as a quick rise at the end of the ageing process. Data collection has been successfully carried out for 22 IGBT samples which can be used as a promising data-mining tool. The trend of the raw sensory of time series data indicates useful and meaningful pattern which can be used for the statistic judgment. The histogram of all samples indicates the normal distribution is the most appropriate statistical distribution, but for simplicity, only four of them are shown in Figure 5-1. The chi-squared has been used to validate the goodness of fit test, and the results are recorded in Table 5-1 [122].

Table 5-1 Chi-Squared Hypothesis Testing [100]

Probability Distribution	**Weibull**	**Gamma**	**Poisson**	**Normal**
H	1	1	1	0
P	0.0336	1.5169e-25	2.4599c-13	0.1542

It is noted that the null hypothesis (H=goodness-of-fit to PDF) will be accepted if the H value is zero and P=U [0, 1] greater than the default value at significance level a=0.05. To this end, amongst all data sets, the four IGBT raw data sets for simplicity of computation and testing have been chosen and are shown in Figure 5-3. The y-axis represents the V_{CE} (voltage) value, while the x-axis represents the number of cycles (time), and cycle duration lasts for 6 seconds.

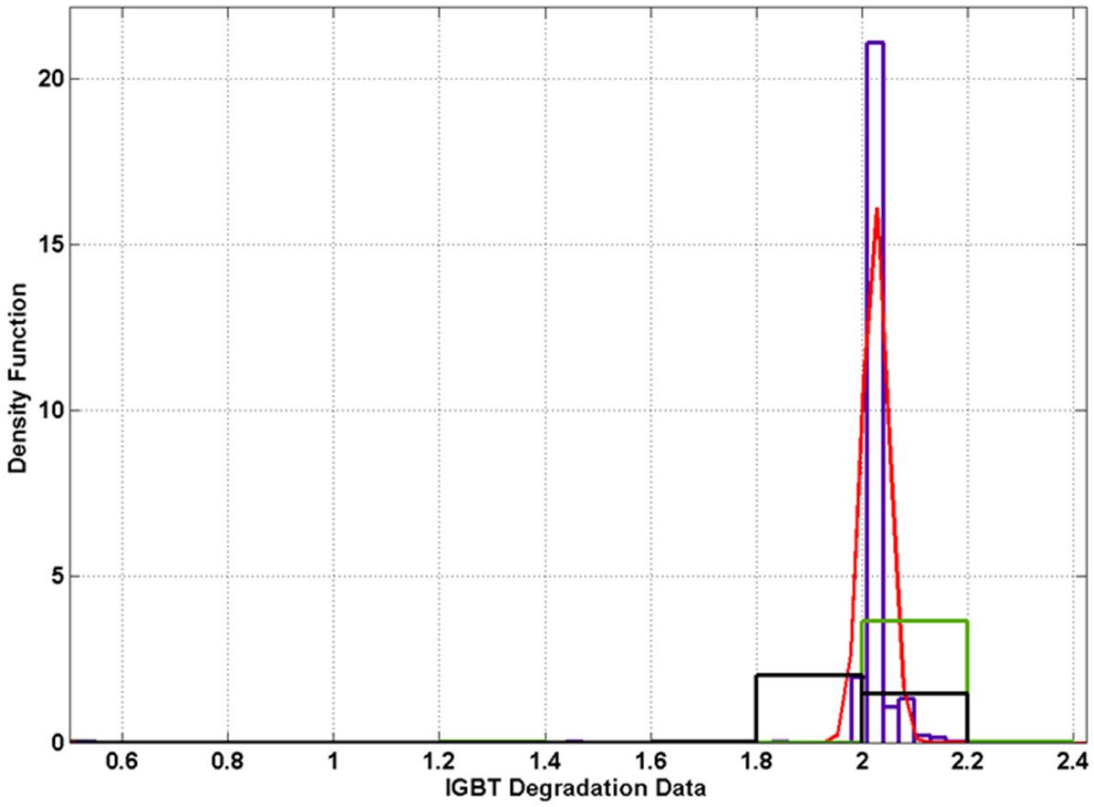

Figure 5-1 Normal distribution best fit to IGBT sample [100]

5.3 Developing the Degradation Model

Figure 5-2 depicts the overall process of the data-mining algorithm development for the IGBT data sets collected from power cycling experiments. Initially, a model is structured from the training data set using artificial neural networks (TDNN, neural fuzzy network, etc.). Subsequently, the trained model is used with the test data to estimate the current health of the component. This process continuously tracks the degradation health state of the component and is used as a performance degradation assessment [123]. This is then used with a trapezoidal rule for calculating the area under the estimated curve to predict the remaining useful life of the IGBT (discussed in more detail in the next section). The outline of the algorithm is described in Figure 5-2.

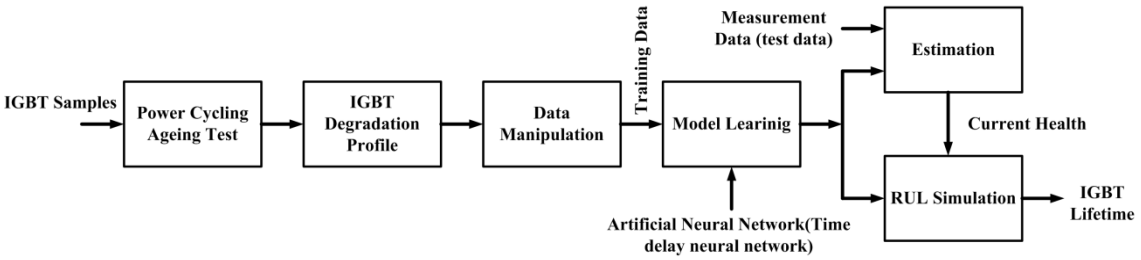

Figure 5-2 Outline of the proposed data-mining prognostics approach [100]

5.3.1 Discretization of Ageing Data

Figure 5-3 shows the filtered V_{ce} for four different IGBTs utilised in this thesis. From this figure, it is noted that the data set is comparatively clear and separated into several discrete states possess different deterioration of the IGBT health states. However, the following initial life durations are recognised:

A flat region where a more and less the ageing process began at a signal amplitude of approximately 2V. This region is representing the IGBT's healthy condition for the duration of 2,500 cycles.

A monotonic region where the region was characterised right after flat region by a monotonic increasing trend until reaches discrete manner.

An early degradation sign where the degradation process has clearly progressed in increasing discrete steps until IGBT failure has occurred at about 2.4V.

Failed where the IGBT reaches to failure region after 4,500 life cycles. The life of the IGBT decreases when the amplitude of the V_{CE} has increases abruptly beyond the initially-defined amplitude level corresponding to the healthy normal condition. The degradation process is discretized using a uniform quantization process [22] and each degradation state increases about 0.054V in a discrete manner which corresponds to one wire bond lift off and is due to one bond wire cut off [124].

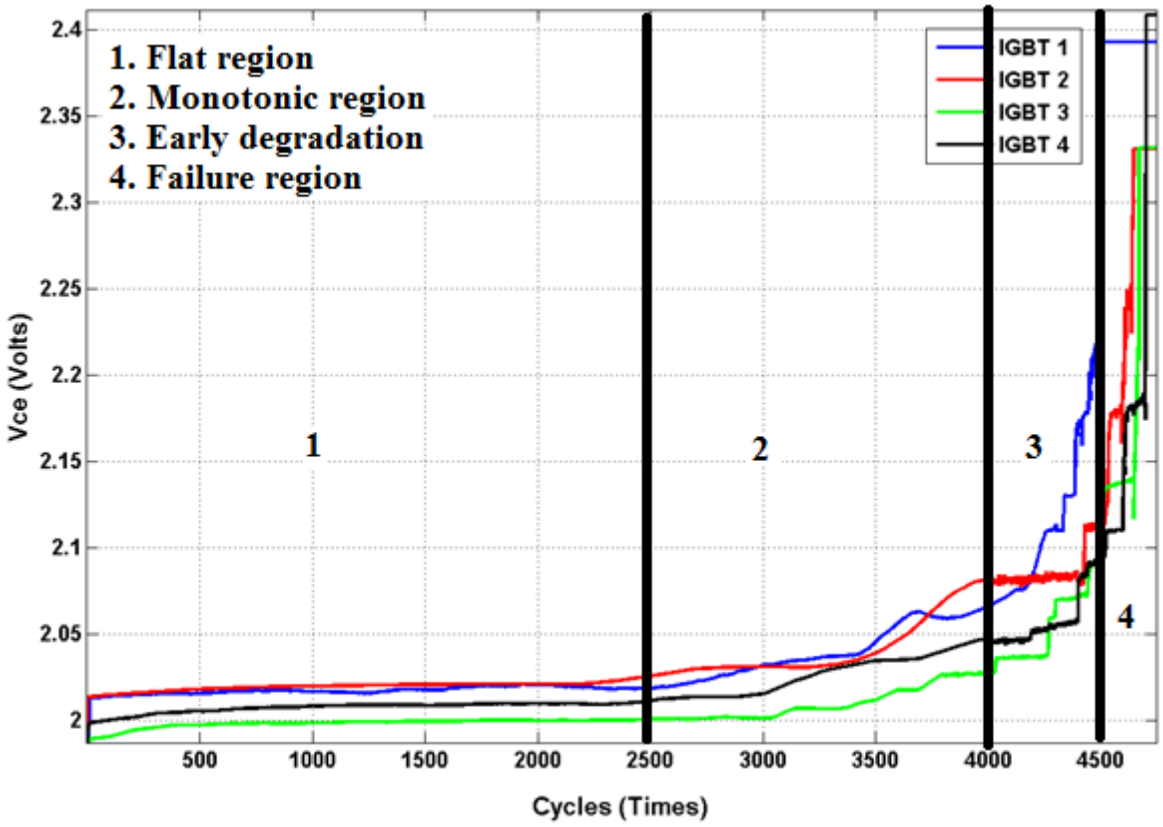

Figure 5-3 Outline of the proposed data-mining prognostics approach [100]

The degradation process is characterised by increasing discrete steps of the V_{CE} (from noise-free data) where the step of each degradation phase is uncorrelated to the subsequent phase. Using a quantized cluster validity index, the phase durations of the run-to-failure of four IGBT samples are obtained and

recorded as given in Table 4-1 IGBT Degradation Phase Duration [17]. The best number of the failure progression occurs at the tenth health state. Thus, degradation undergoes 10 degradation phases using a uniform quantization process for all four IGBT samples wherein each phase lasts for a period of time before the degradation progresses further to the next phase. The next step is about the optimisation of the number of clusters for all IGBT samples.

Genetic algorithms (GA) are robust search engine algorithms that are inspired by the evolutionary idea of genetics (e.g. natural selection). As such, the search engine evaluates the best solution to historical information based on optimising a set of variable parameters or a minimised cost function or a measurement error. The algorithm is typically used for nonlinear problems and is not meant to treat the independent parameters. Therefore, the combined parameters have been taken into account in order to maximise the output [100].

In this method, the GA-based clustering maintains 10 *code vectors* $(C_1, C_2, C_3, \dots, C_i)$ that are assigned to each cluster. And, they are also associated with the sum of the Euclidean distance of the each cluster centres. Select the best fit of the n cluster centres of the raw data set. Then, the clustering can be performed as a solution from the natural evolutionary process to sum the object 'X' with the cluster centre 'C' by appending Euclidean distance. The evaluation of clustering attains the high intra-clustering which a clustering metric 'D' for n number of clusters is:

$$D_{in} = [d_{i1}^n, d_{i2}^n, d_{i3}^n, \dots, d_{i10}^n] = \sum_{i=1}^{n} \sum \|Xin - Ci\| \quad (19)$$

The GA (see Figure 5-5) attempts to minimise the clustering metric. The algorithm searches for optimal validity which then uses the crossover (uniform crossover) as a probabilistic approach for a number of iterations alongside mutation (i.e. substituting a random *code vector* with the training vector). This entails swapping new cluster that addresses the appropriate cluster centre and continues till when to validate validity index as 10 cluster data sets, as shown in Figure 5-4 [125].

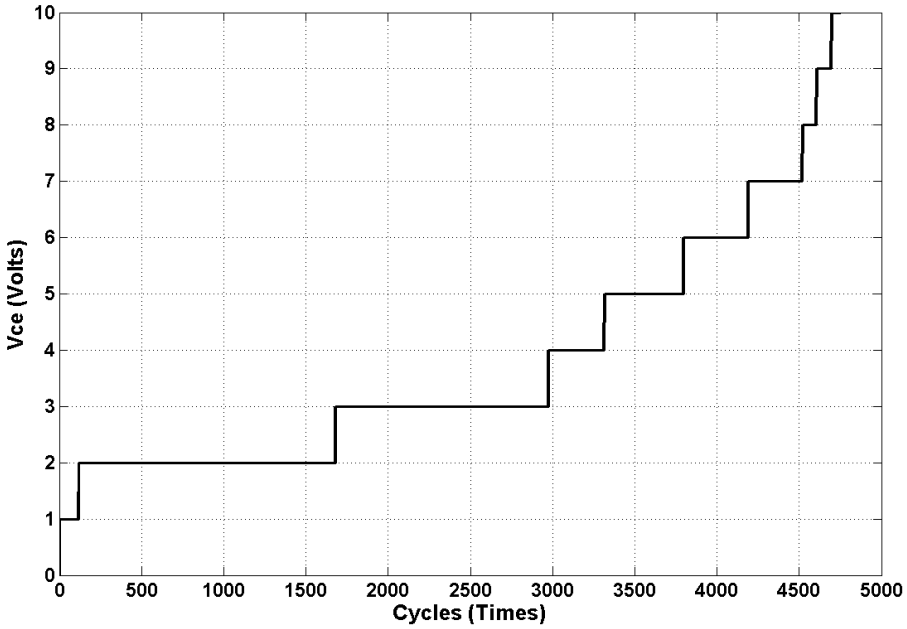

Figure 5-4 Degradation phase after optimisation process [100]

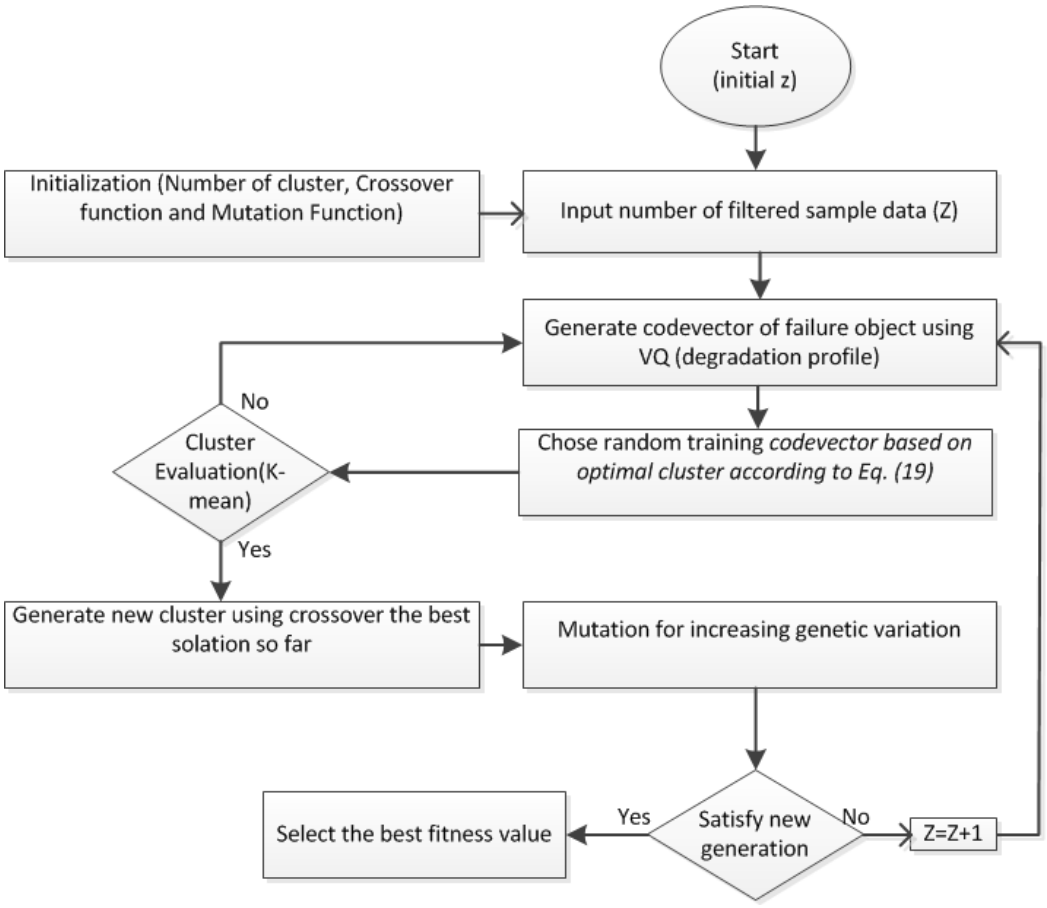

Figure 5-5 GA process

5.3.2 Problem Formulation with TDNN

Time delay neural networks were initially used in speech recognition. TDNN architecture is constructed of mapping a finite number of times series data input into a single output as being shared with weights. It is inspired by feedforward networks but equipped with tap delays of the input's signal which presents the input at a hidden layer at a different time sequence. Thus, it appears as an Auto-Regressive Moving Average model (ARMA).

$$X_t = ß + \sum_{i=1}^{N_D} \sum_{j=1}^{N_P} \emptyset_{ij} X^j{}_{t-i} + \sum_{i=1}^{N_\varepsilon} \theta_i \varepsilon_{t-i} \quad (20)$$

$\sum_{i=1}^{N_\varepsilon} \theta_i \varepsilon_{t-1}$, which is a moving average (MA) part, consists of a series of linear combination of N_ε 'noise' signals, so that ε_{t-1} is a sequence of errors with a constant factor θ_i. As degradation is not limited to linearity as a non-stationary time variant, assume the network forms a non-linear autoregressive model (NAR). Thus, $\sum_{i=1}^{N_D} \sum_{j=1}^{N_P} \emptyset_{ij} X^j{}_{t-1}$ presents a non-linear autoregressive part where N_D is assigned for a number of delays and N_P is the number of polynomial orders. Both ß and $\emptyset_{ij}$ are the constant variables in NARMA and X_{t-i} contains information about the previous input delay as the memory for the network.

A TDNN model is used in this thesis because the IGBT degradation curve of V_{CE} has followed non-homogenous sequential dynamic process data which renders the occurrence of a random event, and this can be efficiently modelled into each individual defective voltage. A TDNN is well defined for deep learning prediction of the model involves with the dynamic of the failure model. The dynamic of the model is stored using time-delayed tap and the nodes are updated by using recursive feedback from the output to the input at the nodal levels for each iteration. As an advantage, the nonlinear relationship feature of the prediction model that incorporates the input parameters and the output parameters can be eased off efficiently. The TDNN is then adapted to associate the prediction model with the complex relationship between multivariate inputs and outputs. This is one of the main advantages of the neural network in general

in that the physical phenomena of the complex system with non-linearity dynamic behaviour can be ignored. And, this effectively recognises the model between multi-dimensional inputs and outputs with unsupervised training. However, this can be a drawback for this technique as the model is unable to interpret the backbone of the physical performance of the system [74]. To include dynamic features of degradation processes and failure mechanisms into the model, the drift voltage (Δv_{ce}) of the degradation is considered to be an index of health states, which if not equal to zero, can be presented as wire bond lift off process. The duration of each degradation process is used as an associated failure time $\lambda_i^{N_i}$ for the input of the TDNN model [126]. The topology of the proposed TDNN model (see Figure 5-6) is comprised from one layer for each input and output. And, one hidden layer with four number of delayed of inputs signals (V_{CE} and ΔV_{CE}) which are introduced to the input layer. All the layers are connected with appropriate weights [127].

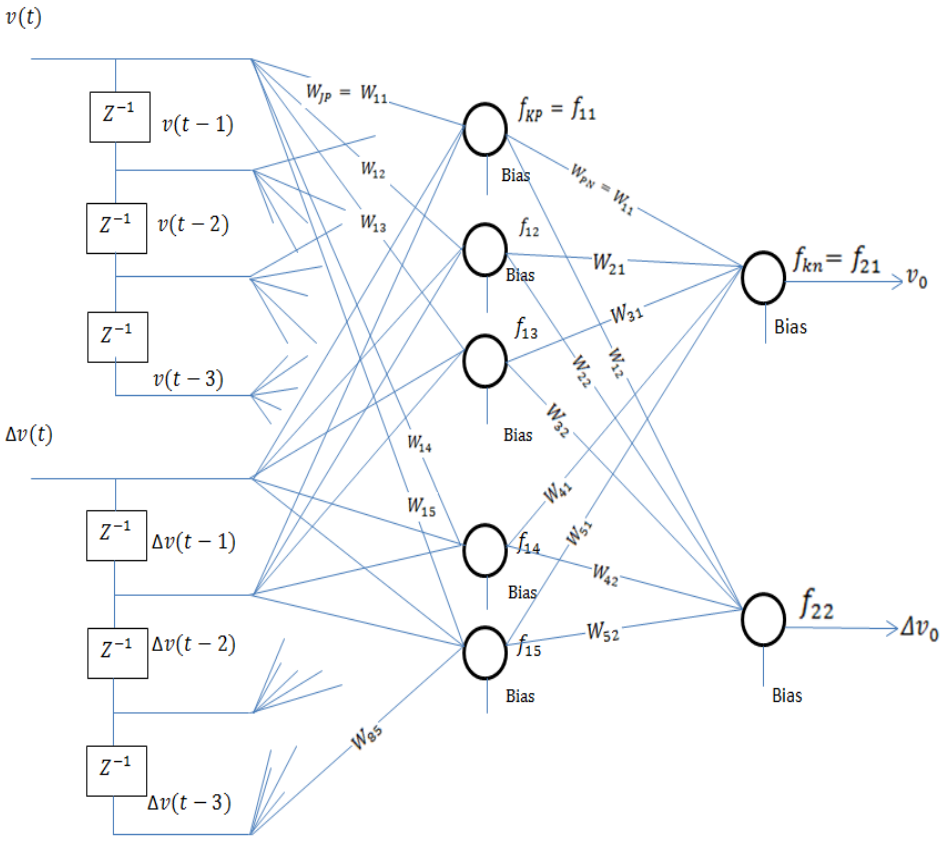

Figure 5-6 Architecture of the proposed TDNN model [100]

The proposed TDNN model directly uses V_{CE} (on state) measurement values and the rate of the measurement is changed, i.e. dynamic of the actual measurement at current inspection t and previous inspection points $t_d = [(t-0), (t-1), (t-2), (t-3)]$ assigned as the inputs' time delay. The model takes into account all these measurement points and changes of the measurement points, all at the same time and at three previous measurement points in order to develop a precise model for prediction of the future health state of the IGBT component in real time. Increasing the number of input nodes would add on more weights and be time-consuming for optimisation of the weights. Consequently, model training which has more inspection points would not improve the model's estimation capability.

The neurones' functions are set as $f(\sum_m (a_m w_m))$ where f is the neuron's activation function as sigmoid $(1 - \frac{1}{e^x})$ and w_m is the synapses' weight associated with the mth input of the neuron in general. Hence, the neuron's output at the hidden layer is constructed in Equation (21) [128] as f_{kp} where K={1, 2} is the layer's number (k=1 for hidden, and 2 for output layer); p={1, 2, ..., 5} is the neuron number at the hidden layer. The synapses' weight between jth input neuron (j= {1, 2, ..., 8}) and the pth neuron at the hidden layer is presented as W_{jp}. Considering two sets of delayed inputs from v and Δv, the neuron's output at the hidden layer is given by Equation (21) where k=1, and time delay t_d with d={0, 1, 2, 3} [129], [130]:

$$f_{kp} = \sum_{P=1}^{5} f_{1p} = \sum_{p=1}^{5}(b_{kp} + f((\sum_{j=0}^{3} w_{(j+1)P} v_{j(t-t_j)}) + (\sum_{j=0}^{3} w_{(j+5)P} \Delta v_{j(t-t_j)}))) \quad (21)$$

where W_{jp} is a two-dimension matrix constructed from all synapses' weights between inputs and the hidden layer's neurones:

$$W_{jp} = \begin{bmatrix} w_{11} & \cdots & w_{15} \\ \vdots & \ddots & \vdots \\ w_{81} & \cdots & w_{85} \end{bmatrix}$$

Similarly, the outputs of neurones, f_{kn}, are obtained from Equation (22) where k=2, n={1, 2} is the neuron's number at the output layer, and W_{Pn} is the synapses' weight between the pth neuron at the hidden layer and the nth neuron at the output layer. The f_{kn} forms the output model of the TDNN which describes the estimation and dynamic of the process using the initial constructed model [36].

$$f_{kn} = f_{2n} = \sum_{p=1}^{5}(b_{2p} + f(w_{pn}f_{1p})) \quad (22)$$

where W_{pn} is a two-dimension matrix constructed from all synapses' weights between the hidden layer's neurones and the neurones of the output layer:

$$W_{pn} = \begin{bmatrix} w_{11} & w_{12} \\ & \vdots \\ w_{51} & w_{52} \end{bmatrix}$$

A TDNN topology including all the synapses' weights and parameters of the neurones' activation functions are predefined to fit in the condition monitoring failure measurement. Then, the four IGBTs' ageing data set samples are used for training the model using cross-validation techniques. During the training process through a number of iterations, the model is adjusted with the weights and biases to converge the output of the desired model and optimisation is performed to minimise the error as much as possible to render the best-fit prognostics model. To that end, MSE is used to evaluate the performance of the desired model to computed output values. The model is trained by 150 iteration times and the MSE incredibly becomes increasingly lower where the final estimation error reaches 0.0333 and the gradients of the output model with respect to weights obtained by $\frac{\partial f_{kn}}{\partial W_{pn}}$ is optimised with Levenberg-Marquardt. The details of the LM for optimisation of the TDNN can be found in [131].

5.3.3 Procedure of Learning Algorithm of the Proposed TDNN

The procedure of the proposed TDNN method is shown in Figure 5-7. The explanation of the flowchart of the proposed algorithm is provided below [132], [114]. The flowchart is executed with the following three steps: 1) data manipulation; 2) model training; 3) propagation.

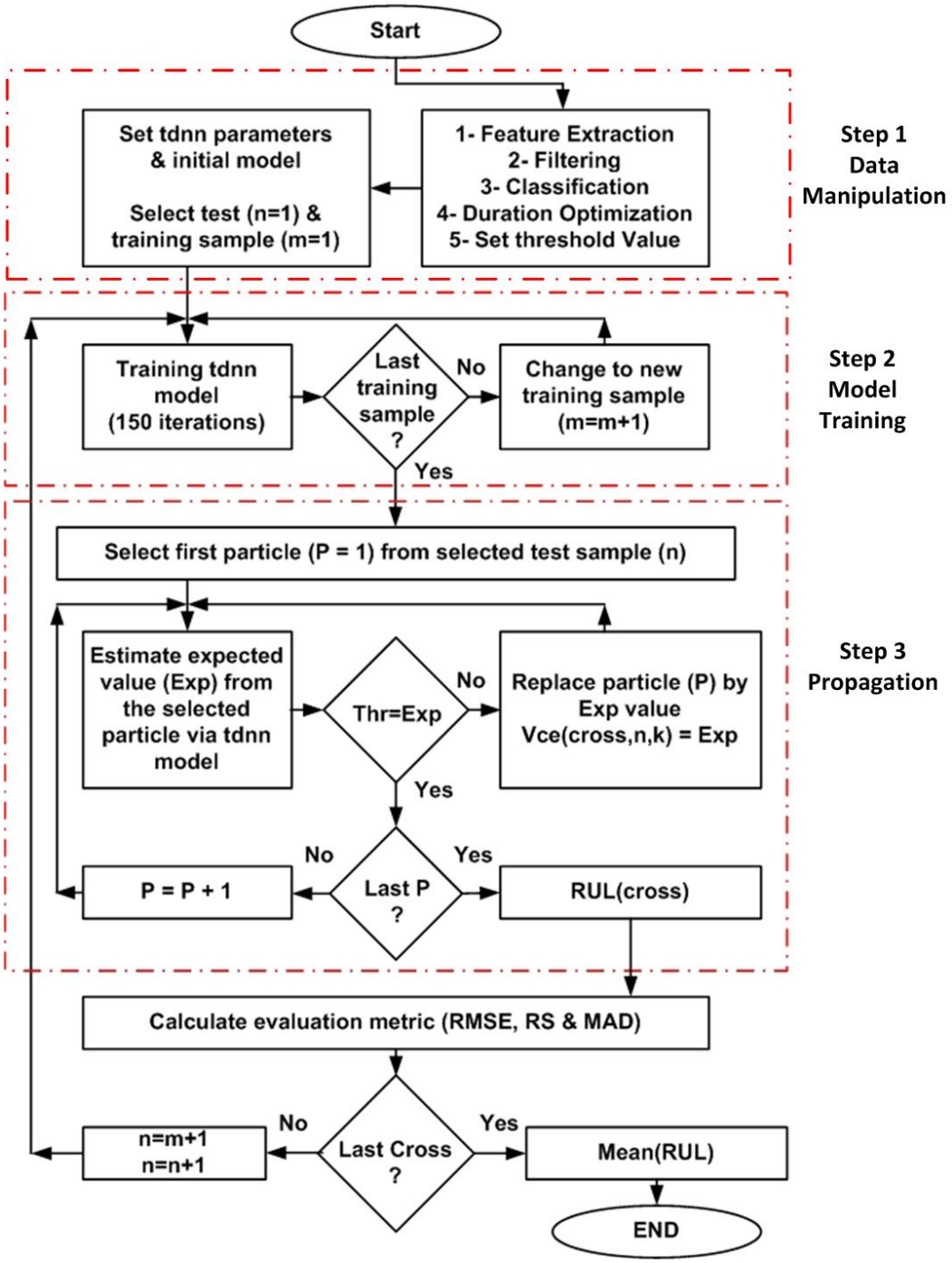

Figure 5-7 Algorithm of the proposed TDNN method [100]

Step 1: We start from the available run-to-failure IGBTs' historical data, which includes the degradation process values from the precursor parameter V_{CE} at inspection points for the power cycling ageing measurement. The low-pass filter is used to filter the noises that are populated inside the data set. The duration of the degradation phase for all data sets is optimised using maximum likelihood estimation, the results of which will be used for the classification using K-mean clustering on the data set. The threshold value is generally set based on expert knowledge, in this case at three times greater than the standard deviation of the flat region where the degradation exponentially starts to rise with a rapid gradient.

This almost deviates by ±15% from its original value [62]. In this dataset, we attempted to set the threshold state at 7 that is almost the critical discrete level. This will represent the catastrophic failure in order to validate the prognostics model and algorithm. The classified data for a failure history is used for the development of the TDNN to estimate the future health state of the IGBTs in real time. The model starts to build up with two input parameters V_{CE} and ΔV_{CE} in conjunction with two hidden layers where the first hidden layer includes 5 neurones and the second layer contains 2 neurones. The two input parameters are assisted with three tapped delay lines as embedding local memory into both the input and hidden layers which provide the dynamic ability to the model structure. The first data set (m=1) is peaked up for training the TDNN model and the second data set (n=1) is chosen as a test data for model validation [133].

Step 2: Training the TDNN model is a stochastic process and depends on the initial weights and is adjusted using the LM method which also requires the training data set and the testing data set. The training of the model is conducted using time series data and the difference in time-related to the pattern, to estimate the number of the sequence of states that corresponds to the currently observed health state for 150 iterations. The training process is completed using cross-validation techniques surely due to the overcoming dissatisfaction of availability of a lower number of data sets. Therefore, all data sets are

partitioned to be used for both training and testing which limits the overfitting model with the training data set. The last training sample is checked before the data set reaches the last data set (Cross Number) for testing. And, if Cross Number is remaining, thus, the learning algorithm continue simply run both the training and the testing sample incrementing by one. This process repeats until 4 failure histories to construct the TDNN training model and validation of the model (see Figure 5-8 for the cross-validation; cross=1,..,4). Four failure history data sets are divided into three training sets and one testing set. The model learns from three samples and is validated with one sample and the learning model will replicate once the first sample becomes the last sample/last cross in the algorithm for validation. The model learns to estimate the failure degradation phase but if the current health state based on the measurement point needs to be identified, then the mean of the RUL results from each of validation represents the final results [100].

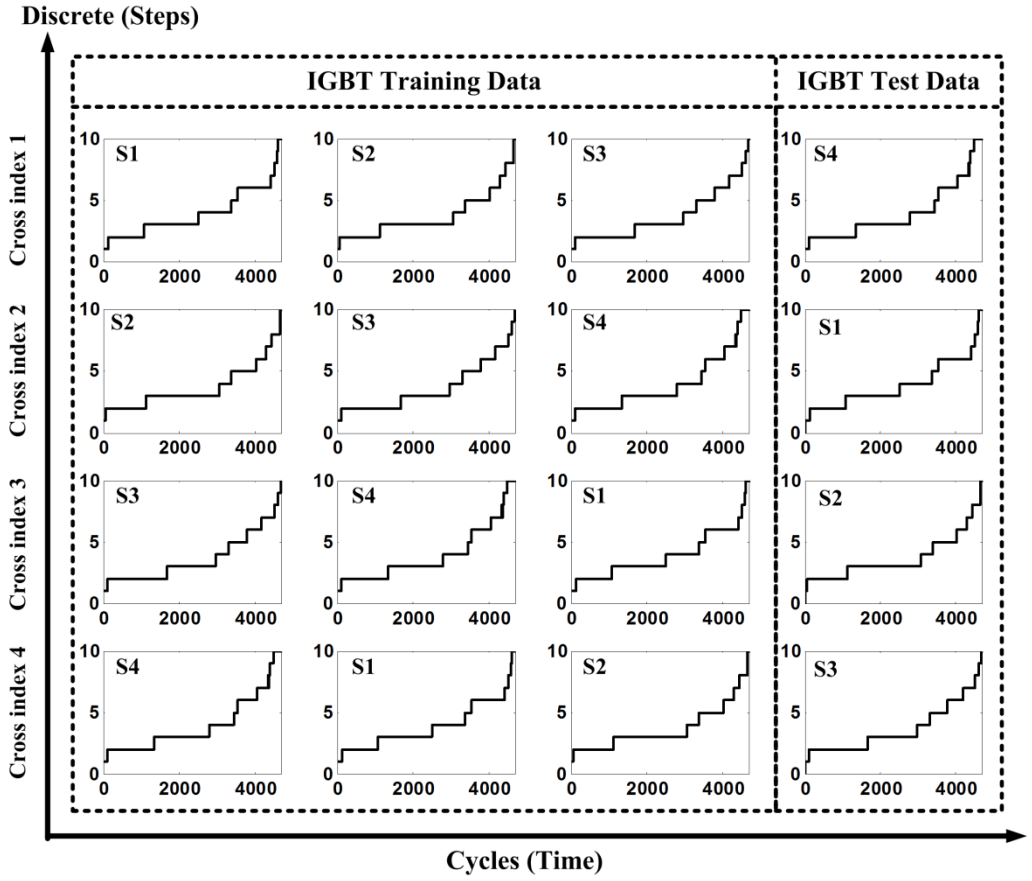

Figure 5-8 TDNN training and testing modelling for IGBTs' failure data set [100]

Step 3: The end-of-life (EoL) of the IGBTs can be calculated by peaking up the first particle from the selected data set as the measurement value at the current state which will be propagated through the degradation model until the threshold value. The availability of the new inspection particle will be checked out once the estimation value reaches the predefined threshold value if the new inspection particle is available. Therefore, the number of particles will be incremented by one until the last particle. The propagation process continues when the measurement point is greater than the length of the last particle and it then moves to calculate the RUL and then the prognostics evaluation metric, such as RMSE, RS and MAD. If the expected value or estimated value has not reached the threshold value, then the current inspection particle will be updated by an estimated value of the measurement parameter. As the recursive algorithm progressing the degradation phase until it reaches a significant promising threshold state. The LM algorithm for the TDNN training is run four times, and the trained TDNN corresponding to the lowest prediction performance MSE after 626 epochs is 3.9805e-06.The prediction performance is shown in Figure 5-9, which is almost mapping the test data (e.g. input measurement data) to the train TDNN model [100].

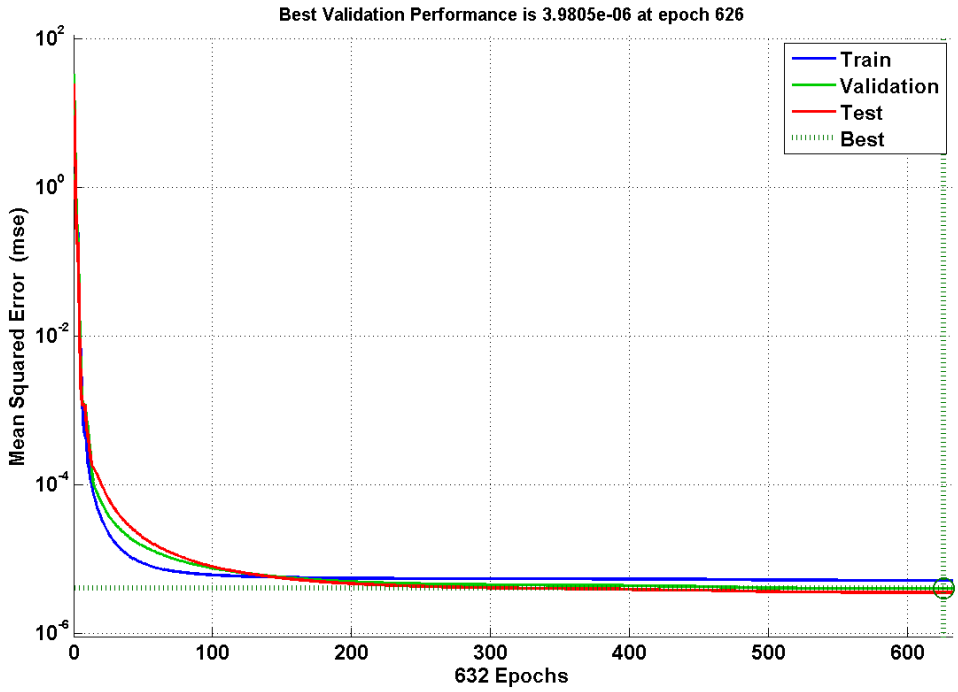

Figure 5-9 Performance of the proposed TDNN [100]

The degradation duration for the estimation model is quite random for each testing model and the number of degradation phases varies slightly. The estimation degradation is assumed to have followed a probability distribution. Given the fact that all samples are comparatively continuous time series data sets, therefore as a solution, normal distribution from the chi-squared test is selected. Results using Gamma and Poisson distributions are presented in [17]. In this chapter, we present results from the normal distribution and compare it with Gamma and Poisson distributions, and their validity is evaluated. In a normal distribution, mean μ and variance σ^2 parameters in Equation (23) are estimated in order to obtain the best fit PDF for each degradation phase.

5.4 Degradation Model Estimation Optimisation

MLE has been used again to maximise the density probability function (i.e. normal distribution function) of the estimation results. A normal distribution as shown in Equation (23) is the probability distribution of the IGBT estimated degradation phase (x_i) given normal parameter μ and σ^2 [134].

$$y = f(x_i|\mu,\sigma^2) = \left[\frac{1}{\sqrt{2\pi\sigma^2}} e^{\frac{-(x-\mu)^2}{2\sigma^2}}\right], x_i \geq 0 \quad (23)$$

The MLE method is used to estimate the underlying rate parameters' sample mean μ and the variance σ for the normal process in order to generate these counts. Again, the joint probability mass function is needed to formulate MLE; in this case, x_i, because it is a discrete random variable of the positive integers [115]. Since all discrete random variables are independent, the product of the individual density functions can be obtained.

$$\mathrm{P}[\mathrm{x}_1, \mathrm{x}_2, \ldots, \mathrm{x}_\mathrm{n}|\mu,\sigma^2] = \prod_{\mathrm{n}=1}^{\mathrm{N}}(2\pi\sigma^2)^{-n/2}\exp\left(\frac{-1}{2\sigma^2}\sum_{j=1}^{n}(x_j-\mu)^2\right) \quad (24)$$

The next step is to calculate the maximum of this probability mass function with respect to μ, σ. However, simplifications in [116] make it possible to find the maximum of the probability mass function from a maximum of μ, σ in the form of Equations (26) and (27).

$$\log(\mu, \sigma^2; x_1, \dots, x_n) = \frac{-n}{2}\ln(2\pi) - \frac{n}{2}\ln(\sigma^2) - \frac{1}{2\sigma^2}\sum_{j=1}^{n}(x_j - \mu)^2 \quad (25)$$

Then, take the derivative and set $\frac{\partial}{\partial_\mu}, \frac{\partial}{\partial_\sigma} = 0$

$$\widehat{\mu_n}\ MLE = \frac{1}{n}\sum_{j=1}^{N} x_n \quad (26)$$

$$\widehat{\sigma_n}^2 MLE = \frac{1}{n}\sum_{j=1}^{n}(x_j - \hat{\mu})^2 \quad (27)$$

It is desirable to find some estimator which would be as close to the true value ($\hat{\lambda}MLE$). This is consistent with having the estimated value makes the observed data more probable which maximizes the chances of getting the results data. Using the MLE method to estimate the best fit of the modelling parameter, the estimator $\hat{\mu}$ equals the sample mean and the estimator $\hat{\sigma}^2$ equals the unadjusted sample variance for a normal distribution [116]. According to Table 4-1, the number of health states for each of the four components' health estimation is 10 non-homogenous discrete phase durations. The MLE function is employed for each health state (HS) of the four components as in Equations (28) and (29) and the results are presented in Table 5-2 [22].

$$\mu_{(HS)_j} = \frac{1}{n}\sum_{n=1}^{4}\sum_{j=1}^{10} HS_j \quad (28)$$

$j = 1, \dots, 10$ *number of health states*

$n = 1, \dots, 4$ *number of IGBT components*

$$\sigma_{(HS)_j} = \frac{1}{n} \sum_{n=1}^{4} \sum_{j=1}^{10} HS_j \quad (29)$$

Table 5-2 MLE Parameters of Estimated Duration [100]

Parameters	μ	δ
Model 1	1.75	0.5
Model 2	104.75	30.685
Model 3	1207.5	264.138
Model 4	1526.25	283.491
Model 5	545	263.920
Model 6	344.25	262.699
Model 7	515	264.054
Model 8	213	111.758
Model 9	104.25	71.978
Model 10	56.25	52.506

5.5 RUL Calculation Algorithm

In this chapter, simulation of RUL presents as the useful life calculation for the IGBT component at each measurement time. The approach depends on the IGBT failure model estimation and the normal distribution based on the optimised duration parameter.

The process of the RUL calculation and its related simulation algorithm are processed based on the fact that the maximum estimated lifetime of the IGBT is divided into a number of estimated durations. Failure at each estimated duration is progressed in a different manner which results in different rates of degradation, known as estimated degradation phases (τ), as discussed in the previous section (see Figure 5-8). Estimated degradation phases result from the TDNN model, and present a number of health states that the IGBT may experience in real time. Considering n number of τ, the life of a health state is

calculated in normalised form (in respect to summation of τ) using the following equation [100]:

$$HSL_i = t_{thr} \cdot \frac{\tau_i}{\sum_{j=1}^{n} \tau_j} i = \{1, 2, \dots, n\} \quad (30)$$

where HSL_i presents a period that i^{th} health state life will last for a number of cycles between a starting cycle (t_s) and an ending cycle (t_n); and t_{thr} is the maximum real lifetime of the IGBT that is not necessarily equal to the total τ, because total τ is the accumulation of estimated values. A normal PDF (f(t)) is assigned to each HSL, wherein the centre and variance of f(t) are the mean of cycles occurring in the HSLi ((t_s+t_n)/2) and the difference of the maximum and the minimum cycles of the HSLi (t_s-t_n), respectively. As each HSL has an area of 1 and different variance values, accordingly, HSLs will have different maximum probabilities. A per-unit HSL is obtained by the following equation [100]:

$$HSL_{pu_i} = \frac{f_i(t)}{\sum_{k=1}^{n} \int_{t_0}^{\tau} f_k(t)} i = \{1, 2, \dots, n\} \quad (31)$$

where HSL_{pui} is i^{th} HSL in per-unit form, $f_i(t)$ is the normal PDF for the i^{th} estimated degradation duration, and t_0 is the operation time at the measurement point. The probability of estimated duration for each inspection time (PDLT) is:

$$PDLT_i = HSL_{pu_i} . \tau_i i = \{1, 2, \dots, n\} \quad (32)$$

$i = 1, \dots, p$ = number of duration lives

$j = 1, \dots, k$ = number of particles for each duration life

The simulation of the RUL calculation is given in the flowchart of the proposed algorithm in Figure 5-10. The approach depends on the IGBT failure model estimation and the normal distribution based on the optimised duration parameter. A time delay neural network approach for the degradation modelling is constructed and sweeping the estimation value under the normal distribution curve for each estimated degradation phase (τ_i) until the end of the component's life or it can be swept up to a predefined threshold value. Then, the RUL (i.e. mean and confidence levels) is calculated using the distribution of estimated values based on the area of each estimated degradation phase by MCS [100].

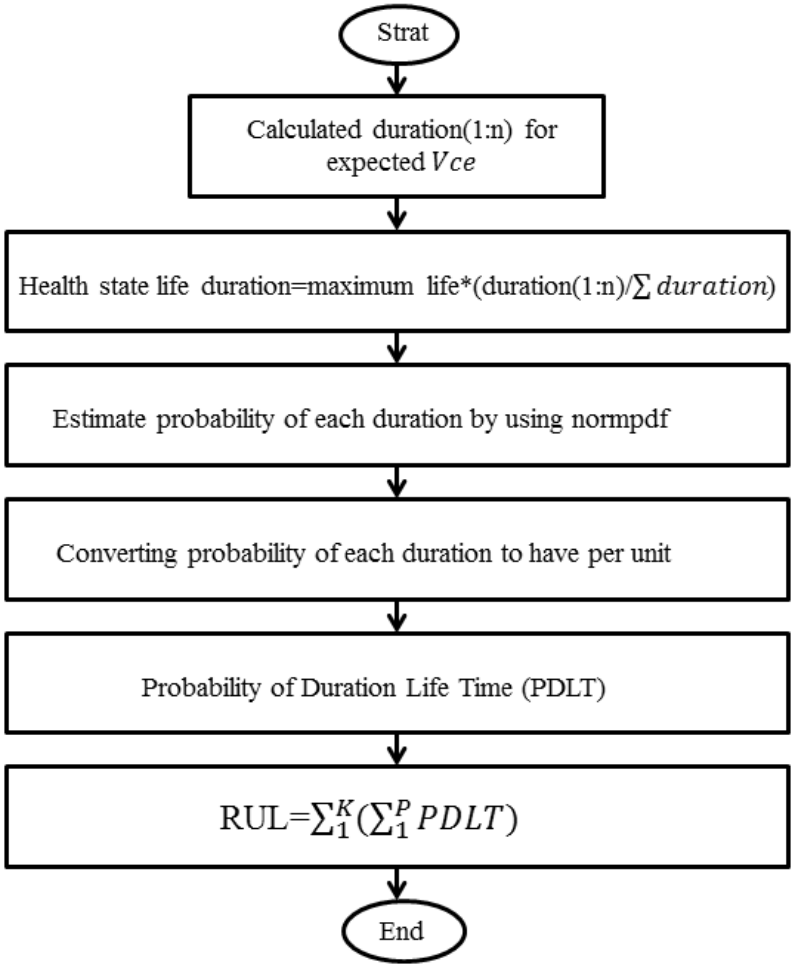

Figure 5-10 RUL calculation approach algorithm [100]

Figure 5-11 show an example (i.e. IGBT sample number 4) of HSL_{pu} results. The results were computed based on a normal distribution model which shows the area under each curve equivalent to one unit per duration. The oscillated blue, red and green curves show the mean of the area per unit, 10% and 90% deviation confidence bounds of the area per unit, respectively. The oscillations present the degradation process and the RUL predictions are also carried out at each moment of the degradation process. Hence, the RUL prediction occurs throughout the whole process of the IGBT degradation experiment. For instance, the observation peaks at measurement 1,500 cycles (cycle per second) where the black area under the each oscillation cycle presents the duration life per unit till it reaches its maximum life which is slightly above 4,000 cycles (Figure 5-11) [100].

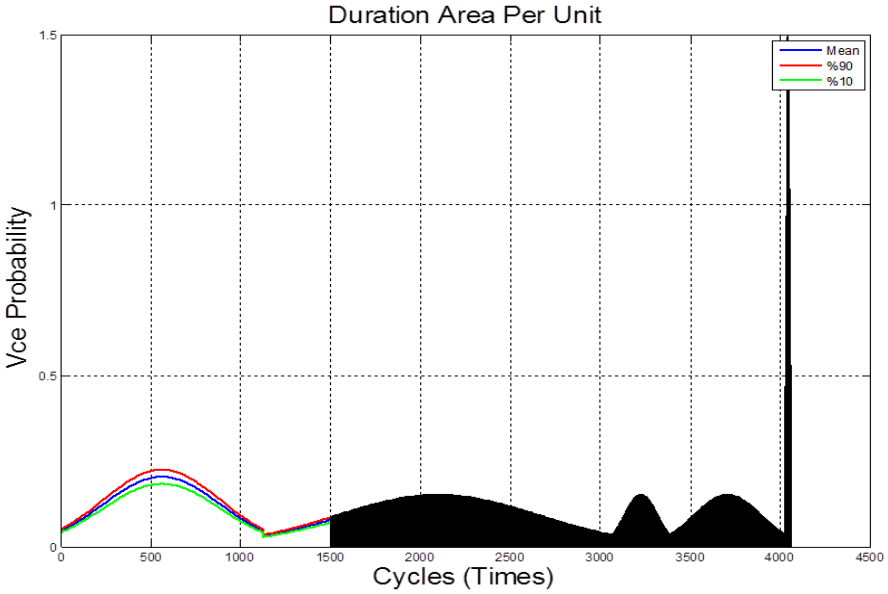

Figure 5-11 Normalisation of the duration life [100]

5.5.1 Hybrid RUL Simulation Results

The RUL prognostics results which have been estimated by the TDNN and fused with the probabilistic approach to reflect the discrete change in the degradation state are expressed by a series of polylines. The prognostics simulation is a process from the beginning of the healthy state condition of the IGBT running to the threshold value at 7 (e.g. # degradation phase). The V_{CE} as a

degradation indicator is monitored and the relevant sensor data during the on-state are recorded at each cycle where the degradation related to the packaging failure mode has caused the IGBT to fail.

Figure 5-12 shows four IGBT samples of RUL simulation results. The RUL result is computed using the statistical approach based on the estimation results from the TDNN failure model. The results are promising for early failure findings and improve decision-making based on confidence levels. The straight black, red and green oscillatory lines are used as the real RUL and it's 10 and 90 percentile deviation confidence bounds, respectively. These three lines present the accuracy of the prognostics estimation during each degradation transient. The blue plot indicates the mean value of the RUL simulation.

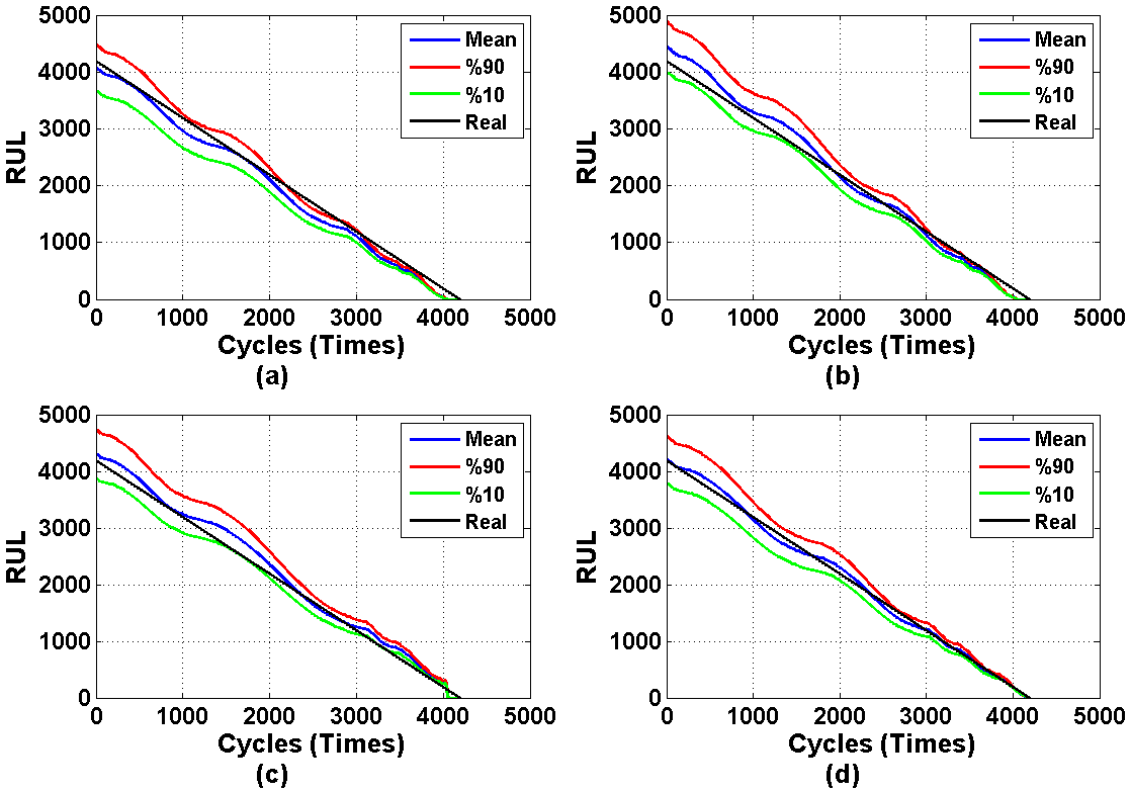

Figure 5-12 Hybrid RUL simulation

At the beginning of the RUL rendering, all prediction plots diverge from the real RUL value. As the operating time is rendered toward the end of the IGBT life, the 10 and 90 percentile confidence bounds significantly converge to the real

RUL value where the accuracy of the life estimation is vital rather than at the beginning of the device life. The confidence bounds initially offer meaningful information as the normal distribution is associated with mean and standard deviation. However, the confidence bounds lie very close to the mean value as the degradation process reaches the end of the ageing process. Confidence levels provide assurance so that we can comfortably rely on the performance of an aged system. The critical point to consider is that the accuracy of prognostics models has always been under doubt and remains to be under margins of confidence levels [100], [135].

5.6 Hybrid Estimation Error

In this chapter, RMSE and RA are used to assess the precision of the proposed prognostics performance for all durations of failure progression, and the results are compared against an extended KF [1]. Basically, RA measures the error in RUL calculation relative to the real RUL at a specific time index determined by predicted values while prediction is performed by a model or an estimator [136]. Due to the nature of degradation data that may widely differ from one sample point to the next sample, mainly where wire bonds lifted off, RA might provide us with a more accurate metric to evaluate the performance of prognostics models [1], [113]. The range of RA values is between zero and one, where the best performance evaluation score is absolute 1. RA can be evaluated at multiple time variants. Therefore, it conveys the estimation results' accuracy at a specific time.

If y_{i_λ} is the real RUL value at time index i_λ, then $\hat{y_{i_\lambda}}$ is the estimated RUL distribution at i_λ , so that RA can be calculated using Equation (34):

$$\text{RA}=100\left(1-\frac{\left|y_{i_\lambda}-\hat{y_{i_\lambda}}\right|}{y_{i_\lambda}}\right) \tag{34}$$

The performance of the proposed prognostics technique is summarised in Table 5-3 and Table 5-4 using RMSE and RA metrics for each life duration, respectively. Table 5-5 also compares the RMSE values of the proposed technique with the RMSE values from [17] that employ Gamma and Poisson probability distributions in a Markov chain probabilistic approach. It is observed from the metric that the proposed fusion technique has considerably improved prediction for all degradation phase processes compared to the stochastic model based approach. In general, the hybrid approach is proved to be a versatile approach for both prediction processes and RUL calculation and presents better RMSE values. Furthermore, it offers significant decision-making benefits because the 90 and 10 percentiles confidence width bounds are narrow realistically close to the mean during the whole prediction. This will provide meaningful information for decision-makers due to the fact that most of the occurrence of the estimated failure data is disseminated within standard deviation. According to the RA values based on the proposed approach, the IGBT test sample number 1 has the largest RA value. Therefore, it presents a more accurate predictive failure model amongst all four IGBTs and can be employed as a precise prognostics model. From [1], extended KF-based prognostics presents maximum RA (97.052) as a significant prognostics performance. Based on our approach, it can be noted from Table 5-4 that RA incredibly gives better results for all four samples in average 99.9.

Table 5-3 RMSE Hybrid Prognostics Performance Metric up to a Predefined Threshold Value [100]

Degradation Phase	IGBT 1	IGBT 2	IGBT 3	IGBT 4
1	1.15	1.15	1.16	4.28
2	1.10	1.12	0.85	4.14
3	0.89	0.93	0.84	3.58
4	0.90	0.90	0.87	3.45
5	0.94	0.87	0.91	3.28
6	0.97	0.84	0.91	3.17

Table 5-4 RA Hybrid Prognostics Performance Metric up to a Predefined Threshold Value [100]

Degradation Phase	IGBT 1	IGBT 2	IGBT 3	IGBT 4
1	99.9703	99.9433	99.9738	99.9994
2	99.9774	99.9466	99.9747	100.00
3	99.9905	99.9380	99.9579	99.9912
4	99.9924	99.9245	99.9487	99.9747
5	99.9939	99.9233	99.9492	99.9714
6	99.9940	99.9249	99.9511	99.9678

Table 5-5 RMSE Probabilities Prognostics Performance Metric [100]

RMSE %	IGBT 1	IGBT 2	IGBT 3	IGBT 4
Normal	0.9917%	0.9683%	0.9233%	3.65%
Poisson	28.6%	20.0%	25.8%	27.2%
Gamma	33.17%	33.97%	34.85%	33.19%

5.7 Summary

The main contribution of Chapter 5 is the development and implementation of a TDNN failure model of IGBTs for indication of the current health state and fuses with the principle of the area under the curve for RUL calculation. To this end, the area of the breaking region of the failure model is fitted with a probabilistic distribution function (i.e. normal distribution function). In addition, MCS is utilised in the algorithm to generate the calculation area up until the threshold value to approximate the IGBT's RUL. Overall, the IGBT degeneration model is built based on IGBT failure mechanism and degradation characterisation. The stochastic approach and MCS are used to calculate the area under the estimated degradation phases and the precursor parameter, collector-emitter voltage (V_{CE}), is integrated to develop the prognostics algorithm for predicting the IGBT's RUL. Comparison with the results of RUL prediction is shown in Table 5-3 and Table 5-4 which show that for all four samples, the first samples present significantly small RMSE and

large RA values. The implementation of the developed prognostics framework could be applied to provide advance warning of failures, thereby preventing costly power electronic system downtime and failures. The TDNN failure model can perform much more efficiently when it fuses with the statistical approach for failure RUL prediction results in some IGBTs. The combined model in this chapter is only based on the normal distribution, established and implemented in IGBT RUL prediction [100]. The next chapter will present the radically novel prognostics model for IGBT which the prognostics model can be generalised in a per-unit form. Then, its features are adjusted depending on the application, working condition, and dynamic of changes.

6 IGBT Knowledge-Based Prognostics Model

There is a need for an efficient prognostics algorithm that is embeddable and able to improve on the current prognostics models. A positive aspect of this approach is that the IGBT failure model developed using fuzzy logic adapts prognostics model with the fuzzy nature of failure mechanisms. Actually, this method is like an adaptive neuro-fuzzy inference system (ANFIS). Current state-of-the-art prognostics algorithms, notably those based on Markov probabilistic models, are computationally-intensive and not applicable to real-time embedded applications. Creating a real-time prognostics tool to predict degradation in power electronic modules in their working environment is an importunate request for predicting reliability and life consumption from various consumers of power electronic modules [14]. Fuzzy logic and neural networks are knowledge-based techniques that are frequently employed for forecasting. In general for power electronics, prognostics methods require sufficient reliable data, such as current, voltage and temperature, to develop a precise model to determine RUL based on the historic health information of the power electronic module. However, in the fuzzy approach due to make use of uncertainty, and calibrates vagueness to create a more robust model at low computational cost.

In this chapter, the IGBT failure model is used to generate run-to-failure data in different testing conditions. The data set has the similar fashion to power cycling ageing test data. In fact, electrical parameters, such as V_{CE} and junction temperature (T_j) during its operation, are monitored as precursor parameters. Modelling prognostics based on fuzzy sets which are constructed by input membership function pass through the input layer and real life estimation can be seen as an output layer. This also is connected by output membership

functions. Fuzzy knowledge enables the model to acquire expert knowledge from degradation profiles that ultimately use back propagation to minimise the estimation error of the failure parameter. ANFIS can be assigned as a knowledge-based model and has the advantages of the fuzzy logic (FL) and artificial neural network (ANN). Attention is focused on using time series data in the form of a history of time interval data as input which is being adapted with a dynamic notion of the input variables. In the proposed ANFIS prognosis model, the dynamic of each defect's phase is presented in failure trend to demonstrate the development of the failure over time. The detailed of the early stage of the deterioration of the component and the environmental loading conditions are monitored and considered to be used as the inputs to determine failure process. And then, they are employed to determine the remaining useful life of the power electronic module in lifetime models [13].

The method is proposed in such a way that by combining the operational working condition and the on-state collector-emitter voltage can adjust the model to be scalable and generated the weighed data which fit in degradation pattern. This has been constructed using a per-unit approach which quantifies explicitly the variation in usage conditions. The proposed method illustrates based on soft computing method (ANFIS) which has used a fusion of per-unit of failure data and its conditions to estimate the lifetime of in-service power electronic module.

6.1 Operational Scalable Prognostics Approach

A per-unit model/system [137] has been proposed to express the system quantities as fractions of a defined base unit quantity, for instance in power system analysis, engineering economic analysis, estimating cost models, etc. It is a simple but useful approach in which RUL estimation is made for a single unit that is a per-unit prognostics model. Then, the total RUL estimation is presented in percentage instead of actual RUL values. However, to improve the accuracy of prognostics while the operation condition is changed, the prognostics model

partitions the total RUL estimation into the number of segments. Each segment is developed based on degradation patterns under specific working conditions. Then, ANFIS is utilised and trained to recognise how component/system degradation is changed from one pattern to another while working conditions are changed. We believe that the ISHM system will greatly benefit by a per-unit prognostics model in which degradations under different working conditions are characterised into patterns useful for natural computing-based pattern recognition. The advantage of this approach is that it will enable RUL to be estimated while working conditions are also changed in the real-time process. However, RUL is presented as life percentage rather than actual values.

The various techniques to conduct accelerated ageing tests under different working/operational conditions, such as thermal cycling, power cycling, and electro-thermal cycling, are presented in [138]. It is worth mentioning that an additional step known as feature extraction is also an important initial step which involves investigating what signals should be monitored to allow prognostics to be successfully developed based on the features extracted from those signals. The damage model created is then used for obtaining the initial threshold (Th) under normal operating conditions, ideal RUL (IR), and a prognostics model. Suppose the system has been monitored by a number of measurement points through its life period collected inside a validation/test profile. RUL estimation is a process to sweep measurement points from the first to the last point, and for each particular point, estimate when degradation in the system is progressed to the threshold level (Th) where the system is aged enough to be known as a damaged system. Then, RUL at the measurement point is accounted as the numbers of iterations (also known as Cycle Time, CT) that need to be performed from the chosen measurement point (mp) to the point that the damaged state propagates to the threshold (Th). The RUL of systems is expressed with lower and upper confidence levels accounted. For instance, Figure 6-1 presents IR, estimated RUL, 10% and 90% confidence levels when the system is under normal operating conditions (presented by index n, IRn). The life

of the system is assumed to be ended under normal working conditions where Th_n crosses the IR_n representing EOL.

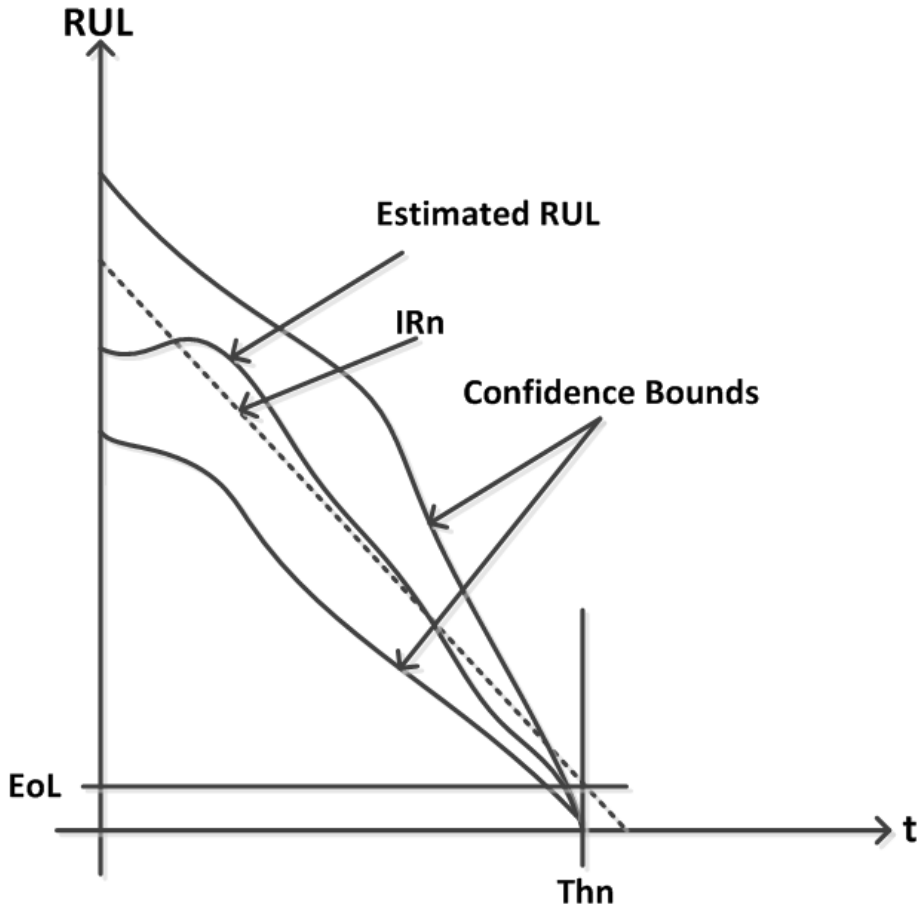

Figure 6-1 Normal working condition [139]

It is still challenging to consider effects of all various working conditions to accurately estimate RUL. As working conditions vary during the system's lifetime, degradation is processed at different rates so that the threshold (Th) may occur at different points (CTs) (Figure 6-2). In comparison with Figure 6-1 that presents estimated RUL continues to decrease under normal working conditions, the estimated RUL (Figure 6-2) progresses random decrease and increase depended on the changes in the working conditions. However, the trends of both RUL in Figure 6-1 and Figure 6-2 are life reduction toward EOL and 0. The next section describes the estimation of RUL under variable working

conditions using natural computation. Figure 6-2 expresses what maximum life expectancy at each working condition is, and how RUL is reduced as systems perform under different working conditions. The threshold is the point at which the system gets to EOL that is a specific percentage of its overall lifetime.

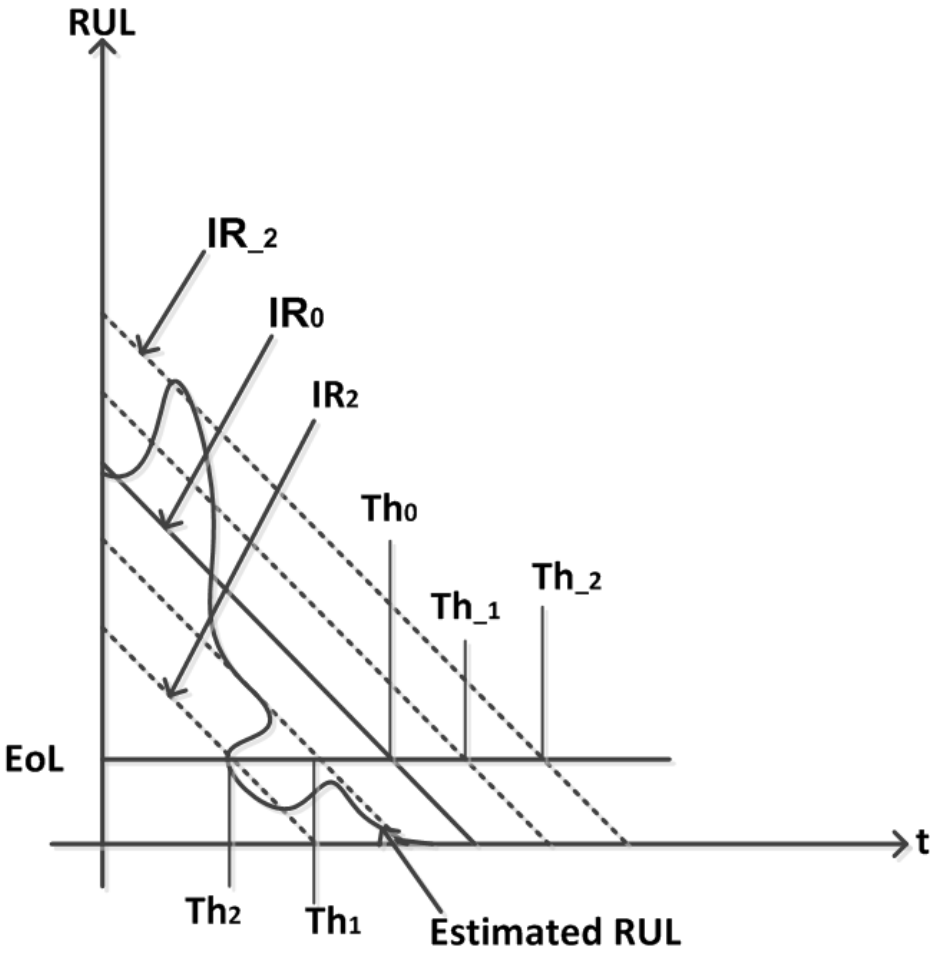

Figure 6-2 Variable working condition [139]

6.2 ANFIS Prognostics Model using Per-Unit Approach

Consider a single component so that its degradation model can be expressed using a number of parameters under specific operating conditions declared by the second set of parameters; for instance, the voltage across the IGBT as a parameter of the degradation model and temperature as working conditions. Figure 6-3 presents an ANFIS model as a black box that can be used

for building a per-unit prognostics model by defining base values of the per-unit model when the component is under normal operating conditions. Then, per-unit quantities are calculated by dividing the actual value of any parameter (under any operating condition) by its specific base value. For instance, the per-unit value of parameter X(t) that has a base value Xbase is calculated as Xpu(t) =X(t)/Xbase. Table 6-1 provides base and per-unit quantities for an IGBT component. All based values are accounted for the component under normal operating conditions.

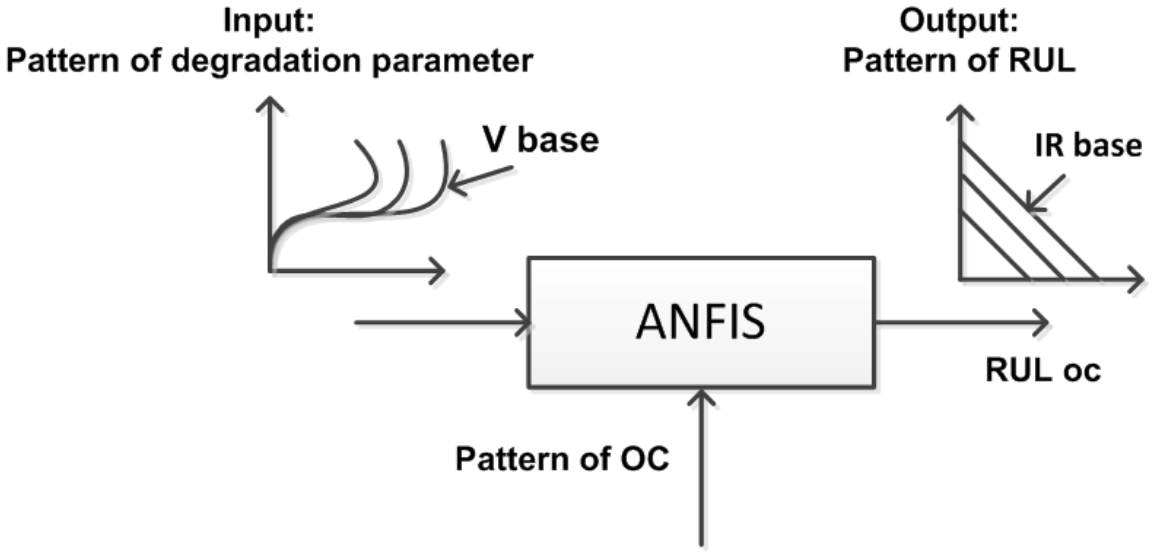

Figure 6-3 ANFIS-based per-unit prognostics technique [139]

Table 6-1 Per-Unit Quantities [139]

Base	Description	Per-Unit
S_{base}	Switch power loss	$S_{pu}(t)=S_{wc}(t)/S_{base}$
V_{base}	V_{ce_sat}*	$V_{pu}(t)=V_{wc}(t)/V_{base}$
I_{base}	I_{c_sat}**	$I_{pu}(t)I_{wc}(t)/I_{base}$
Th_{base}	Threshold	$Th_{pu}(t)=Th_{wc}(t)/Th_{base}$
T_{base}	Temperature	$T_{pu}(t)=T_{wc}(t)/T_{base}$
CT	Cycle time	$CT_{pu}(t)=CT_{wc}(t)/CT_{base}$
*V_{ce_sat}: Collector-emitter saturation voltage **I_{c_sat}: Collector saturation current		

As presented in Table 6-1, there is also a base value and per-unit parameter for CT so that the prognostics model fits the life of the component under any operating condition (OC) within the same window. This unifies the created prognostics model for any application under any OC and stress. Hence, the degradation model is formulated in per-unit form by Equation (35) [139]:

$$D_{pu}(CT_{pu},oc_{pu}) = f(CT_{pu},oc_{pu}) / \max(D_{base}) \quad (35)$$

where D is the actual parameter used to develop the degradation model; $O_C = \{0, \pm1, \pm2, \ldots\}$ refers to the operating condition for $O_C = 0$ under normal operating conditions, $O_C > 0$ when the conditions worsen, and $O_C < 0$ when conditions are modified; f refers to the function of the degradation model under condition O_C; and max is the maximum function. And also, max is applied on D representing D as a normalised parameter with a maximum value of the degradation model under normal OC. If points of EoL for different operating conditions are located on the vertical line as shown in Figure 6-2, then the ideal RUL (IRpu) is obtained from Equation (36). It develops IR_{pu} as a line equation for each OC [139].

$$IR_{pu}(CT_{pu}) = EOL\ (1+(CT_{pu}-Th_{pu})/(CT_{npu}-Th_{pu})) \quad (36)$$

where IRpu is the ideal RUL in per-unit form, EoL is a constant value of end of life, CTnpu=max(CTn/CTbase) is per-unit of cycle time under normal operation conditions equal to one. This approach divides the prognostics models into segments while each segment is created from the per-unit degradation model, and related base values correspond to a specific working condition. Hence, in real-time operation, the RUL at each measurement point is estimated by firing the right segments of the prognostics model. The fired segment is changed as O_C varies through the lifetime of the system/component. The ANFIS neuro-fuzzy

system in Figure 6-3 is trained to recognise working conditions and to fire the right segment of the prognostics model that finally results in RUL estimation. To train such a neuro-fuzzy RUL estimator, per-unit forms of the damage model and RUL under different working conditions are used as inputs, and output parameters, respectively. In fact, training patterns are generated by collecting Dpu, oc and IRpu in vectors. However, ΔDpu can be also included as an additional input variable to improve the accuracy of the ANFIS-based RUL estimator by looking to the dynamic of the damage model (Table 6-2).

Table 6-2 Training Pattern [139]

Pattern	Input			Output
1	OC_1	$Dpu_1(1)$	$\Delta Dpu_1(1)$	$IRwc_1(1)$
2	OC_1	$Dpu_1(2)$	$\Delta Dpu_1(2)$	$IRwc_1(2)$
To be continued to pattern m-1				
m	OC_1	$Dpu_1(m)$	$\Delta Dpu_1(m)$	$IRwc_1(m)$
m+1	OC_2	$Dpu_2(1)$	$\Delta Dpu_2(1)$	$IRwc_2(1)$
m+2	OC_2	$Dpu_2(2)$	$\Delta Dpu_2(2)$	$IRwc_2(2)$
To be continued to pattern n-1				
n	OC_3	$Dpu_2(n)$	$\Delta Dpu_2(n)$	$IRwc_2(n)$
To be continued for all OC_k				

6.2.1 Characterization of Ageing Data

Junction temperature, power loss and duty cycle are just some of the parameters that are worth considering as the working condition of IGBTs. However, in general, it is known that saturated collector-emitter voltage (V_{CE_sat}) is measured when the IGBT is switched on. Thus, V_{CE_sat} is dropped to its minimum value, and the current through the collector (I_C) will be increasing and elevates the junction temperature. Depending on the I_C, the IGBT may have a positive or negative temperature coefficient for V_{CE_sat} so that V_{CE_sat} increases at high I_C, and it decreases at lower I_C with an increase in temperature [140]. This means that both the IGBT junction temperature and I_{C_sat} have a significant impact on the performance of the IGBT. Hence, V_{CE_sat} is used as a degradation parameter, and the temperature is used as an explicit part of the model for scaling working condition parameter whereas in this simulation is

performed for a fixed maximum I_{C_sat}. Alternatively, the power loss of the IGBT can also be used for accounting both I_{C_sat} and temperature as working conditions. However, to reduce complexity, we focus on temperature. Figure 6-4 for instance, IV characteristic may present positive or negative temperature coefficient for the V_{CE_sat} and is considered for working condition of IGBT. Thus, it also shows the collector current (I_C) in conducting state as a function of the V_{CE} at different junction temperatures. It is important to note that operating about 40A, the conduction losses decrease with increasing temperature. And for higher current, the conduction losses increases slightly. In this case, it is considered an increase in nominal current and a junction temperature increases from 25°C to 150°C can be observed. This region is an effective operational lifetime quality for the IGBT. We notice that the V_{CE} is relatively higher for high temperatures. However, at some point of higher temperature, the mobility of electrons at conduction mode is saturated and collision between electrons provokes the on-state resistance (Ron) becomes higher. [141].

It is well understood that due to the ageing of the wire bonds, solder joints and die of IGBTs, the short circuit current is decreased while the on-state voltage $V_{CE\ (ON\text{-}state)}$ is increased [142]. This will result in an increase in the forward resistance of the IGBT. This will also can be correlated with the evolution of Al metallization resistance during degradation of IGBT [142]. Considering the IGBT as a switch, it has two working modes: on-state is when the IGBT is switched on and off-state is when the IGBT is switched off, respectively. During the on-state mode, the IGBT's voltage across the collector-emitter is dropped down because the channel of the IGBT is saturated; and so, its resistor, R_{on}, is reduced to less than 1 ohm. On the other hand, the IGBT's channel is cut off for an off-state mode that causes the current through the collector-emitter of the IGBT to be dropped down to almost 0, meaning R_{off} is highly increased. Due to degradation, the on-state and off-state values of the IGBT are changed resulting in changes in R_{on} and R_{off} as well. To summarise, any degradation caused by thermo-mechanical and electrical stress will result in changes in energy losses that increase junction temperature as well as the

temperature of wire bonds and solder joints. The accumulation of effects resulting from various stresses causes cracks in the die, wires and the overall package of the IGBT. This subsequently results in an increase in R_{on}, $V_{CE\ (ON\text{-}state)}$ and power loss of the IGBT that increases thermal stress.

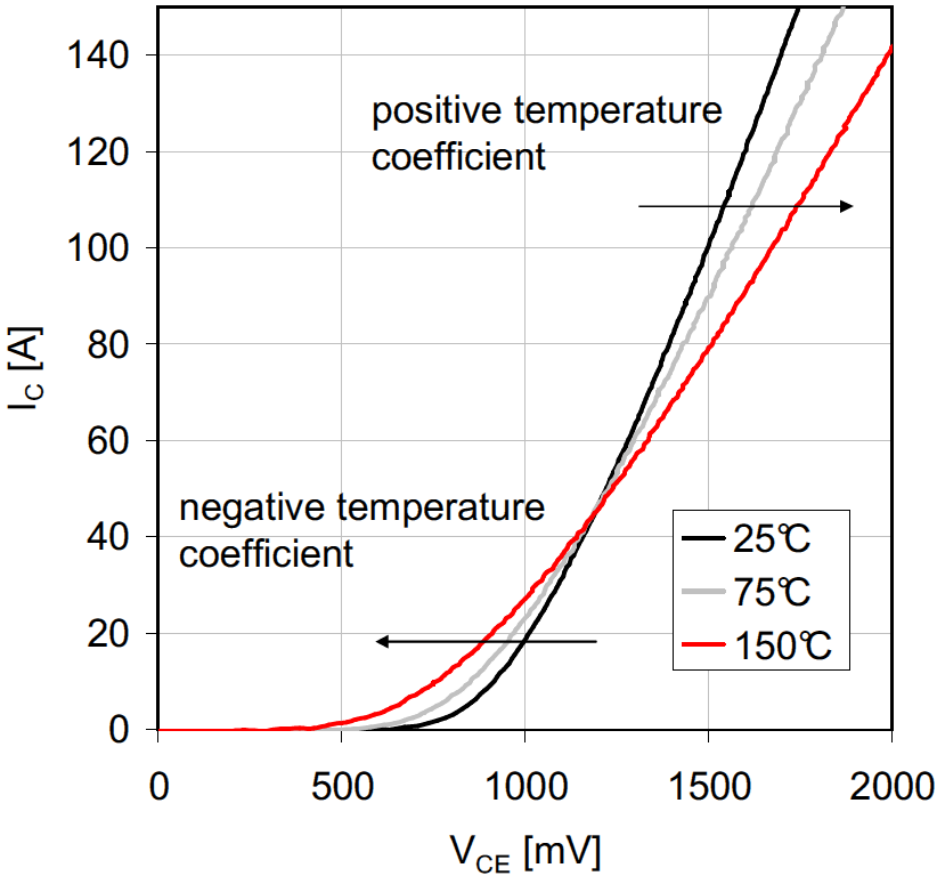

Figure 6-4 Example of IV characteristics for IGBT [139]

6.2.2 Discretisation of Ageing Data

The previous V_{CE} data sets shown in Figure 6-5 have been considered and are chosen as precursor parameters in this chapter from the experiment data, providing the best degradation indicator to crack propagation leads to wire bond lift off in comparison to other measurable parameters [82], [17]. In this regard, the IGBT's power is cycled so that the IGBT's temperature is kept between minimum and maximum limits (T_{min} and T_{max}, respectively). Through each cycle, the IGBT is switched on to increase the temperature from T_{min} to T_{max}, and then

it is switched off to reduce the temperature from T_{min} to T_{max}. Each iteration is known as a cycle time ($t_{cyc} = t_{off} + t_{on}$) comprising from t_{off} and t_{on} for when the IGBT is switched off and on, respectively. Cycle time causes IGBTs to slowly develop irregularities, degradations and faults which eventually get to the point of malfunction, indicating that the IGBT is damaged. $V_{CE\ (on\text{-}state)}$ and $I_{CE\ (off\text{-}state)}$ (including load, the temperature of IGBT and environment as working condition parameters) could be known as the best parameters to monitor the IGBT's failure during the first stage.

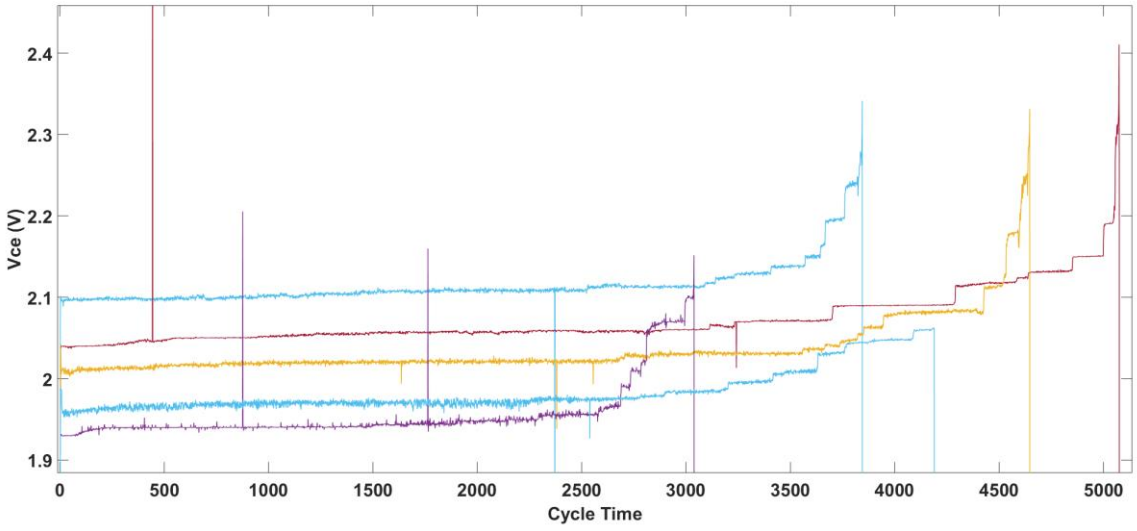

Figure 6-5 Run-to-failure data for five IGBTs of the same type [139]

The power cycling test is repeated for 22 IGBTs (with 600V/75A), and all the monitored parameters including on-state voltage, off-state current, junction temperature are saved within the n^{th} degradation profile for the chosen n^{th} IGBT under ageing test, $1 \leq n \leq 22$ and $n=\{1, 2, \ldots, 22\}$. However, for simplifying the process, we proceed with just one set of working conditions, a fixed T_{min}, T_{max} and load. Run-to-failure results of power cycling tests conducted on five samples of the same IGBT are shown in Figure 6-5. Tests are processed under working conditions of T_{min}=60°C and T_{max}=120°C. The following failure patterns can be modelled with Equation (37) [139]:

$$V_{CE\,(sat)} = \sum_i (P_{i1} + P_{i2}\,(1\text{-}exp\,((t\text{-}P_{i2})/P_{i4})) \quad (37)$$

where V_{CE_sat} is the collector-emitter saturation voltage of the IGBT, t is the time index (when the sample has been taken), Pi1 to Pi4 are parameters which define per-unit damage patterns, EoL, Thresholds, and IR; and finally, i={1, 2, ..., 6} is the number of clusters detected in the IGBT's failure data using the K-means and silhouette clustering tools of MATLAB. The spikes in all samples are due to solder fatigue stress that appears as an intermittence fault.

Equation (37) provides specific training information needed to initialize the ANFIS network. Then, two IGBT samples from the degradation profile in Figure 6-5 are used to generate training patterns. The other two samples in Figure 6-5 are used for validation purposes. Initial V_{CE_sat} either from Equation (3) or samples in Figure 6-5 create temperature-based derivatives corresponding to the working condition in Figure 6-4. Using the training pattern in Table 6-1, inputs are constructed from V_{CE_sat} specified by Equation (37) to initialise the ANFIS), and two IGBT degradation profiles from Figure 6-5 (used for damage model parameters) along with temperature-based IGBT variations given in Figure 6-4 (used for the working condition of IGBT). Training patterns for the output of the ANFIS system are also created using Equation (36). Considering 6 clusters for each V_{CE_sat} and five different temperatures {40, 60, 80, 100, 120°C} create 30 different training patterns. However, to improve the accuracy of the ANFIS system, 100 samples at different CTs from each cluster have been taken into account. This increases the number of training patterns to 6,000 [139].

Both V_{CE_sat} and the junction temperature (T_J) as a working condition (W_C) or O_C are driven by power switching fed to the i^{th} input sets which determines an initial fuzzy set.

A_i^j, for $i = 1, 2, 3$, B_i^j for $i = 4, 5, 6$ and C_i^j for $i = 7, 8, 9$

As, they have associated with the j^{th} fuzzy rule to stablish fuzzy logic inference engine whereas, the output of the inference engine is constructed from real RUL (i.e. IRpu). Both the per unit of V_{CE} (i.e. Dpu) and T_J indicate the occurrence of

random events whereas the per unit of ΔV_{CE} (i.e. ΔDpu) is taken into account as a dynamic of health states of the model to present crack growth propagation in the die-attached solder joint for improving accurate prediction during the lifetime calculation process. In the ANFIS structure uses fuzzy Sugeno model reasoning. Two initial steps of filtering and classification are required to filter rapid changes due to noise and spikes and to eliminate redundant information by taking just one sample from each cluster. These steps speed up the process of RUL estimation. A solution that also reduces uncertainties is the buffering technique [72]. It can be noted in Figure 6-6 that the first element of the V_{CE} fetches into the FIFO buffer frame and upon second arrival is shifted the next part, and will carry on till both partitions of the buffer size (10) are occupied with sensory data. This phenomenon is essential to overcome initial aggression of the sensory noises. The monitored signals are shifted in the FIFO (First-In First-Out stack) one by one, and the mean value of the available data in the FIFO is then used for the RUL estimation. FIFO has a fixed storage length, so that shifting a new sample to the FIFO will release the sample that had already been shifted into the stack at the earliest time. At the same time, ΔV_{CE} is determined from two obtained mean values of the first and second buffer size of the V_{CE} variable, and the W_C data is buffered, as shown in Figure 6-6, for the buffer size (10). The estimation of RUL system reasoning will be improved by applying FIFO. The RUL from such a system is estimated in per-unit form and can be used to present the remaining useful life of the system in percentage rather actual remaining life time. After noise reduction, all four input variables [143]:

$$x_i=\{V_{ce}(t), \Delta V_{ce}(t-1), W_c(t)\}$$

For i=1, 2, 3

which is assigned to three inputs of the membership functions, low, medium and high, as linguistic labels in layer zero, Therefore, sigmoid membership functions

are used to calculate the membership grade at each node in layer 1. These membership functions μ (0) define by scaling between 0 and 1 how representative the local degradation models are for a certain value Vce, as shown in the following:

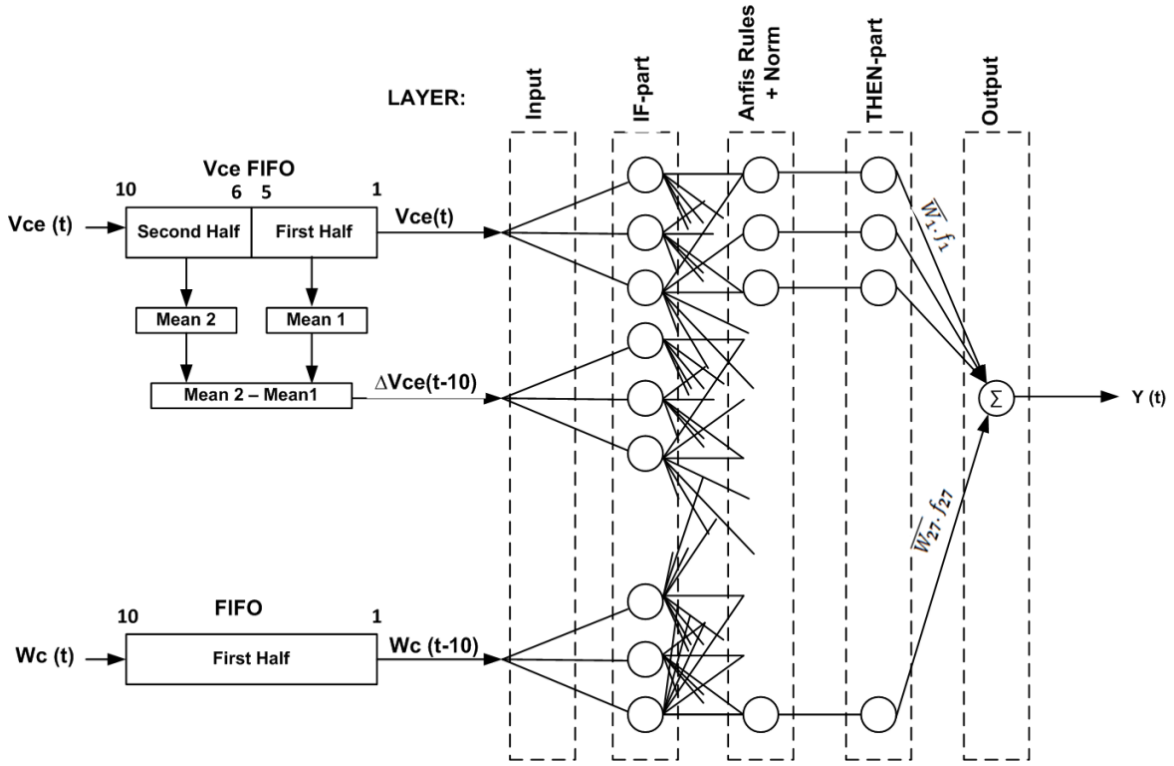

Figure 6-6 Structure of the proposed ANFIS model [143]

$$\mu_{A,B,C}(x_i) = \{low_{x_i}, medium_{x_i}, high_{x_i}\} = \frac{1}{1+\left|\frac{x-c_{ij}}{a_{ij}}\right|^{2b_{ij}}}$$

For i=1, 2, 3; j=1, 2… 27

where $\mu_{A,B,C}$ is the output signal of the layer 1 with respect to the i^{th} input parameter and j^{th} fuzzy rule, and three premise parameters (a_{ij}, b_{ij}, c_{ij}) of the Sigmoid function are optimised using back propagation via the gradient descent

method and changing the shape of the membership function instead of just using data to choose parameters [144].

$\{\mu.A_i^j(x_i), \mu.B_i^j(x_i), \mu.C_i^j(x_i)\}$

At the fourth layer, the T-norm operator performs j=27 fuzzy rules which after are required to firing strength of rule. The output of the fuzzy rules at each node in layer three will represent the firing strength of the 27 fuzzy rules, for instance as follows [143], [145]:

Rule 1: IF V_{ce}, ΔV_{ce} and W_c are

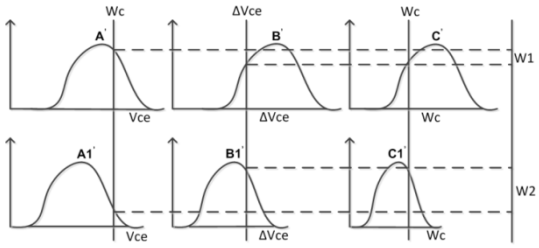

THEN $f_1 = d_1^1 V_{ce} + d_2^1 \Delta V_{ce} + d_3^1 W_c + d_4^1$

THEN $f_1 = d_1^2 V_{ce} + d_2^2 \Delta V_{ce} + d_3^2 W_c + d_4^2$

Then, the rule firing strengths is normalised, which follows as:

$$W_j = \prod_{i,j} \mu.A_i^j(x_i)\mu.B_i^j(x_i)\mu.C_i^j(x_i)$$

For i=1, 2, 3; j=1, 2… 27

$$\overline{W}_J = \frac{W_j}{\sum_j W_j}$$

where the normalised firing strengths output is adapted to a node function $\overline{W_J}.f_j$. All incoming signals at single node output are computed as an overall output using a Takagi-Sugeno type model. As shown in the following:

$y(t) = \sum_j \overline{W}_J . f_j$

where f_j is formulated with consequent parameters $\{d_1^j, d_2^j, d_3^j, d_4^j\}$ and optimised using the least squares method. After the linearisation all input signals, the output $y(t)$ predictor of the ANFIS presents as follows:

$$y(t) = \sum_j \overline{w}_j \left(d_1^j V_{ce}(t) + d_2^j \Delta V_{ce}(t-1) + W_c d_3^j (t) + d_4^j\right) \quad (37)$$

j=1, 2, 3…27

6.3 ANFIS Prognostics Results

To demonstrate the proposed operational scalable prognostics result, we tested the approach based on 4 run-to-failure IGBT test samples, all of which have different working conditions. The algorithm was implemented and tested in MATLAB. The testing data set used as measurement data is rendered point by point to estimate the online RUL. As the results are in per unit; therefore, considering EoL for estimation value where IGBT is already damaged for any CT_{pu} more than 0.72. The best results of RUL estimation presents from validation phase with RMSE of 0.081 as the model performance precision is shown in Figure 6-7. This figure presents how the RUL of a single IGBT is reduced and scalable to track deterioration under different working conditions, even though the degradation profile of the IGBT that has been used for validation is obtained from ageing accelerated tests under a fixed working condition variation of T_{min}=60°C and T_{max}=120°C temperatures. With a scalable ANFIS prognostics model, the online prediction results retrieved are good convergences of the degradation model using reference engine rules that are most similar to the degradation pattern. To gain insight into the proposed prognostics approach, we shall analyse the results in more detail. Consider the light blue (i.e. IRn), green (i.e. IR60), red (i.e. IR80), cyan (IR100) and magenta (IR120) lines of the true RUL for all different operating conditions, and the estimated RUL. The estimated RUL in the scattered black plot can be observed at the beginning of the data rending which has converged to around IRn between

0 to 0.14 CTpu in ambient temperature. However, as the temperature rises up to 60°C, the estimated plot will be expected to close IR60 from 0.14 to 0.25 CTpu and the RUL estimation continues around their associated real values as observed in Figure 6-7. The ANFIS model estimator is converging to its real value up to the point where the junction temperature tracks the operating condition at different life spans per unit [139].

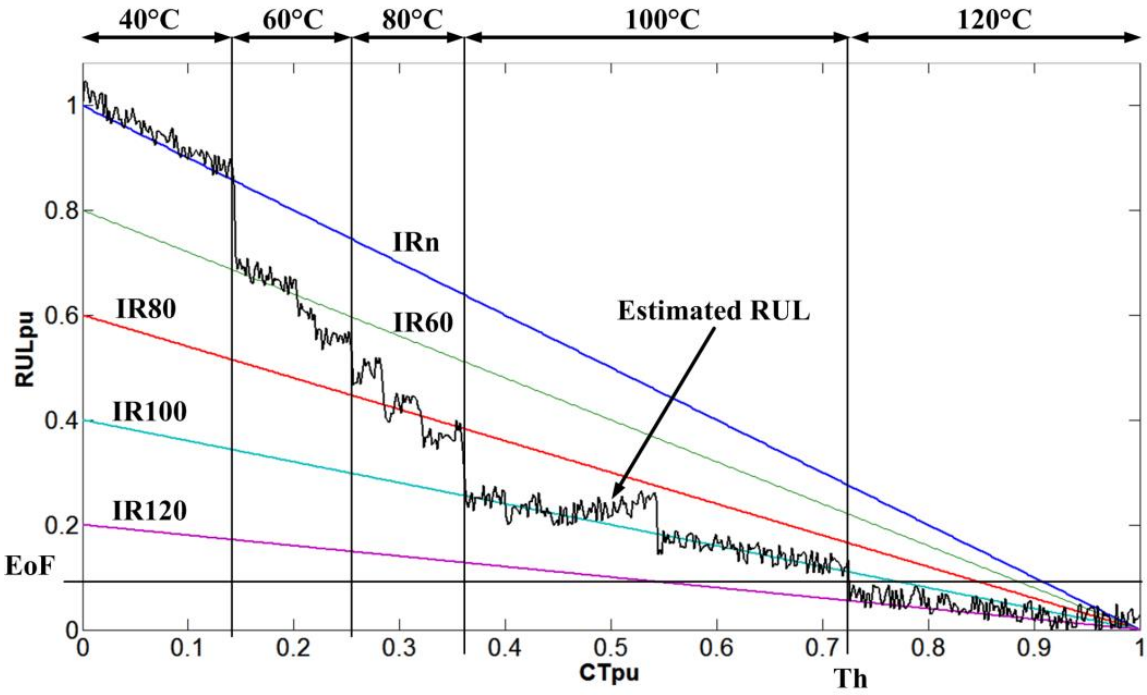

Figure 6-7 Operational scalable RUL estimation using ANFIS-based per-unit prognostics model [139]

In contrast to the scalable ANFIS-based per-unit prognostics model, the prediction RMSE value decreases for non-scalable ANFIS based per-unit prognostics model as the OC deviates away from one nominal condition to another. The estimation is simulated up until the last degradation phase as the predefined threshold state. As is noted from

Figure 6-8, the precision of the estimated RUL converges as the scattered blue mean prediction plot approaches the black real failure RUL. The RUL associated with wide confidence intervals (90% and 10%) are shown by the red and green plots respectively, which provide meaningful information for maintenance. At the beginning of the RUL simulation, the confidence bound is

quite divergent and fluctuated with the mean RUL but as it progresses to the device's EoL, it becomes convergent with the mean and real values. In contrast to the ANFIS prognostics model, RUL results for the Gamma probabilistic model, as shown in

Figure 6-9, is relatively different from the true RUL with an RMSE of 0.2520. However, the prediction results progress smoothly towards EoL in comparison to the ANFIS results. The RUL estimation of both methods was evaluated by comparing the RMSE of the estimated RULs. The results prove that the ANFIS model has significantly improved prognostics performance and reducing the RMSE value to 0.0176 [17].

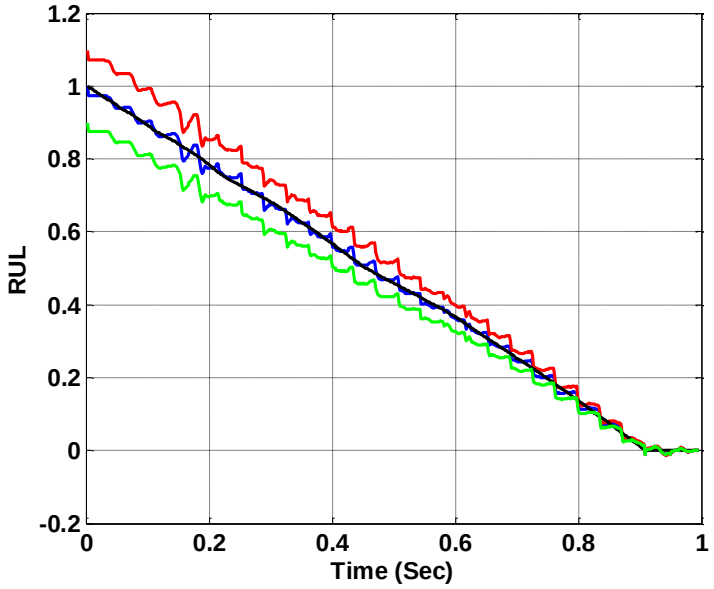

Figure 6-8 RUL estimation using ANFIS-based per-unit prognostics model [143]

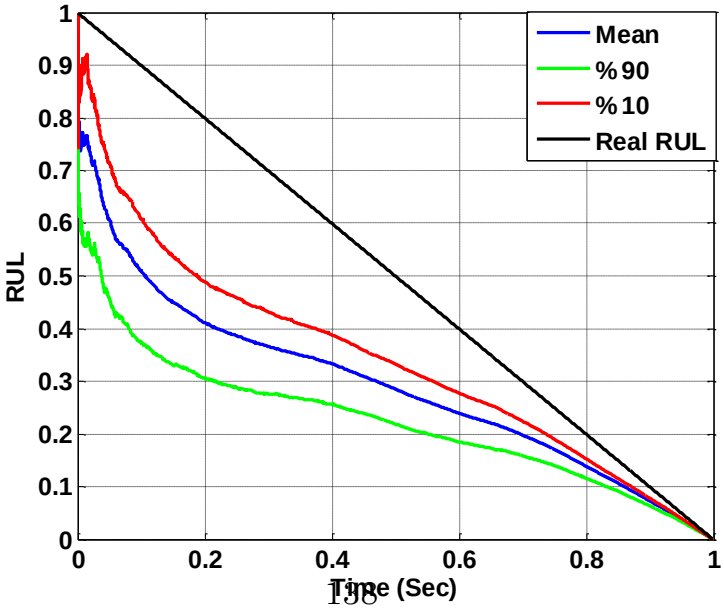

Figure 6-9 RUL estimation using Gamma-based per-unit prognostics model [143]

6.4 Summary

There are still difficulties in estimating the remaining useful lifetime of components while prognostics models are created based on damage parameters neglecting changes in the working conditions. This chapter presents a novel technique using an ANFIS neuro-fuzzy system that unifies prognostics models suitable to be used in different working conditions. This is achieved by creating a per-unit prognostics model and transferring components' features, behaviour under different working conditions, and degradation models to the ANFIS system.

It is concluded that the ANFIS model infusion with failure dynamics and working conditions enhance prognostics performance. In addition to prognostics accuracy, it is important to emphasise that the implemented algorithm is able to perform real-time prognostics calculations. In contrast to the current state-of-the-art prognostics, this chapter presents a lightweight simulation-based prognostics approach applicable to on-board embedded applications which we aim to do in future research. The results indicate the ANFIS model infusion with failure dynamics enhances prognostics performance using the cross-validation technique. In addition to prognostics accuracy, it is important to emphasise that the implemented algorithm is able to perform real-time prognostics calculations. However, the probabilistic model is associated with MCS to generate a random large number of degradation paths up until a predefined threshold during propagation presents time-consuming RUL calculation.

The next chapter will present the development of an electro-thermal model for estimating junction temperature which used to develop physics-of-failure for reliability assessment when the failure of an IGBT is emulated in a DC-DC power converter. Furthermore, a stress minimisation control strategy

has been implemented to reduce the stress condition and increase the lifetime of the device in critical situations.

7 IGBT Physics-of-Failure Prognostics Approach and Thermal Stress Reduction

Commercial reliability prediction programmes for electrical and electro-mechanical stress, including Mil-HDBK-217, 217-PLUS, PRISM, Telcordia and FIDES, still use traditional reliability prediction methods, [146], [147]. These are empirical methods based on statistical data and the average performance of a large number of identical products. In essence, these methods account little for the mechanisms of complex in-service failures. It is, therefore, not surprising that the results obtained from these methods do not always correlate well with actual failures in the field.

Since IGBT power semiconductors are one of the most costly components in power electronic converters, it is beneficial to investigate the long-term reliability and the sizing of the semiconductors used in power converters. On the other hand, due to increased demands for dynamically-controlled safety systems from customers, requests for a continuous monitoring system which tracks and identifies trends in and sources of component degradations prior to failure has been provided. This is because high product availability which is one of the main demands of customers could not be fulfilled by conventional maintenance strategies, such as corrective and preventive maintenance strategies [148]. Therefore, the reliability of these power electronic modules is vital for the commercial success of various types of renewable energy sources and manufacturers. In addition, it is a prerequisite for the components to be available in downtime lifecycles. Certainly, this requirement has put a lot of effort into diagnostic and prognostics for efficient maintenance operation through

automated tests and verifications [92]. Due to harsh environment conditions, particularly in hostile environments such as power conversion applications and their operating load conditions, IGBTs will be subject to electro-thermal and mechanical stress in situations where the early life stage is rapidly degraded [85]. As a result, high reliability becomes an essential issue in power electronic modules, which are a significant part in renewable energy applications, such as wind turbine farms, biomass and solar panel technologies [109]. On the other hand, prevention of power electronic module failure is impossible. Therefore, creating real-time early failure prediction and online estimation of remaining useful life of used power electronic switches in renewable systems is essential.

This requires us to tackle challenges in a) decreasing the stress level of active switches when they are in their failure region, and b) life extension of critical devices. However, to meet these requirements, it is necessary to expand knowledge and techniques in the following areas:

- Critical components
- Dominant failure
- Failure stress analysis.

In comparison with traditional converters, SEPIC has been introduced as a suitable candidate for reducing the overall stress of active power switches in hard operating conditions [24].Figure 7-1: This converter topology is capable of operating in both buck and boost modes with a simple control design. This is because these new topologies benefit from coupled inductors promising for the high-voltage applications at a small demanding duty cycle. As a result, the noise and the ripple current that are important factors for any DC-DC converter are incredibly reduced [24]. Furthermore, it uses fewer power switches, which as an advantage reduces power dissipation, essential in increasing overall reliability.

However, in spite of key advantages of such converters, the reliability of the SEPIC DC-DC converter during the degradation process occurring in the switching device (IGBT) have not been well investigated for industrial

applications, e.g. PV. The topology of the converter consists of active switches, such as an IGBT/MOSFET, and a Schottky diode, and passive devices to regulate output voltage from an input voltage that varies from above to below the output voltage. The current flowing through various circuit components, when stored magnetic energy in inductor L1 during off mode, continues to flow through passive device capacitor C_1 and discharge through another passive device inductor L_2 during ON cycle. A capacitor C_{in} is used to reduce the effect of the internal parasitic noise of the input power supply. The passive device inductors (L_1, L_2) and capacitors (C_1, C_2) with active devices are connected to form the power delivery to the output in both off and on modes.

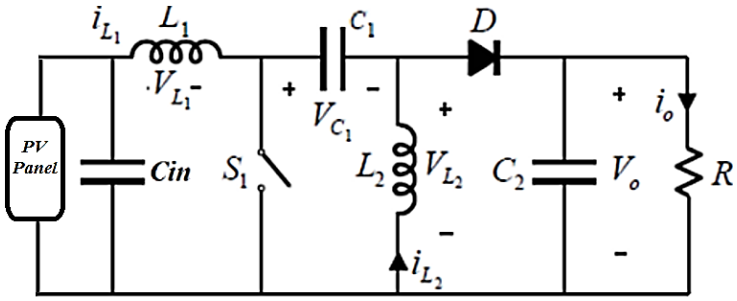

Figure 7-1 SEPIC DC-DC converter topology

The following section will present the testbed design to measure the electrical and temperature parameters in real time.

7.1 Measurement Testbed Set Up

The SEPIC DC-DC converter has been designed and implemented for the testing capability of performing accelerated ageing tests. The proposed test rig is designed for the validation of decelerated stress control strategy for power electronic switches. The PCB design has adequate space to accommodate gate controlled of TO-247 IGBT packages with standard currents capability ranging from 1A to 50A. The accelerated ageing test is performed in a standard power cycle manner and via a high-tech real-control desk base instrumentation kit (i.e. dSPACE, DS1004). In this chapter, a real-time control loop platform for the power converter is implemented using a dSPACE DS1104 controller board which

has the capability of a discrete controller with a sampling rate 500 KHz. And also, used with Real-Time Interface (RTI), it is fully programmable and perfectly supports the MATLAB/Simulink function model with the I/O interfaces and to configure all I/O to the real hardware design. The electrical and temperature signals, such as on state V_{ce} and the IGBT base plate, are measured using analogue to digital converters (ADCs) with 16-bit resolution, ±10V input range and 10KHz signal-to-noise ratio (SNR). Thus, it is recorded in real-time according to test condition respectively. In order to measure the temperature of the power switch, an LM35 (rated for a full -55°C to 150°C range) mounted integrated circuit sensor at the back surface of the baseplate with an electrical output proportional to the temperature. The DC-DC converter includes measurement capability with a built-in input and output LTS 25-NP current sensor 25A. The primary main board was developed to allow hosting four converters comparing the PV panel characteristics, the MPPT algorithm and ageing for identical switches simultaneously. This hardware allocates 60A terminals block of the CAMDEN-CTB77VP range for the input/output power connection of the converter block and one terminal also is given for converter's ICs. In addition, it allows hosting five BNC I/O ports which are connected to the ADC channels of the dSPACE for the measurement of the I/O voltage and current for the converter. Furthermore, as shown in Figure 7-2 sending PWM signal command using slave DSP I/O channels with 10 PWM channels and 14 bits of digital I/O (TTL) to control gate driver (L6388E) of the IGBT/MOSFET for switch control.

There are a few components in power converters which are subject to reliability assessment, and ignoring their reliability will increase system downtime.

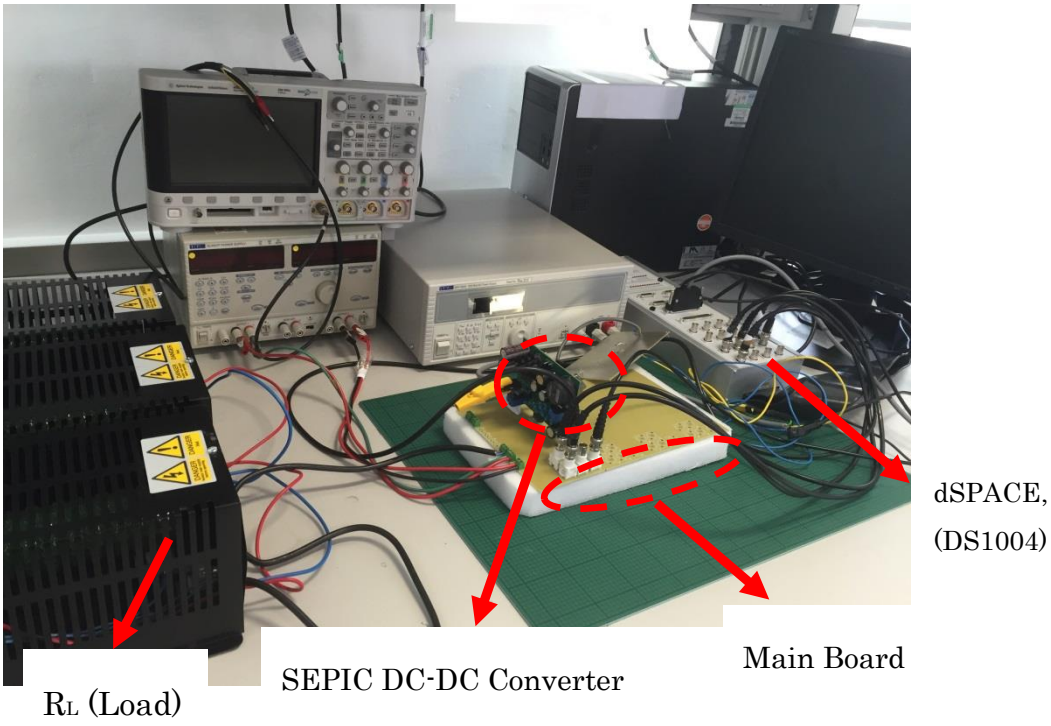

Figure 7-2 Real-time experimental test rig

7.2 Dominant Power Electronic Critical Components

It is widely known that power switches are the most critical components subject to thermo-mechanical stresses for any DC-DC converters, including the SEPIC converter. The potential of failure of various components used in the architecture of converters has been studied in the *Military Handbook for Reliability of Electronic Equipment,* MIL-HDBK-217F, summarised in Table 7-1 [149], [150]. As active switches are the dominant critical components subject to failure, this chapter mainly focuses on the reliability of power switches of the SEPIC DC-DC converter.

Table 7-1 Critical Components in Power Electronics Applications

Component	Type
Active Switches	IGBT, MOSFET
Diodes	Schottky power diodes

Capacitors	Dry aluminium electrolytic capacitors

In this regard, our experiments demonstrate qualitative thermal distribution at the surface of the SEPIC DC-DC converter using an infrared Fluke thermal camera shown in Figure 7-3. Our experiments have performed and corresponded to the input voltage 30V, 3A duty cycle 0.4, and 10-minute duration. After the snapshot integration at the surface of the PCB, the mean temperature reading is 64°C for the hotspot area detected around the IGBT and lower temperature readings for other components. This obviously indicates that the IGBT is the critical component when subjects to high thermal cycling during its operation.

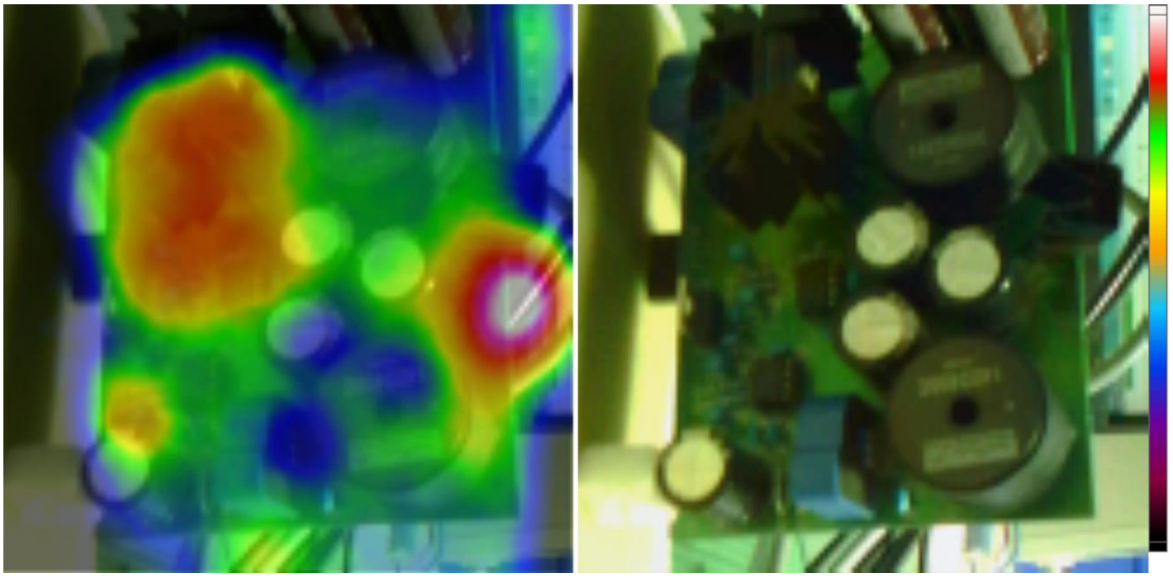

Figure 7-3 Temperature measurement of proposed converter using Fluke thermal camera

Therefore, the reliability of the IGBT needs to be assessed when exposures to failure injection in a similar fashion to wire bond joint failure as the dominant failure in IGBT packaging. Increasing the junction temperature with high-temperature change exposure causes die attached solder failure in a short period and by long-term exposure to small temperature changes causes wire bond solder joint failure. Therefore, each of these failure mechanisms has the different

potential of failure rates and model-based failure which increase the cost of overall lifetime estimation of the device in service. The current state-of-the-art failure mechanisms of power electronic modules (PEMs), notably the dominant failure based on packaging failures, is wire bond lift off under cyclic thermal loading conditions [84].

The difference in thermal expansion coefficients due to different materials inside the IGBT packaging introduces thermal stresses in the component [109]. In common operating conditions, the power dissipated by the silicon flows through multiple layers inside the IGBT until it is dissipated in the base plate by natural or forced convection. The solder, connecting the IGBT to the base plane, is seen as the weakest link in the assembly due to its high expansion coefficient α_{Sn-Ag} compared with the rest of the materials. This will introduce cycling shear stresses on the solder material, which becomes the most critical issue affecting the reliability of the component.

Because operating temperatures are relatively high compared with the melting point of the solder, low temperature creeps deformation occurs in a single transient stage, in which the creep rate decreases continuously over time [151]. In order to assure the structural integrity of the component, a fatigue analysis has been performed as failure stress analysis using two different approaches [151]. The following section discusses thermo-mechanical stress in an IGBT to present fatigue failure in solder joints.

7.3 Physics of Solder Failure Mechanisms

Although the SEPIC DC-DC converter benefits from a number of advantages, such as an impedance network at the input of the converter, and better shoot through switching state during the switching on mode, it still suffers from various failure mechanisms. As already mentioned in the introduction, the dominant failures of converters are related to the power switches of converters, mainly in wire bonds and solder joints. Obviously, it is wise to mention that SEPIC DC-DC converters present better reliability compared to traditional

converters as the new topologies involve fewer switches that improve the reliability and performance of systems [152]. Additionally, SEPIC DC-DC converters are good candidates to regulate the output power to desire value according to maximum power point tracking (MPPT). It is a suitable converter to characterise the solar panels, curves of short circuit current (I_{sc}) and open circuit voltage (V_{oc}) at different environment conditions. It also has the capability of changing the duty cycle to operate at each maximum power point.

Regardless all these positive features of SEPIC converter, the thermal stress of the active power switches due to the harsh environment has a direct impact on quality of the converter and limits the converter in its nominal operating condition. As has been mentioned before, IGBTs are one of the active devices in SEPIC DC-DC converters that are subjected to thermo-mechanical stresses and nonlinear strains during their operating conditions that affect the life prediction of the component.

In this regard, research conducted in [153] demonstrates a 3D Finite Element Analysis (FEA) analysis of the IGBT to understand the solder failure mechanism. Following the experimental data presented in Figure 7-4, a thermal load during an operating cycle is defined by the power dissipated in the silicon device, which is around 0.8W during the first 43 seconds. After that, the component is cooled down by natural convection with the surrounding air to 33°C. It is possible to estimate the smaller characteristic length in which is expected in temperature variations comparable with its characteristic value when uses the lower thermal diffusivity ($k/\rho c$) value from the materials and the characteristic time-scale in the cycle, (see Equation (38)).

$$l_d \sim \sqrt{\frac{k}{\rho c}\, t_c} \sim 70\ mm \tag{38}$$

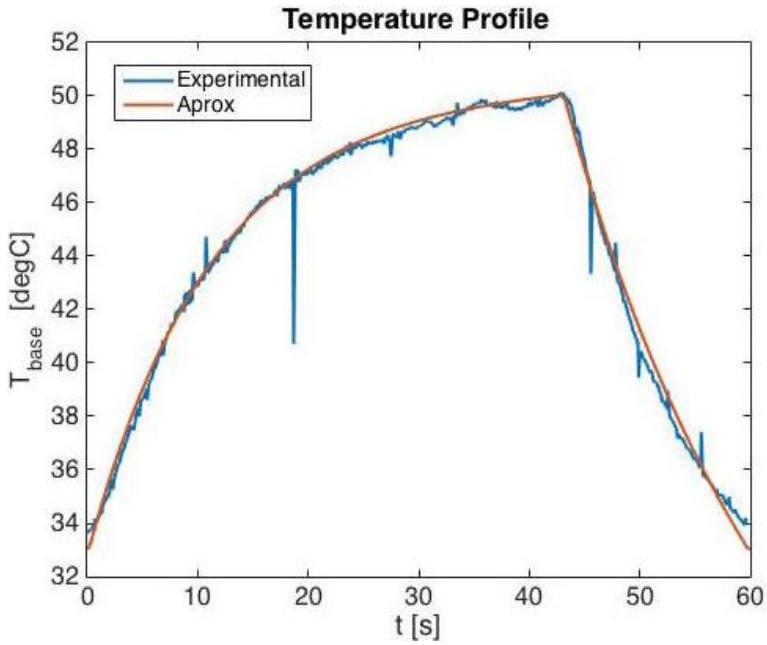

Figure 7-4 Temperature profile of the IGBT in one cycle

Comparing this characteristic length with the dimensions of the studied IGBT ($l \ll l_d$), it can be concluded that the temperature of the component, in first approximation, is just a function of time. In other words, the junction temperature is the same as the base plate temperature and the rest of the components. With this assumption, the FEA is reduced simply to the calculation of the thermal stresses and strains for the temperature profile presented in Figure 7-4.

The SnAg solder material exhibits creep behaviour during its operating conditions. It can be modelled by the Garofalo model [154], [155]. In this model, the creep rate is described by Equation (39), A being the creep rate coefficient, σ_{ref} the reference creeps stress, n the Garofalo parameter, Q the creep activation energy, R the ideal gas constant, T the temperature, s_{ij} the deviatoric stress tensor, and σ_e the von Mises stress.

$$\frac{\partial \varepsilon_{ij}^{c}}{\partial t} = \mathbf{A}\left\{\sinh\left(\frac{\sigma e}{\sigma ref}\right)\right\}^{\mathbf{n}} e^{-\frac{Q}{RT}} \frac{3}{2} \frac{Sij}{\sigma e} \tag{39}$$

The Morrow energy-based fatigue model (Equation (40)) has been implemented. It uses the dissipated creep energy as the damage controlling

mechanism. Since creep is an inelastic process, the dissipated energy can be calculated by integrating the creep dissipation rate (Equation (39)). The model is defined with two constants, the fatigue energy coefficient, $W_f \approx 55E6 \frac{J}{m^3}$, and the fatigue energy exponent, $m \approx -0.69$.

$$\Delta W_d = W_f (2N_f)^m \quad (40)$$

A difference in elastic and thermal properties introduces thermal stress in the component. Although they are not very high, the solder experiences significant inelastic strains (see Figure 7-5).

As was expected, the highest strains and stresses occur in the solder between the substrate and the base plate (see Figure 7-6). This is due to the high thermal expansion coefficient of the SnAg, and the accumulated displacement from the upper materials. The slightly higher value around the corner comes from modelling it as a sharp corner. Nevertheless, the location of the weakest point agrees well with the crack path in real applications [153].

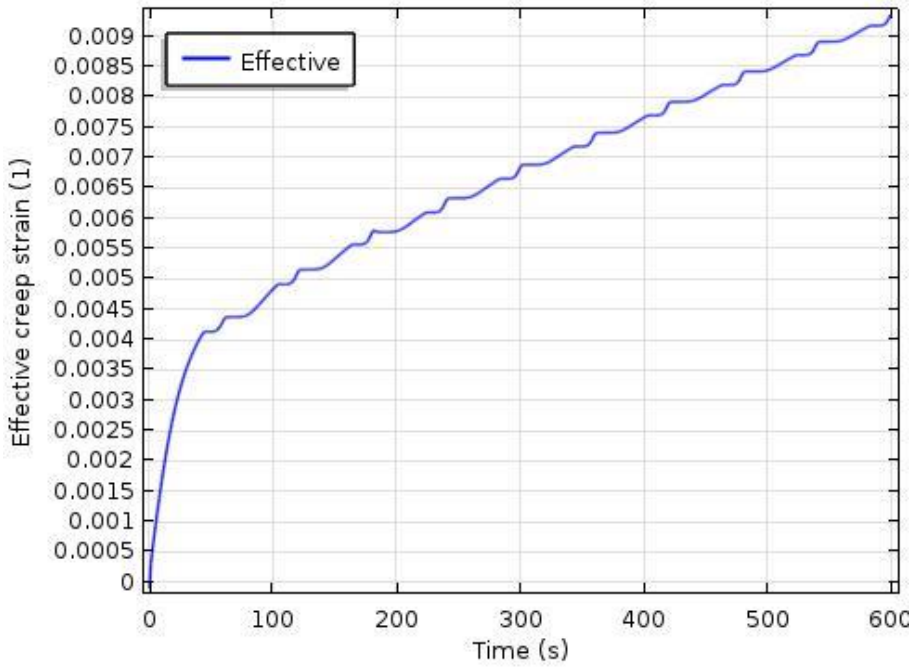

Figure 7-5 Creep strain development in the most critical point of the solder during the first 10 cycles

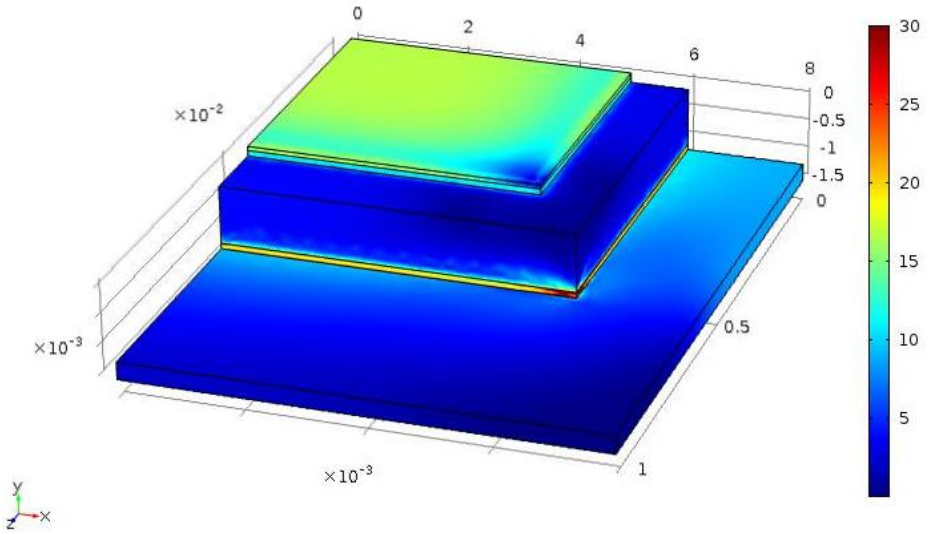

Figure 7-6 Von Mises stress after 10 cycles (units are Mpa)

When nonlinear strains are involved, several cycles need to be simulated to achieve a stable load cycle. Figure 7-7 shows the hysteresis cycle in the critical point.

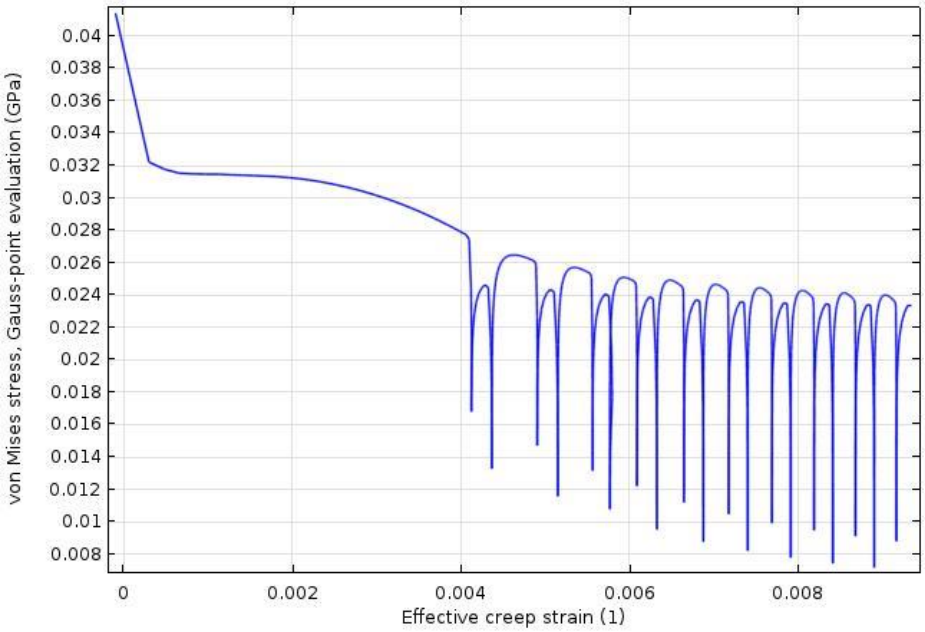

Figure 7-7 Hysteresis cycle in the critical point of the solder

Taking into consideration that the next cycles follow the same trend, with lower values of accumulated strain and less energy dissipated, the fatigue analysis based on the results presented in the last cycle of Figure 7-8 will give a conservative fatigue prediction of around 165,000 cycles.

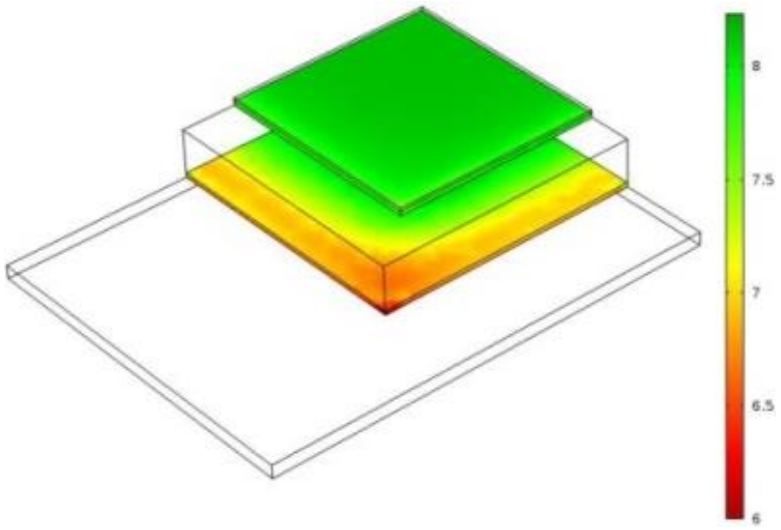

Figure 7-8 Fatigue life predicted on the dissipated creep energy

To sum up, the degradation mechanism comes from a crack initiated in the solder and leads to increaseD thermal variation (ΔT) at the IGBT, which again affects the crack growing rate. This will cause more heat to accumulate at the die-attached solder, which activates the degradation in the silicone by increasing the on-state resistance.

As such, the collector-emitter on-state resistance ($R_{ce(on)}$) exceeds 20% above the nominal value which then, the micro crack growth propagates under inelastic strain from different load conditions, are shown in Figure 7-9. The more the solder heats up, the more the solder joint connection is strained which results in time series of stresses and strains [156].

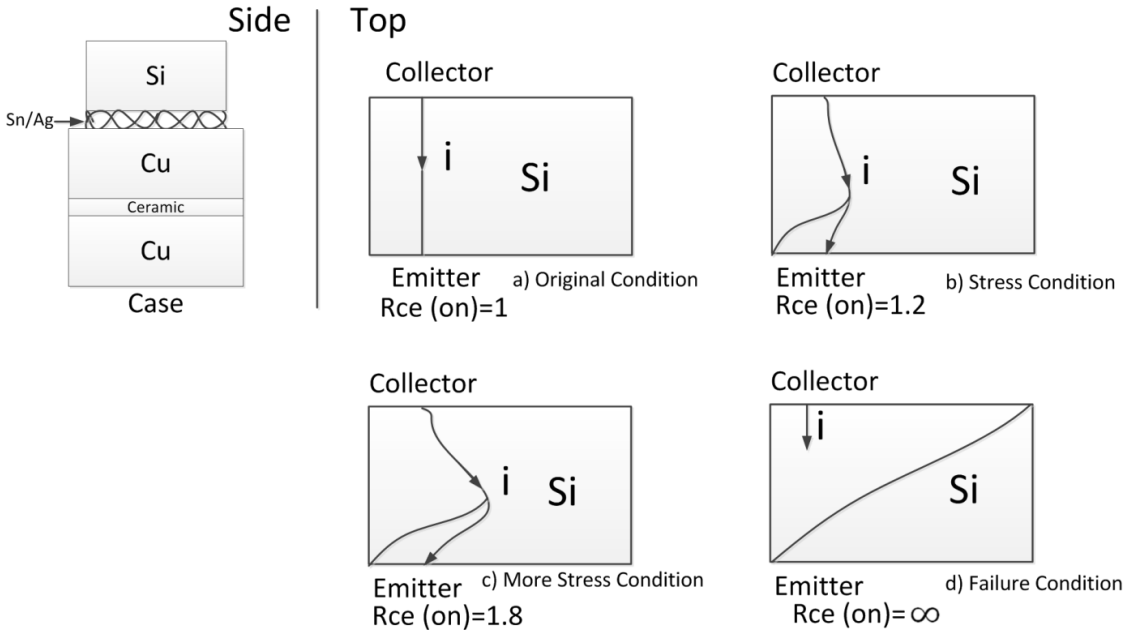

Figure 7-9 Microcrack propagation at die solder attached

The lifetime modelling of the IGBT depends on fatigue life models, which can be shown as a damage-based model to predict the number of cycles to failure of the IGBT.

The time domain fatigue model development requires analysis on the degradation profile is a prerequisite. This will be provided by temperature profile, which is given by reading junction to case temperature as it has abnormality happening due to solder fatigue [58]. This conditional monitoring parameter capability can intervene in control criticality system to prevent system reaches to its catastrophic failure.

7.4 Motivation of Stress Control

Using efficient and reliable switches for power converters and inverters is crucial for enhancing the safety and reliability of a platform. Generally, power converters suffer from failure mechanisms, such as wire bond fatigue, wire bond lift up, solder fatigue and loose gate control voltage, which mainly occur in power

switches. In this thesis, the junction temperature of the IGBT acting as a power switch used in the Impedance-Source DC-DC converter is estimated using an electro-thermal model in order to develop an adaptive thermal stress control (ATSC). The proposed stress control adjusts the reference input of the PI control to extend the life expectancy of the device under the mission. The accuracy of results presented using the modified Coffin-Manson law has been used to determine the life of the IGBT and the lifetime has been successfully increased based on implementing the imperative ATSC and comparing the results with the constant reference input of the PID controller.

There are a number of thermal stress controls for the IGBT that are used for minimising temperature variation [157]. These include active thermal control. A few review papers have covered the thermal stress control approaches for IGBTs.

In [158], Andresen et al proposed active thermal management which limited the output current dependent on the output frequency as the maximum junction temperature is quite high for low-output frequencies.

In [159], Murdock et al implemented a fuzzy region-based controller to regulate the mean temperature (T_m) and junction temperature variation (ΔT_j). This is done by using a proportional-integral-derivative (PID) controller to mitigate the switching frequency and load current proportionally to avoid the junction temperature rising above 110℃.

For all the above thermal stress control approaches, the dynamic of the stress parameter (e.g. junction temperature estimation) has not been considered.

In PV applications, a maximum power point tracking algorithm is a perquisite to deliver desired maximum power from photovoltaic panels. It will be an advance to use a SEPIC DC-DC converter in real-time conditions for this purpose. Thus, it is important to use more reliable power switches (e.g. IGBTs) to improve the efficiency of photovoltaic applications. Thus, it is necessary to have

an accurate and robust CBM technique on board, which has been used for real-time estimation of lifetime consumption.

In order to enhance the reliability of SEPIC DC-DC converters, this thesis aims to employ a physics-of-failure model of the active switch and implement a stress reduction algorithm infusion with a critical control unit. This ultimately reduces the power dissipation for improving life cycles. To meet these key advantages, this chapter will focus on:

Reliability assessment by using the Coffin-Manson rule based PoF model, which integrates the junction temperature of the device with the model. As a precursor parameter for monitoring the health state, the junction temperature is derived from an electro-thermal model to extend the lifetime of the IGBT in downtime [80].

Stress minimisation by introducing a radically novel approach for the development of an adaptive algorithm control for deceleration of the junction temperature stress. It focuses on the degradation data collected from simulation failure propagation conducted particularly for the power switch in the PV module applications under the degradation process occurring in the packaging failure mechanism.

In order to validate the results of the ATSC, a modified empirical equation Coffin-Manson Law is used to calculate the life usage of the device. This will ultimately improve design processes in making robust maintenance schedule policy and efficient reliability assessment. Furthermore, it will be presenting for the life extension of the device. To that end, the junction temperature for the IGBT in the SEPIC DC-DC converter needs to be calculated for non-destructive reliability assessment.

7.5 Junction Temperature Calculation

Since the direct measurement of the IGBT junction temperature is impractical, real-time calculation of the junction temperature needs to use an

appropriate compact electro-thermal model. This model constructs from the thermal parameters (R, C) of the device, which are representing of layers, such as the die, solder, substrate, copper, and baseplate in the thermal RC network structure based. The RC model of the IGBT considers a Foster circuit for the junction to case impedance of the device in Figure 7-10.

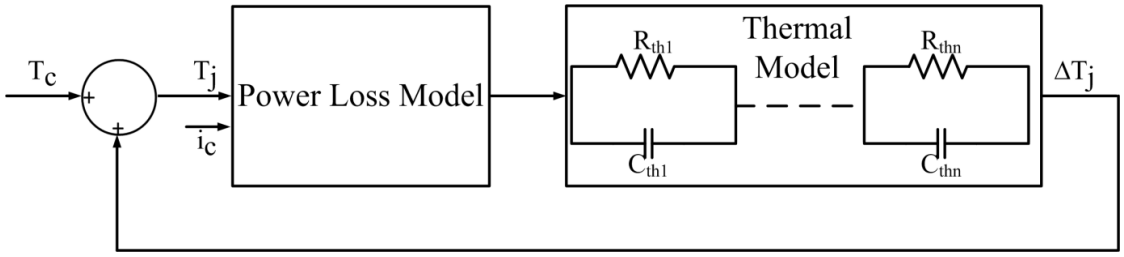

Figure 7-10 Junction temperature estimation

The transient thermal impedance is expressed in Equation (41) at time t. The network can be a n number of time constants and thermal resistances [13].

$$Z_{jc} = \frac{T_j(t) - T_c(t)}{P} = \frac{\Delta T_{jc}}{P_{PULSE}} \tag{41}$$

The peak junction temperature attained during stationary operation when the pulsed power (e.g. power dissipation) flows through the IGBT structure where the transient thermal impedance will be the sum of each structure layer (see Figure 7-11). By means of a coolant system, the reference input temperature of the power converter is set to the ambient temperature. The estimation of the junction temperature is used as a control parameter to adjust the duty cycle to a certain value till the critical temperature cools down under the nominal temperature working condition. The junction temperature will rise up in a short time as the time-dependent heat diffusion in Equation (42) similar to the electric circuit analogue shown in Figure 7-12.

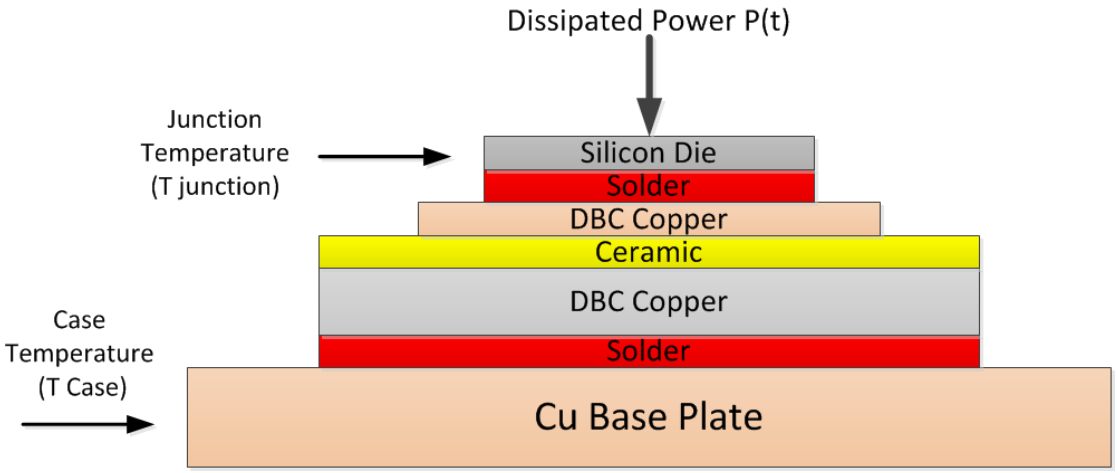

Figure 7-11 IGBT structure layers

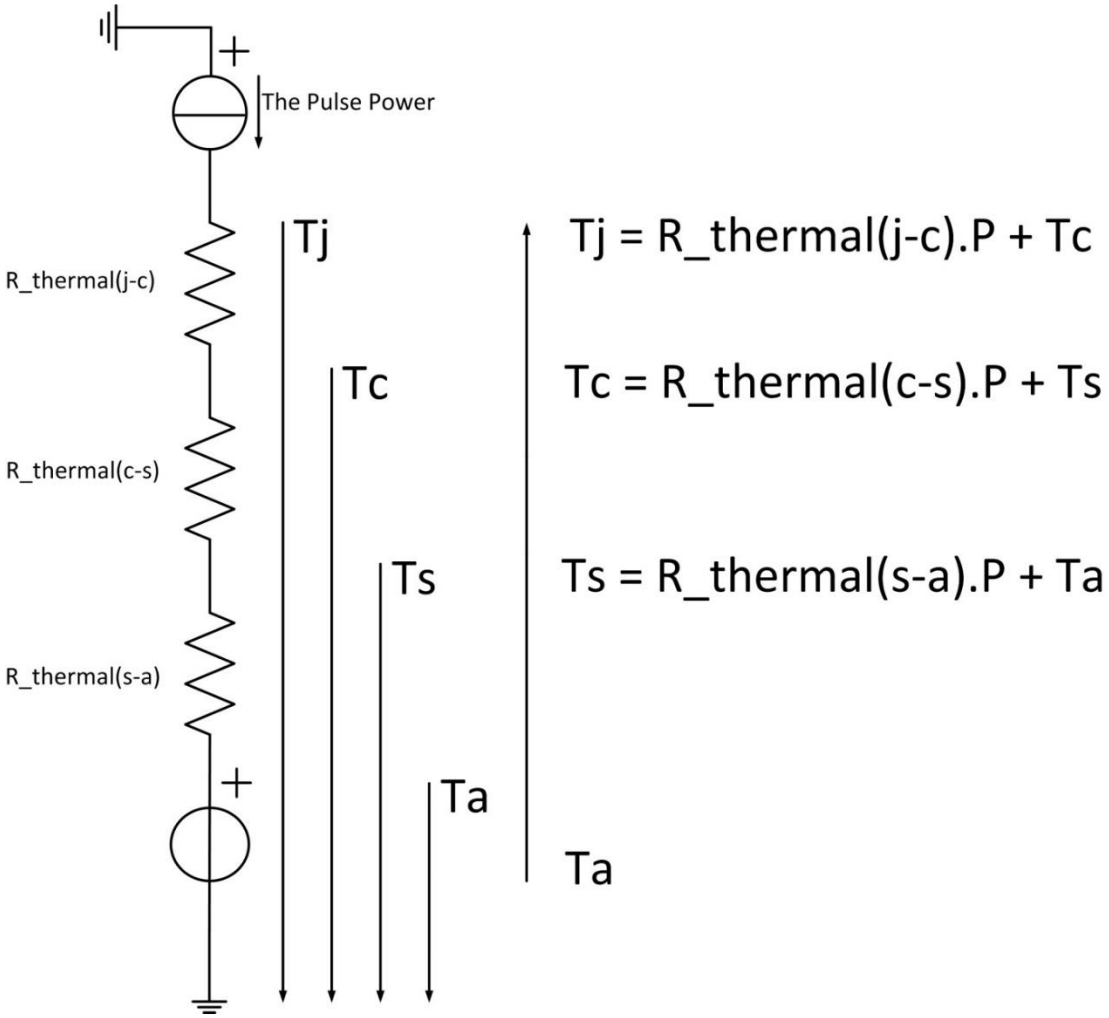

Figure 7-12 Thermal impedance of the IGBT structure

where thermal resistance is defined based on different structure points of the IGBT:

$R\_thermal(j-c)$ is the thermal resistance between the junction and the case (baseplate).

$R\_thermal(c-s)$ is the thermal resistance between the case and the heat sink.

$R\_thermal(s-a)$ is the thermal resistance between the heat sink and the ambient.

$$T_{j(t)} = T_c + P_T.[4t/(\pi R_{th} C_{th})]^{1/2} \quad (42)$$

where T_c is the reference IGBT's case temperature and R_{th} is the thermal resistance of the i number of R_{th} ($℃/Wm$) – C_{th}($Watt.Sec/℃$) for each physical structure of the IGBT. Furthermore, $\tau = R_{th}.C_{th}$ presents the thermal time constant (sec) of the i^{th} RC pairs.

In Equation (42), $P_T(W)$ stands for total power losses of the single device. In a SEPIC DC-DC converter, most of energy losses will be in the IGBT switching and conduction mode. Therefore, freewheeling diode conduction losses are negligible as during turn off switching energy stores in L_2 as shown inFigure 7-1. In this thesis, the SEPIC DC-DC converter is designed for the mid-power solar panel application. Therefore, the conduction loss of the device can be calculated by using three parameters as expressed:

1) On-state collector-emitter voltage ($Vce_{on-state} \equiv V_{CEO}$)

2) On-state collector current ($Ic_{on-state} \equiv I_c$)

3) Collector-emitter on-state resistance (r_c)

where the instantaneous conduction losses can be calculated using a series of these parameters in Equation (43):

$$P_{ct} = V_{CEO}.I_c(t) + r_c.I_c(t)^2 \quad (43)$$

The approximation in mid-power application is given as:

$V_{CEO}.I_c(t) > r_c.I_c(t)$

Therefore, the average losses over a period of T_{sw} in conduction mode can be expressed as:

$$P_{ct} = \frac{1}{T_{sw}} \int_0^{T_{sw}} V_{CEO}.I_c(t)dt = V_{CEO}.I_{cav} \quad (44)$$

Power losses in the IGBT during off and on switching modes are the product of switching energies and the switching frequency (f_{sw}):

$$P_{sw(on-off)} = \left(E_{on-mode} + E_{off-mode}\right).f_{sw} \quad (45)$$

where $E_{on-mode}$ and $E_{off-mode}$ an energy losses are dependent on the blocking voltage and the junction temperature during on and off mode switching, respectively. The energy losses for each event are computed considering the collector current during the fall-time interval and associated with voltage rise-time interval. The total power losses in the IGBT are expressed by the sum of the conduction and switching losses giving:

$$P_T = P_{CT} + P_{sw(on-off)} \quad (46)$$

A real-time numerical simulation was developed to calculate the average power loss conduction using a MATLAB look-up table which is dependent on certain parameters (e.g.V_{CEO}, I_c, and junction temperatures). The look-up table is consulted at switching action, and can interpolate some conditions which are not being given in the data sheet. As an application of the PV, a discrete IGBT with

absolute rating 75A-600V (High –Speed V series) is selected to power up the DC load. The switching energy E_{off} and E_{on} losses rise up due to increases of I_c (collector current), R_G (external gate resistance), T_j and V_{CE}. During the turn on, energy dissipation E_{on} is swiftly increasing with variation of R_G. In a contrast the turn off energy dissipation E_{off} has less dependency on changing of R_G. However, both E_{on} and E_{off} considerably depend on the variation of I_c and temperature changing, as is expressed in Figure 7-13.

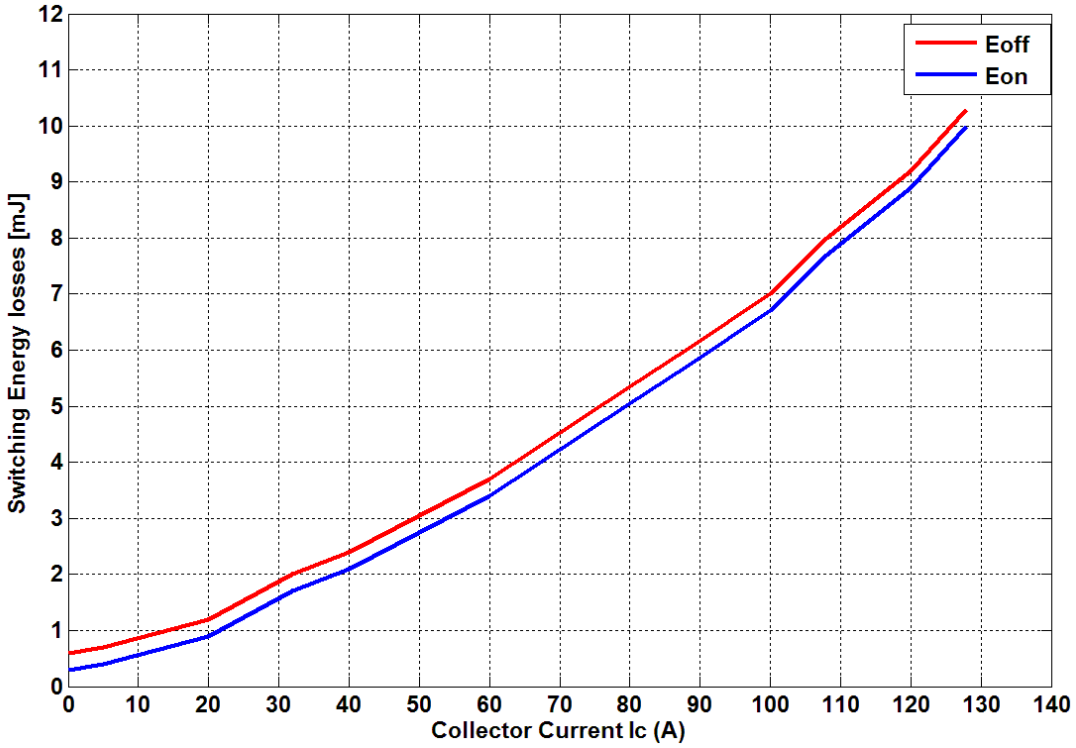

Figure 7-13 Typical FGW75N60HD IGBT switching losses

As a result, the method to calculate both E_{off} and E_{on} equations from Figure 7-13 for a given maximum acceptable junction temperature 175℃ are the outputs switching energy losses in $[mJ]$.

$$E_{on} = 2.3e-7{I_c}^3 + 2.1e-4{I_c}^2 + 0.026I_c + 0.1382 \quad (47)$$

$$E_{off} = 2.4e-7{I_c}^3 + 2.5e-4{I_c}^2 + 0.034I_c + 0.54 \quad (48)$$

The precise switching loss estimation over a PWM switching cycle requires looking at the transient power losses over time. To this end, look-up tables consider a given operating range of different condition measurements such as DC forward blocking voltage, collector current and the junction temperature. The conduction loss curves of the IGBT are performed in three index vectors, such as collector-emitter current, on state collector-emitter voltage and device at two different junction temperatures, which interpolate/extrapolate linearly to get certain temperature values in term of intermediate points. The datasheet is given characteristics of collector-emitter on-state voltage versus collector current at junction temperatures (25℃ and 175℃), which can be used for instantaneous conduction power loss calculation, as shown in Figure 7-14. The typical curve is selected versus gate-emitter 15 volts which in practice IGBT is well triggered with this voltage.

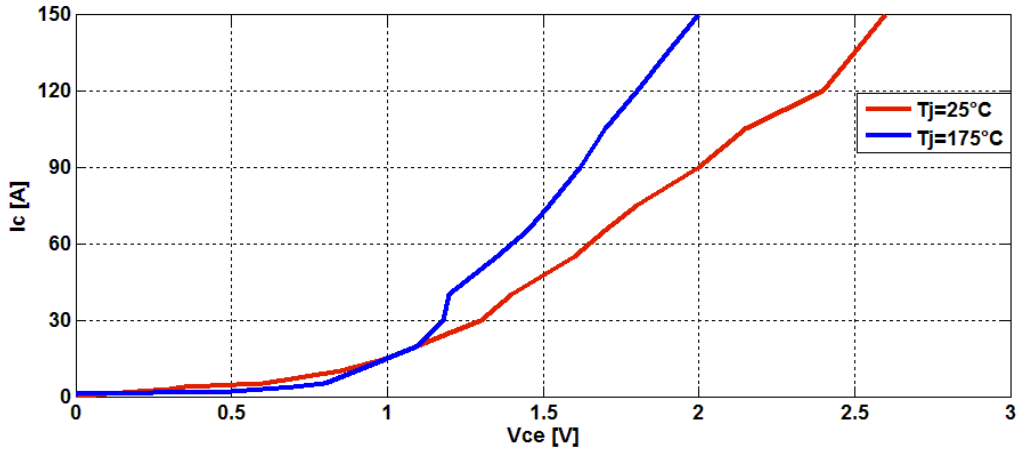

Figure 7-14 Typical FGW75N60HD IGBT output characteristics ($V_{ce} - I_{ce}$) vs junction temperature (25℃ *and* 175℃)

The thermal resistance of the junction to the case has to be minimised by manufacturer design to keep the junction temperature of the IGBT within specific safe conditions. The junction temperature is calculated for a single IGBT (TO 247 packaging) which is manufactured by Fuji Electric and is selected for the features of mid-power loss, low switching surge and noise and high reliability in DC-DC converters. To enable T_j calculation, the $R_{th(j-c)}$ (0.3℃/W) and τ (0.1 Sec) are obtained from the datasheet and effectively $C_{th(j-c)}$ (0.33$Watt.Sec$/℃)

using $\frac{\tau}{R_{th(j-c)}}$ is calculated. In this thesis, what has been ensured, however, is that the maximum junction temperature under the maximum power tracking condition does not exceed the safe margin value for T_j=110℃. The total power losses (see Figure 7-15) are calculated iteratively at the determined junction temperature, which initially is approximated at ambient temperature, and after a few iterative loops, the accurate T_j will reach its stationary value (see Figure 7-16), as shown in Equation (49).

$$T_{j(k)} = P\left(T_{j(k-1)}\right)\left[R_{th(c-a)} + R_{th(j-c)}\right] + T_a \tag{49}$$

where K=1 to n; $T_{j(0)} = T_a$

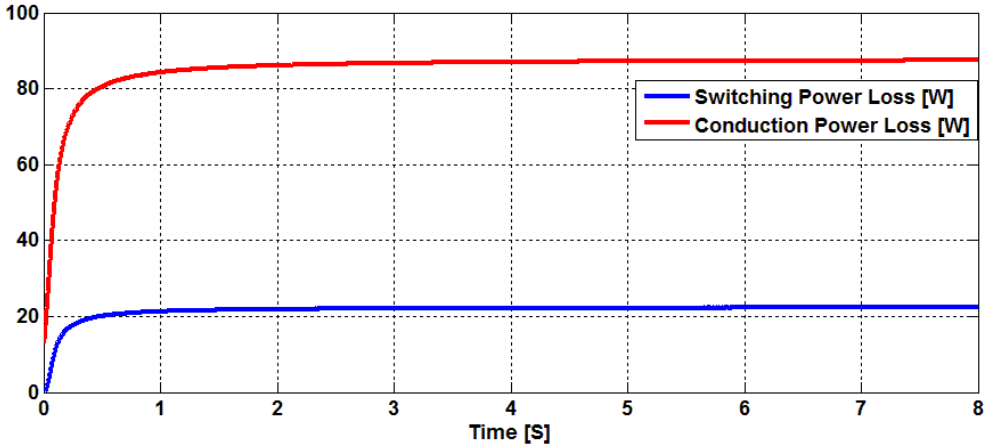

Figure 7-15 Total power loss estimation

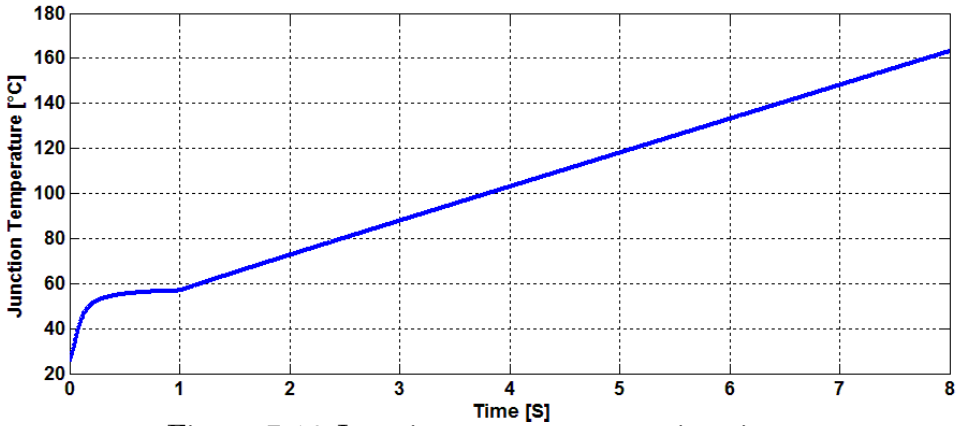

Figure 7-16 Junction temperature estimation

The mission profile is dependent on the junction temperature swings (ΔT_j) which must acquire for indication of stress parameter in the lifetime model [160].

7.6 Damage Profile Modelling Approach

The damage profile collection needs to run in real power cycles to test the lifetime of the device, which is impractical and requires long ageing test time as IGBT life expectancy can last for millions of cycles. Since the novelty of this chapter is about extending the lifetime of the SEPIC DC-DC converter by decelerating failure mechanisms, the damage profile collection needs to be run in real power cycles to test the lifetime of the device. This is quite impractical and requires long ageing test time as IGBT life expectancy can last for millions of cycles. Hence, in simulating, the failure mode is mainly related to wire bond failure has induced in a similar fashion to crack progression at solder joint by increasing the on-state resistance from 0.3Ω-0.75Ω. This is the potential of solder joint fatigue as an important failure mechanism process in power electronic switches The junction temperature increases at 1 sec gradually as a result of failure injection, as shown in Figure 7-16. In this simulation, the ambient temperature is fixed to $24^{\circ}C$ and for given switching frequency 16 KHz. The thermal stress fatigue is considered as the damage profile, which is caused by cyclic temperature in the solder joint. This phenomenon is susceptible to high-temperature thermal cycles, which initiate micro crack propagation, and incorporates the effect of the contraction and compression going. The elastic strain stress law (e.g. the magnitude of thermal cycle ΔT) built up in the solder by n number of given ΔT over the entire temperature scale. This model incorporates a power law (e.g. Arrhenius model) to correspond the fatigue failure model, which can be expressed in Equation (50) [59].

$$N_f = f^{\beta}.\lambda.(\Delta T)^{-\alpha}\exp\left[\frac{E}{K.T}\right] \qquad (50)$$

where f is the frequency of the stress cycle and, α, β are exponent terms as the coefficients of the best fit for the model life time. The coefficient α which ranges from 2 to 3 describes the effect of the severity of the temperature change,

whereas λ is the constant for material properties. the physic terms of the exponential part are the Arrhenius effect E, K and T as the activation energy in eV, the Boltzmann constant ($1.38\times10^{-23}\frac{J}{K}$) and the temperature of failure, respectively.

7.6.1 Exploration of Reliability Using Cycle Counting

The problem posed by the practical device operation is that the thermal cycles are not uniform and that the mean and range change from cycle to cycle, i.e. the load cycle effectively imposes a random thermal cycle to the devices. A method that may be used to correctly account for the number of cycles of each combination of mean and range is applied here to explore the effect of the thermal cycling. This is known as rain-flow cycle counting, which was originally developed for analysing random stress variations in material fatigue by counting the number of complete peak-to-peak cycles experienced.

The time history of the transient temperature profile, in this case, is reduced to a sequence of peaks and troughs. The peaks and troughs are analysed in turn, with a rain flow analogy applied to a rotated copy of the history. By analysing the peaks first, the temperatures at the peak and the next trough are recorded. The analysis moves through the history until the temperature next exceeds this peak, where it is interrupted by a flow from an earlier larger peak or the history ends. At this point, the cycle terminates. The resulting mean and range are, respectively, the average of and the difference between the recorded peak and trough. A half cycle is recorded for this combination of mean and range. The analysis then moves to the troughs and repeats the analysis, adding up the resulting half cycles. Finally, half cycles of opposite sense and the same mean and range are added to give whole cycles. The resulting distribution, or rain-flow matrix, is the number of observed cycles for each combination of temperature mean and range. Although the rain-flow cycle counting method may be used to gather information about the spread of the number of cycles observed with temperature mean and range, it does not relate to the failure rate of the device.

Any method that applies failure estimation to the cycle counting results automatically makes assumptions about the failure mechanisms and the dependence on the temperature mean and range. This method is increasingly used in IGBT lifetime consumed for different spectrum loading conditions (ΔT) as a stress condition. This is estimated by means of using Miner's linear cumulative damage rule, which states the failure phase as the following condition is met as shown in Equation (51) [161]:

$$\sum_{i=1}^{k} \frac{n_i}{N_{f(i)}} = 1 \qquad (51)$$

where i is index, which varies within the range of the number of loads in a spectrum ($1 \leq i \leq k$) and n_i is the number of cycles the IGBT that is exposed to i^{th} temperature swing, whereas $N_{f(i)}$ is the fatigue lifetime for i^{th} load condition. In this chapter, the effective stress range can also be identified using the rain-flow counting method, which is the most suitable algorithm for counting the stress cycle from the fatigue damage profile.

The cycle counting is presented in Figure 7-17 for the IGBT estimated junction temperature profile as it is shown in Figure 7-16. The numbers of cycles are expressed with the temperature swing amplitude.

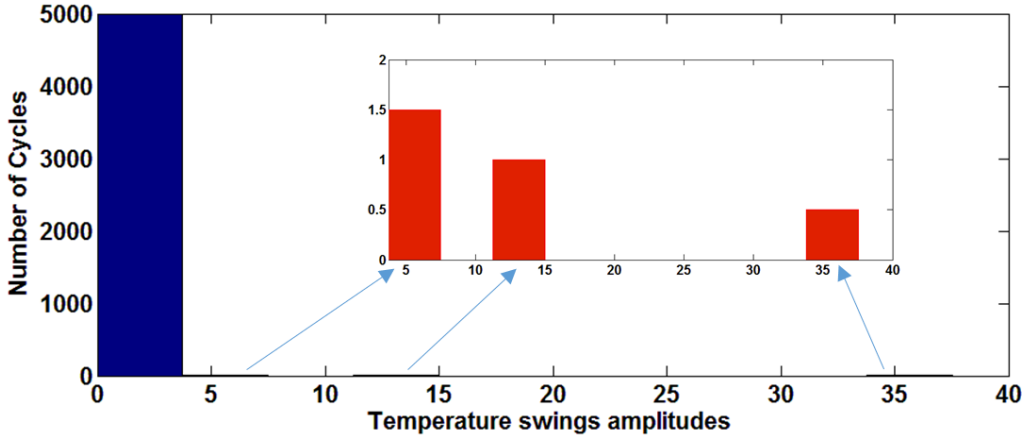

Figure 7-17 Rain-flow histogram of IGBT junction temperature variations before applied stress control

The life usage of the IGBT for the mission profile with predominant temperature stress swings is given in Table 7-2.

Table 7-2 IGBT Lifetime Calculation Results

Temperature Swings	7.5<ΔT℃<11.3	11.3<ΔT℃<15	33<ΔT℃<37	**< 7.5**
Number of Cycles (n_i)	1.5	1	0.5	5000
Mean Temp ℃	153	112	63	45
Number of Cycle to failure ($N_{f(i)}$)	4.1370e+5	4.8743e+5	6.609e+5	1.7332e+5
Life Consumed %	3.6258e-4	2.0516e-4	7.5632e-5	2.8849
Life Consumed after 8 seconds	Almost 3%			

The percentage lifetime consumed calculation for each thermal cycle stress uses Equation (51) to estimate the fraction of total life. Apparently, the total IGBT life usage is due to significant thermal variation stress smaller than 7.5 which significantly have a number of thermal cyclic. To increase the power cycling lifetime of the device requires an adaptive algorithm as the thermal stress amplitude and the number of cycles to failure proportionally reduce [162], [96].

7.7 Adaptive Thermal Stress Control

In this chapter, the stress control algorithm renders to mitigate the junction temperature variation, which generates a non-uniform distribution of hot spots and thermal stress. This approach assumes that the IGBT is degraded as the switching losses relatively increase, and consequently, raises T_j. Observing the junction temperature enables the Adaptive Thermal Stress Control (ATSC) to adjust the duty cycle (D) when the healthy state of device progresses to a degraded state after a one-second simulation run. The duty cycle will be reached to 0.36 at the normal operating condition, and after failure injection without affecting the adaptive control (see Figure 7-18).

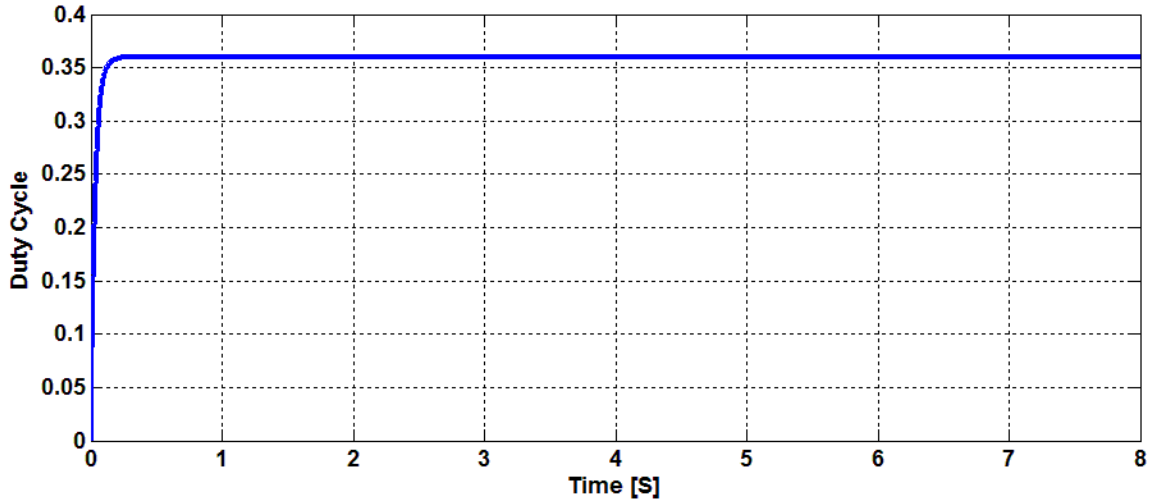

Figure 7-18 Converter duty cycle

Based on the previous discussion, the junction temperature is affected by power losses, which are dependent on the power demands. In order to regulate the desired output of the SEPIC DC-DC converter, the output voltage is sensed and compared with V_{ref} as the error input through the PID controller to generate D which then regulates a pulse width modulation (PWM) with the fix ±15 gate voltage (Vg) which supplies the PWM gate signal to each IGBT/MOSFET switch. The switching frequency and the gate emitter on-state voltage are given from the power switch specification. Under the degradation process, the ratio between the on-state duty cycle and the off-state duty cycle can be varied, and thus the power allocations. The control strategy is required under the failure propagation where the on and off duty cycles will be allocated properly in the ATSC according to the severity of the thermal stress, and varied by adjusting V_{ref} from the output voltage of the MPPT and the output voltage as a feedback parameter loop receiving from the load. Thus, the voltage control loop is composed of a PID voltage controller, an output capacitor C2, and a load. The PI controller effectively is fed with updated V_{ref} according to the reference junction temperature ($T_{j_{ref}}$) as an inner loop which is set to a particular value depending on the IGBT characteristics.

Generally, a PID controller is utilised to ensure the stability of the duty cycle which improves the switching frequency. It is necessary to be used to reduce the steady state error in order to improve the system performance. As a result, the estimated junction temperature gradient declines for the entire target simulation in comparison with $T_{j_{ref}}$ for the determined eight-second simulation performance. This results in improving the converter's life expectancy in downtime by reducing thermal stress and has great impact on DC-DC power converters, as shown in Figure 7-19.

A prototype of the SEPIC DC-DC converter has properly designed to verify the initially proposed simulation at the same rate power of 1.5[kW], with the capability of an output voltage 150[V] and an input voltage of 30-40[V]. Table 7-3 provides the rate of converter's components parameters details. The converter is controlled and simulated via the pulse width modulation (PWM) operation with a carrier frequency of 16KHz.

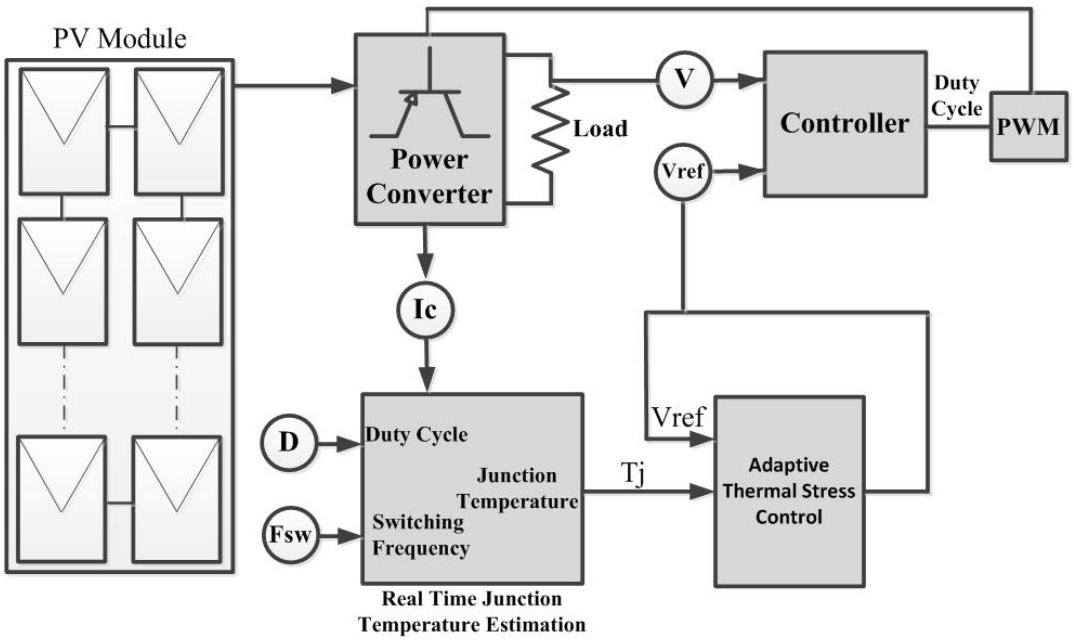

Figure 7-19 Proposed schematic diagram of sensorless thermal stress reduction control

Table 7-3 Component Parameters for Proposed SEPIC Converter

Output power rating	1.5 [kW]	fs	16[KHz]
V1	30-40 [V]	V2	150 [V]
C1	10[μF]	C2	1000[μF]
L1	1[mH]	L2	15[mH]
IGBT		FGW75N60HD	

The dominant failure mechanism of the IGBT, such as bond wire lift up due to solder fatigue progression, is injecting after one second, and it is noted that T_j of the IGBT will rise with slope at 15 and will exceed the defined safe margin value (e.g. 125℃), as shown in Figure 7-16. The proposed ATSC is illustrated in Figure 7-20 assumes the thermal stress can be controlled after the estimated T_j reaches 60℃ where the IGBT is in the normal operating region corresponding to time before it is subjected to deterioration at around 1 sec. The PID control maintains the duty cycle (see Figure 7-18) before T_j rises above 60℃. To increase the converter's lifetime and maintain consistency with the IGBT operating in failure conditions, the control region is designed to reduce the extreme operating condition from over temperature as the duty cycle was regulated between 0.35 and 0.3 (see Figure 7-21) which reduces a total of 40℃ for T_j. In order to intuitively decelerate the temperature rising, the proportional slope rate is determine online and accordingly V_{ref} is adapted and tuned with an effective switching frequency (f_{sw}) rate 16kHz of the device.

The PID controller parameters are determined based on conventional PID tuners (e.g. Ziegler-Nichols tuning) gain calculated method. The photovoltaic panel voltage must track the voltage calculated by the MPPT. The algorithm output will be a reference parameter for PID. The PID controller state feedback can be described as below:

$$d(t) = K_i \int (V_{ref} - V_{in})dt + K_p (V_{ref} - V_{in}) + K_d \frac{d(V_{ref} - V_{in})}{dt} \quad (52)$$

where V_{ref} the output of MPPT algorithm and V_i is the output of the photovoltaic panel. In addition to the two states in the converter, the error is defined as the third state of the system.

$$z \equiv \int (V_{ref} - V_{out})dt \quad (53)$$

Therefore, the new state vector would be:

$$Z = \begin{bmatrix} x \\ z \end{bmatrix} \quad (54)$$

By combining (53) and (52),

$$d = k_i z - k_p C x - k_d C \dot{x} + k_p V_{ref} \quad (55)$$

$$d = -(I + k_d C B_d)^{-1}(k_p C + k_d C A_d)x + (I + K_d C B_d)^{-1} k_i z + (I + k_d C B_d)^{-1} k_p V_{ref} \quad (56)$$

Therefore, the controller equation which can expressed as state feedback $d = K_a Z$ is:

$$d = (I + k_d C B_d)^{-1}[-(k_p C + k_d C A_d)\, k_i]Z + (I + k_d C B_d)^{-1} k_p V_{ref} \quad (57)$$

The final representation of the augmented system may be written as:

$$\dot{Z} = \begin{bmatrix} A_d & 0 \\ -C & 0 \end{bmatrix} Z + \begin{bmatrix} B_d \\ 0 \end{bmatrix} d + \begin{bmatrix} 0 \\ I_{ref} \end{bmatrix} \tag{58}$$

$$V_0 = [C \quad 0]Z$$

where, $d = K_a Z$

The PID parameter gain is calculated as follows:

$$\left[(I + k_d C_z B)^{-1}\left[-\left(k_p C_z + k_d C_z A\right) k_i\right]\right] \equiv [-0.2108 \quad -0.0021 \quad 15.946]$$

Then,

$$\mathrm{k_p} = 0.002483 \quad \mathrm{k_d} = 3.7e-6 \quad \mathrm{k_i} = 75$$

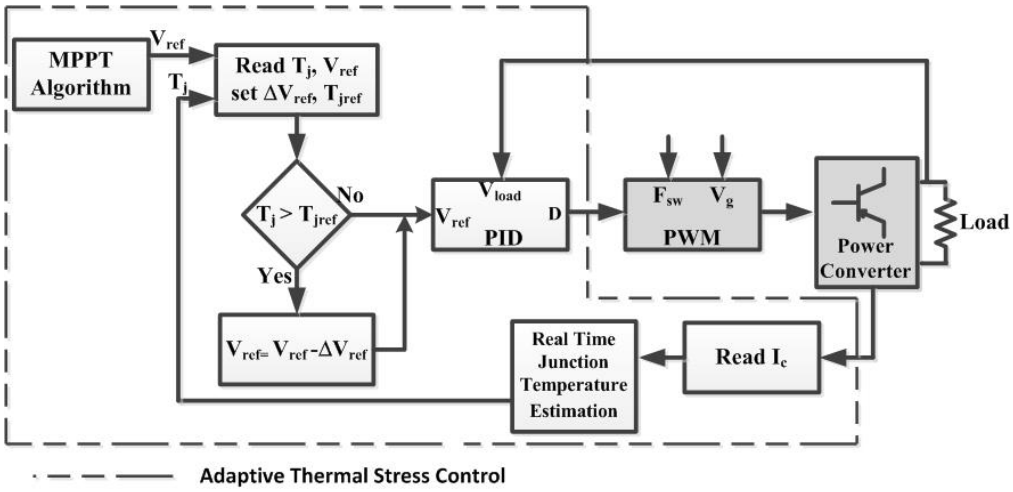

Figure 7-20 Proposed schematic diagram of adaptive thermal stress reduction control algorithm

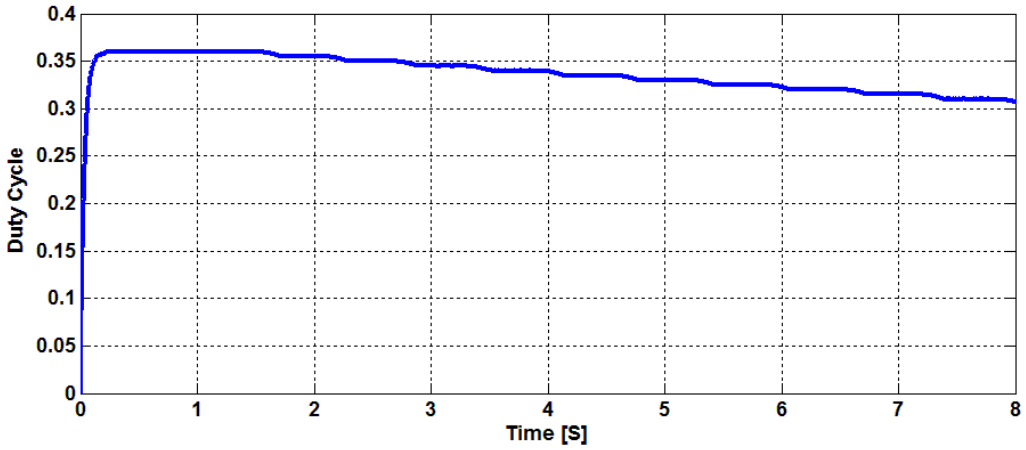

Figure 7-21 Regulated duty cycle with the effect of ATSC control implementation

7.8 Lifetime Extension Results Discussion

As the slope, rate indicates the estimated junction temperature rises above $T_{j_{ref}}$ at 60℃, the ATSC immediately reduces the junction temperature's slope (see Figure 7-23) and clamp the slope at 10. This will be happen by adjusting V_{ref} at 150V from MPPT algorithm according to its dynamic response value ΔV_{ref}. However, following the design specification, the output voltage's limitation does not halt under the appropriate value, which distorts the power demand, as shown in Figure 7-24.

The adaptive stress control part keeps the temperature below 125℃ that allows the IGBT operates in less stress condition until the mission is fulfilled. The most efficient part of the proposed control is about loss reduction which minimises active power losses, as is shown in Figure 7-22. Figure 7-23 shows that the slope of T_j is successfully decelerated, wherein the lower limits of the output voltage is set based on the minimum acceptable output voltage performance as the least limitation of the load demand. Figure 7-24 shows the minimum constrain requirement has been set to 120V, also is depending on the duty cycle, ensuring that the minimum power can be generated from the PV module. In addition reduces the risk of failure of the converter from thermal stress conditions. Moreover, ATSC has extended the lifetime of the IGBT. Furthermore, investigation needs to be performed by applying a rain-flow

algorithm to the junction temperature profile for calculating the device lifetime usage. Interestingly, the device incredibly consumes less lifetime cycles in the form of the inverse-exponentially vs the thermal stress variation amplitude, as shown in Figure 7-25.

The life usage of the IGBT for the mission profile after stress control applied with predominant temperature stress swings has been calculated and is given in Table 7-4.

Table 7-4 IGBT Lifetime Extension Calculation Results

Temperature Swings	2.2<ΔT°C<4.5	13.5<ΔT°C<15.8	20.4<ΔT°C<22.6	<2
Number of Cycles	2	0.5	0.5	5000
Mean Temp °C	51	102.7	64.3	64.5
Number of Cycles to Failure	6.5700e+05	1.8921e+06	1.9934e+06	1.5279e+06
Life Consumed %	3.0442e-06	2.6425e-05	2.5083e-05	0.33
Life Consumed after 8 Seconds	Almost 0.33%			

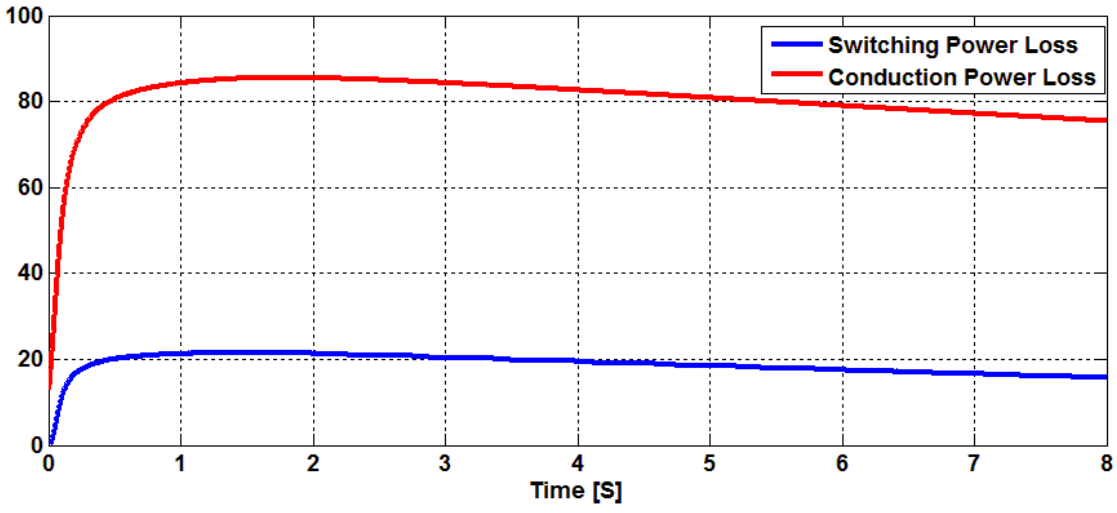

Figure 7-22 Total power loss estimation reduction with the effect of ATSC control implementation

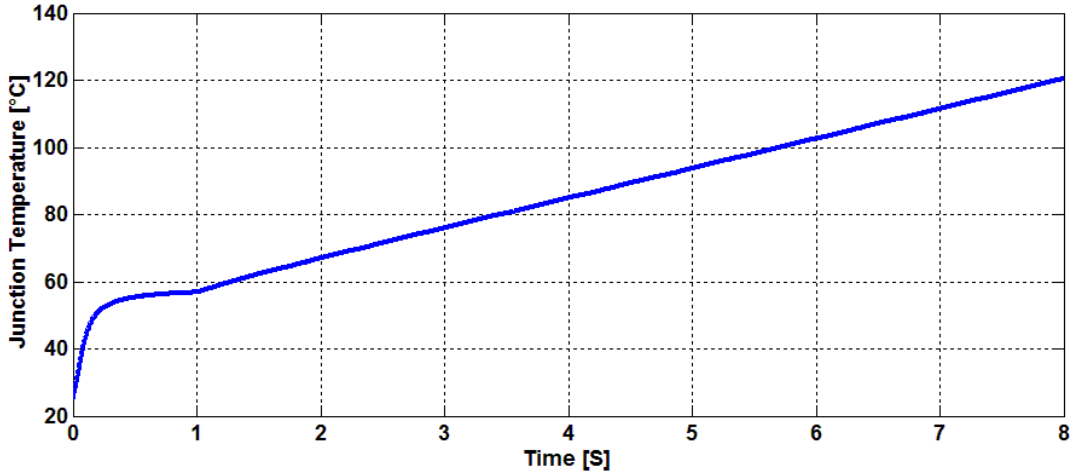

Figure 7-23 Junction temperature reduction with the effect of ATSC control implementation

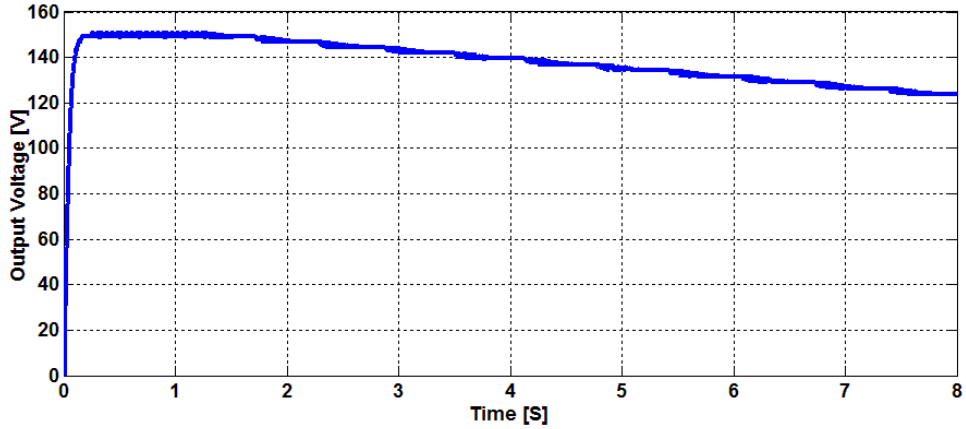

Figure 7-24 Output voltage demand with the effect of ATSC control implementation

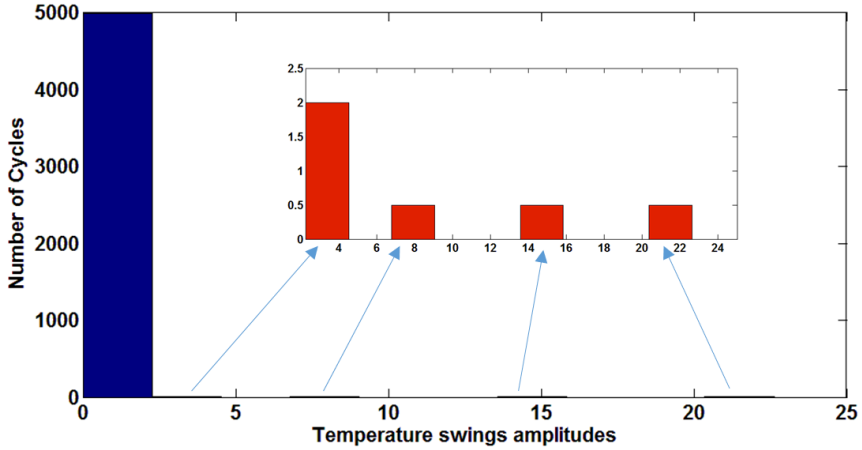

Figure 7-25 Rain-flow cycle counting for IGBT junction temperature stress in the PV after stress control

The results show that the total life consumed by the device using thermal stress control is about 0.33% which means the lifetime is extended by 9 times This is an extremely high improvement compared with when the duty cycle is not a function of thermal stress. Using the proposed control approach has succeeded in minimising the temperature swings to less than 2. This will prevent the converter from reaching the catastrophic failure region, which reduces maintenance costs.

7.9 Summary

This chapter successfully presented the development and implementation of thermal stress control for IGBTs by using the junction temperature as the reference input for the proposed adaptive thermal stress control (ATSC). Furthermore, an increasing life expectancy of the device has been proven by performing the modified Coffin-Manson Law using the estimated junction temperature as a precursor parameter. The calculation of the power losses is well presented to be used in an electro-thermal IGBT model for junction temperature calculation. According to comparative discussion of the IGBT failure mechanism, the IGBT model simulation is propagated with a degradation model as function of the on-state resistance ($R_{s(on-state)}$) and the switching frequency (f_s). This causes the junction temperature (T_j) swings rapid. The life usage calculation proves that the life relatively is extended by comparing with the results of without implementing thermal stress control in simulation and experimental test rig.

It is concluded that the ATSC algorithm is adjusted V_{ref} for PID controller in order to minimise the thermal stress. In contrast to the current state-of-the-art thermal stress control, this chapter presents an adaptive algorithm based on junction temperature variation to decelerate the stress condition, which improves the life usage during failure conditions.

8 Conclusions

In power electronics applications, IVHM is a relatively new concept as compared to mechanical systems. This is because power electronics fault detection has the limitation of monitoring real-time failure mechanism degradation. Furthermore, PHM as a part of the IVHM in power electronics suffers from the limitation of versatile real-time algorithms to pinpoint a condition of the current health state as it requires a light computational process to overcome a huge amount of sensory data. Overall, in this thesis, the PHM presented in novel designs to address all these issues and improved the reliability of the system. This has been tested successfully by implementing new control strategy when the system was injected with the failure mode.

The initial knowledge and techniques needed to develop prognostics for IGBT switches have been presented in the literature. This research, on the other hand, takes the state of the art forward by the development of prognostics policies and roles suitable for increasing the availability of the power electronic modules. In this regard, the hypothesis that has been described in the introduction is tested using structured metrologies presented in Section 1-4. A number of prognostics models has been developed using different techniques, following validation steps to investigate their accuracies, efficiencies and performances. There is still a lack of knowledge to justify the developed models against a particularly successful model. We, however, realise that a physics-based model is a good reference to validate the performance of other techniques. The prognostics implementation policy solution is defined for power electronics in the comparison between different prognostics techniques (i.e. data mining, expert knowledge and hybrid techniques) which have $V_{CE\text{-}on\text{-}state}$ as a precursor parameter.

This is eventually leading us towards the development of knowledge of the prognostics on the collected data which the data was manipulated based on different ageing process presented as a mandatory requirement for data-driven, hybrid and expert knowledge prognostics approach. Additionally, the possibility of the implementing of the prognostics model before reaching catastrophic failure has been investigated. To conduct this, we scientifically looked at:

a) Selecting the parameter that indicates the abnormality and degradation in the device,

b) The necessity of classification of the number of health states for the degradation profile presented in Chapter 4 as an important part of data-mining pattern recognition to explicitly from the raw data to be used for robust failure model learning and building an efficient prognostics algorithm.

c) Utilising a probabilistic model which has been developed from the deterioration phase of the classified data enables the failure model to indicate an incipient fault and the current health state. This, in turn, provides a better RUL calculation due to the elimination of the model uncertainties.

Experiments conducted by this research demonstrate the following strengths:

a) Uncertainties are improved using a Gamma process that comparatively increases the probability of decision-making based on prognostics results.

b) In the model-based approach, it is extremely difficult to mathematically model multi-physics failure mechanisms. As a solution, the hybrid prognostics model, presented in Chapter 5, learns model degradation from the V_{CE} parameter. This technique utilises neural networks, such as TDNN, indicating solder fatigue propagates up until wire bond lift off failure mechanism, and eventually, short circuits occur in

active power switches (IGBTs). As an advantage, the efficiency of the prognostics algorithm is improved by consuming less computational power. Due to the only dependency on the phase duration rather time step, the number of MCS to calculate a mean value for RUL calculation becomes so light.

c) The fusion of the failure model with a novel analytical approach to improve prognostics result in accuracy. In the hybrid approach, novel prognostics employs the trapezoidal rule using MCS for the area under the estimated health state to calculate RUL. The populated uncertainties in model prediction are almost removed by deploying this technique.

d) Prognostics policy and rules are derived from comparisons made on different prognostics approaches conducted on power modules. From results summarised in Table 8-1, it can be realised that:

i. The Gamma process presents a perfect confidence level that makes it more suitable for decision-makers in maintenance strategy. However, the accuracy of the results has been slightly sacrificed.

ii. Normal probabilistic process computationally is very light to be embedded in DSP module, but not be recommended for the maintainer to decide on confidence bounds.

iii. The Poisson model does not make a huge difference in result precision. However, the results do not have an effective confidence bound which not be applicable for decision makers.

iv. In the data-driven approach, Gamma process is a good candidate amongst other probabilities approach for power electronics prognostics implementation and has a good potential of challenging with the hybrid and expert knowledge in future power electronics.

v. The hybrid approach in long term process can be light and computationally-reasonable and accurate for future power electronics health prediction.

vi. Expert knowledge incredibly has improved the accuracy of prediction and tracking O_C online very well. Furthermore, it is very light to be embedded for the power electronics health monitoring driver. In addition maintenance, engineer will be benefited from well-stablished confidence bounds.

The physical model is driven from the origin of the failure mechanism which has given insightful details of failure phenomena, such as creep and fatigue. This will be used for reliability assessment when the life expectancy subjected to be extended in critical situations for power converters.

Table 8-1 Prognostics Implementation Policies for Power Electronics Switches (IGBTs)

Prognostics Models		Light Algorithm/ Less Complexity	Confidence Bounds	RMSE	RA
Data-Driven	Poisson	0.3 ms per measurement point	Narrow	0.254	81.971
	Gamma	0.3 ms	Perfect	0.33795	74.542
	Normal	0.2 ms	Very narrow	0.016	99.947
Hybrid		0.9 ms	Relatively narrow	0.014	99.965
Expert Knowledge	ANFIS-Based per-Unit	0.7ms	Quite good	0.0176	98.832
	Gamma-Based per-Unit	0.4ms	Perfect	0.2520	81.98

Based on these strengths, the results have become more precise compared to latest prognostics results as shown in RA evaluation metrics. The model has learnt from 22 run-to-failure IGBT samples which have been collected from power cycling ageing test. In Chapter 6, the new novel prognostics model presented to be scalable and adapted to operating conditions online. This is often

difficult and complex for PoF model to be integrated with the scalability of the failure conditions. To that end, an adaptive neuro-fuzzy inference system (ANFIS) model has been equipped with a scalable factor in the per-unit format in order to be able to track how fast the system degrades from normal operating conditions.

The simulation of the prognostics results indicates the estimation value almost able to converge to its real RUL. Generally, the per-unit prognostics approach has impressed the predictability results. The knowledge of the end of life is given in percentage which becomes a more user-friendly decision for the maintainer. In this research, we provide a benchmark for prognostics implementation in power electronics to contribute policies for the maintenance engineer in Table 8-1.

Another key element in IVHM is about minimising stress factors in order to reduce unscheduled maintenance. In Chapter 7, the reliability of the SEPIC DC-DC converter is estimated for dominant components which are more subject to thermal stress. The analysis of junction temperature calculation as a source of thermal stress has been carried out for the power switch (IGBT). The experimental temperature measurement profile has been used for 3D-FEA analysis in order to understand how power losses induce failure phenomena, and ultimately become solder crack which eventually kills the device. The novel stress control strategy is enhanced with the critical control when it is necessary to intervene just by adjusting duty cycle in order to reduce power losses. The result of the reliability has been recalculated using Coffin-Manson and Miner's rules with the aid of the rain-flow algorithm and proves that lifetime consumption has been tremendously reduced.

8.1 Future Work

Future work could follow the investigation of the multi-disciplinary physics-of-failure model that advances deep learning parameters to correlate a

few fundamental failure mechanisms in power electronics devices. This has the potential of indication which failure triggers the other, and at what life cycles.

Furthermore, some future work requires collecting data in combination with different accelerated ageing tests and with different load operating conditions to improve the robustness of both hybrid and expert knowledge based prognostics. Also, several revolutionary works could be persuaded to pattern recognition which is about to make similarity search engine that has time series damage profile, working condition and life usage. These all can be converted to time series matrix of objects. This information when it is necessary retrieves and ultimately improves RUL calculation significantly fast. In addition, it is enhanced with a tool of diagnostic, therefore, expecting a lot of improvement in better decision making with having precise details of failures.

References

[1] J. R. Celaya, A. Saxena, C. S. Kulkarni, S. Saha, and K. Goebel, "Prognostics approach for power MOSFET under thermal stress ageing," *Reliability and Maintainability Symposium (RAMS), 2012 Annual Proceedings*, pp. 1–6, 2012.

[2] X.-S. Si, W. Wang, C.-H. Hu, and D.-H. Zhou, "Remaining useful life estimation – a review of the statistical data driven approaches," *Eur. J. Oper. Res.*, vol. 213, no. 1, pp. 1–14, 2011.

[3] M. Musallam and C. M. Johnson, "Real-time compact thermal models for health management of power electronics," *IEEE Trans. Power Electron.*, vol. 25, no. 6, pp. 1416–1425, 2010.

[4] M. Pecht and R. Jaai, "A prognostics and health management roadmap for information and electronics-rich systems," *Microelectron. Reliab.*, vol. 50, no. 3, pp. 317–323, 2010.

[5] N. M. Vichare and M. G. Pecht, "Prognostics and health management of electronics," *Components Package. Technol. IEEE Trans.*, vol. 29, no. 1, pp. 222–229, 2006.

[6] C. Bailey, H. Lu, C. Yin, and T. Tilford, "Integrated reliability and prognostics prediction methodology for power electronic modules," *Aircraft Health Management for New Operational and Enterprise Solutions, IET Seminar*, pp. 1–39, 2008.

[7] Y. Xiong, X. Cheng, Z. J. Shen, C. Mi, H. Wu, and V. Garg, "A prognostic and warning system for power electronic modules in electric, hybrid, and fuel cell vehicles," *Industry Applications Conference, 41st IAS Annual Meeting, Conference Record of the 2006 IEEE*, vol. 3, pp. 1578–1584, 2006.

[8] I. Tumer and A. Bajwa, "A survey of aircraft engine health monitoring systems," *Proc. AIAA*, 1999.

[9] G. . Kacprzynski, M. . Roemer, G. Modgil, A. Palladino, and K. Maynard, "Enhancement of physics-of-failure prognostic models with system-level features," *Aerospace Conference Proceedings, IEEE*, 2002.

[10] N. Costantino, R. Serventi, F. Tinfena, P. D'Abramo, P. Chassard, P. Tisserand, S. Saponara, and L. Fanucci, "Design and test of an HV-CMOS intelligent power switch with integrated protections and self-diagnostic for

harsh automotive applications," *IEEE Trans. Ind. Electron.*, vol. 58, no. 7, pp. 2715–2727.

[11] D. Bilar, "Degradation and subversion through subsystem attacks," *IEEE Secur. Priv.*, vol. 8, no. 4, pp. 70–73.

[12] I. K. Jennions, *Integrated Vehicle Health Management Perspectives on an Emerging Field*. Pennsylvania, USA: SAE International, Warrendale, 2011.

[13] M. Musallam, C. M. Johnson, C. Yin, H. Lu, and C. Bailey, "In-service life consumption estimation in power modules," *13th International Power Electronics and Motion Control Conference, EPE-PEMC 2008*, pp. 76–83, 2008.

[14] N. Patil, J. Celaya, D. Das, K. Goebel, and M. Pecht, "Precursor parameter identification for Insulated Gate Bipolar Transistor (IGBT) prognostics," *Reliab. IEEE Trans.*, vol. 58, no. 2, pp. 271–276, 2009.

[15] L. Zhang, X. Li, and J. Yu, "A review of fault prognostics in condition-based maintenance," *Proceedings of SPIE - The International Society for Optical Engineering*, vol. 6357 II, 2006.

[16] A. Kabir, C. Bailey, H. Lu, and S. Stoyanov, "A review of data-driven prognostics in power electronics," *Electronics Technology (ISSE), 35th International Spring Seminar*, 2012, pp. 189–192, 2012.

[17] A. Alghassi, S. Perinpanayagam, M. Samie, and T. Sreenuch, "Computationally efficient, real-time, and embeddable prognostic techniques for power electronics," *Power Electron. IEEE Trans.*, vol. 30, no. 5, pp. 2623–2634, 2015.

[18] B. Saha, J. R. Celaya, P. F. Wysocki, and K. F. Goebel, "Towards prognostics for electronics components," *Aerospace Conference, 2009 IEEE*, pp. 1–7, 2009.

[19] C. Xiongzi, Y. Jinsong, T. Diyin, and W. Yingxun, "Remaining useful life prognostic estimation for aircraft subsystems or components: a review," *Electronic Measurement & Instruments (ICEMI), 10th International Conference*, pp. 94–98, 2011.

[20] C. Chen and M. Pecht, "Prognostics of lithium-ion batteries using model-based and data-driven methods," *Prognostics and System Health Management (PHM), IEEE Conference*, pp. 1–6, 2012.

[21] C. Hu, B. Youn, and T. Kim, “Semi-supervised learning with co-training for data-driven prognostics,” *Prognostics and Health Management (PHM), IEEE Conference*, pp. 1–10, 2012.

[22] T. Sreenuch, A. Alghassi, S. Perinpanayagam and Y. Xie, "Probabilistic monte-Carlo method for modelling and prediction of electronics component life" International Journal of Advanced Computer Science and Applications (IJACSA), vol. 5, No. 1, 2014, pp.96-104.

[23] S. Sarkar, X. Jin, and A. Ray, “Data-driven fault detection in aircraft engines with noisy sensor measurements,” *J. Eng. Gas Turbines Power*, vol. 133, no. 8, p. 81602, 2011.

[24] S. KUMAR and M. PECHT, “Modelling approaches for prognostics and health management of electronics,” *Int. J. Performability Eng.*, vol. 6, pp. 467–476.

[25] A. Alghassi, S. Perinpanayagam, and I. K. Jennions, “A simple state-based prognostic model for predicting remaining useful life of IGBT power module,” in *Power Electronics and Applications (EPE), 15th European Conference on*, pp. 1–7, 2013.

[26] N. Patil, D. Das, and M. Pecht, “A prognostic approach for non-punch through and field stop IGBTs,” *Microelectron. Reliab.*, vol. 52, no. 3, pp. 482–488, 2012.

[27] M. H. Azarian, R. S. R. Kumar, N. Patil, A. Shrivastava, and M. G. Pecht, “Applications of health monitoring to wind turbines,” *Proc. of the 24th International Conference on Condition Monitoring and Diagnostics Engineering Management*, pp. 304–313.

[28] J. R. Celaya, A. Saxena, S. Saha, and K. F. Goebel, “Prognostics of power MOSFETs under thermal stress accelerated aging using data-driven and model-based methodologies,” *Annual Conference of the Prognostics and Health Management Society*, 2011.

[29] S. Zhang and R. Ganesan, “Multivariable trend analysis using neural networks for intelligent diagnostics of rotating machinery,” *J. Eng. Gas Turbines Power*, vol. 119, no. 2, pp. 378–384, 1997.

[30] O. F. Eker, F. Camci, A. Guclu, H. Yilboga, M. Sevkli, and S. Baskan, “A simple state-based prognostic model for railway turnout systems,” *Ind. Electron. IEEE Trans.*, vol. 58, no. 5, pp. 1718–1726, 2011.

[31] K. Diamantaras, W. Duch, and L. S. Iliadis, *Artificial Neural Networks* -

ICANN 20th International Conference, Thessaloniki, Greece: Springer Science & Business Media, 2010.

[32] C. . Byington, M. Watson, and D. Edwards, "Data-driven neural network methodology to remaining life predictions for aircraft actuator components," *Aerospace Conference Proceedings, IEEE*, vol. 6, pp. 3581–3589, 2004.

[33] J. Martens and I. Sutskever, "Learning recurrent neural networks with Hessian-free optimization," *Proc. 28th Int. Conf. Machine Learn (ICML)*, 2011.

[34] R. C. M. Yam, P. W. Tse, and P. T. L. Li, "Intelligent predictive decision support system for condition-based maintenance," *Int. J. Adv. Manuf. Technol.*, vol. 17, no. 5, pp 383–391.

[35] G. Yu, H. Qiu, D. Djurdjanovic, and J. Lee, "Feature signature prediction of a boring process using neural network modeling with confidence bounds," *Int. J. Adv. Manuf. Technol.*, vol. 30, no. 7, pp. 614–621.

[36] S.-S. Kim, "Time-delay recurrent neural network for temporal correlations and prediction," *Neurocomputing*, vol. 20, no. 1–3, pp. 253–263.

[37] H. Meng, N. Bianchi-Berthouze, Y. Deng, J. Cheng, and J. P. Cosmas, "Time-delay neural network for continuous emotional dimension prediction from facial expression sequences," *IEEE Trans. Cybern.*, 2015.

[38] G. Vachtsevanos and P. Wang, "Fault prognosis using dynamic wavelet neural networks," *AUTOTESTCON Proceedings, IEEE Systems Readiness Technology Conference*, pp. 857–870, 2001.

[39] N. Z. Gebraeel and M. A. Lawley, "A neural network degradation model for computing and updating residual life distributions," *IEEE Trans. Autom. Sci. Eng.*, vol. 5, no. 1, pp. 154–163.

[40] A. Oukaour, B. Tala-Ighil, B. Pouderoux, M. Tounsi, M. Bouarroudj-Berkani, S. Lefebvre, and B. Boudart, "Ageing defect detection on IGBT power modules by artificial training methods based on pattern recognition," *Microelectron. Reliab 2010 Reliab. Compd. Semicond. Work. Progn. Heal. Manag.*, vol. 51, no. 2, pp. 386–391, 2010.

[41] J. Xu and L. Xu, "Health management based on fusion prognostics for avionics systems," *Syst. Eng. Electron. J.*, vol. 22, no. 3, pp. 428–436.

[42] E. Feng, H. Yang, and M. Rao, "Fuzzy expert system for real-time process

condition monitoring and incident prevention," *Expert Syst. Appl.*, vol. 15, no. 3–4, pp. 383–390.

[43] J.-S. R. Jang, "ANFIS: adaptive-network-based fuzzy inference system," *Syst. Man Cybern. IEEE Trans.*, vol. 23, no. 3, pp. 665–685.

[44] K. M. Goh, B. Tjahjono, T. Baines, and S. Subramaniam, "A review of research in manufacturing prognostics," *Industrial Informatics, IEEE International Conference*, pp. 417–422, 2006.

[45] R. B. Chinnam and P. Baruah, "A neuro-fuzzy approach for estimating mean residual life in condition-based maintenance systems," *Int. J. Mater. Prod. Technol.*, vol. 20, no. 1–3, 2004.

[46] A. Alghassi, P. Soulatiantork, M. Samie, S. Perinpanayagam, and M. Faifer, "Relibility enhance powertrain using ANFIS base prognostics model," *Prognostics and Health Management (PHM), IEEE Conference*, pp. 1–6, 2015.

[47] I. K. Jennions, *Integrated Vehicle Health Management: The Technology (Integrated Vehicle Health Management (IVHM))*, Society of Automotive Engineers Warrendale, PA, USA, 2013.

[48] M. Daigle and K. Goebel, "Model-based prognostics under limited sensing," *Aerospace Conference, IEEE*, pp. 1–12, 2010.

[49] J. Luo, K. . Pattipati, L. Qiao, and S. Chigusa, "Model-based prognostic techniques applied to a suspension system," *Syst. Man Cybern. Part A Syst. Humans, IEEE Trans.*, vol. 38, no. 5, pp. 1156–1168.

[50] I. K. Jennions, *Integrated Vehichle Health Management The Technology*. Pennsylvania, USA: SAE International, Warrendale, 2013.

[51] R. Kraus, P. Turkes, and J. Sigg, "Physics-based models of power semiconductor devices for the circuit simulator SPICE," *Power Electronics Specialists Conference, PESC 98 Record, 29th Annual IEEE*, pp. 1726–1731, 1998.

[52] I. F. Kovačević, U. Drofenik, and J. W. Kolar, "New physical model for lifetime estimation of power modules," *Power Electronics Conference (IPEC), 2010 International*, pp. 2106–2114, 2010.

[53] P. James and A. Forsyth, "Accelerated testing of IGBT power modules to determine time to failure," *Power Electronics, Machines and Drives (PEMD 2010), 5th IET International Conference*, pp. 1–4, 2010.

[54] N. Jankovic, Z. Zhou, S. Batcup, and P. Igic, "An advance physics-based sub-circuit model of IGBT," *Industrial Electronics, IEEE International Symposium*, pp. 447–452, 2006.

[55] M. Cotorogea, "Physics-based SPICE-model for IGBTs with transparent emitter," *Power Electron. IEEE Trans.*, vol. 24, no. 12, pp. 2821–2832.

[56] J. Gu, D. Barker, and M. Pecht, "Prognostics implementation of electronics under vibration loading," *Microelectron. Reliab.*, vol. 47, no. 12, pp. 1849–1856, 2007.

[57] M. Musallam, C. Buttay, M. Whitehead, and C. . Johnson, "Real-time compact electronic thermal modelling for health monitoring," *Power Electronics and Applications, 2007 European Conference*, pp. 1–10, 2007.

[58] M. Musallam, C. M. Johnson, C. Yin, C. Bailey, and M. Mermet-Guyennet, "Real-time life consumption power modules prognosis using on-line rainflow algorithm in metro applications," *Energy Conversion Congress and Exposition (ECCE), 2010 IEEE*, pp. 970–977, 2010.

[59] C. Y. Yin, H. Lu, M. Musallam, C. Bailey, and C. M. Johnson, "A physics-of-failure based prognostic method for power modules," *10th Electronics Packaging Technology Conference, EPTC 2008,* pp. 1190–1195, 2008.

[60] H. Huang and P. . Mawby, "A lifetime estimation technique for voltage source inverters," *Power Electron. IEEE Trans.*, vol. 28, no. 8, pp. 4113–4119.

[61] B. Ji, V. Pickert, B. Zahawi, and M. Zhang, "In-situ bond wire health monitoring circuit for IGBT power modules," *Power Electronics, Machines and Drives (PEMD 2012), 6th IET International Conference*, 2012, pp. 1–6, 2012.

[62] Y. Xiong, X. Cheng, Z. J. Shen, C. Mi, H. Wu, and V. K. Garg, "Prognostic and warning system for power-electronic modules in electric, hybrid electric, and fuel-cell vehicles," *Ind. Electron. IEEE Trans.*, vol. 55, no. 6, pp. 2268–2276, 2008.

[63] A. E. Ginart, D. W. Brown, P. W. Kalgren, and M. J. Roemer, "Online ringing characterization as a diagnostic technique for IGBTs in power drives," *IEEE Trans. Instrum. Meas.*, vol. 58, no. 7, pp. 2290–2299, 2009.

[64] H. Lu, C. Bailey, and C. Yin, "Design for reliability of power electronics modules," *Microelectron. Reliab.*, vol. 49, no. 9–11, pp. 1250–1255, 2009.

[65] N. Patil, D. Das, C. Yin, H. Lu, C. Bailey, and M. Pecht, "A fusion approach to IGBT power module prognostics," *Thermal, Mechanical and Multi-Physics Simulation and Experiments in Microelectronics and Microsystems, EuroSimE 2009, 10th International Conference*, pp. 1–5, 2009.

[66] N. Patil, D. Das, K. Goebel, and M. Pecht, "Identification of failure precursor parameters for Insulated Gate Bipolar Transistors (IGBTs)," *Prognostics and Health Management, PHM 2008. International Conference*, pp. 1–5, 2008.

[67] S. Zhou, L. Zhou, and P. Sun, "Monitoring potential defects in an igbt module based on dynamic changes of the gate current," *Power Electron. IEEE Trans.*, vol. 28, no. 3, pp. 1479–1487.

[68] D. L. Goodman, "Prognostic methodology for deep submicron semiconductor failure modes," *Components Packag. Technol. IEEE Trans.*, vol. 24, no. 1, pp. 109–111, 2001.

[69] P. Shetty, D. Mylaraswamy, and T. Ekambaram, "A hybrid prognostic model formulation system identification and health estimation of auxiliary power units," *Aerospace Conference, 2006 IEEE*, 2006.

[70] A. . Garga, K. . McClintic, R. . Campbell, C.-C. Yang, M. . Lebold, T. . Hay, and C. . Byington, "Hybrid reasoning for prognostic learning in CBM systems," *Aerospace Conference, 2001 IEEE Proceedings*, pp. 2957–2969, 2001.

[71] L. Liao and F. Kottig, "Review of hybrid prognostics approaches for remaining useful life prediction of engineered systems, and an application to battery life prediction," *Reliab. IEEE Trans.*, vol. 63, no. 1, pp. 191–207.

[72] M. Samie, S. Perinpanayagam, A. Alghassi, A. M. S. Motlagh, and E. Kapetanios, "Developing prognostic models using duality principles for DC-to-DC converters," *Power Electron. IEEE Trans.*, vol. 30, no. 5, pp. 2872–2884, 2015.

[73] A. Alghassi, M. Samie, and S. Perinpanayagam, "Stochastic RUL calculation enhanced with TDNN-based IGBT failure modeling," *Reliab. IEEE Trans.*, vol. PP, no. 99, pp. 1–16.

[74] J. Z. Sikorska, M. Hodkiewicz, and L. Ma, "Prognostic modelling options for remaining useful life estimation by industry," *Mech. Syst. Signal Process.*, vol. 25, no. 5, pp. 1803–1836, 2011.

[75] V. K. Khanna, *Insulated Gate Bipolar Transistor IGBT Theory and Design*. Wiley-IEEE Press.

[76] B. Jayant Baliga, "Enhancement- and depletion-mode vertical-channel m.o.s. gated thyristors," *Electron. Lett.*, vol. 15, no. 20, pp. 645–647.

[77] J. D. Plummer and B. . Scharf, "Insulated-gate planar thyristors: I—structure and basic operation," *Electron Devices, IEEE Trans.*, vol. 27, no. 2, pp. 380–387.

[78] B. . Scharf and J. D. Plummer, "Insulated-gate planar thyristors: II—quantitative modeling," *Electron Devices, IEEE Trans.*, vol. 27, no. 2, pp. 387–394.

[79] B. J. Baliga, *Fundamentals of Power Semiconductor Devices*, Springer, year.

[80] H. Oh, B. Han, P. McCluskey, C. Han, and B. D. Youn, "Physics-of-failure, condition monitoring, and prognostics of insulated gate bipolar transistor modules: a review," *Power Electron. IEEE Trans.*, vol. 30, no. 5, pp. 2413–2426, 2015.

[81] N. Y. A. Shammas, "Present problems of power module packaging technology," *Microelectron. Reliab.*, vol. 43, no. 4, pp. 519–527, 2003.

[82] G. Sonnenfeld, K. Goebel, and J. R. Celaya, "An agile accelerated aging, characterization and scenario simulation system for gate controlled power transistors," *AUTOTESTCON, 2008 IEEE*, pp. 208–215, 2008.

[83] M.-D. Ker, "ESD (electrostatic discharge) protection design for nanoelectronics in CMOS technology," *Advanced Signal Processing, Circuits, and System Design Techniques for Communications,* pp. 217–279, 2006.

[84] M. Ciappa, "Selected failure mechanisms of modern power modules," *Microelectron. Reliab.*, vol. 42, no. 4–5, pp. 653–667, 2002.

[85] S. Yang, D. Xiang, A. Bryant, P. Mawby, L. Ran, and P. Tavner, "Condition monitoring for device reliability in power electronic converters: a review," *Power Electron. IEEE Trans.*, vol. 25, no. 11, pp. 2734–2752, 2010.

[86] H.-K. Tseng and M.-L. Wu, "Electro-thermal-mechanical modeling of wire bonding failures in IGBT," *Microsystems, Packaging, Assembly and Circuits Technology Conference (IMPACT), 2013 8th International*, pp. 152–157, 2013.

[87] R. Wu, F. Blaabjerg, H. Wang, M. Liserre, and F. Iannuzzo, "Catastrophic failure and fault-tolerant design of IGBT power electronic converters - an overview," *Industrial Electronics Society, IECON 2013 - 39th Annual Conference of the IEEE*, pp. 507–513, 2013.

[88] M. Kobayash and Q. Yu, "Reliability evaluation for specify factor of fatigue on power device," *Prognostics and Health Management Conference, PHM 2010*, pp. 1–6, 2010.

[89] C. Y. Yin, H. Lu, M. Musallam, C. Bailey, and C. M. Johnson, "A prognostic assessment method for power electronics modules," *Electronics System-Integration Technology Conference, ESTC 2008,* pp. 1353–1358, 2008.

[90] C. Bailey, H.-H. Lu, C. Yin, and S. Ridout, "Predictive reliability, prognostics and risk assessment for power modules," *Integrated Power Systems (CIPS), 5th International Conference*, pp. 1–7, 2008.

[91] Y. Xiong, X. Cheng, Z. J. Shen, C. Mi, H. Wu, and V. K. Garg, "Prognostic and warning system for power-electronic modules in electric, hybrid electric, and fuel-cell vehicles," *IEEE Trans. Ind. Electron.*, vol. 55, no. 6, pp. 2268–2276.

[92] A. K. S. Jardine, D. Lin, and D. Banjevic, "A review on machinery diagnostics and prognostics implementing condition-based maintenance," *Mech. Syst. Signal Process.*, vol. 20, no. 7, pp. 1483–1510, 2006.

[93] F. Wakeman, D. Hemmings, W. Findlay, and G. Lockwood, "Pressure contact IGBT, testing for reliability," IXYS Power Semiconductors Application Notes, 2002.

[94] A. Morozumi, Y. Nishimura, and S. Okita, "No Title," *Semicond. Device Method Relaxing Therm. Stress*, 2005.

[95] J. R. Celaya, P. Wysocki, V. Vashchenko, S. Saha, and K. Goebel, "Accelerated aging system for prognostics of power semiconductor devices," *AUTOTESTCON, 2010 IEEE*, pp. 1–6, 2010.

[96] M. Mermet-Guyennet, X. Perpiñá, and M. Piton, "Revisiting power cycling test for better life-time prediction in traction," *18th Eur. Symp. Reliab. Electron Devices, Fail. Phys. Anal.*, vol. 47, no. 9–11, pp. 1690–1695, 2007.

[97] A. Hensler, J. Lutz, M. Thoben, and J. Zachariae, "Power cycling tests at high temperatures with IGBT power modules for hybrid electrical vehicle applications," *3rd Electronic System-Integration Technology Conference (ESTC),* pp. 1–6, 2010.

[98] S. Saha, J. R. Celaya, V. Vashchenko, S. Mahiuddin, and K. F. Goebel, "Accelerated aging with electrical overstress and prognostics for power MOSFETs," *Energytech, 2011 IEEE*, pp. 1–6, 2011.

[99] M. Musallam, C. M. Johnson, C. Yin, H. Lu, and C. Bailey, "Real-time life expectancy estimation in power modules," *2nd Electronics System-Integration Technology Conference, ESTC 2008,* pp. 231–236, 2008.

[100] A. Alghassi, M. Samie, and S. Perinpanayagam, "Stochastic RUL calculation enhanced with TDNN-based IGBT failure modelling," *Reliab. IEEE Trans.*, vol. PP, no. 99, pp. 1–16.

[101] V. Smet, F. Forest, J. J. Huselstein, F. Richardeau, Z. Khatir, S. Lefebvre, and M. Berkani, "Ageing and failure modes of IGBT modules in high-temperature power cycling," *IEEE Trans. Ind. Electron.*, vol. 58, no. 10, pp. 4931–4941, 2011.

[102] J. R. Celaya, P. Wysocki, V. Vashchenko, S. Saha, and K. Goebel, "Accelerated aging system for prognotics of power seminconductor devices," *AUTOTESTCON, 2010 IEEE*, pp. 1–6, 2010.

[103] N. Patil, D. Das, K. Goebel, and M. Pecht, "Failure precursors for Insulated Gate Bipolar Transistors (IGBTs)," *IEEE Trans. Reliab.*, pp. 271–276, 2009.

[104] J. Celaya, P. Wysocki, and K. Goebel, "IGBT accelerated aging data set," *NASA Ames Prognostics Data Repository*. Moffett Field, CA, 2009.

[105] G. Coquery, G. Lefranc, T. Licht, R. Lallemand, N. Seliger, and H. Berg, "High temperature reliability on automotive power modules verified by power cycling tests up to 150°C," *14th Eur. Symp. Reliab. Electron Devices, Fa*, vol. 43, no. 9–11, pp. 1871–1876, 2003.

[106] M. A. Rodríguez-Blanco, A. Claudio-Sánchez, D. Theilliol, L. G. Vela-Valdés, P. Sibaja-Terán, L. Hernández-González, and J. Aguayo-Alquicira, "A failure-detection strategy for IGBT based on gate-voltage behavior applied to a motor drive system," *Ind. Electron. IEEE Trans.*, vol. 58, no. 5, pp. 1625–1633, 2011.

[107] P. Baraldi, F. Cadini, F. Mangili, and E. Zio, "Model-based and data-driven prognostics under different available information," *Probabilistic Eng. Mech.*, vol. 32, no. 0, pp. 66–79, 2013.

[108] K. Goebel, B. Saha, A. Saxena, N. Mct, and N. Riacs, "A comparison of three data-driven techniques for prognostics," *62nd Meeting of the Society*

For Machinery Failure Prevention Technology (MFPT), pp. 119–131, 2008.

[109] B. Ji, V. Pickert, W. Cao, and B. Zahawi, "In situ diagnostics and prognostics of wire bonding faults in IGBT modules for electric vehicle drives," *Power Electron. IEEE Trans.*, vol. 28, no. 12, pp. 5568–5577, 2013.

[110] A. Alghassi, S. Perinpanayagam, M. Samie, and T. Sreenuch, "Computationally-efficient, real-time and embeddable prognostic techniques for power electronics," *Power Electronics, IEEE Transactions*, vol. PP, no. 99. p. 1, 2014.

[111] J. Jiang and X.-P. Zhang, "A novel vector quantization-based video summarization method using independent component analysis mixture model," in *Acoustics, Speech and Signal Processing (ICASSP), 2011 IEEE International Conference*, pp. 1341–1344, 2011.

[112] J. K. Kim, Y. Cho, M. Lee, J. Cha, C. Song, D. S. Kim, and D. Kim, "BetaConcept: a program for Voronoi diagrams, dual structures, and complexes in the plane," *Computational Science and Its Applications (ICCSA), 14th International Conference*, pp. 233–236, 2014.

[113] D. Siegel and J. Lee, "An Auto-Associative Residual Processing and K-means Clustering Approach for Anemometer Health Assessment," Online–Resource.

[114] L. Ma, J.-S. Kang, C.-Y. Zhao, and S.-Y. Liu, "Modeling the impact of prognostic errors on CBM effectiveness using discrete-event simulation," *Quality, Reliability, Risk, Maintenance, and Safety Engineering (ICQR2MSE), 2012 International Conference*, pp. 520–525, 2012.

[115] J. F. Lawless, *Statistical Model and Methods for lifetime Data*, 2nd vol. , Hoboken, New Jersey, Canada: John Wiley & Sons, 2011.

[116] R. B. Millar, *Maximum Likelihood Estimation and Inference*, 1st vol., United Kingdom: John Wiley & Sons, 2011.

[117] S. Sankararaman, M. Daigle, A. Saxena, and K. Goebel, "Analytical algorithms to quantify the uncertainty in remaining useful life prediction," *Aerospace Conference, 2013 IEEE*, pp. 1–11, 2013.

[118] P. Wang, B. D. Youn, and C. Hu, "A generic probabilistic framework for structural health prognostics and uncertainty management," *Interdiscip. Integr. Asp. Struct. Heal. Monit.*, vol. 28, no. 0, pp. 622–637, 2012.

[119] R. M. Crowder, "Electrically powered actuation for civil aircraft," *Actuator*

Technology: Current Practice and New Developments., IEE Colloquium on (Digest No: 1996/110), pp. 5/1–5/3, 1996.

[120] K. Medjaher, D. A. Tobon-Mejia, and N. Zerhouni, "Remaining useful life estimation of critical components with application to bearings," *Reliab. IEEE Trans.*, vol. 61, no. 2, pp. 292–302, 2012.

[121] J. Durbin and S. J. Koopman, *Time Series Analysis by State Space Methods*, Oxford.

[122] A. K. Jain, *Machine Learning and Data Mining in Pattern Recognition*. Springer.

[123] H. Qiu, J. Lee, J. Lin, and G. Yu, "Robust performance degradation assessment methods for enhanced rolling element bearing prognostics," *Intell. Maint. Syst.*, vol. 17, no. 3–4, pp. 127–140, 2003.

[124] B. Ji, V. Pickert, and B. Zahawi, "In-situ bond wire and solder layer health monitoring circuit for IGBT power modules," *Integrated Power Electronics Systems (CIPS), 2012 7th International Conference*, pp. 1–6, 2012.

[125] U. Maulik and S. Bandyopadhyay, "Genetic algorithm-based clustering technique," *Pattern Recognit.*, vol. 33, no. 9, pp. 1455–1465, 2000.

[126] R. Derakhshani and S. A. C. Schuckers, "Continuous time delay neural networks for detection of temporal patterns in signals," *Neural Networks, 2004 Proceedings, 2004 IEEE International Joint Conference*, vol. 4, pp. 2723–2728, 2004.

[127] H. Zhang, M. Ö. Balaban, and J. C. Principe, "Improving pattern recognition of electronic nose data with time-delay neural networks," *Sensors Actuators B Chem.*, vol. 96, no. 1–2, pp. 385–389, 2003.

[128] R. Sitte and J. Sitte, "Analysis of the predictive ability of time delay neural networks applied to the S&P 500 time series," *Syst. Man, Cybern. Part C Appl. Rev. IEEE Trans.*, vol. 30, no. 4, pp. 568–572, 2000.

[129] S. A. Mojarad, S. S. Dlay, W. L. Woo, and G. V Sherbet, "Breast cancer prediction and cross validation using multilayer perceptron neural networks," *Communication Systems Networks and Digital Signal Processing (CSNDSP), 7th International Symposium*, pp. 760–764, 2010.

[130] Y. Tan, C.-Y. Su, and N. Karim, "Neural network based time-delay estimation for nonlinear dynamic systems," *Proc. of the IFAC 15th Triennial World Congress, CD-ROM, Barcelona, Spain*, 2002.

[131] G. Lera and M. Pinzolas, "Neighborhood based Levenberg-Marquardt algorithm for neural network training," *Neural Networks, IEEE Trans.*, vol. 13, no. 5, pp. 1200–1203, 2002.

[132] Z. Tian, "An artificial neural network approach for remaining useful life prediction of equipments subject to condition monitoring," *Reliability, Maintainability and Safety, ICRMS 2009, 8th International Conference*, pp. 143–148, 2009.

[133] F. O. Heimes, "Recurrent neural networks for remaining useful life estimation," *Prognostics and Health Management, PHM 2008, International Conference*, pp. 1–6, 2008.

[134] H. Hirose, A. Todoroki, S. Matsuda, and M. Hikita, "Electrical insulation diagnosing using a new statistical classification method," *Properties and Applications of Dielectric Materials, 8th International Conference*, pp. 698–701, 2006.

[135] M. Samie, S. Perinpanayagam, A. Alghassi, A. Motlagh, and E. Kapetanios, "Developing prognostic models using duality principles for DC-to-DC converters," *Power Electron. IEEE Trans.*, vol. PP, no. 99, p. 1, 2014.

[136] C. Louen, S. X. Ding, and C. Kandler, "A new framework for remaining useful life estimation using Support Vector Machine classifier," *Control and Fault-Tolerant Systems (SysTol), 2013 Conference*, pp. 228–233, 2013.

[137] H. W. Beaty and S. Santoso, *Handbook of Electric Power Calculations*, 4th ed., McGraw-Hill Professional.

[138] J.-M. Thebaud, E. Woirgard, C. Zardini, and K.-H. Sommer, "High power IGBT modules: thermal fatigue resistance evaluation of the solder joints," *Integrated Power Packaging, IWIPP 2000 International Workshop on*, pp. 79–83, 2000.

[139] M. Samie, A. Alghassi, and S. Perinpanayagam, "Unified IGBT prognostic using natural computation," *Digital Signal Processing (DSP), 2015 IEEE International Conference*, pp. 698–702, 2015.

[140] C. O. Maiga, B. Tala-Ighil, H. Toutah, and B. Boudart, "Behaviour of punch-through and non-punch-through insulated gate bipolar transistors under high temperature gate bias stress," *Industrial Electronics, 2004 IEEE International Symposium*, pp. 1035–1040, 2004.

[141] A. Hallouche and A. Tilmatne, "Thermal impact on the power device behaviour: application on the IGBT," *Adv. Electr. Comput. Eng.*, vol. 7 (14),

pp. 53–62.

[142] M. Arab, S. Lefebvre, Z. Khatir, and S. Bontemps, "Experimental investigations of trench field stop IGBT under repetitive short-circuits operations," *Power Electronics Specialists Conference, PESC 2008, IEEE*, pp. 4355–4360, 2008.

[143] A. Alghassi, P. Soulatiantork, M. Samie, S. Perinpanayagam, and M. Faifer, "Relibility enhance powertrain using ANFIS base prognostics model," *Prognostics and Health Management (PHM), 2015 IEEE Conference*, pp. 1–6, 2015.

[144] C. Chen, B. Zhang, G. Vachtsevanos, and M. Orchard, "Machine condition prediction based on adaptive neuro–fuzzy and high-order particle filtering," *Ind. Electron. IEEE Trans.*, vol. 58, no. 9, pp. 4353–4364, 2011.

[145] A. Alghassi, P. Soulatiantork, M. Samie, S. Perinpanayagam, and M. Faifer, "Reliability enhance powertrain using fuzzy knowledge base prognostics model," *Power Electronics and Applications (EPE'15 ECCE-Europe), 17th European Conference*, pp. 1–9, 2015.

[146] B. Ji, V. Pickert, W. Cao, and B. Zahawi, "In situ diagnostics and prognostics of wire bonding faults in IGBT Modules for electric vehicle drives," *IEEE Trans. Power Electron.*, vol. 28, no. 12, pp. 5568–5577, year.

[147] J. Gu and M. Pecht, "Predicting the Reliability of electronic products," *Electronic Packaging Technology, ICEPT 2007, 8th International Conference*, pp. 1–8, 2007.

[148] J. Endrenyi, R. N. Allan, G. J. Anders, S. Asgarpoor, R. Billinton, N. Chowdhury, E. N. Dialynas, R. H. Fletcher, J. McCalley, S. Meliopoulos, T. C. Mielnik, P. Nitu, N. D. Reppen, L. Salvaderi, and A. Schneider, "The present status of maintenance strategies and the impact of maintenance on reliability," *Power Syst. IEEE Trans.*, vol. 16, no. 4, pp. 638–646, 2001.

[149] Y. Song and B. Wang, "Survey on reliability of power electronic systems," *Power Electron. IEEE Trans.*, vol. 28, no. 1, pp. 591–604, 2013.

[150] S. V Dhople, A. Davoudi, P. L. Chapman, and A. D. Dominguez-Garcia, "Reliability assessment of fault-tolerant DC-DC converters for photovoltaic applications," *Energy Conversion Congress and Exposition, ECCE 2009. IEEE*, pp. 2271–2276, 2009.

[151] J. Pelleg, *Mechanical Properties of Materials*, 1st ed., Springer Netherlands, 2013.

[152] Y. P. Siwakoti, F. Z. Peng, F. Blaabjerg, P. C. Loh, and G. E. Town, "Impedance-source networks for electric power conversion part I: a topological review," *Power Electron. IEEE Trans.*, vol. 30, no. 2, pp. 699–716, 2015.

[153] H. Lu, T. Tilford, and D. R. Newcombe, "Lifetime prediction for power electronics module substrate mount-down solder interconnect," *High Density packaging and Microsystem Integration, HDP 2007, International Symposium*, pp. 1–10, 2007.

[154] G. F, "An empirical relation defining the stress dependence of minimum creep rate in metals," *Trans AIME*, vol. 227, p. 351, 1963.

[155] S. BROWN, K. KIM, and L. ANAND, "An internal variable constitutive model for hot working of metals," *Int. J. Plast.*, vol. 5, no. 2, pp. 95–130, 1989.

[156] M. S. Nasrin and F. H. Khan, "Characterization of aging process in power converters using spread spectrum time domain reflectometry," *Energy Conversion Congress and Exposition (ECCE), 2012 IEEE*, pp. 2142–2148, 2012.

[157] H. Wang, M. Liserre, F. Blaabjerg, P. de Place Rimmen, J. B. Jacobsen, T. Kvisgaard, and J. Landkildehus, "Transitioning to physics-of-failure as a reliability driver in power electronics," *Emerg. Sel. Top. Power Electron. IEEE J.*, vol. 2, no. 1, pp. 97–114, 2014.

[158] M. Andresen and M. Liserre, "Impact of active thermal management on power electronics design," *SI ESREF 2014*, vol. 54, no. 9–10, pp. 1935–1939, 2014.

[159] D. A. Murdock, J. E. R. Torres, J. J. Connors, and R. D. Lorenz, "Active thermal control of power electronic modules," *Ind. Appl. IEEE Trans.*, vol. 42, no. 2, pp. 552–558, 2006.

[160] T. Jalakas, D. Vinnikov, and J. Laugis, "Evaluation of different loss calculation methods for high-voltage IGBT-s under small load conditions," *13th Power Electronics and Motion Control Conference, EPE-PEMC 2008,* , pp. 1263–1267, 2008.

[161] M. Musallam, C. Yin, C. Bailey, and C. M. Johnson, "Application of coupled electro-thermal and physics-of-failure-based analysis to the design of accelerated life tests for power modules," *Microelectron. Reliab.*, vol. 54, no. 1, pp. 172–181, 2014.

[162] M. Musallam and C. M. Johnson, “An efficient implementation of the rainflow counting algorithm for life consumption estimation,” *Reliab. IEEE Trans.*, vol. 61, no. 4, pp. 978–986, 2012.